HEPARAN SULFATE PROTEOGLYCANS IN NERVOUS SYSTEM DEVELOPMENT OF *C. ELEGANS*

DISSERTATION
ZUR

ERLANGUNG DER NATURWISSENSCHAFTLICHEN DOKTORWÜRDE

(DR. SC. NAT.)

VORGELEGT DER
MATHEMATISCH-NATURWISSENSCHAFTLICHEN FAKULTÄT

DER

UNIVERSITÄT ZÜRICH

VON

CHRISTA RHINER

AUS

SENNWALD SG

PROMOTIONSKOMITEE

PROF. MICHAEL O. HENGARTNER (VORSITZ, LEITER DER DISSERTATION)

PROF. ESTHER STOECKLI

PROF. ALEX HAJNAL

PROF. HARALD HUTTER

ZÜRICH 2006

To my parents Ruth and Fred

ZUSAMMENFASSUNG

Die Entwicklung eines funktionierenden Nervensystems ist ein hoch komplexer Prozess, der über verschiedene Zwischenschritte abläuft. In einer Anfangsphase müssen Nervenzellen von ihrem Entstehungsort, zu den ihnen vorbestimmten Positionen im neuronalen Netzwerk gelangen. Wenn sie ihren Zielort erreicht haben, senden sie dünne Prozesse aus, Axone, die über weite Distanzen zu anderen Neuronen navigieren, mit denen sie schliesslich synaptische Verbindungen herstellen. Hauptsächlich vier konservierte Proteinfamilien sind bekannt, die als Steuersignale für migrierende Neurone und auswachsende Axone dienen: Netrine, Slits, Semaphorine und Ephrine. Dennoch ist immer noch unklar, wie diese beschränkte Anzahl an Steuersignalen die Ausbildung von hoch differenzierten Steueroptionen für individuelle Neurone kontrollieren kann. Heparansulfatproteoglykane (HSPGe) sind Bestandteil der extrazellulären Matrix, durch welche Axone navigieren. HSPGe tragen unterschiedlich modifizierte Zuckerketten, von denen man vermutete, dass sie Informationen ans Nervensystem weterleiten. Nicht bekannt war jedoch, welche HSPGe an der Entwicklung des Nervensystems beteiligt sind und auf welche Art sie die Entstehung von neuronalen Strukturen kontrollieren.

In dieser Dissertation stelle ich die Resultate meiner Studie über die Funktion der HSPGe in der Entstehung des Nervensystems von *C. elegans* vor. Ich zeige, dass das Zelloberflächen-HSPG syndecan SDN-1 zellautonom in Neuronen funktioniert, um neuronale Migration und axonale Steuerung zu regulieren (Kapitel 2). Die Analyse von Doppelmutanten ordnet SDN-1 in den Slit/Robo Signalweg ein, liefert aber auch Beweise für die Existenz eines parallelen axonalen Steuerungssignalwegs, der von mindestens einem zusätzlichen HSPG kontrolliert wird. Dieses HSPG ist wahrscheinlich das Hauptsubstrat der HS C5-epimerase HSE-5 (Kapitel 2).

Um HSPGe im SDN-1-unabhängigen Signalweg zu identifizieren, habe ich zuerst bestehende HSPG-Mutanten auf neuronale Defekte überprüft und RNAi gegen bekannte HSPGe durchgeführt (Kapitel 3). Mit diesem Ansatz fand ich, dass das extrazelluläre Kollagen XVIII CLE-1 im gleichen Signalweg wie SDN-1 funktioniert, aber ich konnte keine HSPGe des parallelen HS-abhängigen Signalwegs aufdecken.

Deshalb habe ich eine enhancer-screen Strategie entwickelt, um neue Komponenten in beiden HS-abhängigen Signalwegen zu ermitteln. Das Screening für enhancers in einem *hse-5*-mutanten Hintergrund hat 14 enhancer-Mutationen ergeben. Ich habe die sieben stärksten enhancer-Mutationen zurückgekreuzt, charakterisiert und Regionen auf den Chromosomen I, II und IV zugeordnet (Kapitel 4). Es ist wahrscheinlich, dass die isolierten enhancer-Mutationen neue Gene identifizieren werden, die an der SDN-1-abhängigen Axonsteuerung beteiligt sind.

In einem zweiten Projekt habe ich die funktionelle Konservierung von UNC-69 studiert, einem axonalen Steuerprotein in *C. elegans*. Ich konnte zeigen, dass das homologe UNC-69 protein des Huhns stark im Nervensystem exprimiert ist und dass seine Inaktivierung mittels RNAi zu axonalen Steuerdefekten führt (Kapitel 5).

Dies zeigt auf, dass der Fadenwurm *C. elegans* ein starkes Modell darstellt, um neue Regulatoren für die axonale Steuerkontrolle zu entdecken. HSPGe sind hoch konserviert vom Wurm zum Menschen, was die Idee bestärkt, dass gewebespezifische HS Zuckermodifikationen eine wichtige Rolle für die Entwicklung eines komplexen Nervensystems gespielt haben mögen. Es ist deshalb wahrscheinlich, dass im Wurm erkannte Regeln auch bei Säugetieren anwendbar sind und damit zu einem besseren Verständnis der Mechanismen führen, welche die Entstehung des Nervensystems kontrollieren.

SUMMARY

The development of a functional nervous system is a highly complex process and takes place over several intermediate steps. In an initial phase, neurons have to migrate from their place of birth to the positions at which they are destined to function in the neuronal network. Once they have reached their position, they extend thin processes - axons - that navigate over long distances to finally establish synaptic contacts with other neurons. Four main conserved protein families have been identified that serve as guidance cues for migrating neurons and axonal growth cones: netrins, Slits, semaphorins and ephrins. Nevertheless, it is still unclear how a restricted set of guidance molecules is able to give rise to highly differentiated guidance choices of individual axons. Heparan sulfate proteoglycans (HSPGs) are part of the extracellular matrix through which axons navigate. HSPGs carry differentially modified sugar side chains, which have been proposed to convey information to the nervous system. However, it was not known which HSPGs are implicated in neural development and how they function to control neural patterning.

In this dissertation, I present the results of my study on the function of HSPGs in nervous system development of *C. elegans*. I show that the cell surface HSPG syndecan SDN-1 acts cell-autonomously in neurons to regulate neuronal migration and axon guidance (chapter 2). Double mutant analyses place SDN-1 in the Slit/Robo signaling pathway, but provide also evidence for a parallel axon guidance pathway that is controlled by at least one additional HSPG, which is likely to be the main target of the HS C5-epimerase HSE-5 (chapter 2).

In order to identify HSPGs in the SDN-1-independent pathway, I first examined available HSPG mutants for neural defects and performed RNAi against known HSPGs (chapter 3). Using this approach, I found that the extracellular collagen XVIII CLE-1 functions in the same pathway as SDN-1, but did not uncover HSPGs of the parallel HS-dependent axon guidance pathway. Therefore, I developed an enhancer screen strategy to identify new components in both HS-dependent signaling pathways. Screening for enhancers in an *hse-5* mutant background yielded 14 enhancer mutations. I backcrossed and characterized the seven strongest enhancer mutations and mapped them to subchromosomal regions on chromosome I, II and IV (chapter 4). The isolated enhancer mutations are likely to reveal new genes involved in SDN-1-regulated axon guidance signaling.

In a second project, I have studied the functional conservation of UNC-69, a *C. elegans* axon guidance protein. I could show that the chicken homolog of UNC-69 is highly expressed in the developing nervous system of the chicken embryo and that its inactivation by RNAi leads to axon guidance defects (chapter 5).

This shows that the nematode *C. elegans* is a powerful model system to identify new regulators of axon guidance signaling. HSPGs are highly conserved from nematodes to humans, which supports the idea that tissue-specific HS sugar modifications might have been an important factor to generate a complex nervous system. Rules learned in *C. elegans* are thus likely to also apply in mammals, and promise to lead to a better understanding of the mechanisms that control nervous system development.

ACKNOWLEDGMENTS

There are numerous people who have contributed to my scientific education, but here I will just thank those, who have supported me in the past four years in Zurich.

I am very grateful to Adriano Aguzzi, who was my mentor during the diploma thesis at the University Hospital in Zurich. He taught me how to set up good experiments, but also that you have to be passionate about what you are doing in science. I thank Magda Polymenidou, with whom I shared the bench during this year, for scientific discussions and a great friendship.

For the past three years, I have been part of the Hengartner group at the Institute of Molecular Biology. I would like to thank all the past and current lab members who have helped me to perform this work and who created a lively atmosphere in the lab. A special thank goes to Steffi Züllig and Doris Klingele, who introduced me into the basics of *C. elegans* experiments and to Lukas Neukomm, with whom I shared many up and downs in our projects. An extra thank goes also to Ataman Sendoel for numerous afternoon coffee breaks about science and non-science and to Stephan Gysi for reinforcing the neuro group.

Besides my lab members, I am greatly indebted to Hannes Bülow and Oliver Hobert at Columbia University, who taught me how to analyze axon guidance defects in the worm and for comments on the manuscript. Moreover, I would like to thank Matthias Bodmer, who is taking excellent care of the FLP-mapping process.

The members of my thesis committee, Prof. Esther Stoeckli, Prof. Harald Hutter, Prof. Alex Hajnal and Prof. Michael Hengartner, provided me with invaluable advice for the success of this project.

Finally, I would like to thank my advisor Michael Hengartner for his guidance and support. From him I learned how a scientific article should be written and that you should never loose faith.

TABLE OF CONTENTS

ZUSAMMENFASSUNG 3

SUMMARY 5

ACKNOWLEDGMENTS 7

CHAPTER 1: Sugar-Antennae for Guidance Signals: Syndecans integrate Directional Cues for Navigating Neurons

Preface 11

Manuscript (in press) 12

CHAPTER 2: Syndecan Regulates Cell Migration and Axon Guidance in *C. elegans*

Preface 32

Article (re-print) 33

CHAPTER 3: A Systematic Approach to HSPG Function in Neuronal Development of *C. elegans*.

Introduction 47

Results 51

Discussion 61

Material and Methods 66

References 69

CHAPTER 4: Identifying new genes in HS-dependent axon guidance signaling

Introduction 73

Results 76

Discussion 85

Material and Methods 89

References 90

CHAPTER 5: Studying *C. elegans* axon guidance genes in higher vertebrates: Conserved functions for UNC-69 and UNC-76?

Preface 94

Article (re-print) 95

Supplementary Results 121

Material and Methods 125

References 126

CHAPTER 6: Perspectives

Axon guidance: past and present research 128

HSPGs in *C. elegans* nervous system development: An Outlook 129

Concluding remarks 132

References 132

CHAPTER 1

Sugar-Antennae for Guidance Signals: Syndecans integrate Directional Cues for Navigating Neurons

PREFACE

This review will be published in the Cell Biology Domain of TheScientificWorldJOURNAL this year (manuscript in press). It focuses on the role of heparan sulfate proteoglycans and specific heparan sulfate modifications for various aspects of nervous system development. I have written the manuscript, which was later edited by Prof. Michael Hengartner.

Sugar-Antennae for Guidance Signals: Syndecans and Glypicans integrate Directional Cues for Navigating Neurons

Christa Rhiner[1,2] and Michael O. Hengartner[1,2]*

[1]Neuroscience Center Zurich ,[2]Institute of Molecular Biology, University of Zurich, Winterthurerstrassse 190, CH-8057, Switzerland.

** Corresponding author: michael.hengartner@molbio.unizh.ch*

Phone: + 41 44 635 31 40 Fax: + 41 44 635 68 61

Keywords: axon guidance, neuronal migration, heparan sulfate proteoglycans (HSPGs), syndecan, glypican, *C. elegans*

Domains: Cell Biology, Developmental Biology, Genetics (worms), Neuronal Function, Neuroscience, Molecular Biology.

Abstract

Attractive and repulsive signals guide migrating nerve cells in all directions when the nervous system starts to form. The neurons extend thin processes – axons – that connect over wide distances with other brain cells to form a complicated neuronal network. One of the most fascinating questions in neuroscience is how the correct wiring of billions of nerve cells in our brain is controlled. Several protein families are known to serve as guidance cues for navigating neurons and axons. Nevertheless, the combinatorial potential of these proteins seems to be insufficient to sculpt the neuronal network and the appropriate formation of connections. Recently, heparan sulfate proteoglycans (HSPGs), which are present on the cell surface of neurons and in the extracellular matrix through which neurons and axons migrate, have been found to play a role in regulating cell migration and axon guidance. Intriguingly, the large number of distinct modifications that can be put onto the sugar side chains of these proteoglycans would in principle allow for an enormous diversity of HSPGs, which could help in regulating the vast number of guidance choices taken by individual neurons. In this review, we will focus on the role of the cell surface HSPGs syndecan and glypican and specific HS modifications in promoting neuronal migration, axon guidance and synapse formation.

Nerve cells communicate over an immense number of established contacts called synapses. The formation of such connections in neural maps is complex and occurs over several intermediate steps: In an early phase, neurons that are generated from neuronal stem cells have to migrate from their place of birth to the place at which they are destined to differentiate and function. For example, large populations of neurons in the developing mammalian brain are known to travel extensively along different routes in parallel to the brain surface to reach their target area. Other neurons, emigrate radially along specialized glia cells and give rise to the multiple layers of the human cortex [1]. In the latter case, the processes of radial glia are used as guide wires for the migrating neurons. This form of migration, however, is a modern invention, unique to higher vertebrates. In classical forms of neural migration, the neurons are guided by secreted or cell surface-bound attractive or repulsive cues and by interactions with extracellular matrix proteins. In this way, a migrating neuron is exposed to a wealth of different stimuli and molecular gradients while navigating to its often-distant target position. How does a neuron integrate all these signals? How is it able to veer slightly more to the right than its neighbour who is heading the same general direction? Why

does it stop after its remarkable journey at precisely its intended final location? These questions reappear later, when neurons start to send out axons that have to establish synaptic contacts with a target cell over a long distance. While migrating neurons and axonal growth cones do not possess a brain GPS (global positioning system) device, recent findings suggest that they utilize at least one sort of signal integrating and fine-tuning instrument: Heparan sulfate proteoglycans (HSPGs) that are mounted antennae-like on the cell surface and regulate guidance signals via their sugar side chains. HSPGs are a family of highly conserved proteoglycans that consist of membrane-anchored and secreted protein core to which several highly modified heparan sulfate (HS) polysaccharide chains are attached [2, 3, 4]. Syndecans and glypicans are the two main cell surface HSPGs, whereas agrin and perlecan are found in the extracellular matrix (Figure 1). Here, we will focus mainly on the role of syndecans and glypicans in nervous system development.

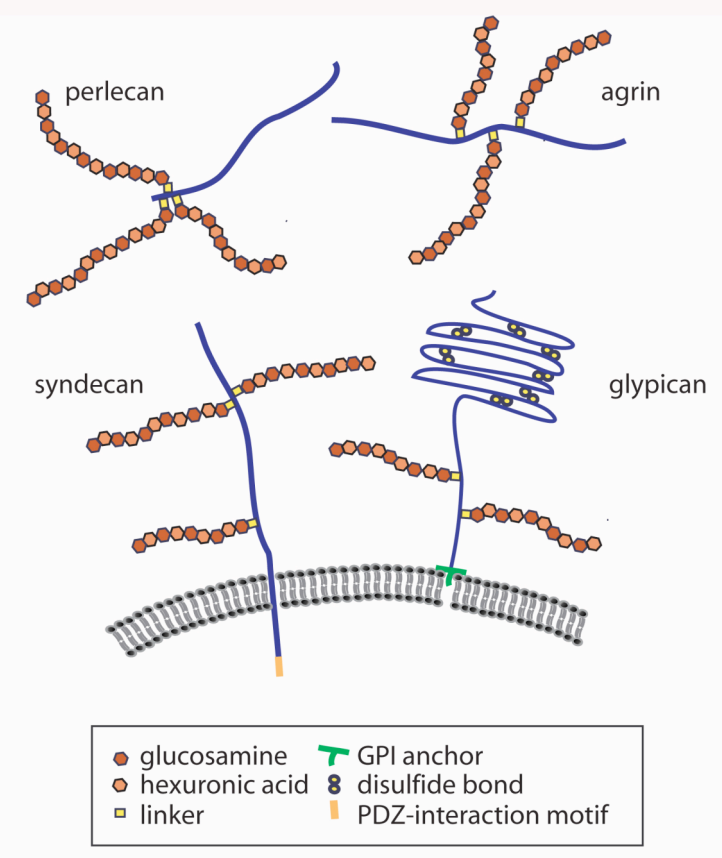

Figure 1: Cell surface and extracellular HSPGs Syndecans and glypicans are integral membrane proteins. Syndecan is a single-pass transmembrane protein with a short conserved cytoplasmic domain containing a C-terminal PDZ-interacting motif. HS side chains are attached to the extracellular domain of the core protein at conserved Serine residues. Yellow boxes represents a typical tetrasaccharide linker region, which connects the HS chain to the serine. The glypican core protein forms a globular domain, which is stabilized by conserved disulfide bonds and linked to the cell surface via a GPI-anchor. In contrast to syndecan, the major HS attachment sites in glypican are located proximal to the membrane. Perlecan and agrin are large multidomain proteins that contain several HS attachment sites. They both exist as multiple isoforms that are generated by alternative splicing and are found in basement membranes of many tissues.

Signals from Outer Space: Extracellular binding partners of HSPGs

The highly modified HS chains of HSPGs are known to interact with an enormous range of extracellular ligands and therefore control multiple cellular responses in both developmental and pathological processes [5, 6]. Growth factors, morphogens, axon guidance cues, antithrombin and extracellular matrix components, all seem to end up in the tentacles of HS side chains.

Fibroblast growth factors (FGFs) are probably the best-studied molecules that directly bind to HS and where the specific HS sequence required for ligand binding is known [7]. Crystal structures have shown that HS, FGF and its receptor form a ternary complex on the cell surface [8, 9]. Since HSPGs are essential for efficient FGF signaling, as well as for other ligand-recptor interactions, they are thought to serve as co-receptors in several signaling pathways [2]. HSPGs are also known to interact with axon guidance cues. The presence of HS increases the affinity of Slit, a repellent secreted by midline cells, for its receptor roundabout (Robo), which is compatible with a co-receptor function of HSPGs. If cultured olfactory bulb axons are treated with heparinase to remove HS from the cell surface, they no longer respond to the repulsive effect of Slit [10]. Moreover, biochemical co-purification has revealed a direct binding of Slit to glypican-1 [11, 12] and of Slit and Robo to *Drosophila* syndecan (Sdc) [13]. The axon guidance cue semaphorin 5A was also found to physically interact with syndecan-3 in the rat brain [14] as well as anosmins, which are conserved secreted proteins that regulate cell migration and axon branching. A recent study could shown that the *C. elegans* anosmin-1 KAL-1 binds specifically to modified HS of syndecan and glypican [15].

Ephrins and Ephrin receptors represents yet another axon guidance system that seems to co-operate with HSPGs. EphB2 can tyrosine-phosphorylate the cytoplasmic domain of syndecan-2, a signaling event involved in the maturation of dendritic spines [16]. This study points to the role of certain HSPGs as possible independent signal transducers. On the other hand, syndecans on muscle cells are also thought to act in *trans* as ligands in the case of their interaction with the neuronal receptor protein tyrosine phosphatase (RPTP) LAR, which binds to the HS chains of *Drosophila* syndecan and glypican with nanomolar affinity [17].

Morphogens are secreted signaling molecules that differentially regulate cell fate in a concentration-dependent manner during development. HS chains help generating morphogen gradients and are required for proper signaling levels of the Wnt/Wingless (Wg), transforming

growth factor-β (TGF-β) and Hedgehog (Hh) pathways in the *Drosophila* wing [18, 19, 20]. For the morphogen decapentaplegic (Dpp), a TGF-β family member, it was shown that extracellular diffusion of Dpp relies on the presence of cell surface glypicans since Dpp failed to move across double mutant clones for both *Drosophila* glypicans, whereas Dpp signal transduction in a cell was dependent on dynamin-mediated endocytosis [21]. In this case, the HSPG glypican can be viewed as an active transporter that promotes Dpp movement along cell surfaces, thereby restricting its extracellular diffusion.

Besides morphogens, guidance cues and growth factors, the list of molecules that require HS for activity includes matrix proteins (e.g., laminin, collagens, tenascin), coagulation factors (antithrombin), lipolytic proteins (apolipoprotein E, low-density lipoprotein) and components of the inflammatory response (chemokines, selectins) [3]. These interactions have to be interpreted with caution, however, since many HS ligands were identified using heparin, an unusual HS produced by mast cells, which contains extended N-sulfation domains.

Transducing the right frequency: Synthesis of HS antennae

How can several developmental progammes rely on the same type of amplifying molecule without creating strong interferences? A closer look at how these molecular glyco-antennae are assembled provides some explanations for their versatile abilities to fine-tune numerous signaling pathways.

HS synthesis occurs in the Golgi, where HS polymerases generate a non-sulfated sugar backbone, which is attached to the HS core protein (Figure 2). HS chains begin with a characteristic tetrasaccharide linker (-Xyl-Gal-Gal-GlcA-) that is first attached to Serines within conserved Ser-Gly sequences on the protein core [3]. The linker tetrasaccharide serves as a primer for HS polymerases that add alternating residues of glucuronic acid (GlcA) and N-acetyl glucosamine (GlcNAc), the sugar building blocks of HS chains. The different sugar residues are all transferred from sugar nucleotides by individual Golgi enzymes [3]. (Figure 2). These early steps of HS assembly, such as the generation of sugar nucleotides or the synthesis of the tetrasaccharide linker are common to the synthesis of other glycosaminoglycans like chondroitin sulfate (CS) and dermatan sulfate (DS). As a result, genetic removal of the enzymes involved in these early synthetic steps causes a broad range of defects. In *C. elegans*, mutations in such “early” enzymes cause maternal-effect lethality due to defects in embryonic development and aberrant vulva formation, which has led to their classification as *squashed vulva* (*sqv*) genes (Figure 2) [22].

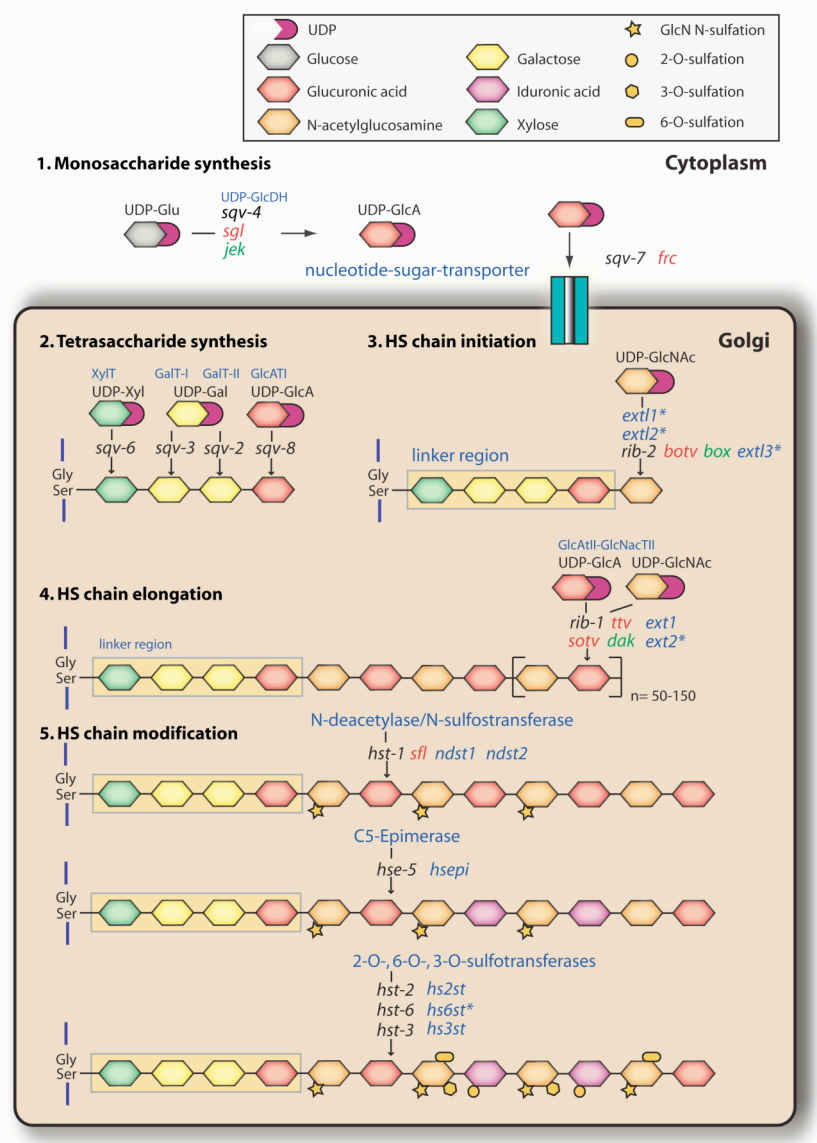

Figure 2. Heparan Sulfate Synthesis and Modification
HS synthesis starts in the cytoplasm with the synthesis of monosaccharides, which are subsequently transported into the Golgi where they are incorporated into a conserved tetrassaccharide linker. HS polymerases catalyze the addition of glucuronic acid and N-acetyl glucosamine to the linker to form the HS sugar backbone. This backbone is later modified by a C5-epimerase and various sulfotransferases giving rise to complex modification patterns. Mutants for enzymes involved in HS synthesis and modification are shown in black (*C. elegans*), red (*Drosophila*), green (zebrafish) and blue (mouse). Enzymes are abbreviated as follows: GalTI, galactosyltransferase I; GalTII, galactosyltransferase II; GlcATI, glucuronyltransferase I, GlcATII; glucuronyltransferase II; GlcNACTI, N-acetylglucosamine transferase I; GlcNAcTII, N-acetylglucosamine transferase II; NDST, N-deacetylase/N-sulfotransferase; UDP-GlcDH, UDP-glucose dehydrogenase; XylT, xylosyltransferase. *botv*, *brother of tout velu*; *box*, *boxer*; *dak*, *dackel*; *ext, exostosin; extl, exostosin-like; frc*, *fringe connection*; *jek*, *jekyll*; *sfl*, *sulfateless*; *sgl*, *sugarless*; *sotv*, *sister of tout velu*; *sqv*, *squashed vulva*; *ttv*, *tout velu*. * No mouse knock-out available yet.

Likewise, the genetic removal of HS polymerases causes a complete lack of HS, which interferes with multiple signaling pathways leading to severe patterning defects and lethality [18, 23, 24, 25]. Mammals have five genes encoding for HS polymerases (Ext1, Ext2, Extl1,

Extl2, Extl3) [26], whereas flies have three (*tout-velu* (*ttv*), *brother of ttv*, *sister of ttv*) [18, 19, 20] and worms two (*rib-1*, *rib-2*) [24, 27]. Mice lacking exostosin 1 (Ext1) function exclusively in neurons die perinatally with severe brain patterning defects, including absence of olfactory bulbs, cerebellum and corpus callosum [23]. Non-conditional Ext-1 knock-out mice already die during gastrulation [28]. In Zebrafish, the Ext family members Ext2 (dackel; dac) and Extl3 (boxer; box) play a role in the sorting of retinal axons in the optic tract and in fin and branchial arch development. Maternal contribution of Ext2 and Extl3 are thought to prevent early developmental defects in these mutants [29]. In general, these results clearly underscore the importance of HS for early development. But to gain insight into the meaning of the many possible HS modifications and how their combination and arrangement might lead to the vast density of information possibly specified by these sugar hieroglyphs, more selective ablations need to be analyzed.

Deciphering the HS code: Analysis of HS modifications

Once theHS precursor chains are assembled, the sugars are modified by several waves of HS-modifying enzymes. After deacetylation and N-sulfation of extensive regions by N-deacetylases/N-sulfotransferases (NDSTs), selected glucuronic acid units of the HS backbone are converted to iduronic acid by a glucuronyl C5-epimerase. Finally, several highly selective sulfotransferases (HS 2O-, 6O- and 3O-sulfotransferases) introduce different O-sulfation motifs along the extending HS side chains [3] (Figure 2). The HS modifications are not distributed uniformly; rather, microdomains of extensively modified sugars are surrounded by unmodified stretches. The result is an enormous diversity in HS chain sequences [4]. Not only can an almost endless combination of motifs be created this way, but also the length of the individual sugar chains is variable (from 50 to 150 disaccharides). By analyzing mutants that lack specific HS-modifications, it has been possible to decipher the role played by many of these modified HS sequences.

N-sulfation is unique to HS and does not occur in related CS, DS or keratan sulfate. Four mammalian NDSTs have been identified, which are likely to have different substrate-binding preferences, but only one isoform is present in *Drosophila* (*sulfateless*) and *C. elegans* (*hst-1*). *Ndst1* knock-out mice die at birth due to lung failure or partly in utero with skull and forebrain malformations [30, 31]. A detailed analysis of *Ndst1*$^{-/-}$ brains revealed lack of the hippocampal and anterior commissure reminescent to loss of EXT1 function in the central

nervous system [32]. *Sulfateless* flies are defective in morphogen (wg, hh, dpp) and growth factor signaling and show segment polarity defects [21, 33, 34]. The drastic effects of loss of NDST function, comparable to complete lack of HS, indicate that the replacement of N-acetyl by N-sulfate groups in the HS sugar backbone is probably required for multiple signaling pathways in early development. It is conceivable that N-sulfations do not confer selective binding properties for certain ligands, but rather serve as a structural hallmark required more generally for HS-ligand interactions. It is well documented that loss of NDST1 in mice does not only affect N-sulfation levels, but also strongly reduces the content of 2-O sulfated HS [35]. Therefore, the observed phenotype is not only caused by decreased N-sulfation, but results from a more broad alteration in the HS modification pattern.

Specific roles of HS-motifs have emerged when research focused on enzymes involved in later events in HS modification. Biochemical analysis showed that different mammalian tissues indeed do have distinct HS fingerprints [35], but deciphering this potential "HS-code" represents a major challenge. Lack of 2-O sulfation motifs in the mouse, for example, abolishes kidney formation, but also affects the development of the eyes and the skeleton [36]. RNAi of the 6-O sulfotransferase in flies interferes with tracheal development causing embryonic lethality [37]. In Zebrafish, knock-down of HS6ST-2, but not HS6ST-1, impairs vascular branching [38]. Interestingly, vascular development and axon guidance are partially regulated by the same factors. 6-O sulfations could therefore be utilized by either system to control the formation of complex branching patterns.

In all organisms analyzed so far, there is only one gene encoding for the C5-epimerase. HS epimerase knock-out mice lack kidneys and show defects in lung and skeletal development leading to their death after birth [39]. In contrast, epimerase mutants in *C. elegans* are viable and fertile, but show specific axon guidance defects of midline interneurons and commissural motoneurons [40]. Axon guidance defects can also be observed in worms lacking 6-O and 2-O sulfotransferase activity [40, 41]. A careful analysis of the various neural phenotypes revealed that the individual HS-modifying enzymes are required for distinct but partially overlapping axon guidance and cell migration events [40]. These findings did not only provide the first evidence for a role of HS-modifying enzymes in nervous system development, but also implied that each modification is indeed required to convey specific information to developing neurons. This prompted Hobert and collegues to postulate the existence of a "sugar code" specified by individual motifs present in a given HS, which could

be regulated in a tissue-specific manner depending on the expression profile of HS-modifying enzymes and distinct HS core proteins. That glycosylation motifs can contain information was nicely demonstrated previously in the elucidation of the "glycan code" of the endoplasmatic reticulum [42]. There, Asn-linked glycans serve as maturation and quality control tags for proteins in the early secretory pathway and the carbohydrate composition encodes crucial indications about structure, localization and age of synthesized glycoproteins.

The understanding of sugar biology has been lagging for many years because of major technical challenges. The good news is that many of these have been overcome in the last years. Certainly, the analysis of sugar function (glycomics) promises to shed light on numerous molecular mechanisms relying on glycosylated molecules. Nevertheless, in the case of HSPGs, there is accumulating evidence that their function depends not only on the HS sugar chains, but also on features of the corresponding core protein.

HS core proteins: Syndecan tunes cell migration signaling

Syndecans are transmembrane proteins, whereas glypicans are attached to the cell surface via a GPI-anchor. The cytoplasmic domain of syndecan is highly conserved and contains a PDZ-interaction motif at its C-terminus (Figure 1). By contrast, the extracellular domain of syndecan shows only little sequence conservation. Mammalian syndecans can be cleaved off the cell surface by metalloproteinases, at least in cell culture experiments [2]. A physiological role for shed syndecan was demonstrated in mice, where soluble syndecan-1 regulates the chemotactic response of neutrophils in the inflammatory response [43]. Mammals have four syndecan and six glypican genes. In mice, the inactivation of a single syndecan gene does not result in obvious phenotypes. This is probably due to redundancy between the different family members, which can compensate partly for each other's function [2, 44]**.** In contrast, the *C. elegans* and *Drosophila* genomes encode a single syndecan and contain only one (*C. elegans*) or two (*Drosophila*) glypican genes. Their simplicity has been exploited in the last two years to study the function of different HS core proteins in neural development [13, 45, 46, 47, 48]. The analysis of a *C. elegans* syndecan *sdn-1* null mutant revealed a role for this HSPG in neuronal migration [47]. In the worm, SDN-1 is highly expressed in neurons during early development and is also detected at lower levels in the nervous system of adult animals [47, 49]. In the absence of SDN-1, several groups of neurons fail to migrate or stop prematurely on their migration route. Interestingly, similar neuronal migration defects are found in *sdn-1*

mutants that express a truncated syndecan lacking the two major HS attachment sites [47, 49]. In these mutants, SDN-1 is not detectable anymore by an anti-HS antibody, but staining with an antibody directed against a conserved phosphorylation site in the SDN-1 intracellular domain shows that the expression pattern of at least the phosphorylated form is not affected by the truncation [49]. These findings strongly suggest that it is the lack of HS, rather than loss of the syndecan core protein, that is responsible for the observed migration defects of neurons. Expression of a *sdn-1* cDNA under the control of a pan-neuronal promoter is sufficient to restore correct migration in *sdn-1* mutants, suggesting a cell-autonomous function of SDN-1 in neuronal migration [47].

Several groups revealed that neuronal migration requires specific modifications of the HS chains. For example, lack of 2-O sulfation motifs on HS significantly impair neuronal migration in *C. elegans* [40, 41, 47]. Since *C. elegans* offers the possibility to build double or triple mutants of HS core proteins and different HS modifying enzymes, it is possible to address more challenging questions such as which combination of modifications are needed on a given HSPG member (and at what time) to regulate a specific guidance choice of a neuron in vivo. First studies of this type indicated that at least one additional HS core protein, which carries 2-O sulfated and epimerized HS, teams up with syndecan to ensure the correct migration of neurons [47]. The identity of this additional HSPG remains to be determined.
Remarkably, syndecans might also be involved in the invasive behavior of transformed cells since these proteoglycans are often deregulated in tumors [50, 51]. Indeed changes in syndecan levels influence the adhesion between cells in culture [52, 53]. The genetically amenable model organisms will hopefully permit a more detailed analysis of the biological underpinnings of HS-dependent cell migration.

Cell surface HSPGs function in axon guidance and synapse morphogenesis

A role for HSPGs in nervous system development was first reported in 1992, when Wang and Denburg showed that adding heparinase, an enzyme that degrades HS, to the culture medium of developing cockroach embryos caused guidance errors of several pioneer axons. They obtained the same effect when adding exogenous HS chains as competing molecules for putative HS ligands, whereas addition of other GAGs did not disturb axonal pathfinding [54]. Similarly, optic nerve fibers in *Xenopus* failed to reach their target area in the optic tectum

when exposed to HS showing a high affinity for FGF-2, whereas HS with a high affinity for FGF-1 had no effect [55].

More recent efforts have concentrated on determining which family of HSPGs are implicated in axon guidance and responsible for the observed effects. From these studies, the HS core protein syndecan clearly emerged as a key player in nervous system development [13, 17, 45, 46, 47, 48]. Syndecan null mutants of *Drosophila* and *C. elegans* both show midline axon guidance defects [13, 45, 47]. In addition, loss of syndecan affects embryonic development of motoneurons in worms as well as in flies [17, 47] and axon guidance in the fly visual system [46]. Similar to the findings on neuronal migration, syndecan was found to act cell-autonomously in neurons to mediate axon guidance at the *Drosophila* midline [13, 45], but showed a cell-nonautonomous way of interaction with LAR to control the patterning of *Drosophila* embryonic motoneurons [17]. Genetic removal of glypican in flies and worms does not cause the characteristic midline guidance phenotypes seen in syndecan mutants [45, Rhiner C. and Hengartner M., unpublished results], but the *Drosophila* glypican gene *dally-like* (*dlp*) is required for axon guidance in the fly visual system [46].

What about extracellular HSPGs in axon guidance? There is some evidence that agrin might also participate in axonal pathfinding: an agrin gradient can provoke repulsive growth cone turning of cultured *Xenopus* spinal neurons [56]. Although agrin-deficient mice show defects in terminal arborization of nerves [57], there is no direct evidence for a function of agrin during axon guidance in vivo. Finally, examined perlecan mutants in flies and worms do not display midline guidance errors [45, Rhiner C. and Hengartner M., unpublished results]. This observations have to be taken with caution, however. To evaluate the effect of loss of perlecan UNC-52 function in *C. elegans*, only *unc-52* RNAi and mutations that affect a subset of the alternatively spliced perlecan/UNC-52 forms could be analyzed since strong *unc-52* alleles cause early embryonic lethality. In summary, cell surface bound HSPGs, especially syndecan, contribute critically to correct axon guidance in genetic model organisms. It will be interesting to see whether syndecans and glypicans also regulate axon guidance in higher vertebrates.

Recent findings in the fly have revealed a novel role of syndecan and Dlp for different aspects of synapse organization [48]. Both cell surface HSPGs colocalize at *Drosophila* neuromuscular junctions (NMJs) and appear to control distinct synaptic processes: syndecan promotes the growth of presynaptic terminals, whereas Dlp is implicated in active zone

formation required for normal electrophysiologic responses. Because the RPTP LAR regulates NMJ growth and active zone structure in *Drosophila* [58] and was shown to directly bind to syndecan and glypican [17, 48], double mutant analysis were performed to elucidate the underlying signaling pathway. Epistasis experiments, combined with assaying LAR signaling output by phosphorylation of Enabled suggested a model in which syndecan and Dlp compete for LAR binding to promote or inhibit its activity, respectively [48]. These findings represent the first evidence that distinct HSPGs might function as competitive ligands to modulate signaling in the synapse. It was already known for a long time that the HSPG agrin is crucial to induce the postsynaptic clustering of acetylcholine receptors in synaptogenesis [57], but it seems now that also cell surface HSPGs play an important part in synapse formation.

Regulation of Slit/Robo signaling by syndecans

How does syndecan contribute to axon guidance? Genetic interaction analyses in *Drosophila* and *C. elegans* have suggested that syndecan acts in the Slit-Robo signaling pathway. Consistent with this hypothesis, Slit can bind to HS in vitro [11, 12, 13]. In *Drosophila*, the introduction of one copy of a mutant allele for a robo receptor (robo or robo2) or slit into a syndecan loss-of-function background causes defects similar to those observed in the homozygous robo mutants [13, 45]. Moreover, complete loss of Slit function in syndecan null worms does not further increase midline-crossing errors compared to either single null mutant, suggesting that syndecan and Slit act in the same signaling pathway [47].

Slits are conserved repellent guidance cues, secreted by cells at the midline to prevent axons expressing the Slit-receptor Robo from crossing the midline. But what is the role of syndecan in this signaling event? Based on the above findings, HS on syndecan has been proposed to act as molecular antennae on neurons, helping to modulate the reception of the Slit signal that is broadcasted by the midline cells. The HS sugar antennae could for example influence the efficacy of the signaling event (quantitative modulation) by binding to and locally increasing the concentration of the diffusing Slit signal. Syndecan mutant flies indeed show a different extracellular distribution of extracellular Slit compared to the wild type, which could be the cause of impaired signal transduction by Robo receptors and consequent midline guidance errors [13]. On the other hand, overexpression of *Drosophila* syndecan in neurons or in midline cells does not disturb Slit signaling [45]. This observation suggests that HS chains

must do more than just serve as ligand gatherers for a limiting guidance cue. Another possibility is that HS is required to modulate the specificity of the Slit/Robo interaction (qualitative modulation). Indeed, certain HS modifications are crucial for some guidance choices but not for others [40, 47]. It is therefore possible that a ligand needs to be presented to the receptor in the context of a specific HS motif to achieve maximal signaling impact. It is tempting to speculate that a neuron could fine-tune its response to a general signal by subtly changing the large number of distinct modification patterns that can be put onto HS. The "sugar code hypothesis" goes even further and suggests that specific HS modifications could provide instructional cues to "recruit" ligands and mediate their binding to the cognate receptor. Such a model predicts that the ectopic introduction of specific HS modifications in a given cell could lead to activation of a signaling pathway that is usually inactive in this cell.

To think that the function of HSPGs is solely mediated by the HS chains seems too simplistic however. Several studies provide evidence for core protein-specific functions. Although pan-neuronal overexpression of *Drosophila* glypican Dlp can compensate for loss of syndecan in certain axon guidance events [13, 46], it increases defects in the context of synaptic development [48]. On the other hand, syndecan overexpression never seems to improve neural defects of *dlp* mutants [46]. It is therefore likely that many signaling events also depend on the nature of the HS core protein. In order to solve this question, future experiments will require comprehensive structure/function analysis of the various HSPGs to determine the regions that are crucial for regulation of guidance signaling.
Syndecans are extremely versatile HSPGs since their cytoplasmic domains also allow interaction with intracellular binding partners. Several PDZ-domain proteins such as syntenin, CASK/LIN-2, synbindin and synectin [59, 60, 61, 62, 63] have been shown to bind to the C-terminus of syndecans, although the in vivo relevance of these interactions still needs to be further characterized. Phosphorylation of the syndecan cytoplasmic domain was found to be essential for inside-out signaling that specifies the left-right looping of the heart and gut in *Xenopus* [64]. Although a phosphorylated form of syndecan SDN-1 has been found to be prominently expressed at the nerve ring of *C. elegans* [49], direct evidence for syndecan-dependent inside-out signaling in nervous system development is still lacking.

Neurons seem to require syndecan to modulate their response to guidance cues present in the extracellular matrix. This regulation needs to be dynamic and is most likely achieved through a combinatorial control of HS-modifying enzyme expression, syndecan cell surface exposure

and shedding by metalloproteinases. Different syndecan family members as well as the HS-modifying enzymes indeed show tightly regulated spatio-temporal expression patterns [65, 66] underscoring their suitability as dynamic regulators of axon guidance signaling.

Despite the emerging evidence that differentially modified HS could endow individual neurons with unique HS fingerprints to regulate their sensitivity to ligands, they are not the only molecules capable of generating a vast number of structurally different forms. Neurexins, cadherins and cadherin-related neuronal receptors also show a high degree of molecular diversity, generated via extensive alternative splicing [67, 68, 69]. An even more striking example is the *Drosophila* gene Dscam, which can potentially generate 38'016 mRNA forms through alternative splicing [70]. This large diversity of isoforms is required for the correct wiring of neurons in the somatosensory system of the fly [71]. According to the chemo-affinity hypothesis, proposed by Roger Sperry in 1963, the high degree of specificity by which neurons connect to each other must either derive from a enormous number of different affinity-labels or from a small set of signals that provide positional information by forming overlapping concentration gradients [72]. The discovery of HSPGs as regulators of axon guidance signaling indicates that reality might lie somewhere between these two extremes, and that specificity can be achieved by combining gradients of relatively few guidance cues with highly variable "co-receptors" that fine-tune the responses of cells to these gradients.

Concluding remarks

Dedicated biochemical and genetic efforts have greatly enhanced our knowledge about the complex structure of HS and its diverse roles in many developmental processes including neuronal migration, axon guidance and synapse formation. Nevertheless, there is still much that we do not know. For example, distinct molecular mechanism have been proposed for the role of HSPGs in different neuronal contexts including functions as receptors, co-receptors, (competitive) ligands and as molecules that function to transport or enrich ligands on the cell surface or that target receptors to specific cell membrane domains such as lipid rafts [73]. What determines which mechanism a given HSPG will utilize? What are the specific motifs present in the molecular glyco-antennae of HSPGs? The ligand binding sequence on HS is only known for very few factors. More sophisticated analysis of HS composition and ligand-binding sites will be a key to understand the regulatory role of HSPGs such as syndecan and

set the basis for the design of inhibitors. What are the functions mediated by the core proteins? Who do they talk to? Elaborate genetic screens will certainly allow to isolate further components of HSPG-dependent signaling. Finally, from an evolutionary and medical point of view, it will be interesting to learn whether these versatile glycoproteins also contribute to nervous system development and function in higher vertebrates. Much exciting research remains to be done.

Acknowledgements
This work was funded by the Swiss National Science Foundation (MOH), the Ernst Hadorn Foundation (MOH) and the Forschungskredit of the University of Zurich (CR).

References

1. Marin O, Rubenstein JL (2001). A long, remarkable journey: tangential migration in the telencephalon. Nat Rev Neurosci. 2: 780-790.

2. Bernfield M, Gotte M, Park PW, Reizes O, Fitzgerald ML, Lincecum J, Zako M (1999). Functions of cell surface heparan sulfate proteoglycans. Annu Rev Biochem. 68: 729-777.

3. Esko JD, Selleck SB (2002). Order out of chaos: assembly of ligand binding sites in heparan sulfate. Annu Rev Biochem. 71: 435-471.

4. Lindahl U, Kusche-Gullberg M, Kjellen L (1998). Regulated diversity of heparan sulfate. J Biol Chem. 273: 24979-24982.

5. Sasisekharan R, Shriver Z, Venkataraman G, Narayanasami U (2002). Roles of heparan-sulphate glycosaminoglycans in cancer. Nat Rev Cancer. 2: 521-528.

6. Topczewski J, Sepich DS, Myers DC, Walker C, Amores A, Lele Z, Hammerschmidt M, Postlethwait J, Solnica-Krezel L (2001). The zebrafish glypican knypek controls cell polarity during gastrulation movements of convergent extension. Dev Cell. 1: 251-264.

7. Nakato H, Kimata K (2002). Heparan sulfate fine structure and specificity of proteoglycan functions. Biochim Biophys Acta. 1573: 312-318.

8. Ornitz DM (2000). FGFs, heparan sulfate and FGFRs: complex interactions essential for development. Bioessays. 22: 108-112.

9. Pellegrini L, Burke DF, von Delft F, Mulloy B, Blundell TL (2000). Crystal structure of fibroblast growth factor receptor ectodomain bound to ligand and heparin. Nature. 407: 1029-1034.

10. Hu H (2001). Cell-surface heparan sulfate is involved in the repulsive guidance activities of Slit2 protein. Nat Neurosci. 4: 695-701.

11. Liang Y, Annan RS, Carr SA, Popp S, Mevissen M, Margolis RK, Margolis RU (1999). Mammalian homologues of the Drosophila slit protein are ligands of the heparan sulfate proteoglycan glypican-1 in brain. J Biol Chem. 274: 17885-17892.

12. Ronca F, Andersen JS, Paech V, Margolis RU (2001). Characterization of Slit protein interactions with glypican-1. J Biol Chem. 276: 29141-29147.

13. Johnson KG, Ghose A, Epstein E, Lincecum J, O'Connor MB, Van Vactor D (2004). Axonal heparan sulfate proteoglycans regulate the distribution and efficiency of the repellent slit during midline axon guidance. Curr Biol. 14: 499-504.

14. Kantor DB, Chivatakarn O, Peer KL, Oster SF, Inatani M, Hansen MJ, Flanagan JG, Yamaguchi Y, Sretavan DW, Giger RJ, Kolodkin AL (2004). Semaphorin 5A is a bifunctional axon guidance cue regulated by heparan and chondroitin sulfate proteoglycans. Neuron. 44: 961-975.

15. Hudson ML, Kinnunen T, Cinar HN, Chisholm AD (2006). C. elegans Kallmann syndrome protein KAL-1 interacts with syndecan and glypican to regulate neuronal cell migrations. Dev Biol. 294: 352-365.

16. Ethell IM, Irie F, Kalo MS, Couchman JR, Pasquale EB, Yamaguchi Y (2001). EphB/syndecan-2 signaling in dendritic spine morphogenesis. Neuron. 31: 1001-1013.

17. Fox AN, Zinn K (2005). The heparan sulfate proteoglycan syndecan is an in vivo ligand for the Drosophila LAR receptor tyrosine phosphatase. Curr Biol. 15: 1701-1711.

18. Bornemann DJ, Duncan JE, Staatz W, Selleck S, Warrior R (2004). Abrogation of heparan sulfate synthesis in Drosophila disrupts the Wingless, Hedgehog and Decapentaplegic signaling pathways. Development. 131:1927-1938.

19. Han C, Belenkaya TY, Khodoun M, Tauchi M, Lin X, Lin X (2004). Distinct and collaborative roles of Drosophila EXT family proteins in morphogen signalling and gradient formation. Development. 131: 1563-1575.

20. Takei Y, Ozawa Y, Sato M, Watanabe A, Tabata T (2004). Three Drosophila EXT genes shape morphogen gradients through synthesis of heparan sulfate proteoglycans. Development. 131: 73-82.

21. Belenkaya TY, Han C, Yan D, Opoka RJ, Khodoun M, Liu H, Lin X (2004). Drosophila Dpp morphogen movement is independent of dynamin-mediated endocytosis but regulated by the glypican members of heparan sulfate proteoglycans. Cell. 119: 231-244.

22. Herman T, Hartwieg E, Horvitz HR (1999). sqv mutants of Caenorhabditis elegans are defective in vulval epithelial invagination. Proc Natl Acad Sci U S A. 96: 968-973.

23. Inatani M, Irie F, Plump AS, Tessier-Lavigne M, Yamaguchi Y (2003). Mammalian brain morphogenesis and midline axon guidance require heparan sulfate. Science. 302: 1044-1046.

24. Morio H, Honda Y, Toyoda H, Nakajima M, Kurosawa H, Shirasawa T (2003). EXT gene family member rib-2 is essential for embryonic development and heparan sulfate biosynthesis in Caenorhabditis elegans. Biochem Biophys Res Commun. 301:317-323.

25. Perrimon N, Bernfield M. Specificities of heparan sulphate proteoglycans in developmental processes (2000). Nature. 404: 725-728.

26. Zak BM, Crawford BE, Esko JD (2002). Hereditary multiple exostoses and heparan sulfate polymerization. Biochim Biophys Acta. 1573: 346-355.

27. Kitagawa H, Egusa N, Tamura JI, Kusche-Gullberg M, Lindahl U, Sugahara K (2001). rib-2, a Caenorhabditis elegans homolog of the human tumor suppressor EXT genes encodes a novel alpha1,4-

N-acetylglucosaminyltransferase involved in the biosynthetic initiation and elongation of heparan sulfate. J Biol Chem. 276: 4834-4838.

28. Lin X, Wei G, Shi Z, Dryer L, Esko JD, Wells DE, Matzuk MM (2000). Disruption of gastrulation and heparan sulfate biosynthesis in EXT1-deficient mice. Dev Biol. 224: 299-311.

29. Lee JS, von der Hardt S, Rusch MA, Stringer SE, Stickney HL, Talbot WS, Geisler R, Nusslein-Volhard C, Selleck SB, Chien CB, Roehl H (2004). Axon sorting in the optic tract requires HSPG synthesis by ext2 (dackel) and extl3 (boxer). Neuron. 44: 947-960.

30. Fan G, Xiao L, Cheng L, Wang X, Sun B, Hu G (2000). Targeted disruption of NDST-1 gene leads to pulmonary hypoplasia and neonatal respiratory distress in mice. FEBS Lett. 467: 7-11.

31. Ringvall M, Ledin J, Holmborn K, van Kuppevelt T, Ellin F, Eriksson I, Olofsson AM, Kjellen L, Forsberg E (2000). Defective heparan sulfate biosynthesis and neonatal lethality in mice lacking N-deacetylase/N-sulfotransferase-1. J Biol Chem. 275: 25926-25930.

32. Grobe K, Inatani M, Pallerla SR, Castagnola J, Yamaguchi Y, Esko JD (2005). Cerebral hypoplasia and craniofacial defects in mice lacking heparan sulfate Ndst1 gene function. Development. 132: 3777-3786.

33. Lin X, Perrimon N (1999). Dally cooperates with Drosophila Frizzled 2 to transduce Wingless signalling. Nature. 400: 281-284.

34. Lin X, Buff EM, Perrimon N, Michelson AM (1999). Heparan sulfate proteoglycans are essential for FGF receptor signaling during Drosophila embryonic development. Development. 126: 3715-3723.

35. Ledin J, Staatz W, Li JP, Gotte M, Selleck S, Kjellen L, Spillmann D (2004). Heparan sulfate structure in mice with genetically modified heparan sulfate production. J Biol Chem. 279: 42732-42741.

36. Bullock SL, Fletcher JM, Beddington RS, Wilson VA (1998). Renal agenesis in mice homozygous for a gene trap mutation in the gene encoding heparan sulfate 2-sulfotransferase. Genes Dev. 12:1894-1906.

37. Kamimura K, Fujise M, Villa F, Izumi S, Habuchi H, Kimata K, Nakato H (2001). Drosophila heparan sulfate 6-O-sulfotransferase (dHS6ST) gene. Structure, expression, and function in the formation of the tracheal system. J Biol Chem. 276: 17014-17021.

38. Chen E, Stringer SE, Rusch MA, Selleck SB, Ekker SC (2005). A unique role for 6-O sulfation modification in zebrafish vascular development. Dev Biol. 284: 364-376.

39. Li JP, Gong F, Hagner-McWhirter A, Forsberg E, Abrink M, Kisilevsky R, Zhang X, Lindahl U (2003). Targeted disruption of a murine glucuronyl C5-epimerase gene results in heparan sulfate lacking L-iduronic acid and in neonatal lethality. J Biol Chem. 278: 28363-28366.

40. Bulow HE, Hobert O (2004). Differential sulfations and epimerization define heparan sulfate specificity in nervous system development. Neuron. 41: 723-736.

41. Kinnunen T, Huang Z, Townsend J, Gatdula MM, Brown JR, Esko JD, Turnbull JE (2005). Heparan 2-O-sulfotransferase, hst-2, is essential for normal cell migration in Caenorhabditis elegans. Proc Natl Acad Sci U S A. 102: 1507-1512.

42. Hebert DN, Garman SC, Molinari M (2005). The glycan code of the endoplasmic reticulum: asparagine-linked carbohydrates as protein maturation and quality-control tags. Trends Cell Biol. 15: 364-370.

43. Li Q, Park PW, Wilson CL, Parks WC (2002). Matrilysin shedding of syndecan-1 regulates chemokine mobilization and transepithelial efflux of neutrophils in acute lung injury. Cell. 111: 635-646.

44. Hartmann U, Maurer P (2001). Proteoglycans in the nervous system--the quest for functional roles in vivo. Matrix Biol. 20: 23-35.

45. Steigemann P, Molitor A, Fellert S, Jackle H, Vorbruggen G (2004). Heparan sulfate proteoglycan syndecan promotes axonal and myotube guidance by slit/robo signaling. Curr Biol. 14: 225-230.

46. Rawson JM, Dimitroff B, Johnson KG, Rawson JM, Ge X, Van Vactor D, Selleck SB (2005). The heparan sulfate proteoglycans Dally-like and Syndecan have distinct functions in axon guidance and visual-system assembly in Drosophila. Curr Biol. 15: 833-838.

47. Rhiner C, Gysi S, Frohli E, Hengartner MO, Hajnal A (2005). Syndecan regulates cell migration and axon guidance in C. elegans. Development. 132: 4621-4633.

48. Johnson KG, Tenney AP, Ghose A, Duckworth AM, Higashi ME, Parfitt K, Marcu O, Heslip TR, Marsh JL, Schwarz TL, Flanagan JG, Van Vactor D (2006). The HSPGs Syndecan and Dallylike bind the receptor phosphatase LAR and exert distinct effects on synaptic development. Neuron. 49: 517-531.

49. Minniti AN, Labarca M, Hurtado C, Brandan E (2004). Caenorhabditis elegans syndecan (SDN-1) is required for normal egg laying and associates with the nervous system and the vulva. J Cell Sci. 117: 5179-5190.

50. Bernfield M, Kokenyesi R, Kato M, Hinkes MT, Spring J, Gallo RL, Lose EJ (1992). Biology of the syndecans: a family of transmembrane heparan sulfate proteoglycans. Annu Rev Cell Biol. 8:365-393.

51. Inki P, Jalkanen M (1996). The role of syndecan-1 in malignancies. Ann Med. 28:63-67.

52. Rapraeger AC. Molecular interactions of syndecans during development (2001).
Semin Cell Dev Biol. 12: 107-116.

53. Dobra K, Andang M, Syrokou A, Karamanos NK, Hjerpe A (2000). Differentiation of mesothelioma cells is influenced by the expression of proteoglycans. Exp Cell Res. 258:12-22.

54. Wang L, Denburg JL (1992). A role for proteoglycans in the guidance of a subset of pioneer axons in cultured embryos of the cockroach. Neuron. 8:701-714.

55. Walz A, McFarlane S, Brickman YG, Nurcombe V, Bartlett PF, Holt CE (1997). Essential role of heparan sulfates in axon navigation and targeting in the developing visual system.
Development. 124: 2421-2430.

56. Xu X, Fu AK, Ip FC, Wu CP, Duan S, Poo MM, Yuan XB, Ip NY (2005). Agrin regulates growth cone turning of Xenopus spinal motoneurons. Development. 132: 4309-4316.

57. Gautam M, Noakes PG, Moscoso L, Rupp F, Scheller RH, Merlie JP, Sanes JR (1996). Defective neuromuscular synaptogenesis in agrin-deficient mutant mice. Cell. 85: 525-535.

58. Kaufmann N, DeProto J, Ranjan R, Wan H, Van Vactor D (2002). Drosophila liprin-alpha and the receptor phosphatase Dlar control synapse morphogenesis. Neuron. 34: 27-38.

59. Grootjans JJ, Zimmermann P, Reekmans G, Smets A, Degeest G, Durr J, David G (1997). Syntenin, a PDZ protein that binds syndecan cytoplasmic domains. Proc Natl Acad Sci U S A. 94: 13683-1368.

60. Cohen AR, Woods DF, Marfatia SM, Walther Z, Chishti AH, Anderson JM (1998). Human CASK/LIN-2 binds syndecan-2 and protein 4.1 and localizes to the basolateral membrane of epithelial cells. J Cell Biol. 142: 129-138.

61. Hsueh YP, Yang FC, Kharazia V, Naisbitt S, Cohen AR, Weinberg RJ, Sheng M (1998).
Direct interaction of CASK/LIN-2 and syndecan heparan sulfate proteoglycan and their overlapping distribution in neuronal synapses. J Cell Biol. 142: 139-151.

62. Ethell IM, Hagihara K, Miura Y, Irie F, Yamaguchi Y (2000). Synbindin, A novel syndecan-2-binding protein in neuronal dendritic spines. J Cell Biol. 151: 53-68.

63. Gao Y, Li M, Chen W, Simons M (2000). Synectin, syndecan-4 cytoplasmic domain binding PDZ protein, inhibits cell migration. J Cell Physiol. 184: 373-379.

64. Kramer KL, Barnette JE, Yost HJ (2002). PKCgamma regulates syndecan-2 inside-out signaling during xenopus left-right development. Cell. 111: 981-990.

65. Ford-Perriss M, Turner K, Guimond S, Apedaile A, Haubeck HD, Turnbull J, Murphy M (2003). Localisation of specific heparan sulfate proteoglycans during the proliferative phase of brain development. Dev Dyn. 227: 170-84.

66. Sedita J, Izvolsky K, Cardoso WV (2004). Differential expression of heparan sulfate 6-O-sulfotransferase isoforms in the mouse embryo suggests distinctive roles during organogenesis. Dev Dyn. 231: 782-794.

67. Missler M, Fernandez-Chacon R, Sudhof TC (1998). The making of neurexins.
J Neurochem. 71: 1339-1347.

68. Takeichi M, Matsunami H, Inoue T, Kimura Y, Suzuki S, Tanaka T (1997). Roles of cadherins in patterning of the developing brain. Dev Neurosci. 19: 86-87.

69. Wu Q, Maniatis T (1999). A striking organization of a large family of human neural cadherin-like cell adhesion genes. Cell. 97:779-790.

70. Schmucker D, Clemens JC, Shu H, Worby CA, Xiao J, Muda M, Dixon JE, Zipursky SL (2000). Drosophila Dscam is an axon guidance receptor exhibiting extraordinary molecular diversity. Cell. 101: 671-684.

71. Chen BE, Kondo M, Garnier A, Watson FL, Puettmann-Holgado R, Lamar DR, Schmucker D (2006). The molecular diversity of Dscam is functionally required for neuronal wiring specificity in Drosophila. Cell. 125: 607-620.

72. Sperry RW (1963). Chemoaffinity in the orderly growth of nerve fiber patterns and connections. Proc Natl Acad Sci U S A. 50: 703-710.

73. Lee JS, Chien CB (2004). When sugars guide axons: insights from heparan sulphate proteoglycan mutants. Nat. Rev. Genet. 5: 923-935.

CHAPTER 2

Syndecan Regulates Cell Migration and
Axon Guidance in *C. elegans*

PREFACE

In this article, we report our findings on the function of *C. elegans* syndecan in nervous system development. The syndecan null mutant was initially isolated by Prof. Alex Hajnal and Erika Fröhli. Erika Fröhli backcrossed the mutant and performed the northern blot experiment. I conducted all the double mutant analysis and characterized the neural phenotypes of *sdn-1* mutants as well as other phenotypes. I also cloned most of the constructs and generated the integrated *sdn-1::gfp* lines to study the expression pattern of syndecan. Stephan Gysi did most of the microinjections for the rescue experiments and helped me with the quantification of several rescue lines. I composed the figures and wrote the manuscript, which was then edited by Prof. Alex Hajnal and Prof. Michael Hengartner.

Syndecan regulates cell migration and axon guidance in *C. elegans*

Christa Rhiner[1,2], Stephan Gysi[1], Erika Fröhli[3], Michael O. Hengartner[1,2,*] and Alex Hajnal[3]

[1]Institute of Molecular Biology, University of Zurich, 8057, Switzerland
[2]Neuroscience Center, 8057, Zurich, Switzerland
[3]Institute of Zoology, University of Zurich, 8057, Switzerland
*Author for correspondence (e-mail: michael.hengartner@molbio.unizh.ch)

Accepted 17 August 2005

Development 132, 4621-4633
Published by The Company of Biologists 2005
doi:10.1242/dev.02042

Summary

During nervous system development, axons that grow out simultaneously in the same extracellular environment are often sorted to different target destinations. As there is only a restricted set of guidance cues known, regulatory mechanisms are likely to play a crucial role in controlling cell migration and axonal pathfinding. Heparan sulfate proteoglycans (HSPGs) carry long chains of differentially modified sugar residues that have been proposed to encode specific information for nervous system development. Here, we show that the cell surface proteoglycan syndecan SDN-1 functions autonomously in neurons to control the neural migration and guidance choices of outgrowing axons. Epistasis analysis suggests that heparan sulfate (HS) attached to SDN-1 can regulate guidance signaling by the Slit/Robo pathway. Furthermore, SDN-1 acts in parallel with other HSPG core proteins whose HS side chains are modified by the C5-epimerase HSE-5, and/or the 2*O*-sulfotransferase HST-2, depending on the cellular context. Taken together, our experiments show that distinct HS modification patterns on SDN-1 are involved in regulating axon guidance and cell migration in *C. elegans*.

Key words: Axon guidance, *C. elegans*, Cell migration, Heparan sulfate proteoglycan, Syndecan

Introduction

During nervous system development, migrating cells and axonal growth cones are guided by extracellular stimuli to their final position in the body. Although several major families of attractive and repulsive guidance cues have been characterized, it is not clear how the presence of multiple directional cues are integrated by a single outgrowing axon while leaving other neurons unaffected. Recent findings indicate that heparan sulfate proteoglycans (HSPGs) act as crucial modulators of axon guidance choices (Lee and Chien, 2004). HSPGs are present both on the cell surface and in the extracellular matrix, where they modulate cellular responses to extracellular signals in various developmental and pathological processes (Sasisekharan et al., 2002; Topczewski et al., 2001). Their function in nervous system development has long been presumed, but only recent genetic studies have provided in vivo evidence for their role in axon pathfinding (Bülow and Hobert, 2004; Inatani et al., 2003; Johnson et al., 2004; Lee et al., 2004; Steigemann et al., 2004).

HSPGs consist of a secreted or membrane-anchored protein core to which several heparan sulfate (HS) polysaccharide chains are attached (Bernfield et al., 1999; Esko and Selleck, 2002; Lindahl et al., 1998). Once the HS chain is synthesized, specific enzymes – including sulfotransferases and an epimerase – modify the individual sugar moieties, resulting in complex modification patterns (Lindahl et al., 1998). A complete lack of HS abrogates multiple signaling pathways essential for early development, resulting in severe patterning defects and lethality (Inatani et al., 2003; Bornemann et al., 2004; Herman et al., 1999; Morio et al., 2003; Perrimon and Bernfield, 2000). Together with the biochemical studies, these observations led to the hypothesis that HSPGs act as co-receptors that bind and sequester extracellular signals in the extracellular matrix (Bernfield et al., 1999; Perrimon and Bernfield, 2000).

By contrast, genetic removal of enzymes that secondarily modify HS, including sulfotransferases and an epimerase, demonstrated that specific modifications are needed for distinct axon guidance choices (Bülow and Hobert, 2004). Hence, it has been proposed that individual HS modifications in a given area or on specific neurons give rise to a 'sugar code' that regulates axon guidance by modulating specific receptor-ligand interactions. So far it is not known, however, which core proteins are crucial in this process and how they function to modulate axon guidance signaling. Syndecans and glypicans are the two major families of cell surface-bound HSPGs (Fig. 1A). In mice, the inactivation of a single syndecan gene does not result in any obvious phenotype, probably due to redundancy between the family members (Hartmann and Maurer, 2001; Bernfield et al., 1999).

Syndecan mutant flies display a Robo-like midline phenotype, which can be rescued by overexpression of either syndecan or the two *Drosophila* glypican genes *dally* and *dally-like* (Johnson et al., 2004; Steigemann et al., 2004). Furthermore, it was found that lack of syndecan affects the distribution of the midline repellent Slit, which provides the first indication of how HSPGs might function (Johnson et al., 2004).

Unlike mammals, which have four syndecan family members, the *Caenorhabditis elegans* genome contains one

single syndecan (*sdn-1*) gene. We show here that *C. elegans* syndecan SDN-1 functions autonomously in neurons to ensure correct cell migration and axon guidance. Epistasis analysis indicates that *sdn-1* participates in the Slit/Robo signaling pathway, which acts in parallel with a second, currently unknown, guidance system that relies on a different combination of sugar modifications on a distinct HSPG core protein. We therefore propose that at least two distinct HSPG members bearing cell-specific HS modification patterns are involved in regulating axon pathfinding and cell migration.

Materials and methods

C. elegans genetics

Standard methods were used for maintaining and manipulating *Caenorhabditis elegans* (Brenner, 1974). The *C. elegans Bristol* strain N2 was used as wild-type reference in all experiments. Animals were raised at 20°C unless indicated otherwise. The following mutations were used: LG III: *hse-5(tm472)* (Bülow and Hobert, 2004); LGX: *sdn-1(zh20)* (this study), *sdn-1(ok449)* (Minniti et al., 2004), *hst-6(ok273)* and *hst-2(ok595)* (Bülow and Hobert, 2004), *sax-3(ky123)* (Zallen et al., 1998), *slt-1(eh15)* (Hao et al., 2001). All transgenes used to score neuroanatomy were described previously (Bülow and Hobert, 2004; Bülow et al., 2002).

Constructs

The $P_{sdn\text{-}1}$*::sdn-1::gfp* translational fusion construct pAH40 was generated by ligating a 5.7 kb *Bam*HI-*Sph*I fragment covering 2.8 kb of 5′ regulatory sequences and the entire coding region into the pPD95.75 vector (gift of A. Fire, Stanford University), such that the full-length *sdn-1* open reading frame was fused in frame to *gfp*. pAH40 and the *lin-15* rescuing plasmid pL15EK (gift of R. Horvitz) were co-injected (100 ng/μl of each) into *lin-15(n765ts)* animals to obtain transgenic lines. Two independent lines (*opIs170*, *opIs171*) showed similar expression patterns.

$P_{sdn\text{-}1}$*::sdn-1* (pAH46) was made by cloning a 6.9 kb genomic PCR product containing 2.8 kb of 5′ sequences, the entire *sdn-1* coding region and the predicted 3′UTR into the pGEM-T vector. The $P_{dpy\text{-}7}$*::sdn-1*(cDNA) construct was generated by fusion PCR (Hobert, 2002): the hypodermal promoter of *dpy-7* (216 bp) (Gilleard et al., 1997) was fused to the ATG start codon of the *sdn-1* cDNA. The $P_{sra\text{-}6}$*::sdn-1* plasmid (pCR1) and the $P_{unc\text{-}119}$*::sdn-1* plasmid (pCR2) were made by subcloning the *sra-6* promoter (3747 bp) or the *unc-119* promoter (2189 bp) sequence into pPD95.86 (gift of A. Fire, Stanford University), in front of the ATG start codon of the *sdn-1* cDNA. For rescue, worms were injected with 20 ng/μl of pAH46, pCR1 or pCR2, or with 2.5 ng/μl of the fusion construct $P_{dpy\text{-}7}$*::sdn-1*. Constructs were injected together with pTJ1157 (*lin-48::gfp*) and pBluescript SK at 50 ng/μl each, or, for the rescue of HSN migration, with pPD118.33 (*myo-2::gfp*) at 2.5 ng/μl.

Isolation of the *sdn-1* deletion allele

The *sdn-1(zh20)* deletion mutant was isolated from an EMS-mutagenized library consisting of approximately 10^6 haploid genomes, as previously described (Jansen et al., 1997; Berset et al., 2001). DNA pools were screened by nested PCR with the outer primers OAH40 (5′-TGGGTTCATCCAATGCGTATGACC-3′) and OAH49 (5′-CCCTATTCTGTCATTGTACCAC-3′), and the nested primers OAH41 (5′-TTGCCGTACACCGCCATTTCCTC-3′) and OAH48 (5′-AGAATGGCTGTAATCACCGCAACG-3′). The *zh20* deletion removes 1260 bp within the coding region (Fig. 1B). The sequence of the break point is as follows: TTTGCTTCACAC//zh20//GTCGACAGGCAG. The mutant strain was backcrossed six times to N2 before analysis.

Phenotypic analysis

All mutant alleles were backcrossed at least four times before phenotypic analysis. Axon guidance defects were scored in staged young adults or L1 larvae using a Leica DMR microscope. Migration of HSN, ALM and CAN neurons and coelomocytes were scored in adult stages (HSN, ALM, CAN) and L3-L4 stages (coelomocytes).

Statistical analysis

All phenotypes, except defects in guidance and left/right choices of D-type motoneurons (Fig. 6A), were scored as the percentage of animals that were defective, and are shown with error bars denoting the standard error of proportion. Statistical significance was calculated using the z-test. For the defects in D-type motoneurons, error bars give the standard error of the mean and statistical significance was calculated by using Student's *t*-test. If multiple comparisons were made, Bonferroni's correction was applied.

Results

Isolation of a *sdn-1* null allele

The *C. elegans* genome is predicted to code for only two cell surface-bound HSPGs genes, syndecan SDN-1 and glypican GPN-1 (Fig. 1A), and three extracellular HSPGs, agrin (F41G3.8) (Hutter et al., 2000), perlecan UNC-52 (Rogalski et al., 1993) and CLE-1, a homolog of collagen XVIII (Ackley et al., 2001; Halfter et al., 1998).

To study the role of SDN-1 in nervous system development, we first isolated a null allele of *sdn-1*. The deletion allele *sdn-1(zh20)* removes most of the *sdn-1* open reading frame (Fig. 1B). Furthermore, no *sdn-1* transcripts were detected on northern blots of RNA isolated from *zh20* animals (Fig. 1C). Thus, the *sdn-1(zh20)* allele most likely causes a complete loss of SDN-1 function. Homozygous *sdn-1(zh20)* animals are viable, but they show defects in backward locomotion, are variably egg-laying defective and have a slightly reduced brood size (201±42, n=10) when compared with wild-type worms (280±10, n=10).

A recent study carried out with a hypomorphic allele of *sdn-1* reported a role of SDN-1 in vulva development, but did not analyze neuronal phenotypes (Minniti et al., 2004). This published allele, *sdn-1(ok449)*, results in an in-frame deletion and produces a truncated form of SDN-1 lacking the two major conserved HS attachment sites in the extracellular domain (Fig. 1B). The truncated SDN-1 core protein in *ok449* animals could still be detected on western blots by using an antibody directed against the cytosolic tail, but was no longer recognized by a monoclonal antibody specific for HS side chains, indicating that there is considerably less, if any, HS attached to SDN-1 in this mutant (Minniti et al., 2004). We examined the neural phenotypes of both *sdn-1* mutants, but focused our epistasis analysis on the null allele *sdn-1(zh20)*, because the *ok449* deletion may not completely eliminate *sdn-1* function (Table 1).

SDN-1 is necessary for the migration of different cell types

The formation of a functional nervous system starts with the migration of neural cell bodies to their genetically determined position. Thereafter, neurons extend axons that navigate to the target area to finally form synaptic contacts. The migrating neurons and axonal growth cones are guided by similar molecules. For example, UNC-6 Netrin controls both cell and

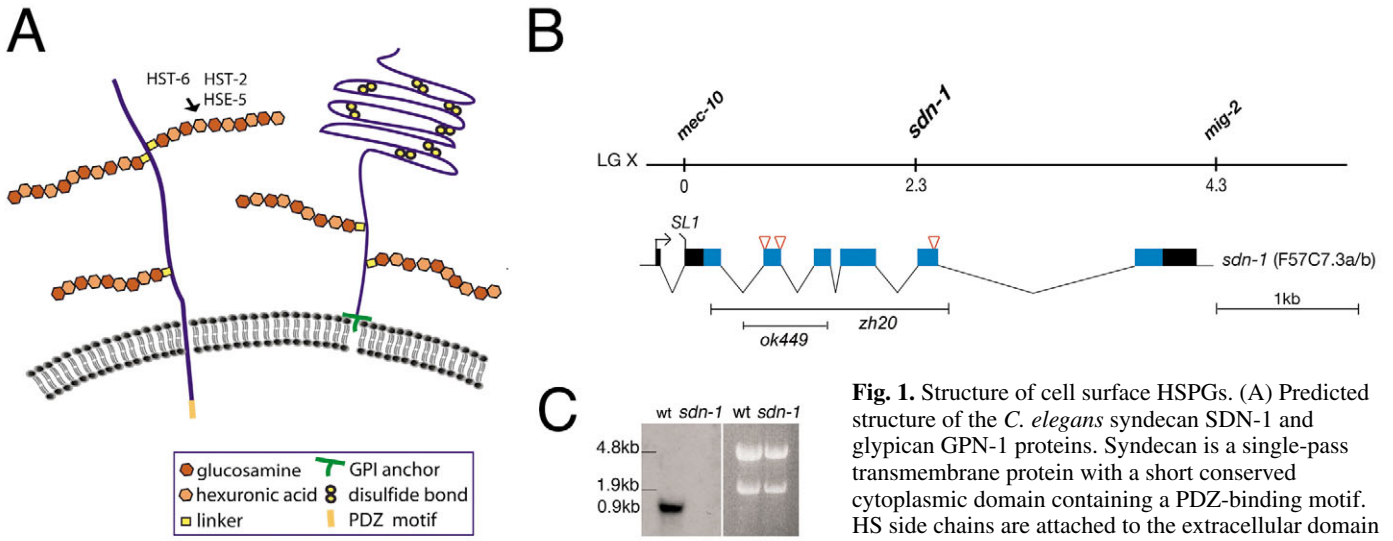

Fig. 1. Structure of cell surface HSPGs. (A) Predicted structure of the *C. elegans* syndecan SDN-1 and glypican GPN-1 proteins. Syndecan is a single-pass transmembrane protein with a short conserved cytoplasmic domain containing a PDZ-binding motif. HS side chains are attached to the extracellular domain of the core protein at conserved serine residues. The yellow box represents a typical tetrasaccharide linker region, which connects the HS chain to the serine. Glypican is attached to the cell surface by a GPI anchor. (B) Genomic structure of the *sdn-1* locus on chromosome X. Boxes represent exons (blue, coding; black, non-coding) and red triangles indicate putative HS attachment sites. Two isoforms of the *sdn-1* mRNA have been predicted to code for identical proteins. The null allele *sdn-1(zh20)* affects exons 1-5. The allele *ok449* was previously shown to produce a truncated syndecan form lacking the two major HS attachment sites (Minniti et al., 2004). (C) Northern blot analysis of *sdn-1*. A single message of approximately 0.9 kb is detected in wild-type worms, whereas no message can be found in *sdn-1(zh20)* mutants. 18S and 28S ribosomal RNAs, as loading controls, are shown to the right.

Table 1. Summary of phenotypes in *sdn-1* mutants

Neurons examined (marker used)	% Animals defective	
	sdn-1(zh20)	Wild type
A. Axon guidance		
Head neurons		
Sensory neurons		
AFD sensory neurons (*oyIs17*)	0	0
Amphid neurons (DiI)	0	0
Ventral cord neurons		
Sensory neurons		
AVM/PVM neurons (*zdIs5*)		
– ventral axon guidance	9±1	1±1
Interneurons		
PVT interneuron (*otIs39*)	0	0
AVK interneurons (*bwIs2*)	36±2	4±1
PVP interneurons (*hdIs26*)	32±3	5±1
PVQ interneurons (*oyIs14*)	49±2	8±1
Command interneurons (*rhIs4*)	0	0
Motoneurons		
HSN motoneurons (*mgIs71*) – axon guidance*	83±4*	9±3
D-type motoneurons (*oxIs12*)		
– fasciculation VNC	37±3	7±1
– midline L/R choice†	2.3†	0.3†
– circumferential growth	66±3	0
– fasciculation DNC	15±7	0
DA/DB motoneurons (*evIs82b*)		
– midline L/R choice†	1.1†	0†
Tail neurons		
Sensory neurons		
Phasmid neurons (DiI)	0	0
B. Cell migrations		
HSN motoneurons (*mgIs71*)	56±3	0
CAN neurons (*otIs33*)	39±2	6±2
ALM sensory neurons (*zdIs5*)	47±4	1±1
Anterior coelomocytes (*otIs121*)	69±2	3±1

*Part of the defects are caused by mispositioned HSN cell bodies.
†Number of commissures that exit the VNC on the inappropriate side/adult.

growth cone migrations along the dorsoventral axis (Chan et al., 1996; Hedgecock et al., 1987). To study the role of SDN-1 in different phases of nervous system development, we crossed *sdn-1* alleles into different reporter strains, in which specific types of neurons are labeled with *gfp* (Table 1). We observed no obvious changes in the overall organization of the nervous system in the major ganglia and nerve bundles in both *sdn-1* alleles when using a pan-neuronal *gfp* marker (data not shown).

When examining single neuron subtypes, however, we observed prominent migration defects of neural cell bodies. The HSN left (L)/right (R) motoneurons normally migrate during embryonic development from the posterior to the mid-body region (Fig. 2A). In both *sdn-1* alleles, the HSN neurons either failed to migrate at all or stopped prematurely before reaching their normal position near the vulva (Fig. 2C,D). A null mutation in the 2*O*-sulfotransferase *hst-2* gene causes similar HSN migration defects, although they are less severe than those observed in *sdn-1(zh20)* animals (Fig. 2E) (Bülow and Hobert, 2004; Kinnunen et al., 2005). By contrast, neither the 6*O*-sulfotransferase HST-6 nor the C5-epimerase HSE-5 is required for HSN migration (Bülow and Hobert, 2004), pointing to a crucial role of 2*O*-sulfated HS in this process. Double-null mutants of *sdn-1* and *hst-2* show significantly more HSN migration defects, indicating that 2*O*-sulfation, although possibly important for SDN-1 function, is also required for, at least, one additional HSPG (Fig. 2E). Loss of HSE-5 similarly enhances the HSN migration defects of *sdn-1* null mutants, whereas removal of HST-6 in a *sdn-1* background shows no increase of migration errors (Fig. 2E). Next, we tested posterior migration of the ALML/R sensory neurons. In the absence of SDN-1, ALML/R neurons stopped prematurely (Table 1). Migration defects of the ALML/R neurons have also been described in mutants for the *C. elegans*

Robo receptor SAX-3 (Zallen et al., 1999). We examined ALM migration errors of both *sdn-1(zh20)* and *sax-3(ky123)* mutants and found comparable defects [47% for *sdn-1(zh20)*, 45% for *sax-3(ky123)*]. In addition, loss of SDN-1 function impaired the posterior migration of the CANL/R neural cell bodies (Table 1).

Finally, we detected a cell migration defect of the macrophage-like coelomocytes, a non-neural cell-type. In wild-type hermaphrodites, four coelomocytes are born and migrate posteriorly during embryogenesis, whereas the two coelomocytes generated in the L1 stage do not migrate (Fig. 2F). In *sdn-1(zh20)* null mutants, the embryonic coelomocytes were often located too far anteriorly, just behind the pharynx (Fig. 2H). In all the cell migration events examined, SDN-1 always appeared to confer a pro-migratory property, irrespective of the direction of cell migration.

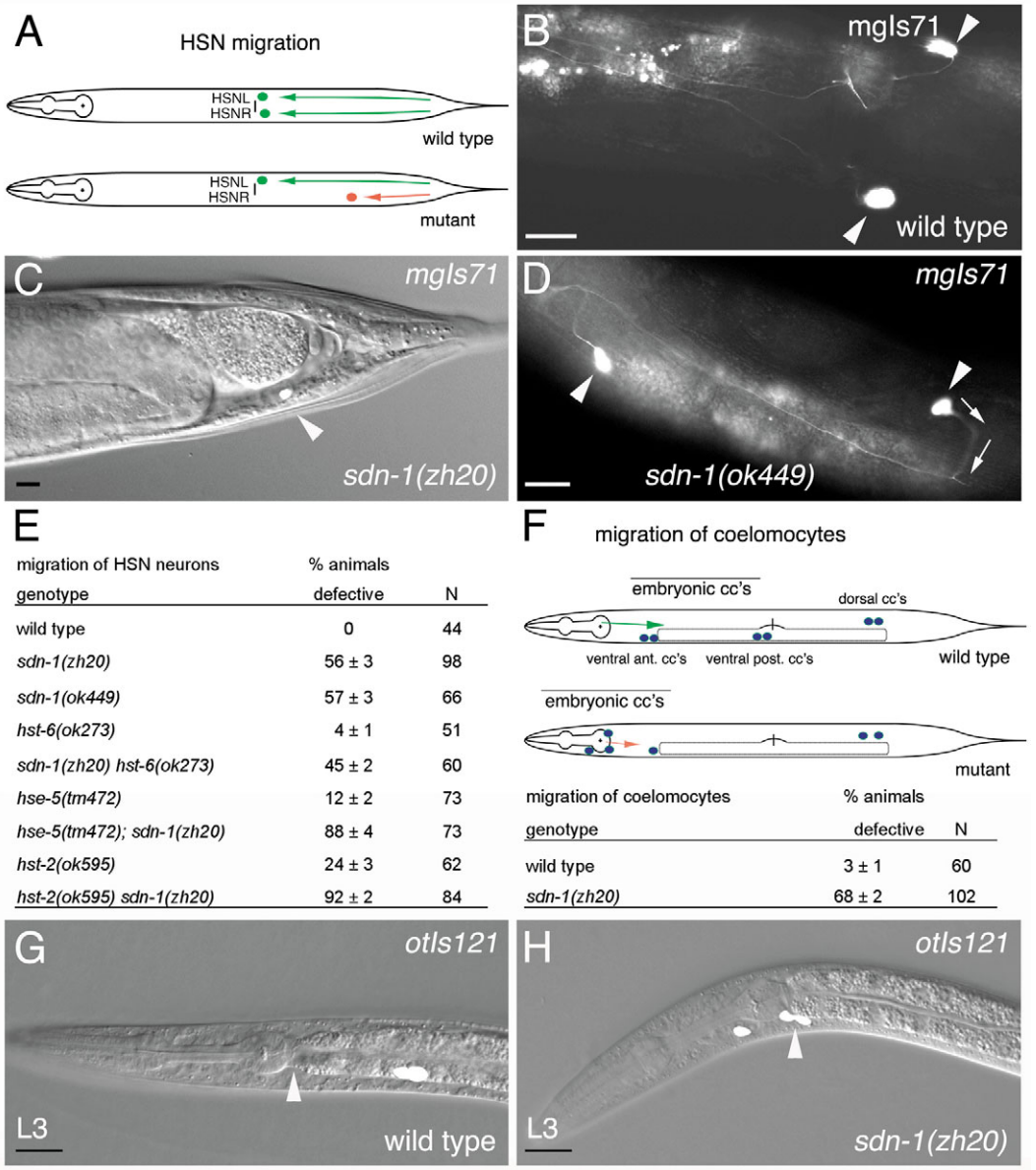

Fig. 2. SDN-1 is required for the migration of neurons and coelomocytes. (A) Schematic depicting the migration of HSN neurons during embryogenesis. (B) In wild-type animals both HSN cell bodies (arrowheads) locate close to the vulva. (C,D) In *sdn-1* mutants, HSN neurons fail to migrate to the vulva from their original position in the tail (C) or stall prematurely anterior to the vulva (D). Axons of mispositioned HSN bodies (arrowheads) that initially grow out incorrectly in a posterior direction eventually turn (arrows) and reach the nerve ring in the head. (E) HSN migration (adult stages) demonstrated by the genetic interaction of *sdn-1* nulls with HS-modifying enzyme mutants. '% animal defective' represents the fraction of animals with at least one defective HSN neuron. Numbers are shown with the standard error of proportion. (F) Schematic of the six coelomocytes in wild-type and *sdn-1(zh20)* hermaphrodites. (G) In the wild type, coelomocytes born in the head migrate caudally during embryonic development, past the intestinal valve that separates the pharynx from the intestine (arrowhead). (H) In *sdn-1* null mutants, coelomocytes are found in the head region, anterior and posterior of the intestinal valve (arrowhead). In order to define anatomical locations, some pictures were taken with DIC optics in the fluorescent channel (C,G,H). N, number of animals scored. Scale bars: 10 μm.

SDN-1 is required for correct axon guidance at the midline

Midline interneurons

Because mutants for the HS-modifying enzymes have previously been reported to display guidance defects of midline interneurons (Bülow and Hobert, 2004), we tested whether *sdn-1(zh20)* null mutants would show similar defects. The ventral nerve cord (VNC) runs along the left and right side of the ventral hypodermal ridge in two separate fascicles. We first examined the guidance of the PVQ interneurons, a pair of bilaterally symmetric neurons located in the tail (Fig. 3A). The PVQL and PVQR axons normally grow out to the head on the left and right side of the midline, respectively, without crossing to the contralateral side (Fig. 3A,B). In both *sdn-1* mutants, PVQ axons inappropriately crossed to the contralateral side or were entirely fused in a single track (Fig. 3C). Most crossover defects (75%) consisted of single or multiple midline crossings of PVQ axons along the entire length of PVQ extention, the remaining 25% showed entirely collapsed PVQ axons. The PVPL/R and AVK interneurons showed comparable crossover defects (Fig. 3F, Table 1).

HSN motoneurons

In contrast to most axons, which join the VNC in the head or the tail, the axons of the HSN neurons join the VNC midway near the vulva and grow anteriorly without crossing the midline (Fig. 3G,H). In *sdn-1(zh20)* animals, HSN axons frequently crossed the midline

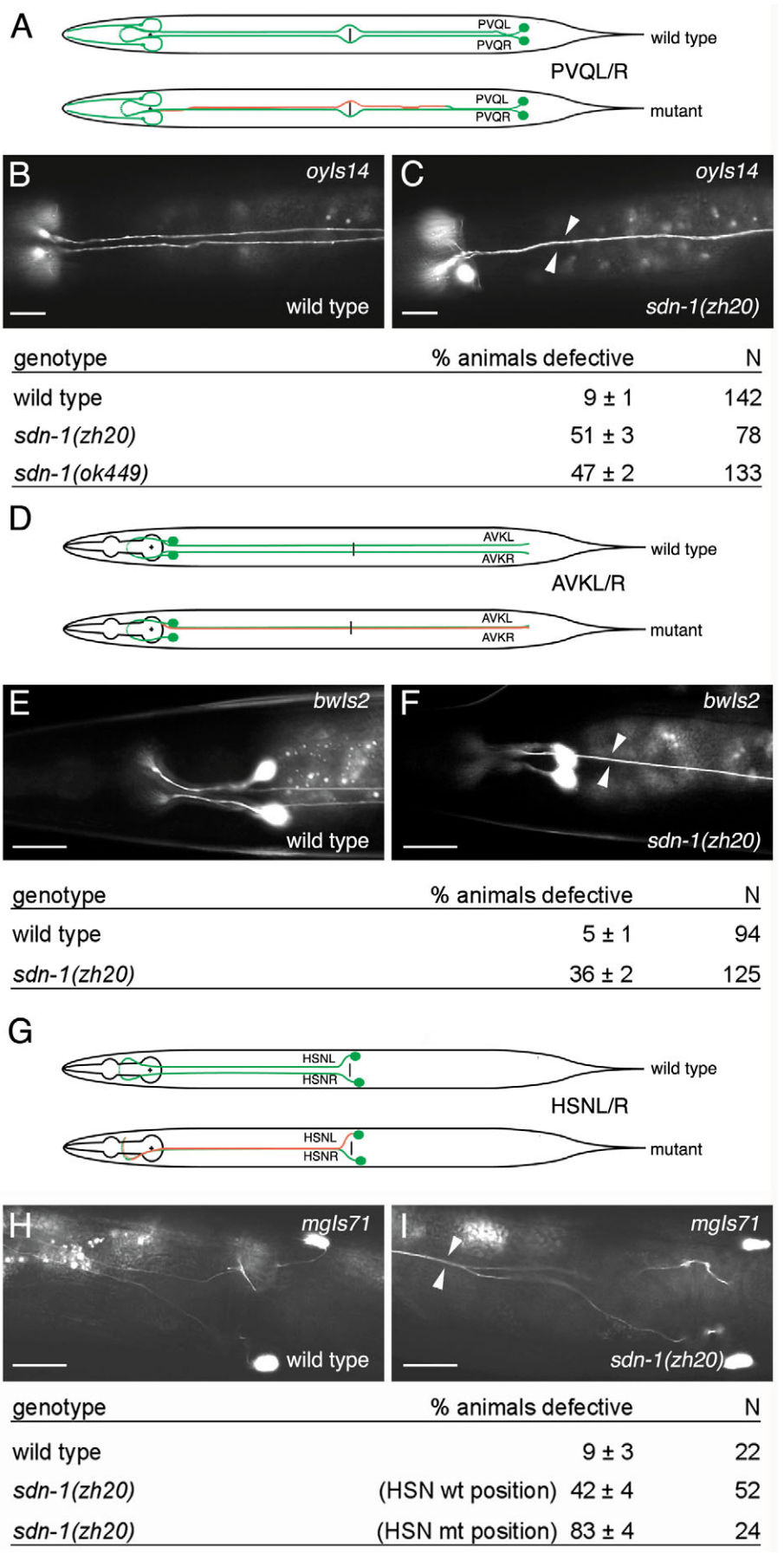

genotype	% animals defective	N
wild type	9 ± 1	142
sdn-1(zh20)	51 ± 3	78
sdn-1(ok449)	47 ± 2	133

genotype	% animals defective	N
wild type	5 ± 1	94
sdn-1(zh20)	36 ± 2	125

genotype	% animals defective	N
wild type	9 ± 3	22
sdn-1(zh20)	(HSN wt position) 42 ± 4	52
sdn-1(zh20)	(HSN mt position) 83 ± 4	24

Fig. 3. *sdn-1* mutants show midline crossover defects of VNC interneurons. (A) Schematic of PVQL/R interneurons. (B) PVQL/R interneurons run parallel to the head in the wild type. (C) PVQ axons inappropriately cross the midline in *sdn-1* mutants, leading to collapsed axon tracks (arrowheads). (D) Schematic of the AVKL/R interneurons. (E) Wild-type AVKL/R run next to each other, whereas midline crossing of AVKL/R axons can be observed in *sdn-1(zh20)* worms (arrowheads) (F). (G) Schematic of HSNL/R motoneurons. (H) HSNL/R stay ipsilateral in the wild type, whereas HSNL/R axons frequently cross to the contralateral side in *sdn-1(zh20)* null mutants (arrowheads) (I). All schematics and photos are ventral views, anterior is to the left. N, number of animals scored. Scale bars: 10 μm.

(Fig. 3I). As mentioned before, the HSN neurons frequently fail to migrate to their normal position in *sdn-1* mutants (Table 1). To determine whether the misplacement of the HSN cell bodies might contribute to the observed guidance defects, we scored HSN pathfinding in animals with wild-type and misplaced HSN neurons separately (Fig. 3I, Table 1). We found that crossover defects occurred in both cases, but were indeed more frequent in animals with mispositioned HSN cell bodies.

Commissures of ventral nerve cord motoneurons

Midline decisions are also made by different types of motoneurons in the VNC. In the case of D-type motoneurons (DD and VD subtypes), axons extend first in the right VNC and then circumferentially grow out on the right side of the animal (with the exception of the two anteriormost DD and VD neurons, which grow out on the left) to form the commissures that connect to the dorsal nerve cord (DNC; Fig. 4A). The axons of the six DD neurons grow out during embryonic development, whereas those of the 13 VD neurons grow out postembryonically. We analyzed *sdn-1(zh20)* and *sdn-1(ok449)* mutants for two major guidance defects: first, the circumferential guidance to the DNC; and, second, the left/right decision during the exit from the VNC (Fig. 4E). In wild-type worms, the commissural axons always reach the DNC where they bifurcate and connect to neighboring branches of the D-type motoneurons to form a continuous DNC fascicle (Fig. 4C,E). In both *sdn-1* mutants, the circumferential outgrowth of commissures was impaired,

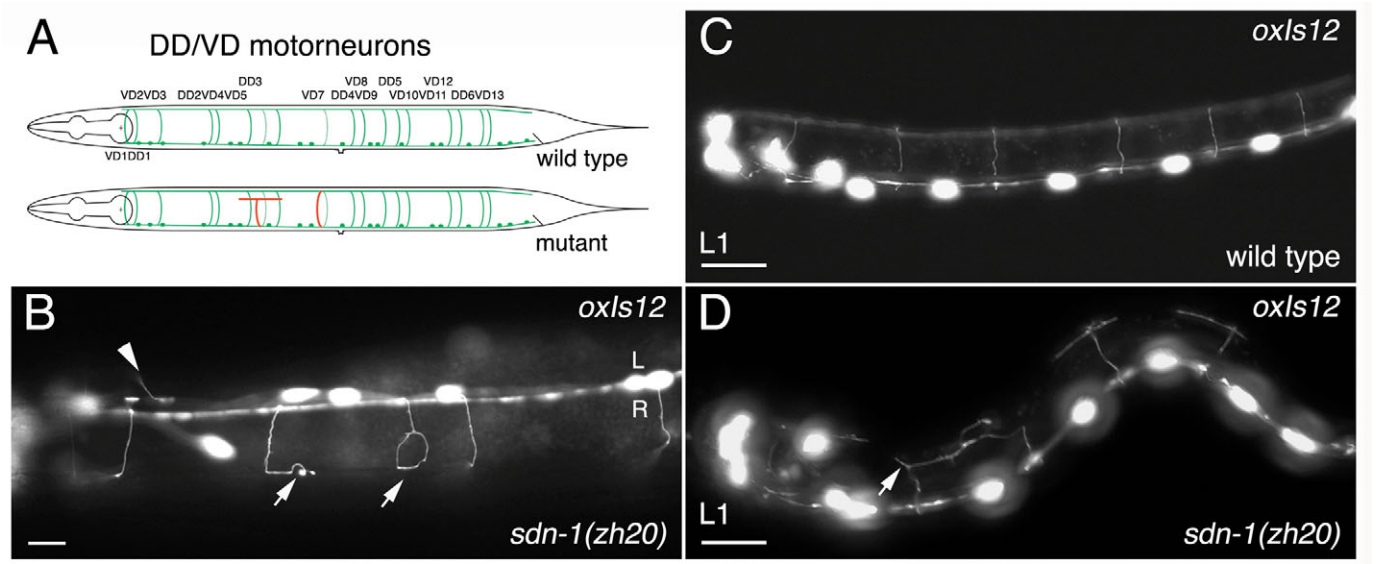

E

% commissural reach (circumf. elong) 1.

	left	N	right	N
wild type	100	23	100	460
sdn-1(zh20)	75	110	92	674
sdn-1(ok449)	84	110	97	698
hst-6(ok273)	91	32	99	278
sdn-1(zh20) hst-6(ok273)	40	161	75	633
hse-5(tm472)	30	223	78	507
hse-5(tm472); sdn-1(zh20)	14	217	20	417

% animals with n inappropriate commissures on the left L/R 2.

0	1	2	3	4	5	6	7	8	N
76	20	3	1	0	0	0	0	0	93
11	21	29	20	9	8	2	0	0	135
12	24	26	16	18	2	2	0	0	50
22	39	20	12	7	0	0	0	0	50
2	10	16	23	23	10	10	5	1	135
0	1	7	15	19	28	17	11	2	87
0	2	22	18	10	20	14	8	6	50

Fig. 4. Loss of SDN-1 affects the guidance and left/right choices of commissural motoneurons. (A) Schematic of DD and VD motoneurons. (B,E) DD/VD commissures in young adults and (C,D) embryonic DD commissures in the L1 larva. (B) Ventral nerve cord (VNC) view of an *sdn-1(zh20)* animal. D-type motoneurons inappropriately grow out on the left side of the animal (arrowhead) or stop prematurely before reaching the dorsal nerve cord (DNC) (arrows). L, left side; R, right side. (C) Six DD commissures form a continuous dorsal nerve cord in the wild-type L1 larva. (D) In *sdn-1* null mutants, DD commissures branch prematurely and fail to reach the DNC (arrow). (E) D-type motoneuron development analyzed for: (1) circumferential outgrowth of DD/VD commissures to the DNC; (2) left/right choice to exit the VNC. (1) N represents the total number of commissures scored. Right and left denote the percentage of commissures that reach the DNC when growing out on the correct (right side) and incorrect side (left side), respectively. Note that guidance is considerably more affected if axons grow out on the wrong side of the animal. (2) N represents the number of animals analyzed. Each column gives the percentage of animals that show the indicated amount (1-8) of commissures inappropriately exiting the VNC on the left side. Scale bars: 10 μm.

especially on the left side of the worm (Fig. 4B,D,E). Furthermore, *sdn-1* mutants showed partial VNC defasciculation and an increased number of commissures inappropriately leaving the VNC on the left side (Fig. 4E, Table 1). The outgrowth of other types of neurons, such as the sensory neurons in the head or the pioneering axons in the VNC, were not affected in *sdn-1(zh20)* null mutants (Table 1).

Taken together, our findings indicate that syndecan SDN-1 is required for several distinct axon guidance and cellular migration events. Interestingly, the *sdn-1(zh20)* axon guidance defects that we describe here are similar to those previously reported in mutants for the HS-modifying enzymes (Bülow and Hobert, 2004), suggesting that SDN-1 might be a major target of these enzymes in the developing nervous system. Moreover, animals expressing the truncated form of syndecan lacking the major HS attachment sites showed qualitatively and quantitatively similar defects to those observed in syndecan null mutants, pointing to a major role of the HS moiety of SDN-1 in regulating cell migration and axonal pathfinding.

SDN-1 is highly expressed in the nervous system

In order to examine the expression pattern of SDN-1, we generated transgenic animals expressing a full-length C-terminally tagged SDN-1::GFP fusion protein. In embryos and L1 larvae, SDN-1::GFP was expressed in many tissues, including neurons, pharynx and hypodermis (Fig. 5A′). In later larval stages and in adult worms, SDN-1::GFP was predominantly expressed in the nervous system, with strong expression in the nerve ring and the VNC motoneurons (Fig. 5B,C,E,F). Apart from the neuronal expression, SDN-1::GFP was also found at a lower level in the hypodermis (Fig. 5D) and the vulval cells (data not shown). Because antibodies directed against the conserved intracellular domain of mammalian syndecan 4 have been reported to specifically detect *C. elegans* SDN-1 in the nerve ring and the vulva (Minniti et al., 2004), the SDN-1::GFP reporter likely reflects the endogenous SDN-1 expression pattern.

SDN-1 functions in neurons to control cell migration and axon guidance

Based on the SDN-1::GFP expression pattern, it is conceivable that SDN-1 could affect neuronal differentiation in a cell non-autonomous manner. In particular, SDN-1 expressed in the hypodermis might regulate the diffusion and thus spatial distribution of secreted guidance cues. Alternatively, SDN-1 might function cell autonomously in the migrating neurons and navigating growth cones to modulate – possibly through its HS chains – the interaction of specific ligand/receptor pairs.

To distinguish between these two possibilities, we expressed a full-length *sdn-1* cDNA under the control of either the hypodermal *dpy-7* promoter ($P_{dpy\text{-}7}$*::sdn-1*) (Gilleard et al., 1997) or the pan-neuronal *unc-119* promoter (Maduro et al., 2000), and tested the rescuing activity of the different transgenes. Interestingly, neuron-specific expression of SDN-1, as well as expression of SDN-1 driven by the endogenous *sdn-1* promoter ($P_{sdn\text{-}1}$*::sdn-1*) rescued the HSN and ALM migration defects of *sdn-1* null mutants (Table 2). By contrast, hypodermal expression of SDN-1 under control of the *dpy-7* promoter had no significant effect on ALM migration, although it did weakly reduce the HSN migration defects (Table 2).

To determine whether cell type-specific expression of SDN-1 was sufficient to rescue the axon guidance defects of the corresponding neurons, we expressed SDN-1 under the PVQ-specific *sra-6* promoter ($P_{sra\text{-}6}$*::sdn-1*). PVQ-specific expression of SDN-1 significantly reduced the crossover defects of PVQ interneurons, with a similar efficiency as expression of SDN-1 under its endogenous promoter (Table 3). By contrast, expression of SDN-1 in hypodermal tissue ($P_{dpy\text{-}7}$*::sdn-1*) showed no rescuing activity. In summary, our data indicate that SDN-1 is likely to act cell autonomously in neurons to promote cell migration and axonal pathfinding.

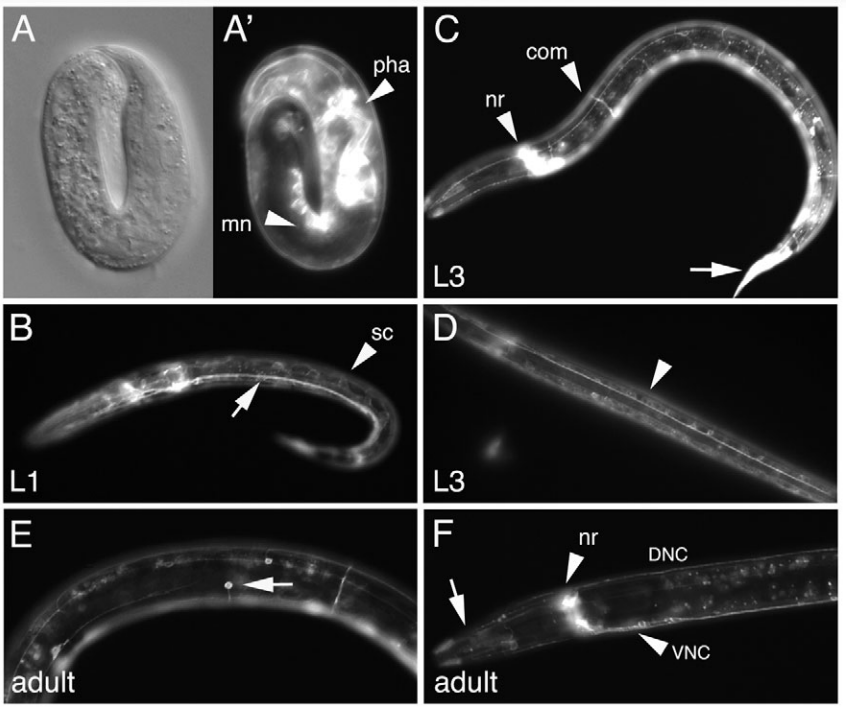

Fig. 5. SDN-1 expression in neural and hypodermal tissue. (A-F) Expression pattern of the translational $P_{sdn\text{-}1}$*::sdn-1::gfp* reporter. (A′) SDN-1::GFP is broadly expressed in the three-fold embryo, and is particularly strong in the pharynx (pha) and the motoneurons (mn) of the VNC. (B) In L1 larvae, expression is seen in the VNC (arrow) and around the seam cells (arrowhead). SDN-1::GFP expression is also visible in embryonic DD commissures (out of focal plane in B). (C) During later larval stages, SDN-1::GFP is predominantly found in the nervous system. The nerve ring (nr), and the VNC motoneurons and commissures (com) show the highest expression levels (arrowheads; B,F), but the reporter is also present in touch neurons (arrow; E) and other sensory neurons in the head (arrow; F). SDN-1::GFP can also be detected at a lower level in the body wall hypodermis (arrowhead; D); expression is stronger in hypodermal tissue in the tail (arrow; C).

Table 2. Rescue of cell migration defects

Genotype	Transgene expression	% Defective HSN	*n*
A. HSN migration			
Wild type	N/A	0	50
sdn-1(zh20)	N/A	55±3	52
sdn-1(zh20); opEx1216 [$P_{sdn\text{-}1}$*::sdn-1*]	Hypodermis, neurons	13±2	62
sdn-1(zh20); opEx1217 [$P_{sdn\text{-}1}$*::sdn-1*]	Hypodermis, neurons	13±3	46
sdn-1(zh20); opEx1218 [$P_{sdn\text{-}1}$*::sdn-1*]	Hypodermis, neurons	14±2	77
sdn-1(zh20); opEx1221 [$P_{unc\text{-}119}$*::sdn-1*]	Pan-neuronal	4±1	75
sdn-1(zh20); opEx1222 [$P_{unc\text{-}119}$*::sdn-1*]	Pan-neuronal	3±1	68
sdn-1(zh20); opEx1224 [$P_{unc\text{-}119}$*::sdn-1*]	Pan-neuronal	7±2	82
sdn-1(zh20); opEx1226 [$P_{dpy\text{-}7}$*::sdn-1*]	Hypodermis	40±3	78
sdn-1(zh20); opEx1227 [$P_{dpy\text{-}7}$*::sdn-1*]	Hypodermis	35±2	130
sdn-1(zh20); opEx1230 [$P_{dpy\text{-}7}$*::sdn-1*]	Hypodermis	31±3	64

Genotype	Transgene expression	% Defective ALM	*n*
B. ALM migration			
Wild type	N/A	0±1	100
sdn-1(zh20)	N/A	42±3	96
sdn-1(zh20); opEx1196 [$P_{sdn\text{-}1}$*::sdn-1*]	Hypodermis, neurons	19±2	68
sdn-1(zh20); opEx1198 [$P_{sdn\text{-}1}$*::sdn-1*]	Hypodermis, neurons	10±2	69
sdn-1(zh20); opEx1199 [$P_{sdn\text{-}1}$*::sdn-1*]	Hypodermis, neurons	13±2	85
sdn-1(zh20); opEx1206 [$P_{unc\text{-}119}$*::sdn-1*]	Pan-neuronal	5±1	82
sdn-1(zh20); opEx1207 [$P_{unc\text{-}119}$*::sdn-1*]	Pan-neuronal	9±2	80
sdn-1(zh20); opEx1208 [$P_{unc\text{-}119}$*::sdn-1*]	Pan-neuronal	6±1	82
sdn-1(zh20); opEx1202 [$P_{dpy\text{-}7}$*::sdn-1*]	Hypodermis	51±4	43
sdn-1(zh20); opEx1204 [$P_{dpy\text{-}7}$*::sdn-1*]	Hypodermis	51±3	63
sdn-1(zh20); opEx1205 [$P_{dpy\text{-}7}$*::sdn-1*]	Hypodermis	32±3	50

sdn-1 interacts genetically with genes encoding HS-modifying enzymes in a context-dependent manner

We next investigated whether we could identify specific modification patterns of HS chains carried by SDN-1 that could confer to the axons the ability to selectively respond to midline guidance cues. To address this issue, we examined double-null mutants between *sdn-1(zh20)* and mutants in the HS-modifying enzymes. As the C5-epimerase HSE-5 and the 2*O*-sulfotransferase HST-2 have previously been shown to act in the same pathway for midline guidance, we concentrated our analysis on HSE-5 and the 6*O*-sulfotransferase HST-6 (Bülow and Hobert, 2004).

For D-type motoneurons, we found that in animals lacking both HSE-5 and SDN-1 the outgrowth of commissures to the DNC was drastically reduced compared with that of either single mutant (Fig. 6A-D′). Moreover, *hse-5; sdn-1* double null mutant L1 larvae showed a highly defasciculated VNC (Fig. 6C′) and most of the embryonic DD commissures failed to reach the DNC (Fig. 6A,B′). We observed a similar range of defects in L4 larvae and adult animals, where most of the DD and VD commissures were misguided and did not connect to the DNC (Fig. 6D′).

Similarly, *sdn-1 hst-6* double-null mutants (L1 larvae and adults) showed more severe phenotypes in D-type motoneurons than did either single mutant alone, but the increase of defects was less pronounced than in *hse-5; sdn-1* double-null worms (Fig. 6A, Fig. 4E). The strong enhancement of the guidance defects observed in *hse-5; sdn-1* double mutants suggests that HSE-5 acts in parallel with SDN-1, i.e. that HSE-5 must modify at least one additional HSPG regulating a parallel signaling pathway. Because *sdn-1 hst-6* double mutants show a detectable enhancement of guidance defects in D-type motoneurons when compared with either single mutant, SDN-1 may not be the only substrate of HST-6 in D-type motoneurons.

To expand these observations in a different cellular context, we also examined the pathfinding of PVQ interneurons. Again, *hse-5; sdn-1* double-null animals showed significantly more

Table 3. Rescue of PVQ guidance defects

Genotype	Transgene expression	% Defective PVQ	*n*
Wild type	N/A	9±2	142
sdn-1(zh20)	N/A	49±4	140
sdn-1(zh20); opEx1159 [P_{dpy7}*::sdn-1*]	Hypodermis	58±4	128
sdn-1(zh20); opEx1160 [P_{dpy7}*::sdn-1*]	Hypodermis	58±5	112
sdn-1(zh20); opEx1161 [P_{dpy7}*::sdn-1*]	Hypodermis	50±5	122
sdn-1(zh20); opEx1162 [$P_{sra\text{-}6}$*::sdn-1*]	PVQ interneurons	22±4	111
sdn-1(zh20); opEx1163 [$P_{sra\text{-}6}$*::sdn-1*]	PVQ interneurons	25±4	111
sdn-1(zh20); opEx1164 [$P_{sra\text{-}6}$*::sdn-1*]	PVQ interneurons	30±4	109
sdn-1(zh20); opEx1165 [$P_{sdn\text{-}1}$*::sdn-1*]	Hypodermis, neurons	37±5	111
sdn-1(zh20); opEx1166 [$P_{sdn\text{-}1}$*::sdn-1*]	Hypodermis, neurons	18±4	109
sdn-1(zh20); opEx1167 [$P_{sdn\text{-}1}$*::sdn-1*]	Hypodermis, neurons	23±4	109

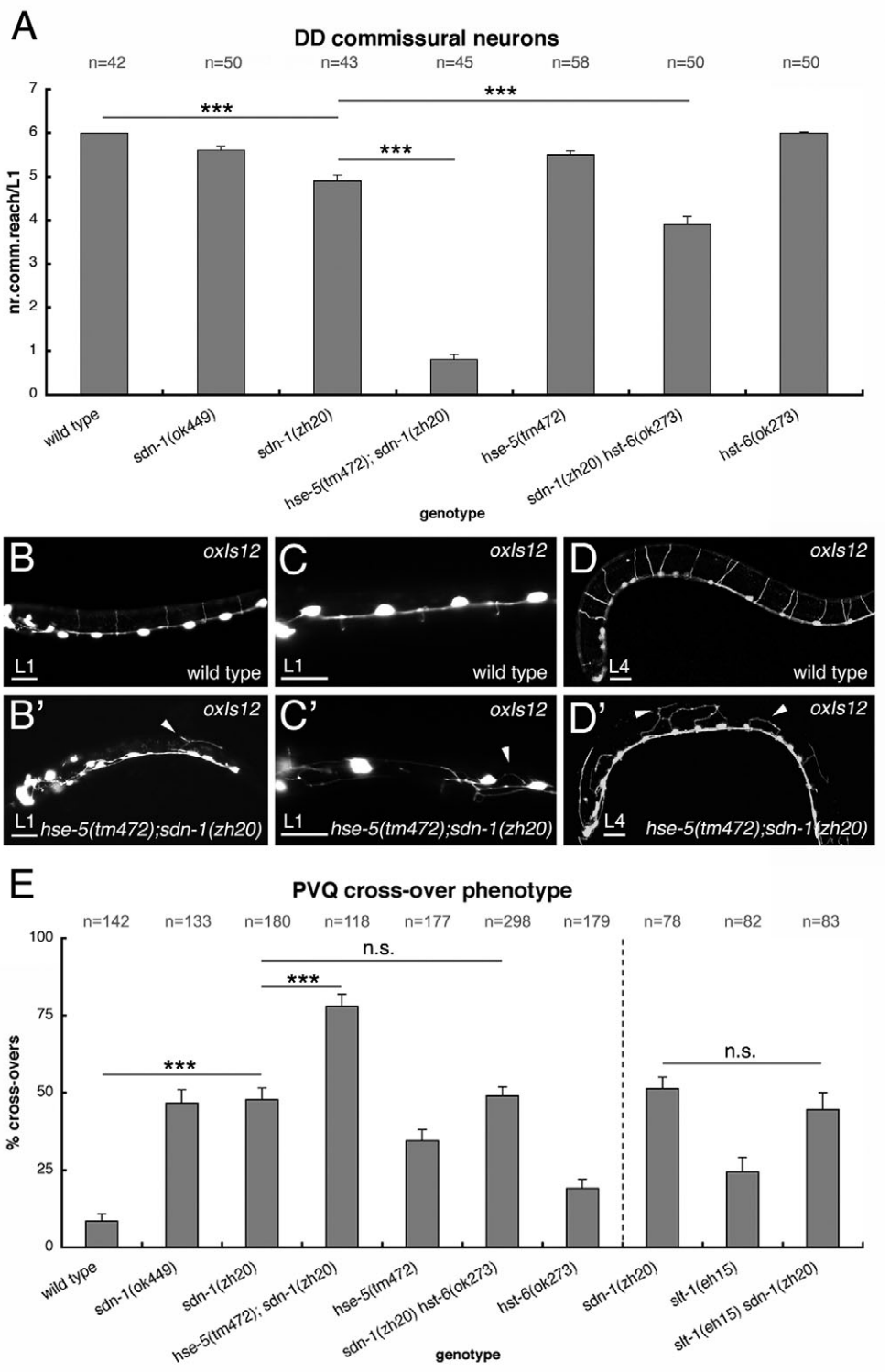

Fig. 6. Double mutant analysis of SDN-1 and HS-modifying enzymes. (A) Circumferential guidance of DD commissures (L1 larvae), as shown by the genetic interaction of *sdn-1* nulls with HS-modifying enzyme mutants. Data represent the number of commissures that reach the level of the DNC per L1 larva. Error bars indicate s.e.m. (B,B′) Analysis of DD commissures in L1 larvae. (B′) In *hse-5; sdn-1* double-null mutants, most DD commissures either fail to grow out dorsally or branch prematurely (arrowhead). (C,C′) VNC view of L1 larvae. (C′) The VNC of *hse-5; sdn-1* double-null mutants is highly defasciculated (arrowhead). (D,D′) DD/VD commissures of L4 larvae. (D′) Circumferential guidance of DD/VD motoneurons is disrupted in *hse-5*; *sdn-1* double mutants (arrowheads). D and D′ show confocal *z*-stack images to visualize all misguided commissures in different focal planes. (E) The PVQ crossover phenotype demonstrated by the genetic interactions of *sdn-1* null worms with HS-modifying enzyme mutants and *slt-1(eh15)*. Error bars indicate the standard error of proportion. Asterisks denote statistical significance as follows: ***P<0.0001; n.s., not significant; *n*, number of animals scored. Scale bars: 10 μm in B-C′; 25 μm in D,D′.

PVQ crossover defects than did either single mutant (Fig. 6E). In most *hse-5; sdn-1* worms, midline crossing had already occurred in the posterior region, leading to completely collapsed PVQ tracts (>50% of crossover defects). In contrast to D-type motoneurons, loss of HST-6 function did not result in a statistically significant enhancement of the *sdn-1* null phenotype. Interestingly, HST-6 is predominantly expressed in neurons, in contrast to HSE-5, which is mainly expressed in the hypodermis (Bülow and Hobert, 2004). This finding, together with our observation that loss of HST-6 function does not lead to more severe PVQ crossover defects in an *sdn-1* null background, suggests that 6*O*-sulfated HS, generated by HST-6, is important for SDN-1 function in PVQ midline crossing. By contrast, in D-type motoneurons, both *hse-5*; *sdn-1* and *sdn-1 hst-6* double-null mutants exhibited additive effects. Thus, signaling in different cellular contexts (D-type motoneurons

versus PVQ) might depend on a different combination of HS modifications.

In summary, the epistasis analysis with HS-modifying enzyme mutants points to the existence of a parallel, SDN-1-independent midline guidance pathway modulated by a distinct HSPG core protein that is a major target of the sugar epimerase HSE-5. Although our results do not exclude the possibility that HSE-5 also modifies SDN-1, the fact that *sdn-1(zh20)* enhances the *hse-5* loss-of-function phenotype indicates that, even in the absence of C5-epimerization, SDN-1 still regulates axon guidance.

SDN-1 acts in the Slit/Robo pathway

As the above experiment showed that syndecan SDN-1 is required for midline guidance, we speculated that SDN-1 might act as a co-receptor in one of the known axon guidance pathways, such as UNC-6/Netrin or Slit/Robo (Hao et al., 2001; Ishii et al., 1992; Zallen et al., 1998). The *C. elegans* genome encodes one Robo receptor (SAX-3) and one Slit homolog (SLT-1), which are both required for ventral axon guidance (Hao et al., 2001). Furthermore, interneurons that are usually separated in the left and right VNC inappropriately cross the midline in *sax-3* and *slt-1* mutants (Hao et al., 2001), a defect similar to the phenotype that we observed in *sdn-1* mutants.

In order to test whether SDN-1 acts in the SLT-1-dependent signaling pathway, we used the presumptive null allele *slt-1(eh15)* (Hao et al., 2001) and compared the phenotype of *slt-1 sdn-1* double-null mutants with that of either single mutant (Fig. 6E). The midline crossing defects in *slt-1 sdn-1* double mutants were no more severe than those of either single mutant, suggesting that SDN-1 acts in the same genetic pathway as SLT-1. Likewise, *slt-1 sdn-1* double mutants did not show enhanced defects of L/R choices of D-type motoneurons (data not shown).

Discussion

The differential modification of HS sugar chains was recently found to be required for various aspects of axon guidance. This observation led to the development of the 'sugar-code hypothesis' (Bülow and Hobert, 2004), which states that tissue-specific sugar side-chain modifications, like tissue-specific alternative splicing or tissue-specific heterodimerization, can modulate and fine-tune the activity of a core protein (in this case the HSPGs). In this study, we show that the HSPG core protein SDN-1 acts autonomously in neurons to direct cell migration and specify axon guidance decisions at the midline. We provide evidence that distinct modification patterns on SDN-1 and at least one additional HSPG core protein allow these proteins to differentially modulate two partially redundant axon guidance signaling pathways.

Syndecan in cell migration

Loss of SDN-1 function interferes with the migration of the HSN, CAN and ALM neurons, which, together with Q neuroblasts, are the only groups of neurons that migrate long distances in *C. elegans*. Because similar ALM migration defects have been reported for mutations in *sax-3*/Robo (Zallen et al., 1999), SDN-1 might also modulate Slit/Robo signaling in cell migration, in addition to its role in the regulation of Slit signaling in midline guidance indicated by our data. However, lack of SDN-1 does not perturb cell migration in general; for example, sex myoblast migration is normal in *sdn-1(zh20)* animals (data not shown). Furthermore, *sdn-1* null mutants exhibit no circumferential distal tip cell (DTC) migration defects. Mutations in the gene encoding perlecan/UNC-52, a basement membrane HSPG, enhance the DTC migration defects of UNC-6/netrin signaling mutants – an effect that can be partially suppressed by mutations disrupting growth factor-like signaling (Merz et al., 2003). Whether SDN-1 also contributes to signaling by EGL-20/WNT, UNC-129/TGF-β or EGL-17/FGF still needs to be determined.

Another candidate pathway that could be regulated by SDN-1 is signaling by integrins. *C. elegans ina-1* α integrin was shown to be required in neurons for the migration of HSN, ALM and CAN neurons (Baum and Garriga, 1997). Intriguingly, *ina-1* mutants also show defects in coelomocyte migration, whereas sexmyoblast migration is normal, similar to the situation we found in *sdn-1(zh20)* null mutants. In addition, cell culture studies have demonstrated a crucial role of the syndecan extracellular domain in regulating the adhesion and invasion of tumor cells, possibly by interacting with integrins (Beauvais et al., 2004; Burbach et al., 2004). Understanding the role of syndecan in cell migration is particularly relevant in light of the role mammalian syndecans play during carcinogenesis. Upregulation of human syndecan 1 in breast and pancreatic cancer, for example, usually correlates with more invasive tumors, although, in other types of cancer, downregulation of syndecan seems to have equally adverse effects (Beauvais and Rapraeger, 2004; Leivonen et al., 2004). In *C. elegans*, SDN-1 could promote cell migration either by modulating the activity of guidance cues or, directly, by regulating cell adhesion.

Syndecan in axon guidance

How might SDN-1 function in axon guidance? A recent study in *Drosophila* has shown that loss of syndecan function affects the extracellular distribution of the ligand Slit, which is secreted by midline cells and might therefore interfere with signal transduction by Robo receptors (Johnson et al., 2004). Neural expression of *Drosophila* syndecan rescued the guidance defects of syndecan mutant flies, whereas the expression of syndecan in midline cells did not (Johnson et al., 2004).

Similarly, our data suggest that *C. elegans* SDN-1 functions in neurons to ensure the correct midline guidance of axons. Cell type-specific expression of SDN-1 in PVQ interneurons partially rescued the midline pathfinding errors of these cells, whereas expression of SDN-1 in the surrounding epidermis failed to rescue. Incomplete rescue of PVQ crossovers, also seen for SDN-1 driven by its endogenous promoter, could be explained by insufficient expression of the rescuing arrays in PVQ neurons due to the lack of an enhancer sequence in the promoters that we used.

Neuronal SDN-1 could act as a co-receptor of specific axon guidance receptors and might thereby enhance the efficacy of the signaling event (quantitative modulation), alter the specificity of the ligand/receptor interaction (qualitative modulation), or both. One good candidate for a receptor that may require SDN-1 for ligand binding is the Slit/SLT-1 receptor SAX-3. *sdn-1* mutants show similar pathfinding errors

as *slt-1* or *sax-3* mutants, and genetic epistasis analysis placed *sdn-1* in the same genetic pathway as *slt-1* in certain cellular contexts (PVQ and D-type motoneuron development).

Alternatively, SDN-1, being a transmembrane protein, could also act directly as a receptor and generate an intracellular signal on its own. For example, *Xenopus* syndecan 2 participates in inside-out signaling that specifies the left-right looping of the heart and gut, which is mediated by PKCγ phosphorylation of the syndecan cytoplasmic domain (Kramer et al., 2002). Beyond their function as (co-)receptors, syndecans may also be involved in the targeting of guidance receptors to specific membrane compartments, such as lipid rafts (Couchman, 2003).

The C terminus of mammalian syndecans has been shown to interact with the PDZ domain of the membrane-associated guanylate kinase CASK (Cohen et al., 1998; Hsueh et al., 1998). The *C. elegans* CASK homolog LIN-2 is required together with LIN-7 and LIN-10 for the basolateral localization of the EGF receptor on vulval precursor cells (Kaech et al., 1998). SDN-1 might therefore be required to anchor the LIN-2/LIN-7/LIN-10 complex to the basolateral plasma membrane and thereby localize the EGF/LET-23 receptor. Although SDN-1::GFP is present on the basolateral side of the primary vulval cells (data not shown), loss of SDN-1 had no effect on EGF receptor localization. However, these observations do not exclude a possible role for SDN-1 in the targeting of axon guidance receptors.

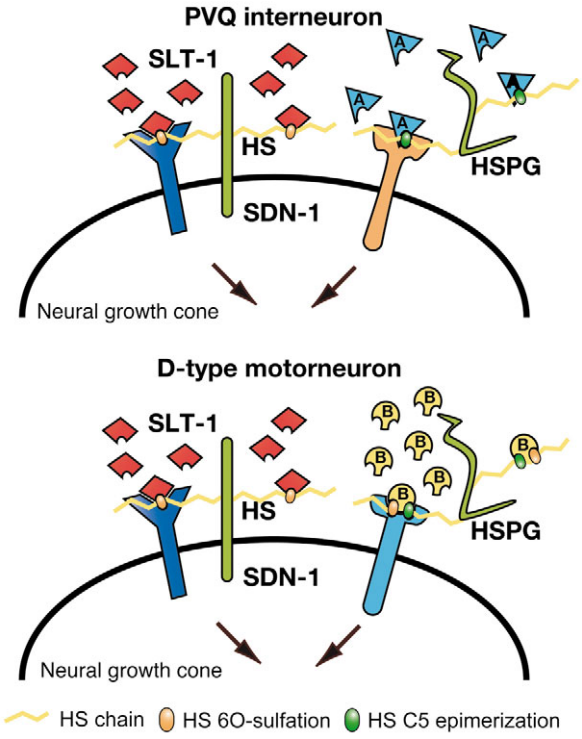

Fig. 7. Model for syndecan function in axon guidance signaling. Syndecan (SDN-1) on the neural growth cone exposes HS chains with 'neuron-specific' sugar modifications, here simplified by 6*O*-sulfations. The HS side chains of syndecan bind specific guidance cues (e.g. SLT-1) and modulate signaling by cognate high-affinity receptors, such as the SAX-3/Robo receptor (co-receptor function). Genetic analysis suggests that parallel signaling to syndecan relies on distinct sugar motifs on additional HSPGs in a context-dependent manner. In PVQ interneurons, this parallel pathway involves HS with epimerization (green), whereas in motoneuron development it involves both epimerization and 6*O*-sulfation. The HS modification patterns may thus define the specificity of different ligand/receptor interactions; A and B represent different ligands.

Syndecan and specific HS modifications

Interestingly, *sdn-1(zh20)* null animals showed comparable phenotypes for PVQ guidance and HSN migration to *sdn-1(ok449)* mutants, which express a mutant SDN-1 lacking the major HS side chains. This observation underlines the importance of the HS side chains and the information encoded in their sugar modifications for correct axon guidance, although it is possible that conformational changes due to the deleted region in the ectodomain or an altered distribution of the truncated SDN-1 form account for the defects observed in *sdn-1(ok449)* mutants. Importantly, we have found that SDN-1 is not the only HSPG controlling the axon guidance of PVQ interneurons and VNC motoneurons. Based on our epistasis analysis, we predict the existence of an additional axon guidance pathway, which relies on HS modifications by the C5-epimerase HSE-5, or on both HSE-5 and the 6*O*-sulfotransferase HST-6 – depending on the cellular context (Fig. 7). As it was shown that HSE-5 acts in the epidermis (Bülow and Hobert, 2004), this parallel pathway may depend on C5-epimerized HS sugars on a, as yet to be identified, HSPG expressed by the surrounding epidermal cells.

C. elegans mutant for glypican GPN-1, the second major cell surface HSPG, do not seem to display axon guidance or cell migration defects (Hannes Bülow and Oliver Hobert, personal communication). In all events that we analyzed (PVQ and DD/VD guidance, HSN migration), *gpn-1(ok377)* failed to enhance the defects of *sdn-1(zh20)* null animals (data not shown), indicating that HSE-5 might modify an extracellular or as yet unknown cell surface HSPG. The UNC-6/Netrin and VAB-1/Ephrin guidance systems act in parallel with SLT-1/Slit signaling to define midline guidance (Zallen et al., 1999), and are thus candidate pathways to be regulated by such proposed epimerized sugar motifs on a HSPG core protein distinct from SDN-1.

In PVQ interneurons, lack of the 6*O*-sulfotransferase HST-6 in worms devoid of SDN-1 did not cause a significant enhancement of crossover defects when compared with *sdn-1* single mutants. Thus, the HS side chains on SDN-1 are likely to be important substrates of HST-6 in PVQ (Fig. 7). HST-6 is, however, also involved in SDN-1-independent signaling, in the context of D-type motoneuron guidance.

Regulation by specific sugar modifications

Our results provide further evidence for the existence of a 'sugar code' on cell-surface and extracellular HSPGs that regulates the differential responses of axons towards the various extracellular guidance cues that they normally encounter. For example, 6*O*-sulfated HS side chains may act as 'molecular antennae' on SDN-1 to enhance the perception of Slit signals, as well as a modulator for the ligand/receptor interaction, while the input from parallel guidance systems could be regulated by extracellular HSPGs carrying C5-epimerized HS chains, with or without 6*O*-sulfation (Fig. 7). In this way, the sensitivity of axons towards Slit signals could be dynamically regulated

through the combinatorial control of HS-modifying enzyme expression and cell surface exposure of SDN-1. Indeed, during an early phase of mouse brain development, the different syndecan family members, as well as the HS-modifying enzymes, show tightly regulated spatiotemporal expression patterns (Ford-Perriss, 2003; Sedita et al., 2004).

The fact that HSPGs are highly conserved from nematodes to humans supports the idea that tissue-specific HS sugar modifications of HSPGs are a key factor that determines the cellular specificity of the different axon guidance systems (Hutter et al., 2000). Rules learned in *C. elegans* are thus likely to also apply in mammals, and promise to lead to a better understanding of the mechanisms that regulate nervous system development.

We thank Hannes Bülow and Oliver Hobert for stimulating discussions and sharing results prior to publication. We thank the CGC and various *C. elegans* researchers for providing strains and markers, the *C. elegans* Knockout Consortium in Oklahoma for providing deletion mutants, Eduardo Moreno and members of the Hengartner and Hajnal laboratories for comments on the manuscript, and Amit Dutt and Doris Klingele for technical support. This work was funded by the Swiss National Science Foundation (M.O.H. and A.H.), the Forschungskredit of the University of Zurich (C.R.) and the Ernst Hadorn Foundation (M.O.H.).

References

Ackley, B. D., Crew, J. R., Elamaa, H., Pihlajaniemi, T., Kuo, C. J. and Kramer, J. M. (2001). The NC1/endostatin domain of *Caenorhabditis elegans* type XVIII collagen affects cell migration and axon guidance. *J. Cell Biol.* **152**, 1219-1232.

Baum, P. D. and Garriga, G. (1997). Neuronal migrations and axon fasciculation are disrupted in *ina-1* integrin mutants. *Neuron* **19**, 51-62.

Beauvais, D. M. and Rapraeger, A. C. (2004). Syndecans in tumor cell adhesion and signaling. *Reprod. Biol. Endocrinol.* **2**, 1-12.

Beauvais, D. M., Burbach, B. J. and Rapraeger, A. C. (2004). The syndecan-1 ectodomain regulates alphavbeta3 integrin activity in human mammary carcinoma cells. *J. Cell Biol.* **167**, 171-181.

Bernfield, M., Gotte, M., Park, P. W., Reizes, O., Fitzgerald, M. L., Lincecum, J. and Zako, M. (1999). Functions of cell surface heparan sulfate proteoglycans. *Annu. Rev. Biochem.* **68**, 729-777.

Berset, T., Hoier, E. F., Battu, G., Canevascini, S. and Hajnal, A. (2001). Notch inhibition of RAS signaling through MAP kinase phosphatase LIP-1 during *C. elegans* vulval development. *Science* **291**, 1055-1058.

Bornemann, D. J., Duncan, J. E., Staatz, W., Selleck, S. and Warrior, R. (2004). Abrogation of heparan sulfate synthesis in *Drosophila* disrupts the Wingless, Hedgehog and Decapentaplegic signaling pathways. *Development* **131**, 1927-1938.

Brenner, S. (1974). The genetics of *Caenorhabditis elegans*. *Genetics* **77**, 71-94.

Bülow, H. E. and Hobert, O. (2004). Differential sulfations and epimerization define heparan sulfate specificity in nervous system development. *Neuron* **41**, 723-736.

Bülow, H. E., Berry, K. L., Topper, L. H., Peles, E. and Hobert, O. (2002). Heparan sulfate proteoglycan-dependent induction of axon branching and axon misrouting by the Kallmann syndrome gene kal-1. *Proc. Natl. Acad. Sci. USA* **99**, 6346-6351.

Burbach, B. J., Ji, Y. and Rapraeger, A. C. (2004). Syndecan-1 ectodomain regulates matrix-dependent signaling in human breast carcinoma cells. *Exp. Cell Res.* **300**, 234-247.

Chan, S. S., Zheng, H., Su, M. W., Wilk, R., Killeen, M. T., Hedgecock, E. M. and Culotti, J. G. (1996). UNC-40, a *C. elegans* homolog of DCC (Deleted in Colorectal Cancer), is required in motile cells responding to UNC-6 netrin cues. *Cell* **87**, 187-195.

Cohen, A. R., Woods, D. F., Marfatia, S. M., Walther, Z., Chishti, A. H. and Anderson, J. (1998). Human CASK/LIN-2 binds syndecan-2 and protein 4.1 and localizes to the basolateral membrane of epithelial cells. *J. Cell Biol.* **142**, 129-138.

Couchman, J. R. (2003). Syndecans: proteoglycan regulators of cell-surface microdomains? *Nat. Rev. Mol. Cell. Biol.* **4**, 926-937.

Esko, J. D. and Selleck, S. B. (2002). Order out of chaos: assembly of ligand binding sites in heparan sulfate. *Annu. Rev. Biochem.* **71**, 435-471.

Ford-Perriss, M., Turner, K., Guimond, S., Apedaile, A., Haubeck, H. D., Turnbull, J. and Murphy, M. (2003). Localisation of specific heparan sulfate proteoglycans during the proliferative phase of brain development. *Dev. Dyn.* **227**, 170-184.

Gilleard, J. S., Barry, J. D. and Johnstone, I. L. (1997). cis regulatory requirements for hypodermal cell-specific expression of the *Caenorhabditis elegans* cuticle collagen gene *dpy-7*. *Mol. Cell. Biol.* **17**, 2301-2311.

Halfter, W., Dong, S., Schurer, B. and Cole, G. J. (1998). Collagen XVIII is a basement membrane heparan sulfate proteoglycan. *J. Biol. Chem.* **273**, 25404-25412.

Hao, J. C., Yu, T. W., Fujisawa, K., Culotti, J. G., Gengyo-Ando, K., Mitani, S., Moulder, G., Barstead, R., Tessier-Lavigne, M. and Bargmann, C. I. (2001). *C. elegans* slit acts in midline, dorsal-ventral, and anterior-posterior guidance via the SAX-3/Robo receptor. *Neuron* **32**, 25-38.

Hartmann, U. and Maurer, P. (2001). Proteoglycans in the nervous system – the quest for functional roles in vivo. *Matrix Biol.* **20**, 23-35.

Hedgecock, E. M., Culotti, J. G., Hall, D. H. and Stern, B. D. (1987). Genetics of cell and axon migrations in *Caenorhabditis elegans*. *Development* **100**, 365-382.

Herman, T., Hartwieg, E. and Horvitz, H. R. (1999). sqv mutants of *Caenorhabditis elegans* are defective in vulval epithelial invagination. *Proc. Natl. Acad. Sci. USA* **96**, 968-973.

Hobert, O. (2002). PCR fusion-based approach to create reporter gene constructs for expression analysis in transgenic *C. elegans*. *Biotechniques* **32**, 728-730.

Hsueh, Y. P., Yang, F. C., Kharazia,V., Naisbitt, S., Cohen, A. R., Weinberg, R. J. and Sheng, M. (1998). Direct interaction of CASK/LIN-2 and syndecan heparan sulfate proteoglycan and their overlapping distribution in neuronal synapses. *J. Cell Biol.* **142**, 139-151.

Hutter, H., Vogel, B. E., Plenefisch, J. D., Norris, C. R., Proenca, R. B., Spieth, J., Guo, C., Mastwal, S., Zhu, X., Scheel, J. et al. (2000). Conservation and novelty in the evolution of cell adhesion and extracellular matrix genes. *Science* **287**, 989-994.

Inatani, M., Irie, F., Plump, A. S., Tessier-Lavigne, M. and Yamaguchi, Y. (2003). Mammalian brain morphogenesis and midline axon guidance require heparan sulfate. *Science* **302**, 1044-1046.

Ishii, N., Wadsworth, W. G., Stern, B. D., Culotti, J. G. and Hedgecock, E. M. (1992). UNC-6, a laminin-related protein, guides cell and pioneer axon migrations in *C. elegans*. *Neuron* **9**, 873-881.

Jansen, G., Hazendonk, E., Thijssen, K. L. and Plasterk, R. H. (1997). Reverse genetics by chemical mutagenesis in *Caenorhabditis elegans*. *Nat. Genet.* **17**, 119-121.

Johnson, K. G., Ghose, A., Epstein, E., Lincecum, J., O'Connor, M. B. and Van Vactor, D. (2004). Axonal heparan sulfate proteoglycans regulate the distribution and efficiency of the repellent slit during midline axon guidance. *Curr. Biol.* **14**, 499-504.

Kaech, S. M., Whitfield, C. W. and Kim, S. K. (1998). The LIN-2/LIN-7/LIN-10 complex mediates basolateral membrane localization of the *C. elegans* EGF receptor LET-23 in vulval epithelial cells. *Cell* **94**, 761-771.

Kinnunen, T., Huang, Z., Townsend, J., Gatdula, M. M., Brown, J. R., Esko, J. D. and Turnbull, J. E. (2005). 2-O-sulfotransferase, *hst-2*, is essential for normal cell migration in *Caenorhabditis elegans*. *Proc. Natl. Acad. Sci. USA* **102**, 1507-1512.

Kramer, K. L., Barnette, J. E. and Yost, H. J. (2002). PKCgamma regulates syndecan-2 inside-out signaling during *Xenopus* left-right development. *Cell* **111**, 981-990.

Lee, J. S. and Chien, C. B. (2004). When sugars guide axons: insights from heparan sulphate proteoglycan mutants. *Nat. Rev. Genet.* **5**, 923-935.

Lee, J. S., von der Hardt, S., Rusch, M. A., Stringer, S. E., Stickney, H. L., Talbot, W. S., Geisler, R., Nusslein-Volhard, C., Selleck, S. B., Chien, C. B. et al. (2004). Axon Sorting in the Optic Tract Requires HSPG Synthesis by *ext2* (dackel) and *extl3* (boxer). *Neuron* **44**, 947-960.

Leivonen, M., Lundin, J., Nordling, S., von Boguslawski, K. and Haglund, C. (2004). Prognostic value of syndecan-1 expression in breast cancer. *Oncology* **67**, 11-18.

Lindahl, U., Kusche-Gullberg, M. and Kjellen, L. (1998). Regulated diversity of heparan sulfate. *J. Biol. Chem.* **273**, 24979-24982.

Maduro, M. F., Gordon, M., Jacobs, R. and Pilgrim, D. B. (2000). The

UNC-119 family of neural proteins is functionally conserved between humans, Drosophila and C. elegans. *J. Neurogenet*. **13**, 191-212.

Merz, D. C., Alves, G., Kawano, T., Zheng, H. and Culotti, J. G. (2003). UNC-52/perlecan affects gonadal leader cell migrations in C. elegans hermaphrodites through alterations in growth factor signaling. *Dev. Biol.* **256**, 173-186.

Minniti, A. N., Labarca, M., Hurtado, C. and Brandan, E. (2004). *Caenorhabditis elegans* syndecan (SDN-1) is required for normal egg laying and associates with the nervous system and the vulva. *J. Cell Sci.* **117**, 5179-5190.

Morio, H., Honda, Y., Toyoda, H., Nakajima, M., Kurosawa, H. and Shirasawa, T. (2003). EXT gene family member *rib-2* is essential for embryonic development and heparan sulfate biosynthesis in *Caenorhabditis elegans*. *Biochem. Biophys. Res. Commun.* **301**, 317-323.

Perrimon, N. and Bernfield. M. (2000). Specificities of heparan sulphate proteoglycans in developmental processes. *Nature* **404**, 725-728.

Rogalski, T. M., Williams, B. D., Mullen, G. P. and Moerman, D. G. (1993). Products of the *unc-52* gene in *Caenorhabditis elegans* are homologous to the core protein of the mammalian basement membrane heparan sulfate proteoglycan. *Genes Dev.* **7**, 1471-1484.

Sasisekharan, R., Shriver, Z., Venkataraman, G. and Narayanasami, U. (2002). Roles of heparan-sulphate glycosaminoglycans in cancer. *Nat. Rev. Cancer* **2**, 521-528.

Sedita, J., Izvolsky, K. and Cardoso, W. V. (2004). Differential expression of heparan sulfate 6-O-sulfotransferase isoforms in the mouse embryo suggests distinctive roles during organogenesis. *Dev. Dyn.* **231**, 782-794.

Steigemann, P., Molitor, A., Fellert, S., Jackle, H. and Vorbruggen, G. (2004). Heparan sulfate proteoglycan syndecan promotes axonal and myotube guidance by slit/robo signaling. *Curr. Biol.* **14**, 225-230.

Topczewski, J., Sepich, D. S., Myers, D. C., Walker, C., Amores, A., Lele, Z., Hammerschmidt, M., Postlethwait, J. and Solnica-Krezel, L. (2001). The zebrafish glypican knypek controls cell polarity during gastrulation movements of convergent extension. *Dev. Cell* **1**, 251-264.

Zallen, J. A., Yi, B. A. and Bargmann, C. I. (1998). The conserved immunoglobulin superfamily member SAX-3/Robo directs multiple aspects of axon guidance in *C. elegans*. *Cell* **92**, 217-227.

Zallen, J. A., Kirch, S. A. and Bargmann, C. I. (1999). Genes required for axon pathfinding and extension in the *C. elegans* nerve ring. *Development,* **126**, 3679-3692.

CHAPTER 3

A Systematic Approach to HSPG Function in Neuronal Development of *C. elegans*.

INTRODUCTION

So far, the only HSPG known to play a role in nervous system development of *C. elegans* is syndecan SDN-1 (Rhiner et al., 2005). It acts in neurons to control neuronal migration and axon guidance and was shown to interact with the Slit/Robo signaling pathway. Nevertheless, there are still important questions that remain to be answered. For example, what is the role of the SDN-1 core protein? Could overexpression of glypican GPN-1, the other main cell surface HSPG, compensate for loss of SDN-1 function? In this context, it also interesting to speculate if a GPI-anchored SDN-1 would suffice to direct migrating neurons indicating that the highly conserved transmembrane and cytoplasmic domain of SDN-1 are dispensable for neuronal pathfinding. A number of PDZ-proteins have been found to interact with the intracellular domains of mammalian syndecans, which all carry conserved PDZ-binding motifs at the very C-terminus of the intracellular domains. It is therefore conceivable that C-terminal addition of GFP could interfere with SDN-1 function. Furthermore, it is not known if SDN-1 is also cleaved and released into the extracellular matrix in the worm and if such shed ectodomains would play a role in the formation of neuronal circuits . To address some of these open questions, I have performed structure/function experiments, in which I tested various constructs for their rescuing activity in *sdn-1* null worms.

But syndecan is most likely not the only HSPG that is required to shape neuronal connections. Our analysis of double mutants lacking SDN-1 and HS-modifying enzymes, provide genetic evidence for a more extensive HS-regulated axon guidance signaling than previously anticipated (Rhiner et al., 2005). Removal of the HS C5-epimerase in an *sdn-1* null background causes a drastic enhancement of axon guidance defects, compared to those observed in either single mutant (Figure 1). This prompted us to posit the existence of at least one additional HSPG, besides SDN-1, which is crucially involved in axon guidance decisions, but functions in a parallel signaling pathway to SDN-1. In principle, this HSPG X could be cell surface-bound or part of the extracellular matrix, based on the properties of known proteoglycans. The C5-epimerase of *C. elegans* is expressed most prominently in the hypodermis and the intestine (Bülow and Hobert, 2004) suggesting that the hypothesized HSPG is produced and eventually secreted by those cells.

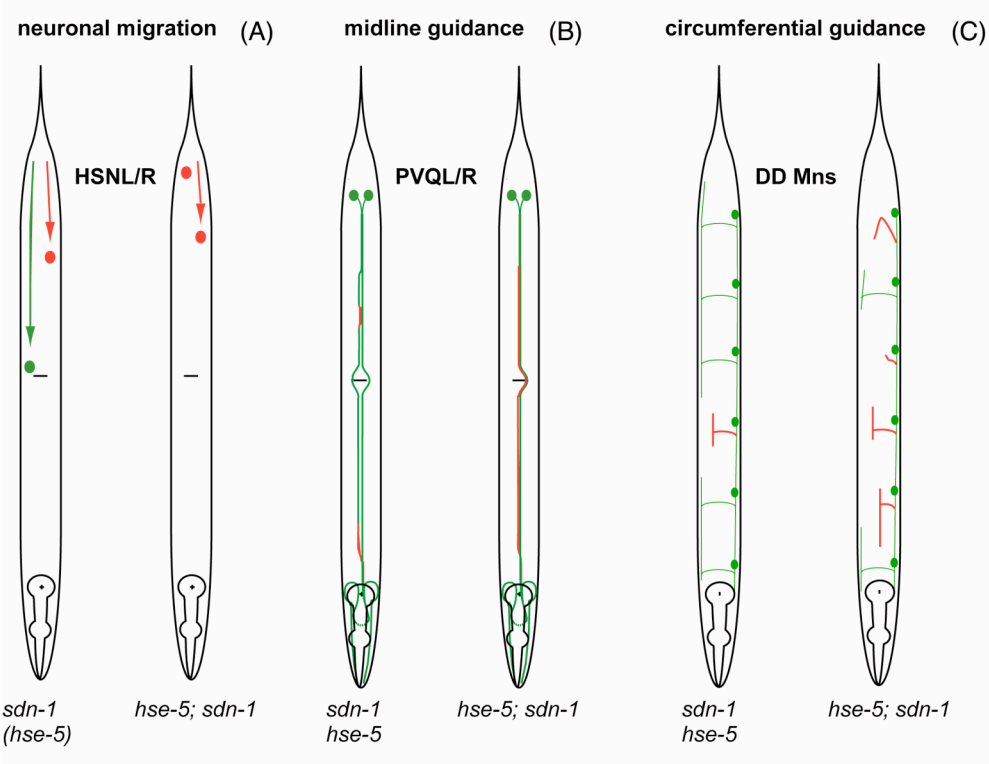

Figure 1. **Additive effects of mutations in *sdn-1* and *hse-5*.** Schematic view of neuronal migration and axon guidance defects in *sdn-1* and *hse-5* single null mutants and *hse-5; sdn-1* double null worms. **(A)**, **(B)** Top view of adult worms. **(C)** Side view of L1 larvae.

Results, mainly obtained in the fly, have established neural functions for GPI-anchored glypicans (Johnson et al., 2004; Johnson et al., 2005; Rawson et al., 2005). This renders the *C. elegans* GPN-1 an attractive candidate for the putative HSPG X. In the worm, GPN-1 is expressed in neuroblasts in the early embryo as determined by several transcriptional and translational *gfp* reporters (Hudson et al., 2006; Bülow H., unpublished results). In later stages, GPN-1 is confined to the pharynx and certain ventral cord motoneurons (Hudson et al., 2006; Bülow H., unpublished results). Together with SDN-1, GPN-1 was shown to participate in anosmin-1-dependent signaling during neuroblast migration in *C. elegans* (Hudson et al., 2006). Another glypican-like protein with an RGD integrin-binding motif is encoded by the gene *lon-2* (Gumienny et al., East Cost Worm Meeting 2004), the function of which still remains to be determined. Apart from membrane-anchored forms, the *C. elegans* genome also contains homologs for all known extracellular HSPGs in mammals (Table 1).

Table 1

Extracellular HSPGs in the nervous system

mouse	*C. elegans*	GAG type	Cellular origin
Agrin	F41G3.15	HS	neurons, muscle (mouse)
Perlecan	UNC-52	HS (CS)	muscle, hypodermis (worm) choroid plexus, blood vessels, glia (mouse)
Collagen XVIII	CLE-1	HS	neurons, muscle (worm) glia of PNS (mouse)
Testican 1-3	C54E4.2	CS/HS	neurons, testis, lung (mouse)

HS: Heparan Sulfate; **CS**: Chondroitin Sulfate

Agrin is a large extracellular HSPG with multiple domains. It is synthesized and released from motoneurons to induce the postsynaptic clustering of acetylcholine receptors at the neuromuscular junction (Glass et al., 1996), but is also expressed by all neurons in the central nervous system (Cohen et al., 1997). *C. elegans* agrin mutants have not been characterized up to date. In the worm, agrin seems to be expressed in the hypodermal ridge, in the pharynx and in several neurons in the head (Hrus A and Chiquet R, unpublished results).

The *unc-52* gene encodes the worm homolog of mammalian perlecan, the major HSPG of the extracellular matrix. Alternative splicing of the large *unc-52* gene yields multiple forms of this multi-domain proteoglycan (Mullen et al., 1999). Mutations in *unc-52* result in progressive paralysis of worms (class I mutations) or in embryonic lethality (two-fold arrest) (class II and III mutations), depending if all or only some of the UNC-52 forms are affected (Brenner 1974; Gilchrist and Moerman, 1992; Rogalski et al., 1995). The paralysis exhibited by carriers of class I mutations is caused by a disrupted attachment of myofilaments to the cell membrane of body wall muscle cells (Waterston, 1988). This suggests that UNC-52 is required to maintain normal muscle structure. The different UNC-52 isoforms are expressed in muscle, in the pharynx and the gonad under a dynamic spatio-temporal control (Mullen et al., 1999). Initially, it was shown that UNC-52 is produced and secreted by muscle cells into the underlying basement membrane (Moerman et al., 1996). Further investigation revealed, however, that also hypodermis-derived UNC-52 contributes to the perlecan pool in basement membranes (D. Moerman, personal communication). Besides muscle development, mutations in *unc-52* are also known to increase the distal tip cell (DTC) migration defects of *unc-6*/netrin mutants, but do not cause defects on their own (Merz et al., 2003). DTC migration gives rise to the U-shaped form of the gonads in *C. elegans*.

Type XVIII collagen is a homotrimeric basement membrane protein, which was shown to carry HS side chains in chicken (Halfter et al., 1998). The *C. elegans* collagen XVIII gene, *cle-1*, encodes three developmentally regulated isoforms: CLE-1A and CLE-1B are mainly expressed in neurons, CLE-1C is additionally expressed in body wall muscles, in the pharynx, head mesodermal cells and the gonadal sheath cells (Ackley et al., 2001). Secreted CLE-1 proteins accumulate in basement membranes that are associated with the nervous system. A deletion in the *cle-1* locus disrupting the C-terminal non-collagenous domain (NC1) was reported to cause neuronal migration and axon guidance defects (Ackley et al., 2001).

Last, the *C. elegans* genome also contains a gene (C54E4.2) homologous to mammalian testicans, which are mixed HS/CS proteoglycans that are highly expressed in the mouse brain, but some forms are specifically found in the testis and the lung (Hartmann and Maurer, 2001). The function of testicans is still unknown. In general, none of the above mentioned membrane-bound or extracellular HSPGs in *C. elegans* have been systematically tested for a role in neural development.

In order to gain a more complete picture of HSPG function in nervous system development, I have tested genetic interactions of *sdn-1* with other available HSPG mutants. The genetic studies were complemented by performing RNAi of HS core proteins in *sdn-1* null mutants. These experiments have shown that the HSPG CLE-1 is also implicated in all guidance events that are affected in *sdn-1* mutants. Moreover, epistasis analysis places CLE-1 in the same axon guidance signaling pathway as SDN-1. On the other hand, this candidate approach has so far failed to uncover additional HSPGs that function in parallel of SDN-1 to control axon guidance. We have therefore initiated a biochemical project to determine all HSPGs in *C. elegans*, by purifying heparan-sulfated proteoglycans, which will then be analyzed by mass spectrometry. Furthermore, I have extended the previous characterization of SDN-1 function. The rescue experiments show, that overexpression of GPN-1 in neurons can not compensate for loss of SDN-1 function suggesting non-redundant roles for the two cell surface HSPGs. In addition, C-terminal fusion of GFP does only slightly impair SDN-1 function. This indicates that proposed intracellular binding proteins are not crucial for SDN-1 function in neuronal migration. The overall data derived from rescue experiments, but also from the analysis of three different *sdn-1* mutants, suggests that HS side chains and eventually the syndecan transmembrane domain are essential for the neuronal function of SDN-1.

RESULTS

GPN-1 and SDN-1 play non-redundant functions in neuronal migration

A deletion in *sdn-1(ok449)* mutants leads to the expression of an extracellularly truncated SDN-1 that lacks the two major HS attachment sites located within the deleted part of the extracellular domain (Figure 2A). These mutants show very similar neural phenotypes as worms that completely lack SDN-1 *(sdn-1(zh20)*). In order to determine if the neuronal migration defects of *sdn-1* mutants can be rescued simply by providing HS on a different core protein, transgenic worms were generated that express *gpn-1* under the control of a pan-neuronal promoter. Analysis of two independent lines showed that overexpression of GPN-1 in neurons does not rescue the ALM migration defects of *sdn-1* mutants, as opposed to pan-neuronally overexpressed SDN-1 (Figure 2A).

In mammals, shed extracellular domains of syndecans are thought to play a regulatory role. To mimic the effect of such shed syndecan domains, a secreted SDN-1 form was expressed in all neurons of *sdn-1* null worms (*sdn-1ΔTM*). The presence of the secreted extracellular SDN-1 domain did not further perturb migration of the ALM neurons in *sdn-1* null mutants. Three independent lines showed no rescue of the ALM migration defects at all, whereas one line displayed slightly improvement migration of ALMs (Figure 2A). Expression of secreted SDN-1 in a wild-type background has not been analyzed yet. In addition, I analyzed axon guidance of D-type motoneurons in a new *sdn-1* mutant, *sdn-1(ev697)*, that might express a secreted form of SDN-1. *sdn-1(ev697)* worms carry a point mutation in the fifth exon of *sdn-1* leading to an early stop before the sequences encoding the SDN-1 transmembrane and cytoplasmic domains (Figure 2B). This mutation potentially transforms SDN-1 into a secreted protein if the product is stable (Schwabiuk M., unpublished results). *sdn-1(ev697)* worms show comparable defects in commissural guidance of motoneurons as *sdn-1(zh20)* and *sdn-1(ok449)* mutants (Figure 2A).

Next, I tested if direct addition of GFP to the C-terminal PDZ-interacting motif might interfere with SDN-1 function. Pan-neuronal expression of GFP-tagged SDN-1 significantly rescued the migration defects of ALM and HSN neurons in *sdn-1* null animals, but the rescue was slightly less efficient compared to untagged SDN-1 (Figure 2A). These findings suggest a minor role of interacting PDZ-proteins for SDN-1 function in neuronal migration. No transgenic lines were obtained with a construct where the syndecan transmembrane domain

was replaced by the GPI-anchor sequence of GPN-1. This GPI-anchored syndecan seemed to be toxic for the worms, maybe due to incorrect folding of the fusion protein.

A

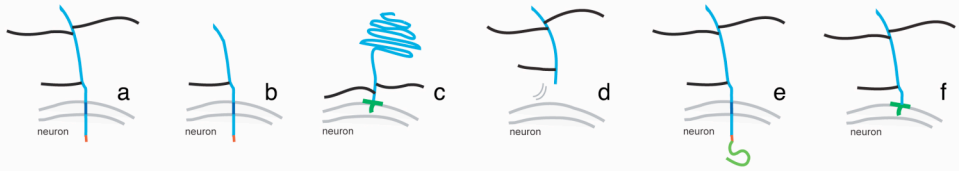

expressed Protein	transgene expression	genotype	N	Neuronal migration	rescue
				ALM (% def.)	
SDN-1 **(a)**	N/A	wild type	100	1 ± 1	N/A
No SDN-1	N/A	*sdn-1(zh20)*	96	42 ± 3	N/A
SDN-1 **(a)**	hypodermis, neurons	*sdn-1(zh20); opEx1198* [$P_{sdn\text{-}1}$*::sdn-1*][1*]	69	10 ± 2	yes
SDN-1 **(a)**	pan-neuronal	*sdn-1(zh20); opEx1206* [$P_{unc\text{-}119}$*::sdn-1*][2*]	82	5 ± 1	yes
GPN-1 **(c)**	pan-neuronal	*sdn-1(zh20); opEx1261* [$P_{unc\text{-}119}$*::gpn-1*][2]	48	52 ± 4	no
	pan-neuronal	*sdn-1(zh20); opEx1262* [$P_{unc\text{-}119}$*::gpn-1*][2]	34	47 ± 4	no
Secreted SDN-1 **(d)**	pan-neuronal	*sdn-1(zh20); opEx1266* [$P_{unc\text{-}119}$*::sdn-1ΔTM*][2]	32	47 ± 4	no
	pan-neuronal	*sdn-1(zh20); opEx1267* [$P_{unc\text{-}119}$*::sdn-1ΔTM*][2]	51	28 ± 4	(yes)
	pan-neuronal	*sdn-1(zh20); opEx1268* [$P_{unc\text{-}119}$*::sdn-1ΔTM*][2]	45	49 ± 4	no
	pan-neuronal	*sdn-1(zh20); opEx1269* [$P_{unc\text{-}119}$*::sdn-1ΔTM*][2]	27	44 ± 5	no
SDN-1::GFP (C-terminal) **(e)**	hypodermis, neurons	*sdn-1(zh20); opEx1264* [$P_{unc\text{-}119}$*::sdn-1::GFP*][1]	30	13 ± 3	yes
GPI-anchored SDN-1 **(f)**	pan-neuronal	*sdn-1(zh20);* [$P_{unc\text{-}119}$*::sdn-1GPI*][2]	-	-	toxic?
				HSN (% def.)	**rescue**
SDN-1 **(a)**	hypodermis, neurons	wild type	50	0 ± 0	N/A
No SDN-1	N/A	*sdn-1(zh20)*	63	56 ± 3	N/A
SDN-1 lacking HS **(b)**	N/A	*sdn-1(ok449)*	66	58 ± 3	N/A
SDN-1 **(a)**	hypodermis, neurons	*sdn-1(zh20); opEx1216* [$P_{sdn\text{-}1}$*::sdn-1*][1*]	62	13 ± 2	yes
SDN-1 **(a)**	pan-neuronal	*sdn-1(zh20); opEx1222* [$P_{unc\text{-}119}$*::sdn-1*][2*]	68	3 ± 4	yes
SDN-1::GFP (C-terminal) **(e)**	pan-neuronal	*sdn-1(zh20);opEx1256* [$P_{unc\text{-}119}$*::sdn-1::GFP*][1]	24	17 ± 4	yes
SDN-1::GFP (C-terminal) **(e)**	pan-neuronal	*sdn-1(zh20);opEx1257* [$P_{unc\text{-}119}$*::sdn-1::GFP*][1]	28	21 ± 4	yes
				DD guidance comm.reach/L1	
SDN-1 **(a)**	N/A	wild type	42	6.0 ± 0	N/A
No SDN-1	N/A	*sdn-1(zh20)*	43	4.9 ± 0.4	N/A
SDN-1 lacking HS **(b)**	N/A	*sdn-1(ok449)*	50	5.6 ± 0.3	N/A
SDN-1 lacking TM and cytoplasmic domain **(d)****	N/A	*sdn-1(ev697)****	51	5.1 ± 0.6	N/A

[1] construct contains *sdn-1* genomic sequence [2] construct contains *sdn-1 cDNA* sequence
[*] best rescuing line is shown out of three (from Rhiner et al., 2006)
[**] the presence of a secreted SDN-1 form has not been confirmed yet on western blot. The *sdn-1* mRNA might als be degraded in *sdn-1(ev697)*.
[***] *juIs76* II [$P_{unc\text{-}25}$*::gfp*] instead of *oxIs12* X [$P_{unc\text{-}47}$*::gfp*] was used to visualize D-type motoneurons. Both *gfp* reporters are equivalent (Bülow and Hobert, 2004).

B

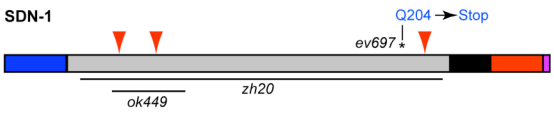

Figure 2. Structure/Function analysis of SDN-1

(A) Table summarizing the results from the structure/function rescue experiments and the analysis of three different *sdn-1* mutants. **(B)** Disruption of the SDN-1 protein by several molecular lesions. The blue box represents the signal peptide and the grey box the extracellular domain. Red arrowheads indicate the positions of putative HS attachment sites. The transmembrane and cytoplasmic domain are shown in black and red, respectively. The last four amino acids form the PDZ-interacting motif (pink).

gpn-1 mutants do not display neural phenotypes

Several deletions in the *gpn-1* locus have been analyzed. The *ok377* deletion disrupts exon three of *gpn-1* (Figure 3A). The group of Enrique Brandan previously reported that they could not see a different HSPG band pattern between wild-type and *gpn-1(ok377)* samples when probed with an anti-HS antibody (Minniti et al., 2004), raising the possibility that *ok377* is not a null allele. To address this question, I have performed quantitative RT-PCR to compare *gpn-1* mRNA levels of wild-type and *gpn-1(ok377)* worms. The result showed that *gpn-1* mRNA is present in *ok377* mutants, although at a lower level (supplementary Figure 1), which indicates that *ok377* is probably a hypomorphic allele. The *tm588* deletion creates a lesion spanning exon four and five of *gpn-1* (Figure 3A). Since exon 4 contains most of the conserved cysteine residues required to stabilize the globular fold of GPN-1, this deletion is likely to cause a complete loss of GPN-1 function. A third deletion in *gpn-1*, *tm595*, has not been analyzed because it essentially overlaps with *ok377*.

To test if GPN-1 is involved in nervous system development, I have crossed several *gfp* reporters into the *gpn-1* mutant background to visualize specific subsets of neurons. The analysis of *gpn-1* single and *sdn-1 gpn-1* double mutants showed that *gpn-1* did not enhance axon guidance defects of *sdn-1* mutants, nor did it cause detectable guidance errors on its own (Figure 3B). Likewise, both examined *gpn-1* mutants exhibited wild-type neuronal migration (data not shown). These results speak against a role of GPN-1 in the formation of the nervous system in *C. elegans*.

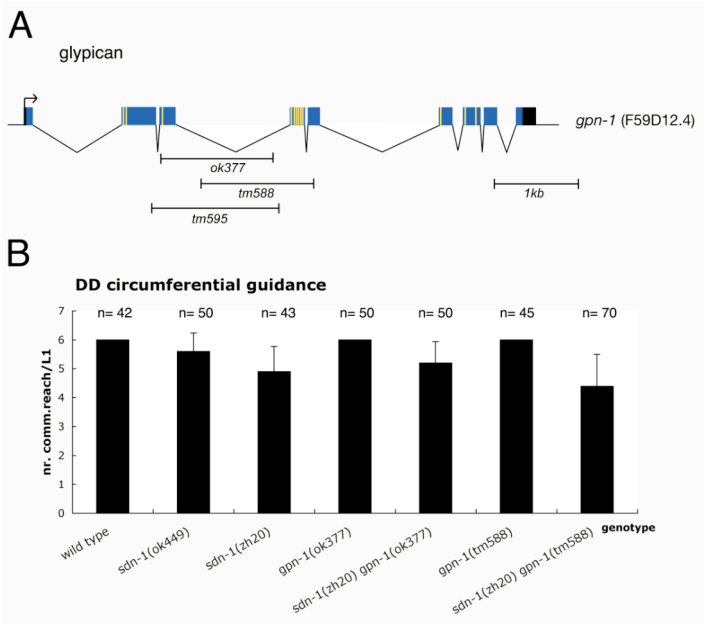

Figure 3. Deletions in *gpn-1* do not affect axon guidance. (A) Genomic structure of the *gpn-1* locus on chromosome X. Boxes represent exons (blue = coding, black = non-coding). Yellow lines indicate conserved cysteine residues. **(B)** Circumferential guidance of DD commissures in L1 larvae. Genetic interaction of *sdn-1* null with *gpn-1* mutants. Data represent the number of commissures that reach the level of the DNC per L1. Error bars indicate the standard deviation.

Class I mutations in perlecan do not increase axon guidance errors of *sdn-1* mutants

In order to test if perlecan might be the HSPG acting in a parallel axon guidace pathway to SDN-1, I used mutations in *unc-52* that cause the progressive paralysis phenotype. The analyzed alleles carry mutations in exon 16 (*e1421*, splice donor) and exon 18 (*e444 and e998,* stop codon) (Figure 4A), which are known to be alternatively spliced (Rogalski et al., 1995). Lesions in these exons therefore only affect some of the perlecan forms produced in the worm. Lethal *unc-52* alleles were not analyzed because the worms die before reaching the L1 larval stage, the earliest stage when development of DD motoneurons can be examined. Mutations in *unc-52* that cause paralysis from the L4 larval stage on did not affect circumferential axon guidance of DD commissurs in L1 larvae (Figure 4B). Moreover, *unc-52; sdn-1* double mutants did not show a significant increase in guidance defects, compared to *sdn-1* single mutants. Similarly, cross-over defects of interneurons at the midline were not enhanced by introducing these *unc-52* mutations into worms devoid of SDN-1 (Figure 4C). Loss of function of certain perlecan forms even seemed to reduce midline-crossing errors of *sdn-1* null mutants, but the suppression was not significant.

In a screen for suppression of the *unc-52* paralyzed phenotype, Erin Gilchrist and Don Moerman isolated a suppressor mutation, *sup-38*, which mapped close to the *dpy-4* gene on chromosome IV (Gilchrist and Moerman, 1992). I also tested an allele of *sup-38* for a potential role in neural patterning since it shows genetic interaction with *unc-52*. Remarkably, worms carrying the *sup-38* mutations showed frequent midline guidance errors (38% animals defective) (Figure 4D). In a double mutant combination with *sdn-1, sup-38* did not augment midline guidance defects of *sdn-1* mutants indicating that it might act in the same signaling pathway as *sdn-1*. Supporting this view, genetic removal of the C-5 epimerase *hse-5* in *sup-38* background caused a significant enhancement of midline cross-overs, as it has been observed in *hse-5; sdn-1* double null mutants (Figure 4D).

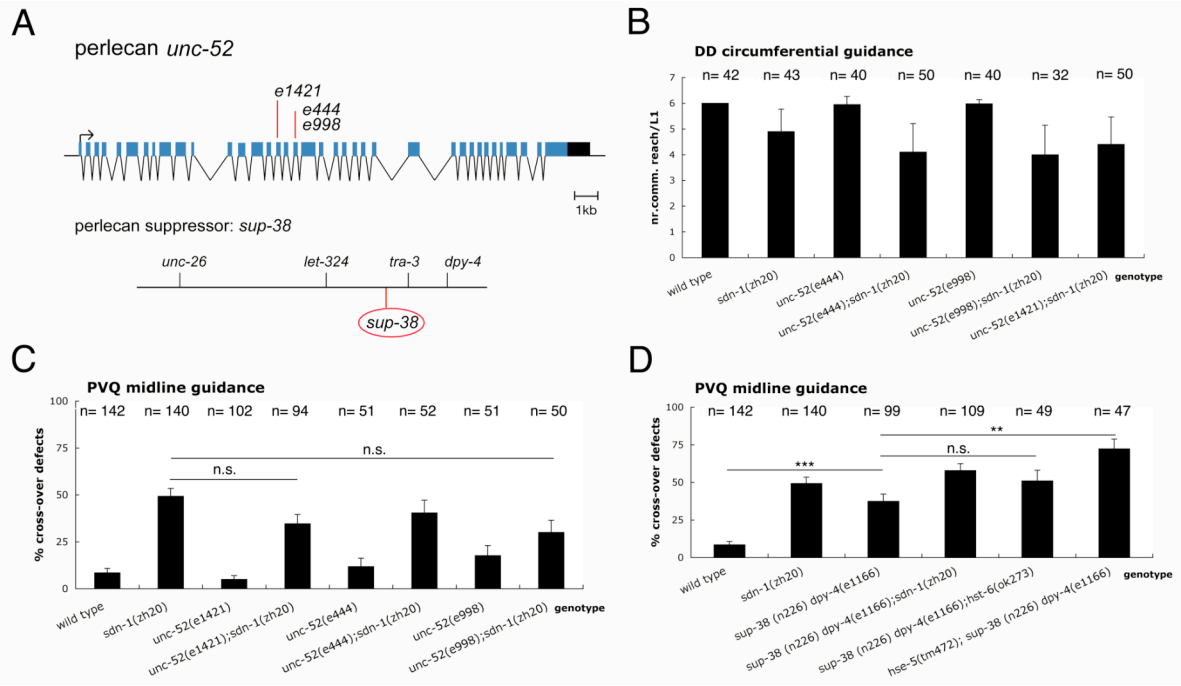

Figure 4. *unc-52* alleles causing progressive paralysis do not interfere with neural development

(A) Structure of the *unc-52* locus on chromosome II. The *unc-52* gene consists of 37 exons (blue boxes = coding, black = non-coding) and spans 20kb. Exons 16, 17 and 18 are alternatively spliced and give rise to perlecan isoforms that vary in the number of NCAM repeats. *e444* and *e998* are nonsense mutations in exon 18; *e1421* alters the splice donor site of exon 16 (Rogalski et al., 1995). The approximate map position of *sup-38*, a suppressor of these perlecan alleles is shown below. **(B)** Circumferential guidance of DD commissures in L1 larvae. **(C, D)** Midline guidance of the left (L) and right (R) PVQ interneuron. The graph depicts the percentage of animals that show aberrant midline cross-overs of ipsilateral PVQs to the contralateral side. Error bars indicate the standard deviation **(B)** or the standard error of proportion **(C, D)**. Asterisks denote statistical significance: * P< 0.01, ** P< 0.001, *** P< 0.0001; n.s. not significant. n, number of animals scored.

Agrin and axon guidance

In collaboration with the group of Ruth Chiquet in Basel, I tested two available agrin mutants for potential axon guidance phenotypes. The structure of the agrin locus in *C. elegans* has been determined by amplifying fragments with SL-1 primers from a cDNA library and was found to encompass 29 exons (Canevascini S and Chiquet R, unpublished results) (Figure 5A). *agr-1(eg1770)* was created by insertion of the *mos-1* transposon into the seventh exon of *agr-1* (Canevascini S and Chiquet R, unpublished results). *tm2051* is a 423 bp in-frame deletion, which removes exon 26 and 27 and thereby parts of the second LamG domain of agrin. Both mutants show absence of agrin staining in the pharynx, compared to the wild type

indicating that they are loss-of-function alleles (Hrus A and Chiquet R, unpublished results). When examined for axon guidance defects, *agr-1* single mutants exhibited wild-type motoneuron development and axonal pathfinding of interneurons at the midline (Figure 5B, 5C). In addition, *agr-1*(*eg11770)* and *agr-1(tm2051)* did not increase guidance defects of *sdn-1* null worms. The two agrin alleles were also evaluated with respect to a possible effect on neuronal migration. Migration defects of the HSN neurons were significantly higher in *agr-1(eg1770); sdn-1* double mutants compared to *sdn-1* or *agr-1* single mutants. However, this enhancement of HSN migration defects was not observed with the *tm2051* allele.

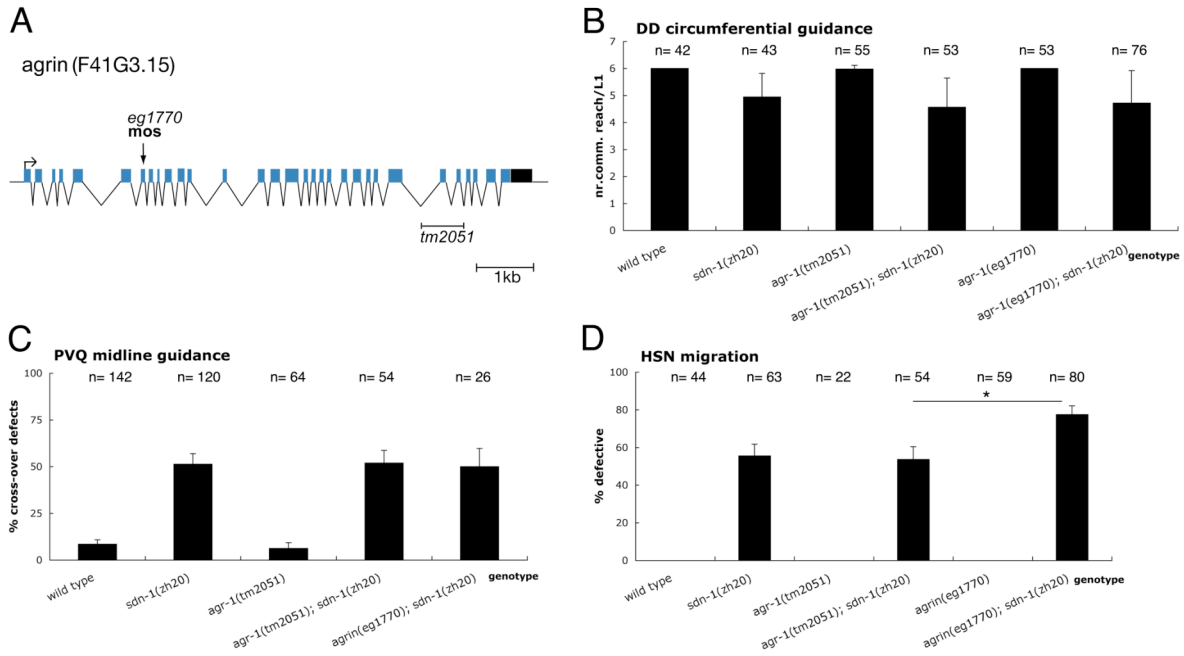

Figure 5. Tested agrin alleles for neuronal migration and axon guidance defects

Presumptive structure of the agrin gene (F41G3.15) in *C. elegans*, located on chromosome II (based on Hrus A and Chiquet R, unpublished results). Agrin is known to be alternatively spliced in other species giving rise to muscle- and neuro-specific isoforms. **(B)** Circumferential guidance of DD commissures in L1 larvae. **(C)** Midline guidance of the PVQ L/R interneurons. **(D)** Neuronal migration of the HSN L/R neurons. The graph depicts the fraction of worms displaying HSN neurons that fail to migrate or stop prematurely. Error bars indicate the standard deviation **(B)** or the standard error of proportion **(C, D)**. Asterisks denote statistical significance: * P< 0.01, ** P< 0.001, *** P< 0.0001; n.s. not significant. n, number of animals scored.

CLE-1 is required for circumferential guidance of motoneurons

A deletion in the worm collagen XVIII gene, *cle-1*, has previously been shown to cause neuronal migration defects of the HSN and ALM neurons (Ackley et al., 2004). The reported defects are qualitatively similar to those seen in *sdn-1* mutants, although the phenotype is less penetrant (27% HSN migration defects in *cle-1(cg120)* versus 55% in *sdn-1(zh20)). cle-1(cg120)* worms carry a 2 kb deletion in the C-terminal noncollagenous domain (NC1) of the *cle-1* gene (Figure 6A). The *cg120* deletion removes three exons that are common to all three *cle-1* splice forms and gives rise to stable truncated CLE-1 proteins (Ackley et al., 2004). By sequence alignment of *C. elegans*, *Drosophila*, chicken and human collagen XVIII, I found two conserved HS attachment sites (S-G) in the entire collagen XVIII protein sequence, which are located in the NC1 domain affected by the *cg120* deletion (data not shown). That loss of HS, rather than the truncation of the CLE-1 protein could be responsible for the neural phenotypes of *cle-1(cg120)* worms, has not been considered in the previous study by Ackley and collegues. However, this first possibility seems to be more likely because of the striking similarities in neural defects of *cle-1* and *sdn-1* mutants.

In addition to neuronal migration defects, *cle-1(cg120)* mutants also show impaired left/right choices of DA/DB commissures to exit the ventral nerve cord (VNC), a phenotype that is also associated with loss of SDN-1 function. In *sdn-1* mutants, additionally left/right decisions and circumferential guidance of D-type commissures are affected. Therefore, it was interesting to determine if *cle-1* is also implicated in development of D-type motoneurons. Indeed, DD commissures in *cle-1(cg20)* mutants branched prematurely and failed to reach the dorsal nerve cord (DNC) (Figure 6B). Next, I generated *cle-1; sdn-1* double mutants to determine if the two HSPGs function in parallel signaling pathways to control motoneuron development. Genetic removal of SDN-1 and the NC1 domain of collagen XVIII did not cause more severe pathfinding errors in DD commissures of L1 larvae, compared to either single mutant indicating that SDN-1 and CLE-1 rather act in the same pathway (Figure 6B).

Based on the genetic data so far, it is still conceivable that various extracellular HSPGs might play redundant roles in axon guidance. If so, removal of a single HSPG might not suffice to decrease extracellular HS below a critical threshold. To address this question, several triple HSPG mutants were analyzed. However, neither *agr-1 unc-52; sdn-1* nor *cle-1; agr-1; sdn-1* triple mutants showed an enhancement of the *sdn-1* null phenotype using the described hypomorphic alleles (Figure 6B).

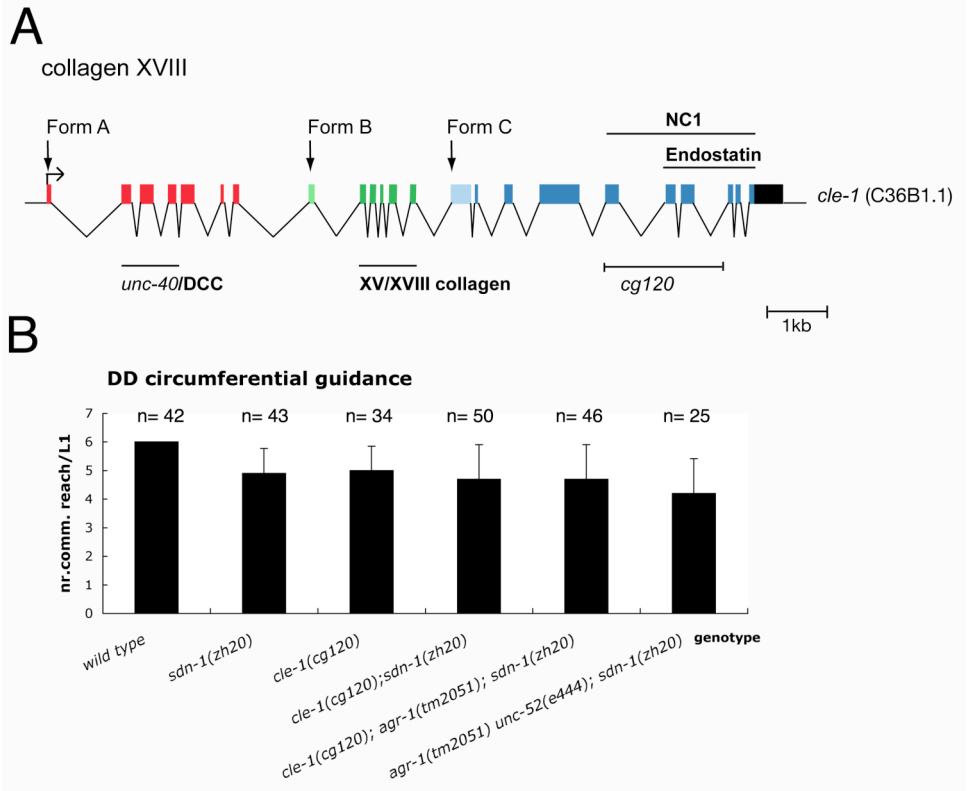

Figure 6. A deletion in *cle-1* causes similar defects as loss of SDN-1 function. (A) Structure of the *cle-1* gene on chromosome I. Three different *cle-1* forms are generated by alternative splicing. Form A-specific exons are red, exons common to form A and B are green and exons shared by all forms are blue. Arrows indicate predicted translation start sites for each isoform (Ackley et al., 2001). **(B)** Circumferential guidance of DD commissures in L1 larvae. Note that triple mutants of *sdn-1* and hypomorphic alleles of two extracellular HSPGs do not display increased guidance defects compared to *sdn-1* null worms.

RNAi of HSPGs

The use of hypomorphic alleles of extracellular HSPGs allows to circumvent the lethality caused by complete loss-of-function mutations. But it bears the caveat that neural phenotypes might not be detectable because the remaining activity of the unaffected isoforms might be sufficient to sustain axon guidance. To corroborate the genetic data with the HSPG mutants, I performed RNAi of HSPGs in *sdn-1* and *lin-35; sdn-1* mutant backgrounds. *lin-35(n745)* was recently shown to sensitize worms to RNAi, especially to enable knock-down of genes in neurons, which are usually refractile to the effect of RNAi (Wang et al., 2005). L1 larvae were grown on bacteria expressing dsRNA against *gpn-1*, *unc-52*, *cle-1* or the empty RNA expression vector as a control and axon guidance was analyzed in L1 larvae of the second

generation. The results showed that commissural guidance defects of DD motoneurons in *sdn-1* null mutants were not significantly altered by RNAi of *gpn-1*, *unc-52* or *cle-1* (Figure 7A).

By contrast, the *lin-35; sdn-1* strain showed a significant increase of axon guidance defects compared to *sdn-1* single mutants, even though *lin-35* did not cause significant guidance errors on its own (data not shown). In combination with *sdn-1*, *lin-35(n745)* also caused significantly more HSN migration defects than *sdn-1* alone (data not shown). *lin-35* encodes the retinoblastoma homolog of *C. elegans* and mutations in the Rb pathway components are known to induce the expression of genes in somatic cells, which are normally limited to germ-line specific P-granules (Wang et al., 2005). Therefore, I considered the enhanced neural defects in *lin-35; sdn-1* mutants as an unspecific effect of generally altered gene expression. Regardless of the elevated background defects, RNAi of the tested HSPGs did not further exacerbate commissural guidance in *lin-35; sdn-1* worms (Figure 7A). On the other hand, *lin-35(n745)* clearly sensitized the worms to the effect of RNAi. RNAi of *unc-52* in the *lin-35; sdn-1* background caused onset of paralysis at the L4 stage and led to embryonic lethality in the second generation, which could not be analyzed for axon guidance therefore (Figure 7A, 7B). In contrast, *sdn-1* null worms with wild-type *lin-35* became paralyzed only as young adults and the second generation mostly survived larval development. RNAi of *cle-1* in the sensitized background caused an egg-laying defective (Egl) phenotype.

Together with the group of Ruth Chiquet in Basel, we also tested RNAi of agrin by injecting agrin dsRNA into the *C. elegans* gonad, but could not detect an effect on circumferential guidance of motoneurons in *sdn-1* mutants (data not shown). To sum up, RNAi of known HSPGs did not lead to an enhancement of the *sdn-1* axon guidance phenotype further supporting the view that they do not represent the major targets of the C5 epimerase HSE-5.

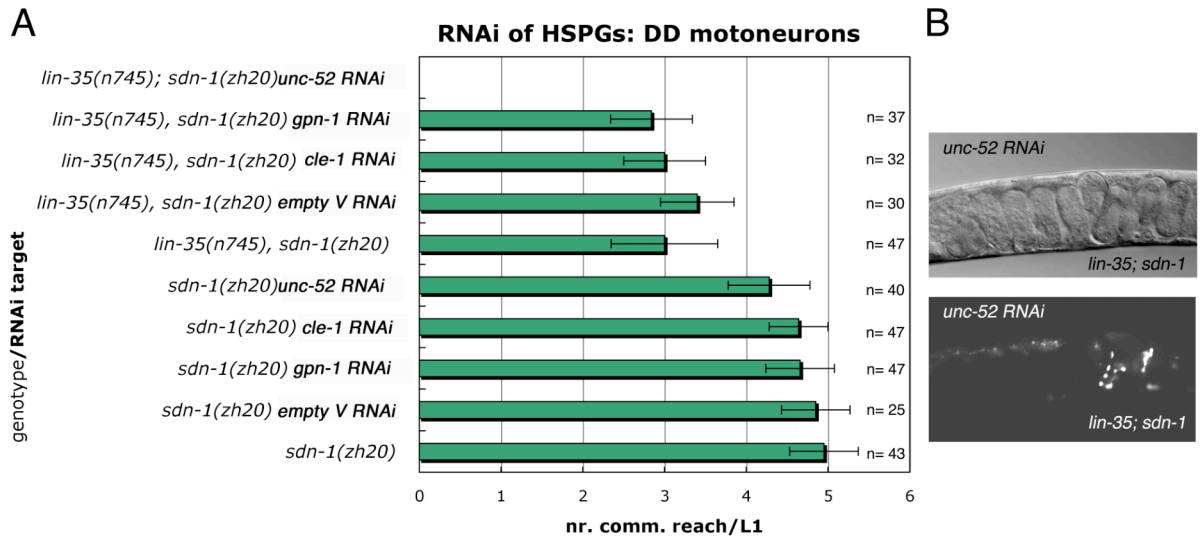

Figure 7. Knock-down of HSPGs in *sdn-1* null mutants

(A) *sdn-1* null L1 larvae were fed with bacteria expressing dsRNA against *gpn-1*, *unc-52*, *cle-1* or the empty RNAi vector as a control. The progeny (L1 larvae) was analyzed for circumferential guidance defects of DD motoneurons. *lin-35(n745)* was crossed into the SDN-1-deficient background to increase the efficacy of RNAi-mediated gene knock-down. **(B)** RNAi of *unc-52* in the *lin-35; sdn-1* strain caused early embryonic lethality of the second generation. Eggs were retained in paralyzed adults and could not be scored for guidance defects. RNAi target genes are indicated in bold type. The upper panel shows the arrested embryos in DIC optics, the lower picture was taken in the fluorescent channel and shows expression of GFP in D-type motoneurons visualized by the *oxIs12* [$P_{unc\text{-}47}$*::gfp*] transgene.

Expression of HSPGs

In order to detect the different HSPGs present in *C. elegans*, worm lysates were subjected to western blot analysis. The core protein of any HSPG can be detected after heparinase III treatment by means of the monoclonal anti-Δ-heparan sulfate antibody (3G10 epitope). This antibody recognizes a neo-epitope generated in the proteoglycan core protein after digestion of HS with the heparinase enzyme (Steinfeld et al., 1996). In total worm lysate, the anti-Δ-heparan sulfate antibody recognized a major band at 50kDa, which is absent in *sdn-1* null worms, and a fainter band at 30kDa (Figure 8). This shows that the SDN-1 protein can readily be detected in unpurified worm lysates. The 30kDa band has been recently reported to correspond to GPN-1 because it was absent in *gpn-1(ok377)* worms (Hudson et al., 2006). In contradiction to this study, I repeatedly observed the presence of the 30kDa band in *gpn-1(ok377)* worms loading 80 μg of protein. Similarly, the group of Enrique Brandan could not

detect a difference in the HSPG pattern of *gpn-1(ok37)* mutants compared to the wild type (Minniti et al., 2004). Using total worm lysate, I was unable to identify other HSPGs than SDN-1, probably also due to technical difficulties with the solubility of the large extracellular proteoglycans. The limited resolution of the WB based on total worm lysate will hopefully be overcome by purifying HSPG fractions (in collaboration with Enrique Brandan). Efforts are ongoing to obtain clean HSPG bands that can be analyzed by mass spectrometry.

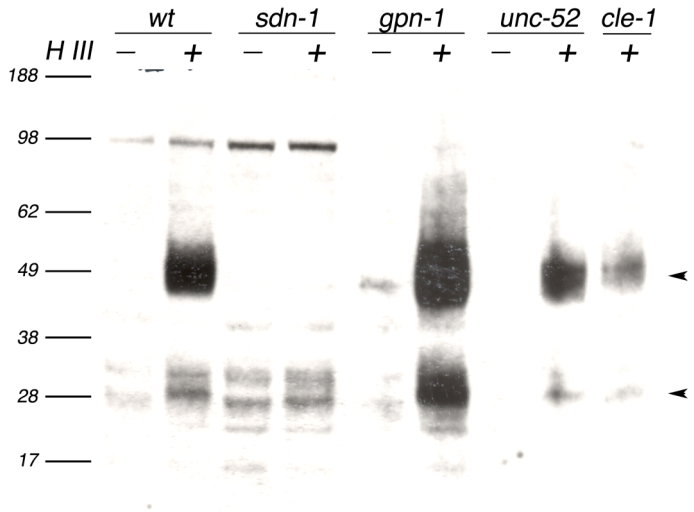

Figure 8. SDN-1 corresponds to a 50kDa core protein bearing HS GAGs. Western blot analysis with samples from *sdn-1(zh20)*, *gpn-1(ok377)* and *unc-52(e444)* mutants and wild-type worms. Lysates were incubated with Heparinase III before gel electrophoresis. Addition of Heparinase III (+HIII) generates a neo-epitope in HS core proteins compared to untreated samples (-HIII), which is recognized by the anti-Δ-heparan sulfate antibody. SDN-1 corresponds to the 50 kDa band that is absent in *sdn-1* null worms. A second protein core is detected as a 30kDa band present in all tested mutants.

DISCUSSION

Based on their highly regulated expression patterns in the brain during axon guidance, HSPGs have long been presumed to play a role in nervous system development. The simplicity of the genetic model organisms *C. elegans* and *Drosophila* allowed to unveil functions of individual core proteins for different aspects of neural development such as neuronal migration, axon guidance and synaptic differentiation (chapter 1). Initial studies focused mostly on the characterization of a single HS core protein in a particular context of nervous system

development. Here, I have analyzed a broad range of available HSPG mutants for defects in neuronal migration and axon guidance. In addition, I have further examined which features of SDN-1 are essential for its crucial role in neuronal migration.

Syndecan: structure and function

In *Drosophila,* overexpression of a glypican could partially compensate for the lack of syndecan, in certain neuronal contexts (Johnson et al., 2004; Rawson et al., 2005). In this study, I show that pan-neural overexpression of GPN-1 in the worm can not substitute for SDN-1 function in neuronal migration (Figure 2A). This underlines that the mere exposure of HS chains on neurons is not sufficient to restore correct migration. If SDN-1 functions as a co-receptor for guidance signals, it is likely that the positions of the HS chains are crucial for determining the geometry of the HS-ligand-receptor interaction. Therefore, it is possible that GPN-1 is not able to compensate for SDN-1 function simply because it carries membrane-proximal HS chains, as opposed to SDN-1, where they are mainly located at the N-terminus. It remains to be shown, if neuronal expression of GPN-1 could partially rescue the midline guidance defects of *sdn-1* null worms as it was observed in *Drosophila* (Johnson et al., 2004).

The fact that GPI-anchored GPN-1 shows no rescuing activity could also point to a requirement for the SDN-1 intracellular domain. Fusing GFP to the C-terminus of SDN-1, next to the PDZ interacting motif, did only slightly impair SDN-1 function (Figure 2A). This could mean that PDZ-proteins might be required to stabilize SDN-1 at the membrane, but they do not crucially contribute to SDN-1 function in neuronal migration. Unfortunately, no lines were obtained with the construct encoding a GPI-anchored syndecan. The altered syndecan structure with a GPI-anchor probably interfered with the folding of the protein. To determine if the intracellular part of SDN-1 is dispensable for neuronal migration, a construct truncating SDN-1 right after the transmembrane (TM) domain might be more suitable. The transmembrane domain of SDN-1 could be important to mediate clustering of SDN-1 proteins at the cell surface. There is evidence that a motif in the transmembrane domain of mammalian syndecan-3 promotes self-association (Asundi et al., 1995). Self-association, mediated by the transmembrane domain, might also be required for SDN-1 function. Notwithstanding these arguments, there is ample evidence that the extracellular HS chains of SDN-1 are the most essential attribute of SDN-1 for regulating neuronal migration and axon guidance. First, mutations in genes encoding for specific HS-modifying enzymes, which do not affect HS core

proteins, cause similar neural phenotypes as those present in *sdn-1* worms (Bülow and Hobert, 2004). Second, *sdn-1*(*ok499)* animals that express a SDN-1 lacking solely a stretch of the extracellular domain where the HS attachment sites are located, show almost identical neuronal defects as *sdn-1* null mutants (Figure 2A). And third, a deletion in *cle-1*, which leads to similar defects in neural patterning as those observed in *sdn-1* null mutants, disrupts the exons that encode the two conserved HS attachment sites in all splice forms of this multi-domain protein. This provides strong evidence for a crucial function of the HS chains in the regulation of axon guidance signaling.

Secreted SDN-1 in the extracellular matrix could potentially bind Slit and form a functional Slit gradient, a mechanism that was proposed for *Drosophila* syndecan in axon guidance (Johnson et al., 2004). However, a secreted SDN-1 form did not rescue the migration defects of ALM neurons in an *sdn-1* null background, in agreement with a proposed cell-autonomous function of SDN-1 (Rhiner et al., 2005). It will be interesting to determine if secreted SDN-1 can antagonize axon guidance signaling by crossing the *sdn-1*ΔTM arrays into a wild-type background. In this case, similar migration and guidance defects might be observed in this transgenic worms as in *sdn-1* null mutants. That an increase in extracellular HS could lead to competition for HS-ligands has already been proposed by Wang and Denburg from their studies in cockroach embryos. In their experiments, addition of exogenous HS caused similar axon guidance errors as enzymatic degradation of the HS of endogenous HSPGs (Wang and Denburg, 1992).

HSPGs in nervous system development

Using a broad spectrum of available deletions in most of the known HSPGs in *C. elegans*, I analyzed their effect on neuronal development, especially their capacity to enhance neural phenotypes of *sdn-1* null worms. Analysis of two *gpn-1* alleles did not reveal a role for GPN-1 in nervous system development (Figure 3). Although I provide evidence that *gpn-1(ok377)* might not be a molecular null allele, the same results were obtained with *gpn-1(tm588),* a likely null allele of *gpn-1*. The lack of a neural phenotype in *gpn-1* mutants is not unexpected considering that GPN-1 is mainly expressed in the pharynx and only transiently present in certain neurons of the VNC (Hudson et al., 2006). In *Drosophila*, the glypican Dallylike Dlp and syndecan are expressed in highly overlapping patterns on the surface of embryonic axons (Johnson et al., 2004) and on terminal boutons of the neuromuscular junctions (Johnson et al.,

2006). Consequently, *dlp* mutants display axon guidance and synaptic defects (Rawson et al., 2005, Johnson 2006). The different expression patterns seem to reflect distinct roles of GPN-1 in *C. elegans*, compared to its counterpart in *Drosophila*. *sdn-1; gpn-1* double mutants do also not display enhanced migration defects of HSN neurons during embryogenesis, but GPN-1 and SDN-1 seem to function redundantly in early neuroblast migration (Hudson et al., 2006). Based on the worm data, GPN-1 plays - if at all - only a minor role for the correct wiring of the nervous system in the worm. To exclude glypicans definitively from the list of HSPGs with potential functions in axon guidance, it will important to examine in addition the function of the glypican-like molecule LON-2.

The role of perlecan UNC-52 in axon guidance was tested by analyzing several hypomorphic perlecan alleles causing the progressive paralysis phenotype in a single and double mutant background with *sdn-1*. As alternative to this genetic approach, perlecan knock-down was titrated using two *sdn-1* deficient strains with different sensitivities to RNAi. The hypomorphic perlecan alleles did not cause axon guidance errors that differed significantly from the wild type, nor did any approach of reducing perlecan function cause a marked enhancement of the *sdn-1* axon guidance phenotypes (Figure 4B,C, Figure 7A). Unfortunately, RNAi of perlecan in the sensitive *lin-35; sdn-1* background did not yield any escaper L1 larvae in the second generation that could have been analyzed for axon guidance defects because all the progeny arrested at early embryonic stages. Therefore, it cannot be excluded that certain perlecan forms, required for embryonic development, also play a role later during axon guidance. Another viable perlecan allele that exhibits no paralysis phenotype, *gk3*, was found to cause low penetrance defects in commissural guidance at the level of the DNC (Don Moerman, personal communication). *gk3* eliminates laminin G domains in domain V of perlecan, whereas the here tested viable point mutations lie within domain IV, which mainly consists of Ig-like repeats. Examining a larger set of mutations in *unc-52* might therefore allow to narrow down the regions in perlecan that might be required for neural development. With respect to axon guidance, the perlecan domain that mediates binding to the basement membrane protein nidogen is of special interest, because nidogen was shown to be required for the correct positioning of longitudinal nerves in *C. elegans* (Kim and Wadsworth, 2000).

Examining a perlecan suppressor, I found that *sup-38* mutants display aberrant midline cross-overs of PVQ interneurons (Figure 4D). The epistasis analysis with *sdn-1* indicated that SUP-38 could potentially act in the same pathway as SDN-1 to control midline guidance. *Sup-38*

mutants also show some defects in circumferential guidance of D-type motoneurons, although the number of commissures that fail to reach the dorsal nerve cord per L1 larvae is low (0.24/L1 compared to 0 in the wild type). Putative null *sup-38* mutations were shown to cause maternal-effect lethality (Gilchrist and Moermann, 1992), which is reminescent of the *sqv* mutants that are defective in HS synthesis. Since *sup-38* was isolated as a dominant suppressor of viable perlecan alleles, the mutation in *sup-38* might be an unusual gain-of-function allele, which further complicates the interpretation of the double mutant analysis. The only key to understand this unexpected link between suppression of a muscle phenotype and axon guidance is probably to elucidate the molecular nature of *sup-38*.

I also analyzed two agrin alleles for potential functions in neural development. Results from the group of Ruth Chiquet in Basel showed that agrin is prominently expressed in the hypodermal ridge at the *C. elegans* midline. In the worm embryo, the left and right fascicles of the VNC are separated by motoneurons (Hobert and Buelow, 2003). During larval development, divisions and fusions of hypodermal cells create the protruding hypodermal ridge as a prominent midline structure. Based on the agrin expression pattern, it was interesting to test if loss of agrin function would impair midline guidance. The results showed that neither of the two available agrin alleles, nor RNAi of agrin by injection, caused midline guidance defects or increased midline cross-overs in an *sdn-1* null background (Figure 5C, data not shown). Furthermore, both agrin alleles did not perturb circumferential guidance of DD commissures nor did they interfere with migration of HSN neurons (Figure 5B, 5D). Increased HSN migration defects were observed in *agrin(eg1770); sdn-1(zh20)* double mutants suggesting that exon 7 of agrin might encode a region of the agrin protein that is relevant for cell migration. In order to obtain more conclusive results, it will be necessary to characterize the various splice forms of agrin and analyze further deletions, which are more likely to abolish agrin function.

Collagen XVIII CLE-1 has already been known to play a role in certain aspects of neural development. Here, I show that CLE-1 is also required for correct circumferential guidance of D-type motoneurons, which has not been tested previously (Figure 6). As in *sdn-sdn-1(ok449),* the deletion in *cle-1(cg120)* affects the two conserved HS attachment sites present in the N-terminal noncollagenous (NC1) domain. The fact, that the observed migration and guidance defects could be the cause of lacking HS and not the loss of parts of

the non-collagenous domain, has not been recognized before. RNAi against *cle-1* causes an Egl phenotype, probably due to misguided HSN neurons. However, *cg120* does not give rise to enhanced circumferential guidance defects when combined with an *sdn-1* null allele (Figure 6B). This genetic data suggests that CLE-1 acts in the same pathway as SDN-1 through a yet unknown mechanism. It is possible that CLE-1 concentrates and presents ligands in the extracellular matrix, which might be necessary to facilitate clustering of SDN-1 and axon guidance receptors.

CONCLUSIONS

This study has led to a better understanding of SDN-1 function in axon guidance. I could show that SDN-1 plays a unique role in modulating neuronal migration that cannot be provided by the cell surface HSPG glypican suggesting distinct properties of individual core proteins. Furthermore, I provide evidence that SDN-1 function in neural processes is largely mediated by its HS side chains, but eventually requires the SDN-1 transmembrane domain. The analysis of multiple deletions in predicted HSPGs and a RNAi approach failed to reveal the major substrate of the C5-epimerase HSE-5, the hypothesized HSPG X. None of the tested alleles significantly enhanced guidance defects of D-type motoneurons in a *sdn-1* deficient background like it is observed in *hse-5; sdn-1* double null mutants. Further analysis with confirmed null alleles might help to uncover neural functions of other HSPGs, in addition to SDN-1.

MATERIALS AND METHODS

Functional rescue study

$P_{\text{unc-119}}$*::gpn-1* (*pCR6*) was created by inserting the *gpn-1* cDNA amplified from a plasmid containing the complete *gpn-1* cDNA (*yk747.2a*) into the *AscI-FseI* site of *pCR3* containing the *unc-119* promoter. $P_{\text{unc-119}}$*::sdn-1ΔTM* (*pCR7*) was generated by introducing an *sdn-1* cDNA lacking the coding sequence for the transmembrane and the intracellular domain of *sdn-1* into the AscI-FseI site of *pCR3*. For $P_{\text{unc-119}}$*::sdn-1GPI* (*pCR4*), the extracellular domain of *sdn-1* was fused to the GPI-anchor sequence of *gpn-1* by PCR assembly from cDNAs (Hobert, 2002). *pCR4, pCR6* and *pCR7* were injected at 10 ng/µl, together with 60 ng/µl *lin-48::gfp* and 40 ng/µl pBluescript SK.

Primers used to generate pCR4 were:

CR1: 5' CGACGGTACCATGGTATTGATATCTG

CR2: 5' TTTGGCGCGCCATGATTCTGAAACTCAATTTCTGC (nested)

CR3: 5' TCAATTTTATCGTCATGTTTTCGCTGCATAGAAGCCATTTGCCAGTGT

CR4 5' CGAAAACATGACGATAAAATTGAAATTG (nested)

CR5: 5' CTCTGTATATACAACTAAGCAATTCAATCAA

CR6: 5' TTTGGCCGGCCTTACCTAGAACATTGAAACAAAGCAGAA

Primers used to generate pCR6 were:

CR6: 5' TTTGGCCGGCCTTACCTAGAACATTGAAACAAAGCAGAA

CR10: 5' TTTGGCGCGCCATGTTTTCTGACACTTTGGCCT

Primers used to generate pCR7 were:

CR2: 5' TTTGGCGCGCCATGATTCTGAAACTCAATTTCTGC

CR9: 5' TTTGGCCGGCCCTGCATAGAAGCCATTTGCCAGTGT

(Restriction sites are shown in blue, the fusion overhang to *gpn-1* sequence in red).

Quantitative RT-PCR

Total RNA was isolated with RNAzol B (Ams Biotechnology) according to the manufacturer's protocol, treated with DnaseI, and further purified with the RNeasy kit (Quiagen). For cDNA synthesis, purified total RNA was reverse transcribed with 250 U MultiScribe Reverse Transcriptase (Applied Biosystems) by using random primers. Relative amounts of *gpn-1* cDNA were subsequently estimated by real-time quantitative PCR in an ABI Prism 7700 Sequence detector system, by using the primers 5'GCAAAGTTCAAGGCTTTTCCAGTGAT3'/5'CTACACAAGTATTCAGGCAAATTTCCAA3', which span the sixth *gpn-1* intron. 18S rRNA was used for the internal standard.

RNAi

RNAi by feeding was performed as described in Fraser at al., 2000. 30-50 staged L1 larvae were placed on NGM agarose plates containing 2mM IPTG and seeded with *E. coli* producing double-stranded RNA (dsRNA). Adults were transferred to new RNAi plates to lay eggs. L1 larvae of the second generation were picked and analyzed for axon guidance defects by fluorescent microscopy.

Western Blot

For protein isolation, worms were washed three times with M9 buffer. 200 µl of glass beads (Sigma) were added to 400 µl of worm pellet and 200 µl of Heparinase III buffer (20mM Tris-HCl, 50mM NaCl, pH 7.4) containing protease inhibitors (PI) (CompleteMini, Roche). Then, worms were lysed by placing the tubes into the bead beater for three times 45s. Lysates were diluted with Heparinase III buffer (homogenates) or centrifuged for ten minutes at 2500 g to remove the supernatant (S1 fractions). Before gel electrophoresis, 30 µl of sample was first incubated with 1 µl of Heparinase III (Sigma) for three hours at 37°C, diluted in Heparinase III buffer with PI. For immunodetection, the monoclonal mouse anti-Δ-heparan sulfate antibody (3G10 epitope) (US Biologicals, USA) was applied 1:1000 and the secondary goat anti-mouse-HRP 1:20'000.

Genotyping

Primers to detect deletions were:

agrin(eg1770):

agr6:	5' TGGGCATACACATTTGGGTTTTCCG
agrmos:	5' GCTGCCTGCAAGGAACAAAAGG
mos2:	5' GCATTCGGTGCGATTCCGCAG

agrin(tm2051):

del1:	5' GCTCCTTCTTGCCATATAACG
del4:	5' CAAACGAGTTCATTAAATTG

cle-1(cg120):

cle-1up:	5' AAGCAAAATGAGTGAATGAAGCC
cle-1 down:	5' AAAGAGGACCTCAAGGACCACC
cle-1del:	5' ACCTTCACAACTTGCCGTCC

gpn-1(ok377), *gpn-1(tm588)*:

HB191:	5' TCCCGTTTTTCTTGGAAATG
HB304:	5' CGGTAGATATGTTGACAAGG
HB305:	5' CCTACAATCATCCAGCAGG

sdn-1(zh20), sdn-1(ok449):

OAH41:	5' TTGCCGTACACCGCCATTTCCTC
OAH139:	5' GTGTATATTTGCCCATCCGG
OAH140:	5' GCCATTCCATGAGACACTGG

sdn-1(ev697):

ev697fw:	5'CTACAGCGGTTTGTGTCGGC
ev697rv:	5'GAAGCCATTTGCCAGTGT

amplify the genomic region containing the mutation at bp 458.

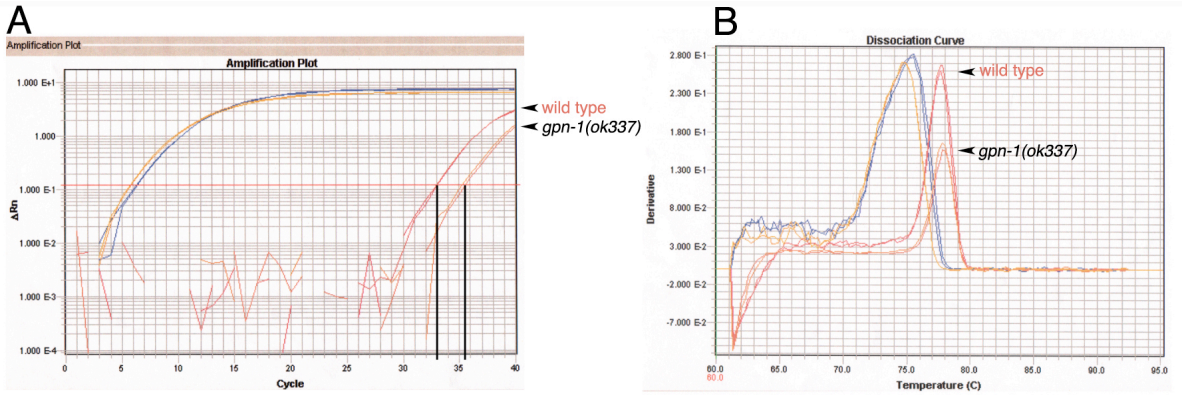

Supplementary Figure 1. QRT-PCR for *gpn-1* mRNA

(A) Quantitative RT-PCR amplification plot. Primer flanking intron 6 of *gpn-1* were used to amplify a 140 nt fragment from *cDNA* of *gpn-1(ok377)* mutants and wild-type worms. Primers for the 18S rRNA were used as an internal standard. To calculate the relative amounts of *gpn-1* cDNA, cycle values were normalized to 18S rRNA. The relative cycle difference of wild-type versus *gpn-1* cDNA was two on a log scale indicating that there was a four-fold reduction of *gpn-1 cDNA* in *ok377* compared to the wild type. The presence of *gpn-1* cDNA in *gpn-1 (ok377)* mutants suggests that *ok377* is not a null allele. **(B)** Dissociation curve of the same experiment.

REFERENCES

Ackley BD, Crew JR, Elamaa H, Pihlajaniemi T, Kuo CJ, Kramer JM (2001). The NC1/endostatin domain of Caenorhabditis elegans type XVIII collagen affects cell migration and axon guidance. J Cell Biol. 152: 1219-1232.

Asundi VK, Carey DJ (1995). Self-association of N-syndecan (syndecan-3) core protein is mediated by a novel structural motif in the transmembrane domain and ectodomain flanking region. J Biol Chem. 270: 26404-26410.

Brenner S (1974). The genetics of *Caenorhabditis elegans*. Genetics. 77: 71-94.

Bulow HE, Hobert O (2004). Differential sulfations and epimerization define heparan sulfate specificity in nervous system development. Neuron. 41: 723-736.

Cohen NA, Kaufmann WE, Worley PF, Rupp F. (1997). Expression of agrin in the developing and adult rat brain. Neuroscience. 76: 581-596.

Fraser AG, Kamath RS, Zipperlen P, Martinez-Campos M, Sohrmann M, Ahringer J (2000). Functional genomic analysis of C. elegans chromosome I by systematic RNA interference. Nature. 408: 325-330.

Gilchrist EJ, Moerman DG (1992). Mutations in the *sup-38* gene of *Caenorhabditis elegans* suppress muscle-attachment defects in *unc-52* mutants. Genetics. 1992 132: 431-442.

Glass DJ, Bowen DC, Stitt TN, Radziejewski C, Bruno J, Ryan TE, Gies DR, Shah S, Mattsson K, Burden SJ, DiStefano PS, Valenzuela DM, DeChiara TM, Yancopoulos GD (1996). Agrin acts via a MuSK receptor complex. Cell. 85: 513-523.

Halfter W, Dong S, Schurer B, Cole GJ (1998). Collagen XVIII is a basement membrane heparan sulfate proteoglycan. J Biol Chem. 273: 25404-25412.

Hartmann U, Maurer P (2001). Proteoglycans in the nervous system--the quest for functional roles in vivo. Matrix Biol. 20: 23-35.

Hobert O (2002). PCR fusion-based approach to create reporter gene constructs for expression analysis in transgenic C. elegans. Biotechniques. 32: 728-730.

Hobert O, Bulow H (2003). Development and maintenance of neuronal architecture at the ventral midline of *C. elegans*. Curr Opin Neurobiol. 13: 70-78.

Hudson ML, Kinnunen T, Cinar HN, Chisholm AD (2006). *C. elegans* Kallmann syndrome protein KAL-1 interacts with syndecan and glypican to regulate neuronal cell migrations. Dev Biol. 294: 352-365.

Johnson KG, Ghose A, Epstein E, Lincecum J, O'Connor MB, Van Vactor D (2004). Axonal heparan sulfate proteoglycans regulate the distribution and efficiency of the repellent slit during midline axon guidance. Curr Biol. 14: 499-504.

Johnson KG, Tenney AP, Ghose A, Duckworth AM, Higashi ME, Parfitt K, Marcu O, Heslip TR, Marsh JL, Schwarz TL, Flanagan JG, Van Vactor D (2006). The HSPGs Syndecan and Dallylike bind the receptor phosphatase LAR and exert distinct effects on synaptic development. Neuron. 49: 517-531.

Kim S, Wadsworth WG (2000). Positioning of longitudinal nerves in *C. elegans* by nidogen. Science 288: 150-154.

Merz DC, Alves G, Kawano T, Zheng H, Culotti JG (2003). UNC-52/perlecan affects gonadal leader cell migrations in *C. elegans* hermaphrodites through alterations in growth factor signaling. Dev Biol. 256: 173-186.

Minniti AN, Labarca M, Hurtado C, Brandan E (2004). *Caenorhabditis elegans* syndecan (SDN-1) is required for normal egg laying and associates with the nervous system and the vulva. J Cell Sci. 117: 5179-5190.

Moerman DG, Hutter H, Mullen GP, Schnabel R (1996). Cell autonomous expression of perlecan and plasticity of cell shape in embryonic muscle of Caenorhabditis elegans. Dev Biol. 173: 228-242.

Mullen GP, Rogalski TM, Bush JA, Gorji PR, Moerman DG (1999). Complex patterns of alternative splicing mediate the spatial and temporal distribution of perlecan/UNC-52 in *Caenorhabditis elegans*. Mol Biol Cell. 10: 3205-3221.

Rawson JM, Dimitroff B, Johnson KG, Rawson JM, Ge X, Van Vactor D, Selleck SB (2005). The heparan sulfate proteoglycans Dally-like and Syndecan have distinct functions in axon guidance and visual-system assembly in Drosophila. Curr Biol. 15: 833-838.

Rhiner C, Gysi S, Frohli E, Hengartner MO, Hajnal A (2005). Syndecan regulates cell migration and axon guidance in C. elegans. Development. 132: 4621-4633.

Rogalski TM, Gilchrist EJ, Mullen GP, Moerman DG (1995). Mutations in the *unc-52* gene responsible for body wall muscle defects in adult *Caenorhabditis elegans* are located in alternatively spliced exons. Genetics. 1995 139: 159-169.

Steinfeld R, Van Den Berghe H, David G (1996). Stimulation of fibroblast growth factor receptor-1 occupancy and signaling by cell surface-associated syndecans and glypican. J Cell Biol. 133: 405-416.

Wang D, Kennedy S, Conte D Jr, Kim JK, Gabel HW, Kamath RS, Mello CC, Ruvkun G (2005). Somatic misexpression of germline P granules and enhanced RNA interference in retinoblastoma pathway mutants. Nature. 436: 593-597.

Wang L, Denburg JL (1992). A role for proteoglycans in the guidance of a subset of pioneer axons in cultured embryos of the cockroach. Neuron. 8:701-714.

Waterston RH (1988). Muscle, pp 281-336 in *The Nematode, Caenorhabditis elegans*, edited by WB Wood. Cold Spring Harbour Laboratory, Cold Spring Harbor, N.Y.

CHAPTER 4

Identifying new genes in HS-dependent
axon guidance signaling

INTRODUCTION

In *C. elegans*, various types of genetic screens have been successfully conducted to identify genes and entire signaling pathways (Jorgensen and Mango, 2002). The most straightforward method for identifying new genes that function in a given process is to screen for more mutants with the same phenotype. This strategy works well, in particular for mutants with a clearly visible phenotype (Brenner, 1974). Alternatively, components of a genetic pathway can also be uncovered in modifier screens (e.g. enhancer or suppressor screens): The screen is performed with a mutant strain that shows a defined phenotypic defect. Worms with second-site mutations after mutagenesis leading to an enhancement or suppression of the initial phenotype will be analyzed. These second-site mutations often identify proteins that are involved in the same process as that disrupted in the starting strain.

In order to find new components of HS-dependent axon guidance signaling in *C. elegans*, the pathfinding of commissural D-type motoneurons was chosen as neural process to be studied for several reasons. First, defects in circumferential guidance of this group of axons are observed in *sdn-1* mutants and all HS-modifying enzyme mutants. Second, the dorsal guidance of the D-type commissures is mainly mediated by UNC-6 (Hedgecock et al., 1990; Ishii et al., 1992), a guidance cue that shows a conserved function across all species. In contrast, midline guidance, for example, is known to be controlled by several partially redundant guidance systems (Zallen et al., 1999). Third, defects in this type of motoneurons result in impaired movement of the worms, whereby the severity of the locomotion phenotype is proportional to the number of commissures that are affected. Therefore, the uncoordinated (Unc) phenotype serves as a rough visible indicator of axon guidance defects of D-type commissures. D-type motoneurons, which include 6 DD neurons and 13 VD neurons, are GABA-ergic motoneurons that innervate the dorsal and ventral body muscles, respectively. During locomotion of the worm, when muscles are contracted on one side, the muscles on the opposite side are relaxed through secretion of the inhibitory GABA neurotransmitter by D-type motoneurons (McIntire et al., 1993). Last, D-type motoneurons were chosen because gfp-marked commissural axons are clearly visible in moving worms as well as anaesthesized animals under the microscope, which facilitates the detection and quantification of the defects.

In previous genetic experiments, we provided evidence that syndecan SDN-1 and the HS C5-epimerase HSE-5 act in parallel pathways, which both impinge on motoneuron axon guidance (Rhiner et al., 2005). D-type commissures show guidance errors in both *sdn-1* and *hse-5* single mutants, but the defects are rather subtle and can only be detected under a high power fluorescent microscope. Screening for mutants using a high power fluorescent microscope is very laborious and greatly limits the number of worms that can be screened. Therefore, I designed two modifier screens that can be performed under a low power dissecting scope. These screens should allow me to identify new components in HS-dependent guidance signaling. In a suppressor screen, *hse-5; sdn-1* double mutants, which are severely uncoordinated (Unc), were mutagenized and the progeny was screened for worms with normal locomotion. Suppressors of the Unc phenotype are likely to identify downstream components of either signaling pathway. The second screen was based on mutagenesis of either *sdn-1* or *hse-5* single mutants, which carry a *gfp* reporter in the background to visualized D-type motoneurons. The F2 generation of the mutagenized worms was screened directly under a high magnification fluorescent dissecting scope for mutants with strong guidance defects of D-type commissures. Enhancer mutations identified in the *sdn-1* null background are likely to identify components of the HSE-5-dependent guidance pathway and vice versa (Figure 1).

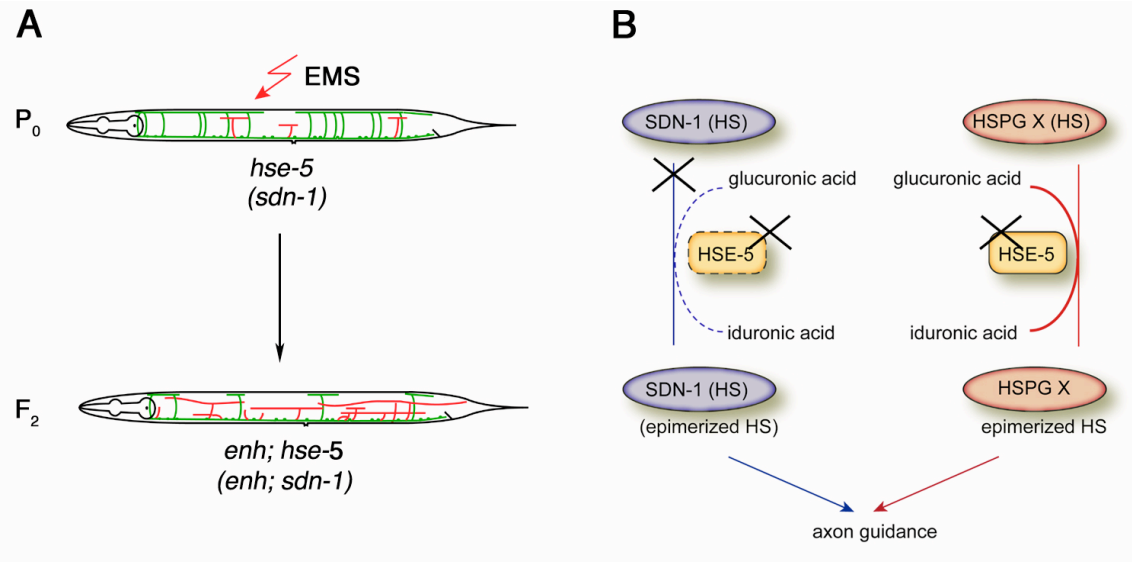

Figure 1. Enhancer screen for commissural guidance defects

(A) Scheme depicting the strategy of the enhancer screen. *hse-5* or *sdn-1* single mutants are mutagenized with EMS. Strains always carry the *oxIs12* (P_{unc-47}*::gfp)* transgene in the background to visualize D-type motoneurons. Adult worms of the F2 generation were screened for animals with severe commissural guidance defects, similar to those observed in *hse-5; sdn-1* double mutants. **(B)** Double null mutants of *hse-5* and *sdn-1* display strongly enhanced commissural guidance defects, compared to either single mutant suggesting that SDN-1 and HSE-5 act in parallel pathways to promote correct axon guidance. HSE-5 might still act on SDN-1, but loss of epimerized HS on SDN-1 probably causes only a subtle impairment of SDN-1 function. Enhancer mutations in the *hse-5* background might identify components in the parallel SDN-1-dependent axon guidance pathway and vice versa. Note that the major substrate of HSE-5, designated as HSPG X, is still unknown.

As I describe below, it was not possible to identify a mutation that markedly suppressed the locomotion defects of *hse-5; sdn-1* double null mutants. On the other hand, the enhancer screens yielded 14 enhancers in the *hse-5* background and one enhancer mutation in *sdn-1* deficient worms so far. I backcrossed the seven strongest *hse-5* enhancers to the *hse-5* null background and characterized the phenotypes of the three times backcrossed strains. The different enhancers cause at least three distinct phenotypes: **I**. a premature stalling and meandering of D-type commissures before reaching the dorsal nerve cord (DNC), **II**. longitudinal instead of dorsal extension of D-type axons in the ventral nerve cord (VNC) and **III.** severe axon outgrowth defects. Using a fragment length polymorphism (FLP) -based mapping strategy, the enhancers *op464* and *op472* have been localized to the left arm of chromosome I (ChI), *op459* to the right arm of chromosome II (ChII) and *op460*, *op462*, *op468* and *op469* to the left arm of chromosome IV (ChIV). Although the genes affected by

the enhancer mutations have not been identified yet, the here-described enhancers are likely to reveal new components involved in SDN-1-dependent axon guidance signaling.

RESULTS

Enhancers of commissural guidance errors in *hse-5* mutants

In order to identify proteins involved in the SDN-1-dependent guidance pathway, *hse-5* mutants were mutagenized with EMS and the F2 generation was searched for worms that display severe defects in circumferential guidance of D-type commissures, e.g. similar to those observed in *hse-5; sdn-1* double mutants (Figure 1). The *oxIs12 (P_{unc-47}::gfp)* reporter was used to visualize motoneuron anatomy. The enhancers were directly identified based on extensive lateral mis-projections of commissures or the absence of a DNC line, which indicated a major lack of commissures. Stephan Gysi, a diploma student who worked with me on this project, screened 11'000 haploid genomes and identified 14 verified enhancer mutations (Gysi S., diploma thesis 2005). Among these, seven enhancers seemed to phenocopy the strong guidance defects of motoneurons observed in *hse-5; sdn-1* double null mutants, whereas the enhancement of guidance defects was less pronounced in the remaining seven candidates. Together, we also started with an identical enhancer screen with *sdn-1* null mutants. We screened 7'500 haploid genomes and have obtained a single enhancer candidate, which showed a significant increase of D-type guidance errors (Gysi S., Diploma thesis 2005). It has to be stated, however, that this results derive from a single round of mutagenesis, which will have to be repeated several times to find more enhancers.

Suppressors of commissural guidance defects in *hse-5; sdn-1* double mutants

For the suppressor screen, *hse-5; sdn-1* double mutants, which are strongly Unc, were mutagenized with EMS. Mutagenized P0's were distributed on big plates and the worms were allowed to grow for several generations until the plates were starved. Then, a part of the starved animals were placed on the edge of a plate that contained bacterial food in the center, and the plate was searched 2 hours and 24 hours later for animals with markedly improved locomotion that might have crawled to the lawn of food. Screening through 30'000 haploid genomes did not identify any clear suppressor of the locomotion defects of *hse-5; sdn-1* double mutants (Gysi S., diploma thesis 2005), suggesting that there likely are no genes – that, through simple loss of function, can suppress the Unc phenotype of *hse-5; sdn-1* double mutants.

Characterization of identified enhancers (*hse-5* mutant background)

In order to examine whether any new *sdn-1* alleles were isolated among the selected *hse-5* enhancers, I sequenced the *sdn-1* locus in all *enh; hse-5* strains, but did not encounter any mutations. Next, I backcrossed the seven strong enhancers three times to the *hse-5* background and quantified the motoneuron defects in L1 larvae (Figure 2).

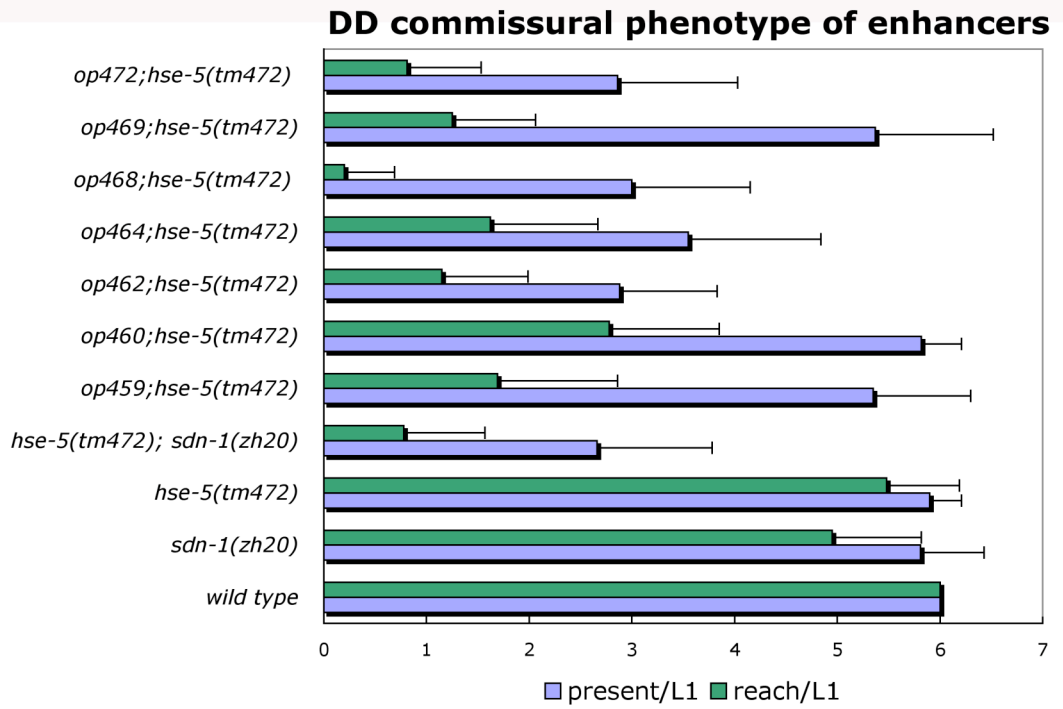

Figure 2. Enhancers that phenocopy the commissural guidance defects of *hse-5; sdn-1* double null mutants. The graph shows the quantification of DD commissural guidance defects in L1 larvae. Blue bars represent the number of commissures that detectably exit the VNC. Green bars show the number of commissures that reach the level of the DNC. The enhancer mutations were generated in the *hse-5* mutant background and all cause severe defects in circumferential guidance to the DNC. Note that *op459* and *op469* do not display the axon outgrowth defects that are typical for *hse-5; sdn-1* double mutants (blue bars). Error bars indicate the standard deviation, n ≥ 40 for all strains.

The five enhancers *op460, op462*, *op464, op468* and *op472*, combined with the *hse-5* mutation, most closely resembled the phenotype of *hse-5; sdn-1* double mutants, where half of the commissures fail to grow out or incorrectly extend in the VNC and only one commissures on average reaches the DNC (Figure 2). In *hse-5* worms carrying the enhancer mutations *op459* and *op469*, almost all the six DD commissures extended visibly, but failed to reach the level of the DNC (Figure 2). *op468* caused highly penetrant outgrowth and

guidance defects in DD motoneurons, which were even more severe than those observed in *hse-5; sdn-1* double mutants.

Besides quantitative differences in the number of outgrowing commissures, the different enhancers also showed qualitative differences in the patterning of D-type motoneuron defects. In *op459; hse-5* and *op469; hse-5* worms, the DD commissures initially grow out normally in a dorsal direction, but then stop prematurely to extend longitudinal uni-or bilateral branches (Figure 3A, 3B, 3G), a phenotype that is reminiscent of *unc-6*/netrin mutants, whereas many commissures in *op462; hse-5* or *op468; hse-5* animals immediately stop growing after exiting the DNC (Figure 3C, 3D, 3F). The commissures of *op464; hse-5* worms also show severe outgrowth defects except for the most posterior commissures, which are usually unaffected (Figure 3E).

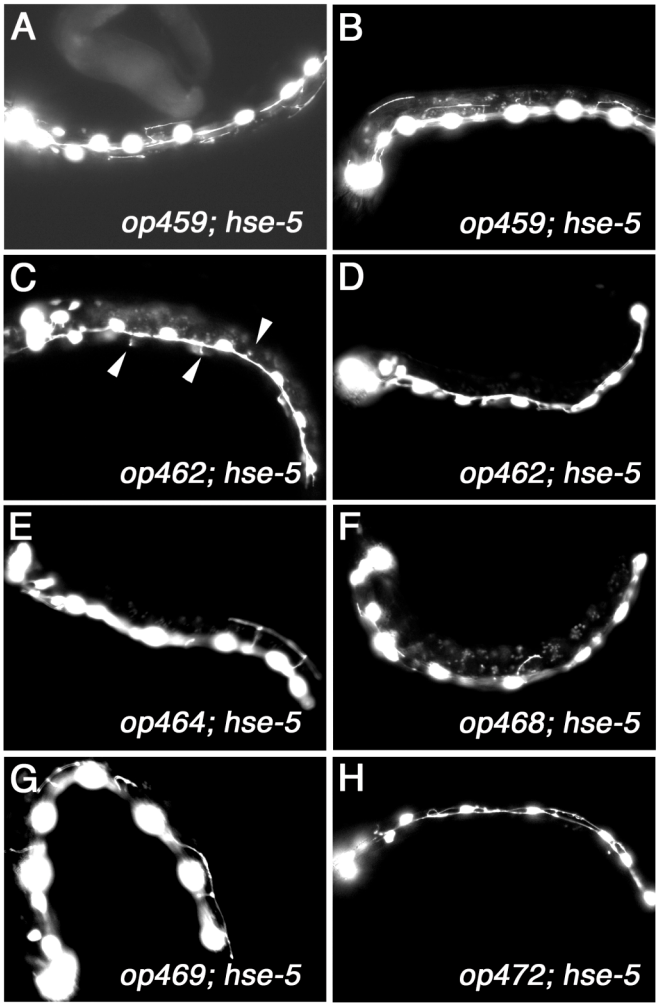

Figure 3. Different enhancers cause distinct commissural phenotypes. DD motoneurons of L1 larvae. Anterior is to the left, dorsal is up in side views (3B, 3D, 3E, 3F, 3G), ventral aspects are shown in 3A, 3C and 3H. In *op459; hse-5* and *op469; hse-5* worms, commissures grow out and mis-project laterally instead of dorsally (3A, 3B). *op462*, *op464, op468,* and *op472* additionally affect outgrowth of commissures (arrowheads 3C, 3D, 3E, 3F, 3H). Note that commissures 5 and 6 are often wild-type in *op464; hse-5* (3E). D-type motoneurons are visualized with the *oxIs12 gfp* reporter.

Locomotion defects and other visible phenotypes

Severely perturbed axon guidance of D-type motoneurons results in impaired backward and forward locomotion of most *enh; hse-5* strains (Table 1). *op462; hse-5* and *op468; hse-5* worms are unable to move backwards when they receive a mechanical stimulus on their head. Furthermore, several of the *enh; hse-5* lines are egg-laying defective (Egl) and exhibit a dumpy body morphology (Dpy), which is also the case for *hse-5; sdn-1* double null mutants. The Egl phenotype could either be the consequence of defects in vulva development or due to defective innervation of vulval muscles by HSN neurons. Since 56% of *hse-5* single mutants show misguided HSN axons (Bülow and Hobert, 2004), the latter possibility seems to be more likely. *op468; hse-5* worms occasionally showed a notched head morphology.

Table 1
Locomotion defects and morphology of *hse-5* enhancer strains

genotype	locomotion		morphology	
	Unc (fw)	Unc (rv) bends	Egl	Dpy
hse-5(tm472)	-	6.8	-	+
op459; hse-5	+	3.3	-	+
op460; hse-5	++	2.5	-	+
op462; hse-5	+++	1.5	++	+
op464; hse-5	+++	2.5	++	++
op468; hse-5	+++	1.5	++	++ (n)
op469; hse-5	++	3	+	+
op472; hse-5	+	5.25	+	+

+ stands for weak, ++ moderate and +++ strong locomotion defects.
Unc (rv) bends indicates the average number of reverse bends performed after tapping on the head of mutants (n = 6), n stands for notched head.

Mapping of enhancer mutations

In order to assign the enhancer mutations to a chromosome, I took advantage of the FLP-mapping method (Zipperlen et al., 2005). The second-site mutations in the *hse-5* mutants have been generated in the standard wild-type strain N2 (*C. elegans* variety Bristol). Therefore, the enhancer mutation is always associated with the Bristol background. For FLP-mapping, the *enh; hse-5* hermaphrodites were crossed to *hse-5* males, which have been backcrossed multiple times to the polymorphic strain CB4856 (*C. elegans* variety Hawaii). Both strains also carried the gfp reporter *oxIs12* in the Bristol and Hawaii background, respectively. In the F2, I selected worms homozygous for the enhancer (e.g. strong guidance defects of D-type commissures) and analyzed them for the distribution of Bristol versus Hawaii FLPs. First, chromosomal linkage was established with two centrally located FLP assays per chromosome

(Zipperlen et al., 2005). The assay mapped *op459* on ChI, *op464* and *op472* on ChII and *op460*, *op462*, *op468* and *op472* on ChIV (Figure 4).

The different enhancers were subsequently fine-mapped using eight different FLP assays along ChI, II and IV (Figure 5). The FLP analysis showed that o*p464* and *op472* both locate to the left arm of ChI, to a 1.9 Mb and 2.9 Mb interval between the FLP markers Zh1-07/Zh1-03 and Zh1-17/Zh1-07, respectively (Figure 5, results shown for o*p464*). *op459* was assigned to the right arm of ChII between Zh2-20/Zh2-12, which corresponds to a 5.4 Mb interval (Figure 5). The remaining four enhancers mapped to the left arm of chromosome IV. For *op460* the interval could be reduced to a 2.8 Mb region between Zh4-05/Zh4-16; *op462* and *op469* were positioned between Zh4-05/Zh4-02, in a 5.2Mb interval and the *op468* mutation must lie somewhere between Zh4-05 and Zh4-21, a large 11.2 Mb interval (Figure 5, data shown for *op462* and *op469*).

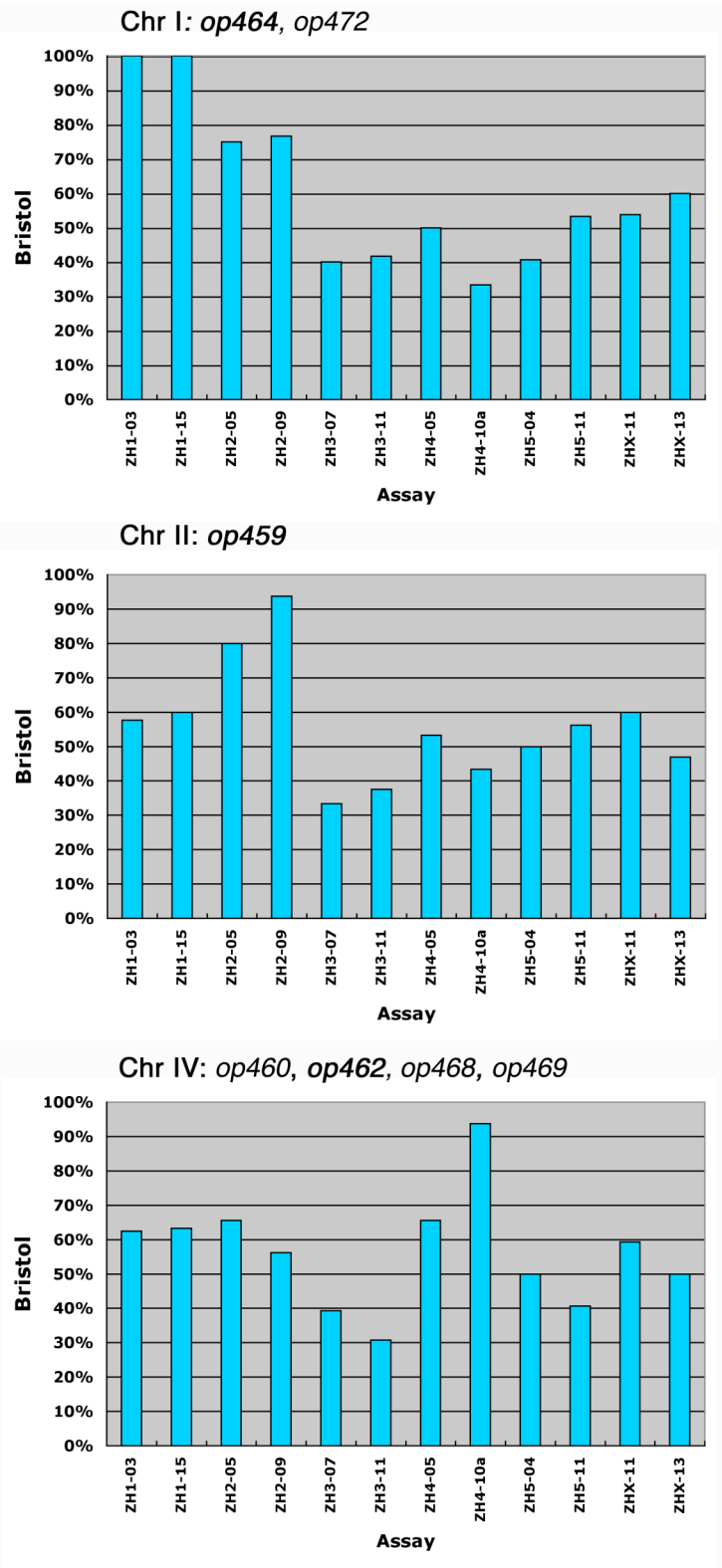

Figure 4. Assignment of enhancer mutations to a chromosome using FLP- mapping. Typical results of Tier 1 assays (Zipperlen et al. 2004) are shown for chromosomes I, II and IV. The graph for chromosome I corresponds to Tier 1 data of *op464*, the graph for chromosome IV represents Tier 1 data for *op462*.

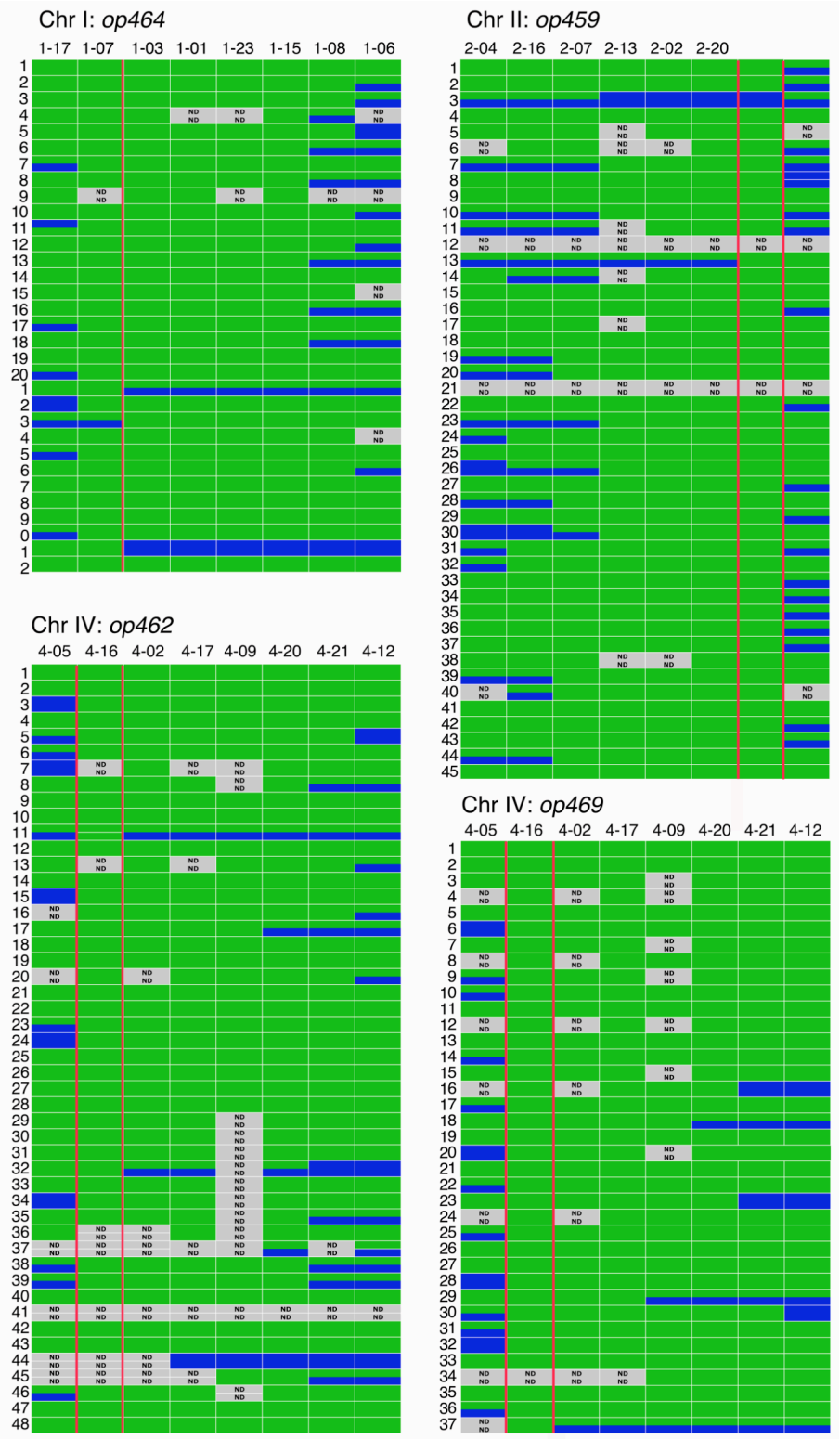

Figure 5. Mapping of enhancers to sub-chromosomal regions. Results of Tier 2 assays (Zipperlen et al. 2004) are shown for *op464*, *op459*, *op460* and *op469*. Blue boxes, Hawaii, green boxes, Bristol. ND, no data because of PCR failure.

Netrin signaling acts independent of syndecan to guide commissural neurons

The described enhancer screen for defects in circumferential guidance could also yield mutants for already known axon guidance receptors and ligands. To address this concern, I have tested if mutations in several key axon guidance systems affect the pathfinding of D-type commissural axons.

The role of the UNC-6/netrin guidance system in dorsal guidance of D-type commissures is well established. UNC-6, which is secreted by epidermoblasts and the pioneer neurons AVG and PVT at the ventral midline, forms a ventral-dorsal gradient (Wadsworth et al., 1996) (Figure 6A). Ventrally extending axons express the UNC-40/DCC receptor that mediates attraction to UNC-6 (Lim et al., 1999), while dorsally migrating axons additionally express the receptor UNC-5. UNC-5 mediates repulsion from UNC-6, together with UNC-40. First, I tested a presumptive null allele of *unc-40, unc-40(e1430)* to confirm these findings. In *unc-40(e1430)* mutants, 50% of the DD commissures in L1 larvae did not reach the DNC (Figure 6C). In *unc-6* and *unc-5* null mutants, about 35% and 26% of the D-type commissures grow out of the VNC, but none of them reaches the DNC (Huang et al., 2003). Therefore, *unc-40(e1430)* was used for double mutant analysis with *sdn-1* and *hse-5* null mutants. *unc-40; sdn-1* double null worms are severely Unc, grow slowly and have a low brood size. Surviving L1 larvae show a strong enhancement of guidance defects compared to either *unc-40* or *sdn-1* single mutants (Figure 6B, 6C). Double mutants of *hse-5* and *unc-40* repeatedly died and viable progeny was never obtained. These results show that the Unc-6/netrin system acts in parallel of HS-dependent signaling for the development of D-type motoneurons. Hence, screening for enhancers in the *sdn-1* and *hse-5* backgrounds could eventually identify mutations in components of the UNC-6/netrin signaling pathway, but most likely only certain hypomorphic alleles since the double mutants with *unc-40* were already semi-viable or lethal.

A null allele of slit *slt-1* and strong hypomorphic alleles of *vab-1*/ephrinR and *ina-1*/integrin did not significantly affect dorsal guidance of DD commissures (Figure 6C). SLT-1 and its receptor SAX-3 are known to play a role in the left/right choices of D-type axons to exit the VNC, but are not involved in dorsal guidance of the commissures (Bülow and Hobert, 2004). Lack of SLT-1 in worms devoid of SDN-1 does not lead to more severe defects of DD motoneurons. *sdn-1 sax-3* double mutants were obtained by taking advantage of *tra-2(q276)* transforming males to bypass the sterility of both strains, but the double mutant could not be maintained. *ina-1*; *sdn-1* double mutants are lethal. *vab-1; hse-5* double mutants showed a

high embryonic lethality. Escaper L1 larvae displayed a detectable increase in guidance errors compared to *hse-5* single mutants, but the enhancement was not as pronounced as in *unc-40; sdn-1* worms. Because null alleles of *vab-1* are lethal (George et al., 1998) and a strong hypomorphic allele of *vab-1* only moderately increases the commissural guidance defects of *hse-5* worms, mutations in *vab-1* are not likely to be selected for in the screen. Last, I tested if wnt signaling could be affected in *sdn-1* or *hse-5* mutants since HSPGs are required for proper wnt signaling in *Drosophila* (Bornemann et al., 2004). To this end, I analyzed the anterior-posterior polarity of PLM neurons in *hse-5*, *sdn-1* and *hse-5; sdn-1* double mutants, but did not find any signs of reversed PLM polarity, a characteristic phenotype of wnt signaling mutants (Hilliard and Bargmann, 2006).

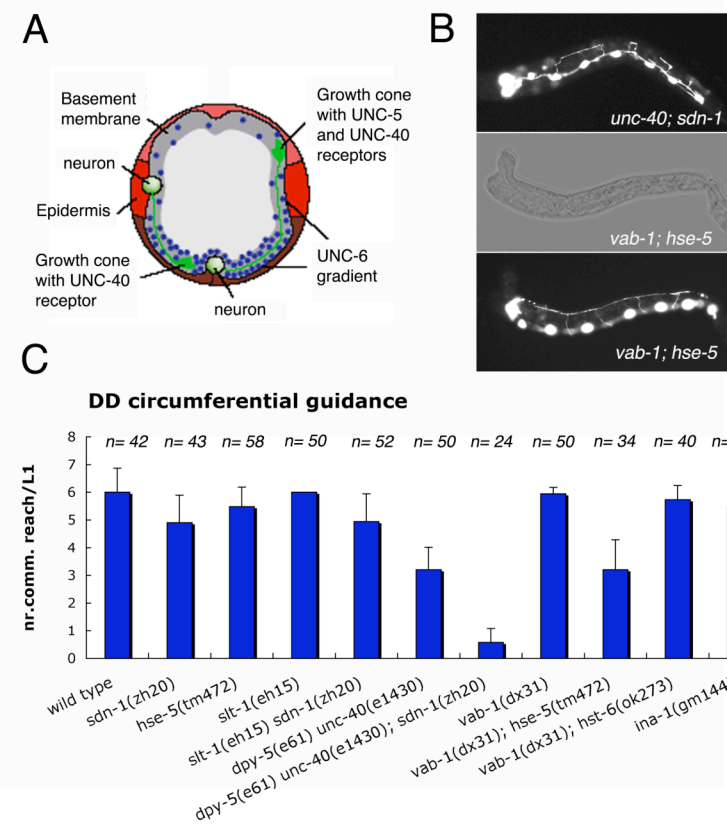

Figure 6. Axon guidance signaling pathways implicated in D-type commissural guidance. (A) Axons extend along the body wall in response to a graded distribution of UNC-6 (blue), which peaks at the ventral midline. Growth cones expressing UNC-40 and UNC-6 migrate dorsally, while those expressing UNC-40 migrate ventrally (adapted from Wadsworth, 2002). **(B)** DD commissures in L1 larvae. **(C)** The graph depicts the number of DD commissures that reach the dorsal nerve cord. Error bars indicate the standard deviation.

DISCUSSION

HSPGs have been recognized as important regulators of axon guidance signaling. Nevertheless, it is not clear which HS core proteins can modulate guidance signals and what are the downstream mediators of this HS-dependent pathway(s). In a screen for enhancers of motoneuron axon guidance defects in *sdn-1* and *hse-5* mutants, which were shown genetically to act in parallel pathways, we have identified seven strong *hse-5* enhancers and one potential *sdn-1* enhancer. The strong *hse-5* enhancers were backcrossed and mapped to different subchromosomal regions on chromosomes I, II and IV (see Figure 7 for an overview). The characterized enhancers might encode genes that impinge directly on SDN-1- dependent axon guidance signaling or another parallel pathway. A suppressor screen, which allowed to screen a large number of mutagenized *hse-5; sdn-1* double mutants for improved locomotion (30'000 haploid genomes), did not yield any strong suppressors. In principle, suppression of one of the two pathways, the SDN-1-dependent or the HSE-5-dependent, should have restored locomotion since the single mutants are not Unc. It could be, that suppression of either pathway is only possible by very rare gain-of-function mutations in a few key regulators and therefore we did not find any suppressors in the screen. On the other hand, we might have missed suppressors because we only looked for suppression of the Unc phenotype, which could be too simplistic, and not for suppression of the motorneuron defects.

Possible enhancers of motoneuron guidance in *hse-5* mutants

Using standard concentrations of mutagen, the frequency at which mutations at any particular locus are recovered is about one null mutation for every 3000-8000 copies of the gene that is analyzed in the screen. Screening through 11'000 haploid genomes, we found seven strong enhancers in at least three different genes considering that *op464* and *op472* on ChI and *op460*, *op462*, *op468* and *op469* on ChIV might be alleles of the same gene. The number of the obtained strong enhancers appears reasonable, compared to the theoretical value. We also expected to recover additional *sdn-1* alleles, which would have validated the screening approach. However, none of the strong enhancers mapped on chromosome X and sequencing confirmed that the *sdn-1* locus is wild-type in all fourteen isolated enhancers indicating that the screen has not reached saturation yet.

The analysis of *unc-40*; *sdn-1* double null mutants revealed that UNC-6/netrin signaling through UNC-40 is independent of SDN-1 and probably also of HSE-5, because of the

lethality of *hse-5; unc-40* double mutants. Loss of SDN-1 function in *unc-40* mutants lead to fully penetrant guidance defects of D-type motoneurons as observed in *unc-5* and *unc-6* null mutants (Figure 6C) (Hedgecock et al., 1990; Huang et al., 2003).

unc-5-dependent signaling in dorsal guidance of motoneurons

The incomplete penetrance of many axon and cell migration defects observed in null alleles of *unc-5*, *unc-6* and *unc-40* mutants was already interpreted as evidence for a second, *unc-5*-independent pathway in dorsal migration by Edward Hedgecock, Joseph Culotti and David Hall in 1990 (Hedgecock et al., 1990). Our results show, that a HS-dependent pathway regulates the dorsal outgrowth of D-type motoneurons, in parallel to UNC-5. These findings imply that hypomorphic *unc-5* alleles could be present among the selected *hse-5* enhancers. *unc-5* is located on ChIV, between the FLP markers Zh4-16 and Zh4-2, outside the mapping interval for *op460*, but still inside the larger intervals obtained for *op462*, *op468* and *op469* (Figure 7). The *unc-40* gene localizes to the center of ChI, distant from the mapping interval of *op472* and *op464* on the left arm of I (Figure 7).

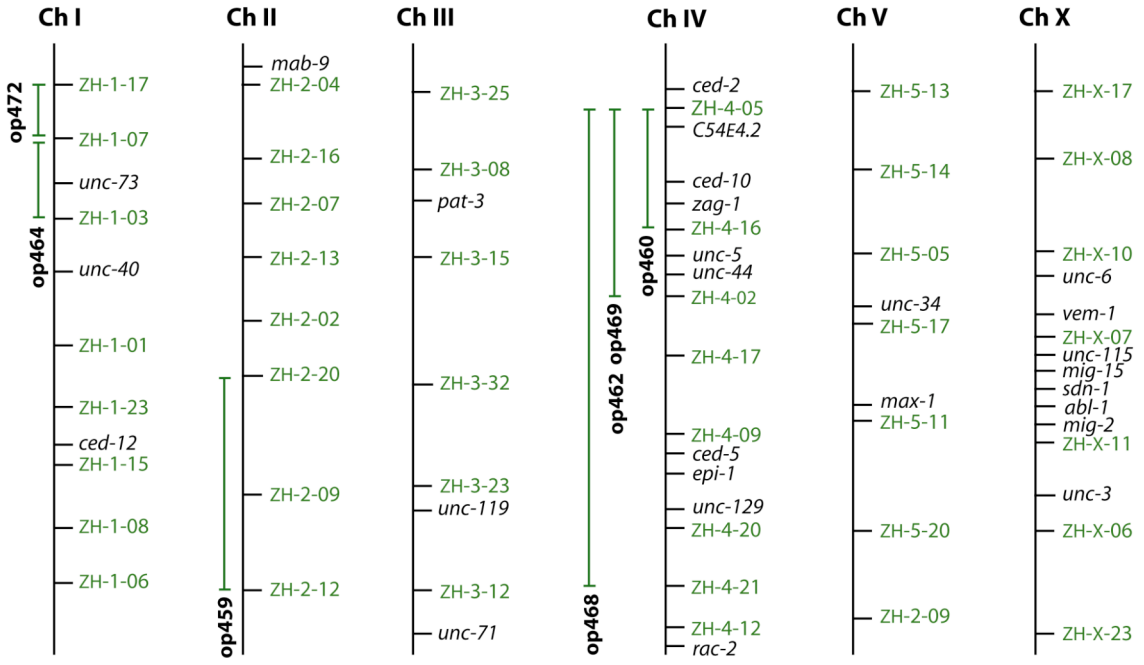

Figure 7. Positions of *hse-5* enhancers and known genes involved in motoneuron development.
Graphic depicting the mapping progress of the seven strong *hse-5* enhancers. Determined FLP-mapping intervals are shown in green. The genes indicated in black have previously been described to play a role in D-type motoneuron development, except for C54E4.2, a gene homologous to mammalian testicans.

When UNC-5 is ectopically expressed in the AVM touch neuron, which normally extends ventrally, the axon is driven to the dorsal side in an UNC-6/netrin-dependent manner (Hamelin et al., 1993). Further genes that are implicated in *unc-5*-mediated axon guidance of D-type motoneurons were identified in a screen for suppression of defects in AVM axon guidance induced by ectopic UNC-5 expression (Colavita and Culotti, 1998). The suppressor screen yielded eight genes, which are required for UNC-5-induced dorsal steering of touch neurons*: unc-6*, *unc-40*, *unc-34*, *unc-44*, *unc-129*, *seu-1*, *seu-2* and *seu-3*. Although these genes were identified under artificially induced conditions, *unc-6*, *unc-40*, *unc-34*, *unc-44* and *unc-129* were all found to be required for the physiologically relevant dorsal guidance of D-type motoneurons controlled by UNC-5 (Colavita and Culotti, 1998). Furthermore, *unc-34*, *unc-44* and *unc-129* mutants also showed circumferential guidance defects of DA/DB motoneurons, which are unaffected in *sdn-1* and *hse-5* worms (Bülow and Hobert, 2004; Rhiner et al., 2005).

UNC-34/Enabled is a conserved profilin-binding protein that regulates actin dynamics and therefore motility of neuronal growth cones (Lanier and Gertler, 2000; Dickson, 2001). In *C. elegans* touch neurons, UNC-34/Ena is the downstream effector of UNC-40-mediated attraction and acts in parallel to Rac and UNC-115/AbLIM (Gitai et al., 2003). UNC-44 is an ankyrin-related protein, which is required for axon outgrowth and guidance for many classes of neurons (Siddiqui and Culotti, 1991; McIntire et al., 1992; Otsuka et al., 1995). Ankyrins are spectrin-binding proteins that link integral membrane proteins to the underlying cytoskeleton (Bennett, 1992). They are known to associate with members of the Ig super-family of cell adhesion molecules (neurofascin, L1, NrCAM) (Davis and Bennet, 1994), which control important aspects of axon guidance (Stoeckli and Landmesser, 1995). Unlike *unc-34* (ChV), *unc-44* is situated within the FLP-interval of *op462, op468* and *op469* on ChIV (Figure 7). *unc-44* mutants show a distinct phenotype for the misguided motoneuron commissures than that observed in *unc-5* worms. In *unc-44* mutants, the commissures often reach the DNC, but in a rather indirect path. In addition, the neuronal cell bodies in the VNC are often mispositioned (McIntire et al., 1992; Colavita and Culotti, 1998). We did not detect any obvious mispositioning of DD neuronal cell bodies in the enhancer candidates on ChIV, but the VNC will have to be examined in more detail to address this question. UNC-129 is a TGF-β homolog that functions non-cell-autonomously to control dorsal guidance of commissural motoneurons in *C. elegans* (Colavita et al., 1998). The *unc-129* gene maps to the

right arm of ChIV, which is still covered by the large preliminary mapping area for *op468* (Figure 7).

Other genes with known roles in commissural guidance

Small GTPases of the Rho family (Rho, Rac and Cdc42) are key regulators of the actin cytoskeleton; they are thought to be the downstream effectors of all axon guidance signaling pathways. The *C. elegans* genome contains three rac-like genes, *ced-10, mig-2* and *rac-2*. D-type motoneurons are unaffected in *mig-2* null mutants, strong hypomorphic alleles of *ced-10* and worms treated with RNAi against *rac-2* (Lundquist et al., 2001). However, *ced-10*; *mig-2* double mutants display severe defects in axon outgrowth and circumferential guidance of D-type motoneurons and exhibit a defasciculated VNC, similar to the defects observed in *hse-5*; *sdn-1* double mutants (Lindquist et al., 2001; Wu et al., 2002; Rhiner et al., 2005). Moreover, *ced-10*; *mig-2* and *hse-5*; *sdn-1* double mutants both display a characteristic Dpy body shape, often with a withered tail, and they are Egl and Unc. This indicates that *ced-10* and *mig-2* act in partially redundant pathways and might act downstream of *hse-5* and *sdn-1*. *ced-10* is located in the sub-chromosomal region defined by the FLP-markers Zh4-05 and Zh4-16 on ChIV (Figure 7). Complete loss-of-CED-10-function is lethal, but hypomorphic *ced-10* alleles could be enhancers of motoneuron guidance defects in a *hse-5* mutant background.

Mutants for the rac regulators CED-2, CED-5 and CED-12 all exhibit mild defects in D-type commissural guidance (Wu et al., 2002). UNC-73, a guanine nucleotide exchange factor (GEF), was shown to act upstream of CED-10 and MIG-2 in the development of D-type motoneurons (Wu et al., 2002). *unc-73* mutants display defects in cell migration, axon outgrowth and guidance (Steven et al., 1998). The gene is located in the FLP-mapping interval on ChI (Figure 7). Mutations in *unc-73* are likely to cause strong commissural guidance defects, independent of *hse-5*, and could therefore also be wrongly selected as enhancer of *hse-5* in the screen.

For further analysis of the enhancer mutations, it will be informative to determine if they are dependent on *hse-5* or if they also cause guidance errors on their own. Preliminary data indicates that enhancement of *op459* is dependent on *hse-5*, whereas *op468* causes commissural guidance defects on its own, but only leads to impaired commissural outgrowth in combination with *hse-5*.

Further proteins involved in development of D-type motoneurons are MAX-1 (required for **m**otoneuron **a**xon **g**uidance), UNC-71, a disintegrin and inactive metalloprotease and the laminin EPI-1 (Forrester and Garriga, 1997; Huang et al., 2002; Huang et al., 2003). Moreover, the patterning of D-type commissures is regulated by UNC-3, an Olf/EBF family transcription factor and MAB-9, a T-box DNA binding protein (Huang et al., 2002; Huang et al., 2003). The conserved protein UNC-119 plays an important role in maintenance of D-type commissures, whereas the Zn-finger homeodomain transcription factor ZAG-1 controls outgrowth and guidance of D-type axons among several other neuron classes (Knobel et al., 2001; Wacker et al., 2003). A direct interaction between the Nck-interacting kinase MIG-15 and the β1 integrin PAT-3 is also thought to contribute to commissural axon navigation (Poinat et al., 2002). In worms lacking VEM-1, a novel membrane protein, not only ventral-dorsal guidance of commissures, but also longitudinal guidance of interneurons is affected (Runko and Kaprielian, 2004). Of all these genes, only *zag-1* on ChIV lies within an enhancer FLP-interval (Figure 7).

The identified enhancers of commissural guidance defects in *hse-5* mutants on ChI and IV might eventually correspond to genes, which were already implicated in motoneuron development such as *unc-5*, *ced-10*, *unc-44* and *zag-1* (ChIV) or *unc-73* (ChI). Genetic complementation tests with theses candidates will show if the enhancers are alleles of the above-mentioned genes or if they represent novel regulators of HS-dependent axon guidance. Additional complementation tests with the enhancers on ChIV and ChI will reveal if they are alleles of the same gene. Previous screens were not conducted in a sensitized background such as the chosen *hse-5*-deficient background here. Therefore it is likely, that at least some of our enhancers will identify novel genes. Indeed, *op459* on ChII is likely to identify a new gene required for motoneuron development since none of the described genes are located in this FLP-interval.

MATERIAL AND METHODS

Enhancer screen

For mutagenesis, staged *hse-5(tm472)* or *sdn-1(zh20)* L4 larvae carrying the *oxIs12* (P_{unc-47}*::gfp*) transgene, were centrifuged for 1 min at 2000rpm in a microfuge and resuspended in 4 ml M9 buffer. 20 µl of ethyl methanesulfonate (EMS) (9.4 M stock solution) (Sigma) were added and the worm suspension was kept for 4h at RT on a rotating wheel. Then, the worms

were washed four times with M9 buffer and distributed onto freshly seeded plates to recover overnight at 15° C. The following morning, young adults were distributed to big seeded plates (3 worms/plate, 12 animals in total). These P0 worms were kept at 15° C and transferred to new plates 2-3 times/per day for about 5 days. The F1 generation was grown at 20°C and removed when the F2 generation reached the L1 larval stage. The number of F1 animals per plate was used to estimate the number of haploid genomes screened. Shortly before screening the F2 for commissural guidance defects, the plates were placed at 4° C to slow down the movement of the worms. Worms were screened on NGM agarose plates to reduce background fluorescence. Commissural phenotypes were examined under a Leica MZ16FA fluorescent dissecting scope with Planapo 2.0x lens.

FLP-mapping

To generate the mapping strain, *hse-5(tm472)* and *oxIs12* were backcrossed individually 12 times to the Hawaii background before crossing them together to obtain *hse-5; oxIs12* Hawaii worms. *hse-5; oxIs12* Hawaii males were crossed to *enh; hse-5* strains generated in the Bristol variety background. F2 animals showing the enhanced commissural phenotype were singled out on plates to lay eggs. 10 F3 worms were lysed and 5 μl of the worm lysate was diluted with 45 μl H_2O for FLP-mapping as described in Zipperlen et al., (2004).

REFERENCES

Bennett V (1992). Ankyrins. Adaptors between diverse plasma membrane proteins and the cytoplasm. J Biol Chem. 267: 8703-8706.

Bornemann DJ, Duncan JE, Staatz W, Selleck S, Warrior R (2004). Abrogation of heparan sulfate synthesis in Drosophila disrupts the Wingless, Hedgehog and Decapentaplegic signaling pathways. Development. 131: 1927-1938.

Brenner S (1974). The genetics of *Caenorhabditis elegans*. Genetics. 77: 71-94.

Bulow HE, Hobert O (2004). Differential sulfations and epimerization define heparan sulfate specificity in nervous system development. Neuron. 41: 723-736.

Colavita A, Krishna S, Zheng H, Padgett RW, Culotti JG (1998). Pioneer axon guidance by UNC-129, a *C. elegans* TGF-beta. Science. 1998 281: 706-709.

Colavita A, Culotti JG (1998). Suppressors of ectopic UNC-5 growth cone steering identify eight genes involved in axon guidance in *Caenorhabditis elegans*. Dev Biol. 194: 72-85.

Davis JQ, Bennett V (1994). Ankyrin binding activity shared by the neurofascin/L1/NrCAM family of nervous system cell adhesion molecules. J Biol Chem. 269: 27163-27166.

Dickson BJ (2001). Rho GTPases in growth cone guidance. Curr Opin Neurobiol. 11: 103-110.

Forrester WC, Garriga G (1997). Genes necessary for *C. elegans* cell and growth cone migrations. Development. 124: 1831-1843.

George SE, Simokat K, Hardin J, Chisholm AD (1998). The VAB-1 Eph receptor tyrosine kinase functions in neural and epithelial morphogenesis in *C. elegans*. Cell. 92: 633-643.

Gitai Z, Yu TW, Lundquist EA, Tessier-Lavigne M, Bargmann CI (2003). The netrin receptor UNC-40/DCC stimulates axon attraction and outgrowth through enabled and, in parallel, Rac and UNC-115/AbLIM. Neuron. 37: 53-65.

Gysi S (2005). A screen for axon guidance genes depending on Heparan Sulfate Proteoglycans in *C. elegans*. Diploma thesis. University of Zurich.

Hedgecock EM, Culotti JG, Hall DH (1990). The *unc-5*, *unc-6*, and *unc-40* genes guide circumferential migrations of pioneer axons and mesodermal cells on the epidermis in *C. elegans*. Neuron. 4: 61-85.

Hilliard MA, Bargmann CI (2006). Wnt signals and Frizzled activity orient anterior-posterior axon outgrowth in *C. elegans*. Dev Cell. 10: 379-390.

Huang X, Cheng HJ, Tessier-Lavigne M, Jin Y (2002). MAX-1, a novel PH/MyTH4/FERM domain cytoplasmic protein implicated in netrin-mediated axon repulsion. Neuron. 34: 563-576.

Huang X, Huang P, Robinson MK, Stern MJ, Jin Y (2003). UNC-71, a disintegrin and metalloprotease (ADAM) protein, regulates motor axon guidance and sex myoblast migration in *C. elegans*. Development. 130: 3147-3161.

Ishii N, Wadsworth WG, Stern BD, Culotti JG, Hedgecock EM (1992). UNC-6, a laminin-related protein, guides cell and pioneer axon migrations in C. elegans. Neuron. 9: 873-881.

Jorgensen EM, Mango SE (2002). The art and design of genetic screens: caenorhabditis elegans. Nat Rev Genet. 3:356-369.

Knobel KM, Davis WS, Jorgensen EM, Bastiani MJ (2001). UNC-119 suppresses axon branching in *C. elegans*. Development. 128: 4079-4092.

Lanier LM, Gertler FB (2000). From Abl to actin: Abl tyrosine kinase and associated proteins in growth cone motility. Curr Opin Neurobiol. 10: 80-87.

Lim YS, Mallapur S, Kao G, Ren XC, Wadsworth WG. Netrin UNC-6 and the regulation of branching and extension of motoneuron axons from the ventral nerve cord of *Caenorhabditis elegans* (1999). J Neurosci. 19:7048-7056.

Lundquist EA, Reddien PW, Hartwieg E, Horvitz HR, Bargmann CI (2001). Three *C. elegans* Rac proteins and several alternative Rac regulators control axon guidance, cell migration and apoptotic cell phagocytosis. Development. 128: 4475-4488.

McIntire SL, Garriga G, White J, Jacobson D, Horvitz HR (1992). Genes necessary for directed axonal elongation or fasciculation in *C. elegans*. Neuron. 8: 307-322.

McIntire SL, Jorgensen E, Kaplan J, Horvitz HR (1993). The GABAergic nervous system of *Caenorhabditis elegans*. Nature. 364: 337-341.

Otsuka AJ, Franco R, Yang B, Shim KH, Tang LZ, Zhang YY, Boontrakulpoontawee P, Jeyaprakash A, Hedgecock E, Wheaton VI, et al. (1995). An ankyrin-related gene (*unc-44*) is necessary for proper axonal guidance in *Caenorhabditis elegans*. J Cell Biol. 129: 1081-1092.

Poinat P, De Arcangelis A, Sookhareea S, Zhu X, Hedgecock EM, Labouesse M, Georges-Labouesse E (2002). A conserved interaction between beta1 integrin/PAT-3 and Nck-interacting kinase/MIG-15 that mediates commissural axon navigation in *C. elegans*. Curr Biol. 12: 622-631.

Rhiner C, Gysi S, Frohli E, Hengartner MO, Hajnal A (2005). Syndecan regulates cell migration and axon guidance in *C. elegans*. Development. 132: 4621-4633.

Runko E, Kaprielian Z (2004). *Caenorhabditis elegans* VEM-1, a novel membrane protein, regulates the guidance of ventral nerve cord-associated axons. J Neurosci. 24: 9015-9026.

Siddiqui SS, Culotti JG (1991). Examination of neurons in wild type and mutants of *Caenorhabditis elegans* using antibodies to horseradish peroxidase. J Neurogenet. 7: 193-211.

Steven R, Kubiseski TJ, Zheng H, Kulkarni S, Mancillas J, Ruiz Morales A, Hogue CW, Pawson T, Culotti J (1998). UNC-73 activates the Rac GTPase and is required for cell and growth cone migrations in *C. elegans*. Cell. 92: 785-795.

Stoeckli ET, Landmesser LT (1995). Axonin-1, Nr-CAM, and Ng-CAM play different roles in the in vivo guidance of chick commissural neurons. Neuron. 14: 1165-1179.

Wacker I, Schwarz V, Hedgecock EM, Hutter H (2003). *zag-1*, a Zn-finger homeodomain transcription factor controlling neuronal differentiation and axon outgrowth in *C. elegans*. Development. 130: 3795-3805.

Wadsworth WG (2002). Moving around in a worm: netrin UNC-6 and circumferential axon guidance in *C. elegans*. Trends Neurosci. 25:423-429.

Wadsworth WG, Bhatt H, Hedgecock EM (1996). Neuroglia and pioneer neurons express UNC-6 to provide global and local netrin cues for guiding migrations in *C. elegans*. Neuron. 16: 35-46.

Wu YC, Cheng TW, Lee MC, Weng NY (2002). Distinct rac activation pathways control *Caenorhabditis elegans* cell migration and axon outgrowth. Dev Biol. 250: 145-155.

Zallen JA, Kirch SA, Bargmann CI (1999). Genes required for axon pathfinding and extension in the *C. elegans* nerve ring. Development. 126: 3679-3692.

Zipperlen P, Nairz K, Rimann I, Basler K, Hafen E, Hengartner M, Hajnal A (2005). A universal method for automated gene mapping. Genome Biol. 6:R19.

CHAPTER 5

Studying *C. elegans* axon guidance genes in higher vertebrates: Conserved functions for UNC-69 and UNC-76?

PREFACE

This research article will be published in the Journal of Biology 5, 2006. An e-publication ahead of print is already available. The paper describes the identification and characterization of a novel protein complex, composed of UNC-69 and UNC-76, which promotes axonal growth and normal presynaptic organization in *C. elegans*. The existence of highly conserved human homologs that can functionally substitute for UNC-69 and UNC-76 in the worm, pointed to a core signaling pathway, which might be present in all animals. In a collaboration with the group of Prof. Esther Stöckli, we could show that the chicken UNC-69 homolog is highly expressed in the developing central nervous system in the chicken embryo and that inactivation of chicken UNC-69 by *in-ovo* RNAi leads to axon guidance defects. I generated the in-situ probes, the dsRNA and performed the hybridization experiments and the whole mount immuno-staining of the embryos. Prof. Esther Stöckli did all the injections and helped me to examine the RNAi phenotype. Dimitris Bourikas helped to set up the experiments and showed me how to dissect chicken embryos.

In the Supplementary Results, I summarize current efforts, which aim to characterize the role of human UNC-69 (SCOCO) and human UNC-76 (FEZ1). These experiments comprise cell culture studies to determine the subcellular localization of the two proteins and the generation of monoclonal anti-SCOCO antibodies, which should provide a powerful tool for future studies in mammals. In addition, I include data obtained from the initial characterization of three *unc-69* suppressors, which were isolated by Cheng-Wen Su in a screen for suppression of the locomotion defects of *unc-69*(*ju69)* worms.

Journal of Biology

BioMed Central

Open Access

Research

The short coiled-coil domain-containing protein UNC-69 cooperates with UNC-76 to regulate axonal outgrowth and normal presynaptic organization in *Caenorhabditis elegans*

Cheng-Wen Su[1,3]*, Suzanne Tharin[4,5,10]*, Yishi Jin[6], Bruce Wightman[7], Mona Spector[5], David Meili[1,2,11], Nancy Tsung[8,12], Christa Rhiner[1,3], Dimitris Bourikas[2,3], Esther Stoeckli[2,3], Gian Garriga[9], H Robert Horvitz[8] and Michael O Hengartner[1,3]

Addresses: [1]Institute for Molecular Biology and [2]Zoological Institute, University of Zurich, Winterthurerstrasse 190, CH-8057 Zurich, Switzerland. [3]Neuroscience Center Zurich, ETH and University of Zurich, Winterthurerstrasse 190, CH-8057 Zurich, Switzerland. [4]Program in Genetics, SUNY at Stony Brook, Stony Brook, NY 11794, USA. [5]Cold Spring Harbor Laboratory, Cold Spring Harbor, NY 11724, USA. [6]Howard Hughes Medical Institute, Department of Molecular, Cellular and Developmental Biology, Sinsheimer Laboratories, University of California, Santa Cruz, CA 95064, USA. [7]Biology Department, Muhlenberg College, Allentown, PA 18104, USA. [8]Howard Hughes Medical Institute, Department of Biology, Massachusetts Institute of Technology, Cambridge, MA 02139, USA. [9]Department of Molecular and Cell Biology, University of California, Berkeley, CA 94720, USA.

Present Addresses: [10]Department of Neurosurgery, Brigham and Women's Hospital, Children's Hospital and Harvard Medical School, 300 Longwood Avenue, Boston, MA 02115, USA. [11]Abteilung für Klinische Chemie und Biochemie, Universitäts-Kinderklinik, Steinwiesstrasse 75, CH-8032 Zürich, Switzerland.[12]Clinigen, Inc., 400 W. Cummings Park #5700, Woburn, MA 01801, USA.

*These authors contributed equally to this work.

Correspondence: Michael O Hengartner. Email: michael.hengartner@molbio.unizh.ch

Published: 00 Month 2006

Journal of Biology 2006, **5:9**

The electronic version of this article is the complete one and can be found online at http://jbiol.com/content/5/4/9

Received: 16 March 2005
Revised: 23 December 2005
Accepted: 5 April 2006

Abstract

Background: The nematode *Caenorhabditis elegans* has been used extensively to identify the genetic requirements for proper nervous system development and function. Key to this process is the direction of vesicles to the growing axons and dendrites, which is required for growth-cone extension and synapse formation in the developing neurons. The contribution and mechanism of membrane traffic in neuronal development are not fully understood, however.

Results: We show that the *C. elegans* gene *unc-69* is required for axon outgrowth, guidance, fasciculation and normal presynaptic organization. We identify UNC-69 as an evolutionarily conserved 108-amino-acid protein with a short coiled-coil domain. UNC-69 interacts physically with UNC-76, mutations in which produce similar defects to loss of *unc-69* function.

In addition, a weak reduction-of-function allele, *unc-69(ju69)*, preferentially causes mislocalization of the synaptic vesicle marker synaptobrevin. UNC-69 and UNC-76 colocalize as puncta in neuronal processes and cooperate to regulate axon extension and synapse formation. The chicken UNC-69 homolog is highly expressed in the developing central nervous system, and its inactivation by RNA interference leads to axon guidance defects.

Conclusions: We have identified a novel protein complex, composed of UNC-69 and UNC-76, which promotes axonal growth and normal presynaptic organization in *C. elegans*. As both proteins are conserved through evolution, we suggest that the mammalian homologs of UNC-69 and UNC-76 (SCOCO and FEZ, respectively) may function similarly.

Background

At its simplest, a neuron is composed of three major structures, a central cell body and two networks of extensively branched membrane structures, the dendrite and the axon. Growing axons respond to a wide variety of extracellular attractive and repulsive signals that direct migration to a fated location. Although many guidance receptors have been identified on extending growth cones, little is known about how activation of receptors mediates coordinated neurite extension. In addition to signaling cues in the extracellular matrix, neurite elongation and growth-cone extension depend on a concerted effort of vesicular transport and regulated membrane addition. For growth cones to extend, vesicles derived from the Golgi apparatus fuse with the plasma membrane by a process of regulated exocytosis [1]. Likewise, synapse formation also requires transport of pre- and post-synaptic components supplied in membranous organelles [2,3]. These vesicles are not only transported but are also differentially sorted into dendrites or axons [4,5]. To fulfill these tasks, intrinsic cytosolic factors are required to regulate transport of the vesicles [6] and to differentially control dendritic versus axonal growth and morphogenesis.

The nematode *Caenorhabditis elegans* has been extensively used to study vesicular transport in neuronal development. For example, monomeric kinesin UNC-104/KIF1A, UNC-116/kinesin heavy chain (KHC), kinesin light chain KLC-2, and various cytoplasmic dynein complex components regulate various vesicle trafficking events [7-9]. KLC-2 might regulate the transport of various axonal and synaptic cargos by recruiting adaptor and regulatory proteins such as UNC-16, UNC-14 and UNC-51 [9,10]. In the absence of UNC-16 (a JNK-scaffolding protein), glutamate receptors and synaptic vesicles containing the synaptobrevin homolog SNB-1 dislodge from the post- and pre-synaptic terminals [7]. UNC-16 binds directly to the tetratricopeptide repeat (TPR) domain of KLC-2, whereas the RUN-domain-containing protein UNC-14 associates with UNC-16 in the presence of KLC-2 [9]. UNC-14 interacts physically with the serine/threonine kinase UNC-51, and both proteins are required for axonal outgrowth [10,11]. Noticeably, although membranous structures with variable size accumulate within axons in *unc-51* [12,13] and *unc-14* [13] mutants, suggesting that both genes are involved in axonal transport, synaptic vesicles are normally clustered in presynaptic terminals in these mutants [13].

C. elegans UNC-76 and its homologs have been implicated in both axonal outgrowth and synaptic transport via association with the heavy chain of Kinesin-1. In worms mutant for *unc-76*, the nervous system is disorganized: the axons fail to extend and axonal bundles are defasciculated [13,14]. In *Drosophila*, Unc-76 interacts with the tail of KHC and is important for transporting synaptic cargos in the axons [15]. The mechanism of UNC-76-mediated transport remains elusive, although there is some evidence that secondary modification by protein kinase Cζ (PKCζ) or polyubiquitination of the fasciculation and elongation protein zygin/zeta 1 (FEZ1), one of the mammalian UNC-76 homologs, contributes to its neurite outgrowth activity [16,17].

In this study we report the cloning and characterization of UNC-69, a small, evolutionarily conserved coiled-coil domain-containing protein that acts as a novel binding partner of UNC-76 in *C. elegans*. Whereas a weak reduction-of-function allele of *unc-69* results in a selective defect in mislocalization of a synaptic vesicle marker, strong *unc-69* mutants show extensive defects in axonal outgrowth, fasciculation and guidance. Mutations in UNC-69 preferentially disrupt membrane traffic within axons. We show that UNC-69 and UNC-76 participate in a common genetic pathway necessary for axon extension and cooperate to regulate the size and position of synaptic vesicles in axons. Moreover, both proteins colocalize as puncta in neuronal processes. We propose that UNC-69 and UNC-76 form a conserved protein complex *in vivo* to regulate axonal transport of vesicles.

Results

unc-69 encodes a conserved short coiled-coil domain-containing protein

unc-69 was identified in a large-scale behavioral screen for uncoordinated (Unc) mutants [18]. *unc-69* loss-of-function *(lf)* mutants move poorly, coil ventrally and are phenotypically similar to other coiler Unc mutants, many of which are defective in axonal outgrowth and guidance. Additionally, *unc-69* mutant hermaphrodites lay more eggs in the absence of food than wild-type worms do (see Additional data file 1), suggesting a defect in the hermaphrodite-specific neurons (HSNs), which control egg-laying behavior.

Previous genetic data placed *unc-69* between *lin-12* and *tra-1* on chromosome III, 0.12 map units to the left of *ced-9* [19]. Using cosmid rescue, we were able to identify the predicted gene *T07A5.6a* (previously named *T07C4.10b*) as *unc-69* (Figure 1a). The *unc-69* gene encodes a 108-amino-acid protein and contains a short coiled-coil domain in its carboxyl terminus (Figure 1b). Although UNC-69 could possibly form a homodimer via its coiled-coil domain, we failed to detect any homophilic interactions of UNC-69 (see Additional data file 1).

The original alleles of *unc-69*, *unc-69(e587)* and *unc-69(e602)*, are both nonsense mutations in the carboxy-terminal half of the protein (see Figure 1b). The *unc-69(e602)* mutation causes a T-to-A transversion and replaces a leucine with an amber stop codon at position 77; *unc-69(e587)* results in a C-to-T transition, changing a glutamine to an amber stop codon at position 86; both of these mutations lie within the well conserved coiled-coil domain. Both *unc-69(e602)* and *unc-69(e587)* are candidate genetic null alleles, as the axon extension and branching defects of the neurons named ALM and AVM were not enhanced significantly when either of these two alleles was placed *in trans* to the deficiency *nDf40* (Table 1, Figure 2).

We also isolated a hypomorphic allele, *ju69*, which results in a G-to-A transition at the start codon and changes the initiator methionine to an isoleucine. Theoretically, the M-to-I substitution (M1I) should abolish translation initiation and hence synthesis of the UNC-69 protein. As the phenotype of *unc-69(ju69)* mutants is much weaker than that of the other two alleles, however, we suspect that a small amount of UNC-69 functional protein is still being produced, either by leaky translation initiation at the original site, or through initiation at the internal, in-frame ATG site at residue 49, which would leave the coiled-coil domain intact. Indeed, overexpression of a mutant fusion protein of UNC-69 with green fluorescent protein (UNC-69(M1I)::GFP) or a carboxy-terminal fragment of UNC-69 (residues 41-108) could partially suppress the locomotion defect of the *unc-69(e587)* mutants (data not shown, and see Additional data file 1).

Finally, we analyzed a small deletion, *ok339*, which completely eliminates the *unc-69* locus. Unfortunately, this deletion also removes the essential neighboring gene *T07A5.5* and was therefore not studied further (see Additional data file 1). Expressed sequence tag (EST) analysis suggested that the *unc-69* locus encodes two splice variants (see Figure 1a and see Additional data file 1). Northern blot analysis of poly(A)$^+$ RNA from mixed-stage worms as well as from embryos revealed a 0.65 kb major transcript (Figure 1c), consistent with the predicted size of the *T07A5.6a* transcript.

UNC-69 is conserved from single-celled eukaryotes to complex metazoans

We found that UNC-69 is highly conserved through evolution and encodes the *C. elegans* homolog of mammalian SCOCO (short coiled-coil protein), a protein recently found to interact with dominant-negative ARF-like 1 (ARL-1) protein in a yeast two-hybrid screen [20]. The *Saccharomyces cerevisiae* UNC-69 homolog, Slo1p (SCOCO-like open reading frame protein), has been shown to interact with Arl3p, a homolog of mammalian ARFRP1, another ARF-like protein, which is involved in endoplasmic reticulum-Golgi and post-Golgi transport [21,22]. Uncharacterized UNC-69/SCOCO homologs can also be found in many other animal species (Figure 3a and Additional data file 1).

All of the UNC-69 homologs are predicted to form a coiled-coil structure near their carboxyl termini (the underlined region in Figure 3a). In an alignment of the *S. cerevisiae*, *C. elegans*, *C. briggsae*, mosquito, fly, *Fugu*, zebrafish, *Xenopus*, mouse and human protein sequences, identity over the coiled-coil regions is 32.6% (Figure 3a). The identity in the coiled-coil region jumps to 73.9% if the yeast sequence is excluded. Except for yeast, an acidic region immediately upstream of the coiled-coil domain as well as a serine/threonine-rich region and a basic region downstream -appear also to be highly conserved. In contrast, the amino terminus of UNC-69 and its homologs is highly divergent, both in length and in amino-acid sequence. The function of UNC-69 proteins seems to be conserved, since expression of human SCOCO as a transgene under the *unc-69* promoter restored locomotion to *unc-69* mutants (Figure 3c).

We assessed the tissue distribution of human *SCOCO* transcripts by probing a human fetal tissue northern blot. This probe detected a single transcript of approximately 2.1 kb in all tissues examined (brain, lung, liver and kidney; Figure 3b). Human *SCOCO* mRNA appeared to be enriched in fetal brain, possibly hinting at a role for SCOCO in mammalian nervous system development.

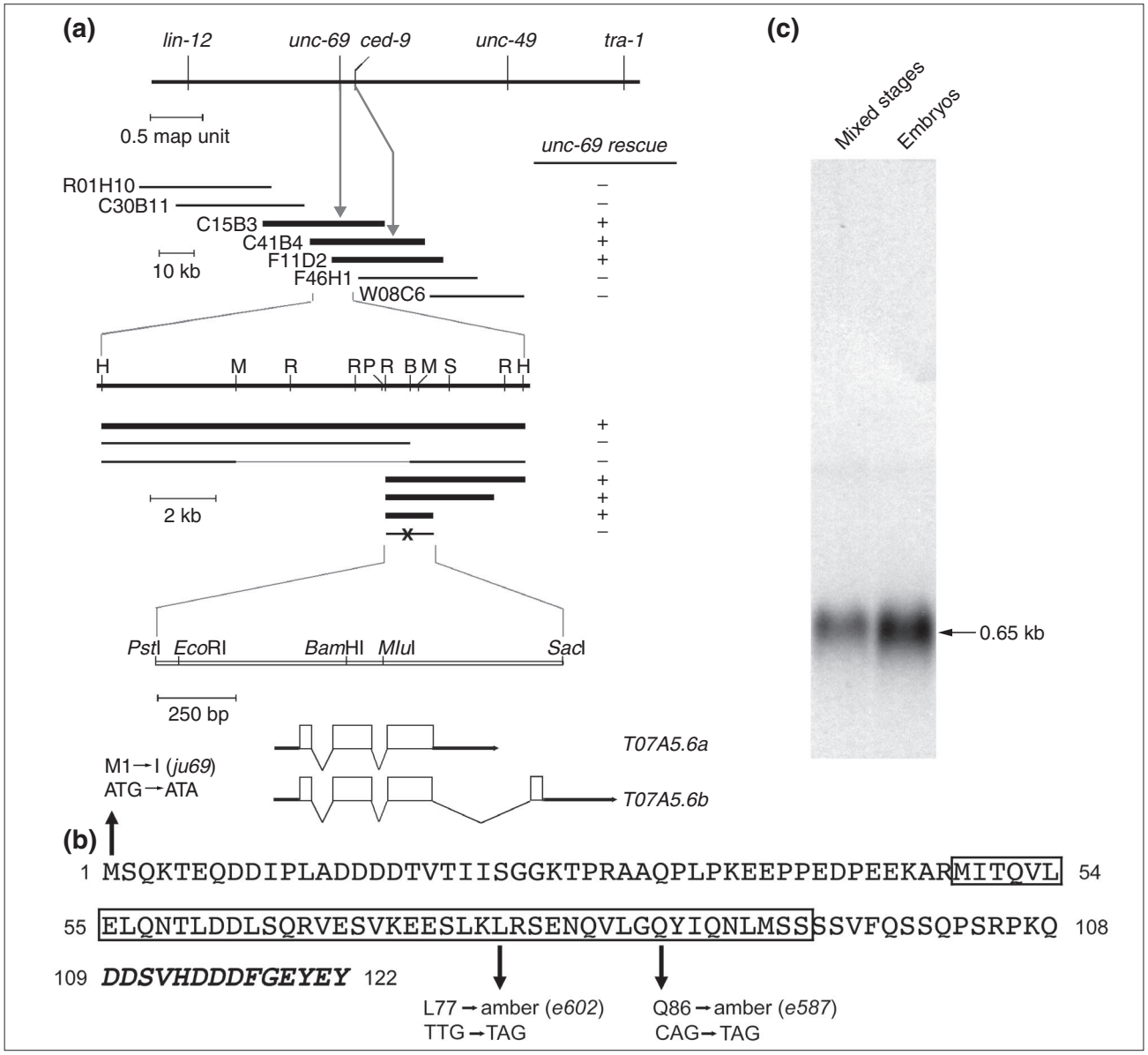

Figure 1
The *unc-69* locus encodes a 108-amino-acid protein with a short coiled-coil domain. **(a)** Genetic and physical maps of chromosome III in the vicinity of the *unc-69* locus. *unc-69* is close to and left of *ced-9*. Cosmids and subclones able to rescue the locomotion defect of *unc-69(e587)* mutants are shown in bold. B: *Bam*HI; H: *Hin*dIII; M: *Mlu*I; P: *Pst*I; R: *Eco*RI; S: *Sac*I. Introduction of a frameshift mutation at the *Bam*HI site in the second exon (denoted with an x) abrogated rescue by the minimal *Pst*I-*Sac*I rescuing fragment. Both splice variants, *T07A5.6a* and *T07A5.6b*, are contained within this fragment. **(b)** The UNC-69 protein sequence. The boxed region is predicted to form a coiled-coil domain. Arrows indicate the positions of the three known *unc-69* mutations. Additional amino acids encoded by *T07A5.6b* are shown in italics (see Additional dataf ile 1). **(c)** Northern-blot analysis of *unc-69* revealed a single major transcript of 0.65 kb (arrow).

UNC-69 is expressed in the nervous system and other tissues from early embryogenesis to adulthood

We generated transgenic animals expressing either amino- or carboxy-terminally *gfp*-tagged *unc-69* fusion constructs under the control of the endogenous *unc-69* promoter. Both translational fusion constructs rescued the Unc phenotype of *unc-69* mutants, suggesting that the fusion proteins were correctly expressed and biologically functional. UNC-69::GFP expression was first detectable

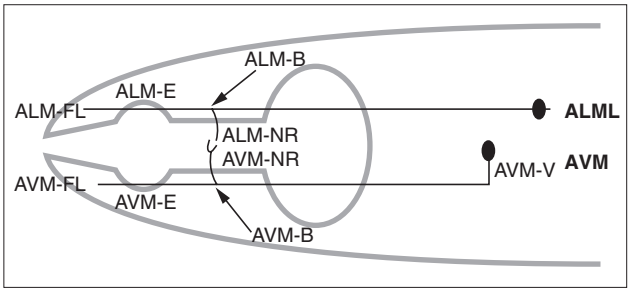

Figure 2
Schematic diagram of the ALM and AVM neurons in *C. elegans*. The different parts of the neurons are given designated letters; see Table 1 for details. Anterior is to the left.

in embryos (Figure 4a,b). In immature neurons, we observed expression of UNC-69::GFP in the processes and growth cones of developing neurites (arrowhead in Figure 4c). In older larvae and adults, UNC-69::GFP was expressed in neurons of the anterior, lateral, ventral and retro-vesicular ganglia in the head, and in neurons of the preanal, dorso-rectal and lumbar ganglia in the tail. The fusion protein was also present in the ventral nerve cord (VNC), in the dorsal nerve cord (DNC), in the dorsal and ventral sublateral nerve cords, and in commissural axons (Figure 4d-f). The reporter was expressed in the neurons named CAN, HSN, ALM, PLM, AVM, PVM, BDU, and SDQR, as evidenced by its localization to the cell bodies of these neurons. Expression of *unc-69* in these latter cells

Table 1

Axon outgrowth and guidance defects in *unc-69* mutants

	ALM defect (%)				
Genotype	B	NR	E	FL	*n*
Wild type	0	0	0	12	113
unc-69(e602)	12	36	77	84	77
unc-69(e587)	15	45	85	89	80
unc-69(e602) (m+z-)	0	4.3	39	91	70
unc-69(e602)/nDf40 (m+z-)	0	7.2	20	72	69
unc-69(e587) (m+z-)	1.4	7.2	43	87	69
unc-69(e587)/nDf40 (m+z-)	0	8.3	20	82	60
*unc-69(e602)**	19	48	62	95	113
*unc-69(e602); opEx[P_{mec-7}::unc-69]**	1	12	2	5	81
*unc-69(e602); opEx[P_{mec-7}::unc-69]**	5	9	6	10	79
*unc-69(e602); opEx[P_{mec-7}::unc-69]**	8	29	0	10	85

	AVM defect (%)					
Genotype	B	NR	E	FL	V	*n*
Wild type	0	0	1	8	0	106
unc-69(e602)	32	27	72	73	2.7	77
unc-69(e587)	64	70	86	87	0	80
unc-69(e602) (m+z-)	1.4	4.3	57	86	0	70
unc-69(e602)/nDf40 (m+z-)	0	0	56	80	0	69
unc-69(e587) (m+z-)	2.9	8.8	56	85	0	69
unc-69(e587)/nDf40 (m+z-)	0	3.6	76	95	0	60
*unc-69(e602)**	46	67	93	100	ND	113
*unc-69(e602); opEx[P_{mec-7}::unc-69]**	0	4	4	4	ND	81
*unc-69(e602); opEx[P_{mec-7}::unc-69]**	8	12	12	23	ND	79
*unc-69(e602); opEx[P_{mec-7}::unc-69]**	11	21	12	13	ND	85

Neurite outgrowth and guidance defects of mechanosensory touch neurons in *unc-69* mutants. The morphology of neurites of ALM (top) and AVM (bottom) neurons (as in the schematic in Figure 2) was scored in different *unc-69* mutants, in *unc-69/nDf40* heterozygotes, and in mosaic animals carrying a functional *unc-69* transgene under the control of the *mec-7* promoter, which directs expression in the six touch neurons. All worms scored had a *P_{mec-4}::gfp* transgene *zdIs5* in the background to allow visualization of the neurite morphology. One ALM neurite was scored per animal. B, failure to form proper branch at the nerve ring; NR, failure of nerve ring branch to fully extend; E: failure to elongate past the branch point; FL, failure to extend fully; V, ventral guidance defect. (m+z-): homozygous mutant animals derived from heterozygous mothers. *These strains also carry a *lin-15(n765)* mutation in the background. All *opEx* transgenes also carry a wild-type copy of *lin-15(+)* as a coinjection marker. ND, not done. *n,* number of worms scored.

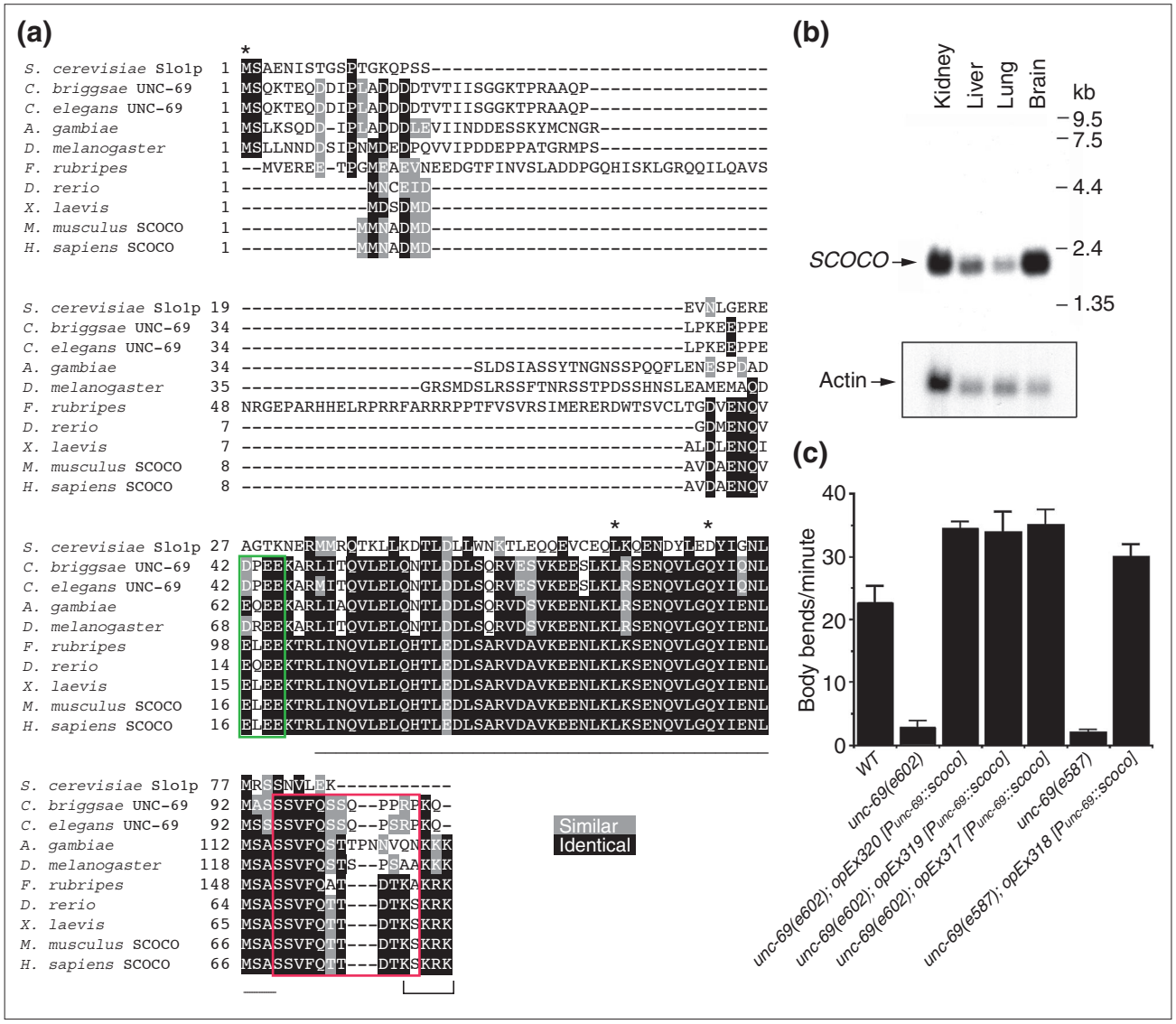

Figure 3
UNC-69 is homologous to mammalian SCOCO. **(a)** Sequence alignment of UNC-69/SCOCO proteins from *S. cerevisiae*, *C. elegans*, *C. briggsae*, mosquito, *Drosophila*, *Fugu*, zebrafish, *Xenopus*, mouse and human. Residues identical in all ten sequences are shaded black; similar residues are shaded gray. The underlined region is predicted in all cases to form a coiled-coil domain. The region boxed in green is acidic, and the region boxed in red is serine/threonine-rich. The bracket indicates the carboxy-terminal basic region. Asterisks mark mutations in *unc-69*. **(b)** mRNA of the human *unc-69* homolog *SCOCO* is enriched in fetal brain and is also present in fetal kidney, liver and lung. **(c)** Expression of human *SCOCO* rescues the locomotion defect of *unc-69* mutant. Movement of the wild type (WT), mutants, and transgenic L4-stage hermaphrodites was scored as complete sine waves per minute. For each genotype $n = 10$. Error bars represent the standard error of the mean.

was confirmed using an *unc-69::LacZ::NLS* fusion (data not shown). Taken together, these results indicate that *unc-69* is expressed widely, perhaps ubiquitously, in the *C. elegans* nervous system.

Expression of UNC-69::GFP was also observed in non-neuronal cells. In larvae and adults, we occasionally observed UNC-69::GFP expression in body-wall muscle (data not shown). We also observed UNC-69::GFP in the excretory canal, in the distal tip cells, in the spermatheca and, less frequently, in hypoderm and gut (Figure 4e, and data not shown). The expression in these non-neuronal cells was variable, however, and might not reflect the endogenous expression pattern of *unc-69*.

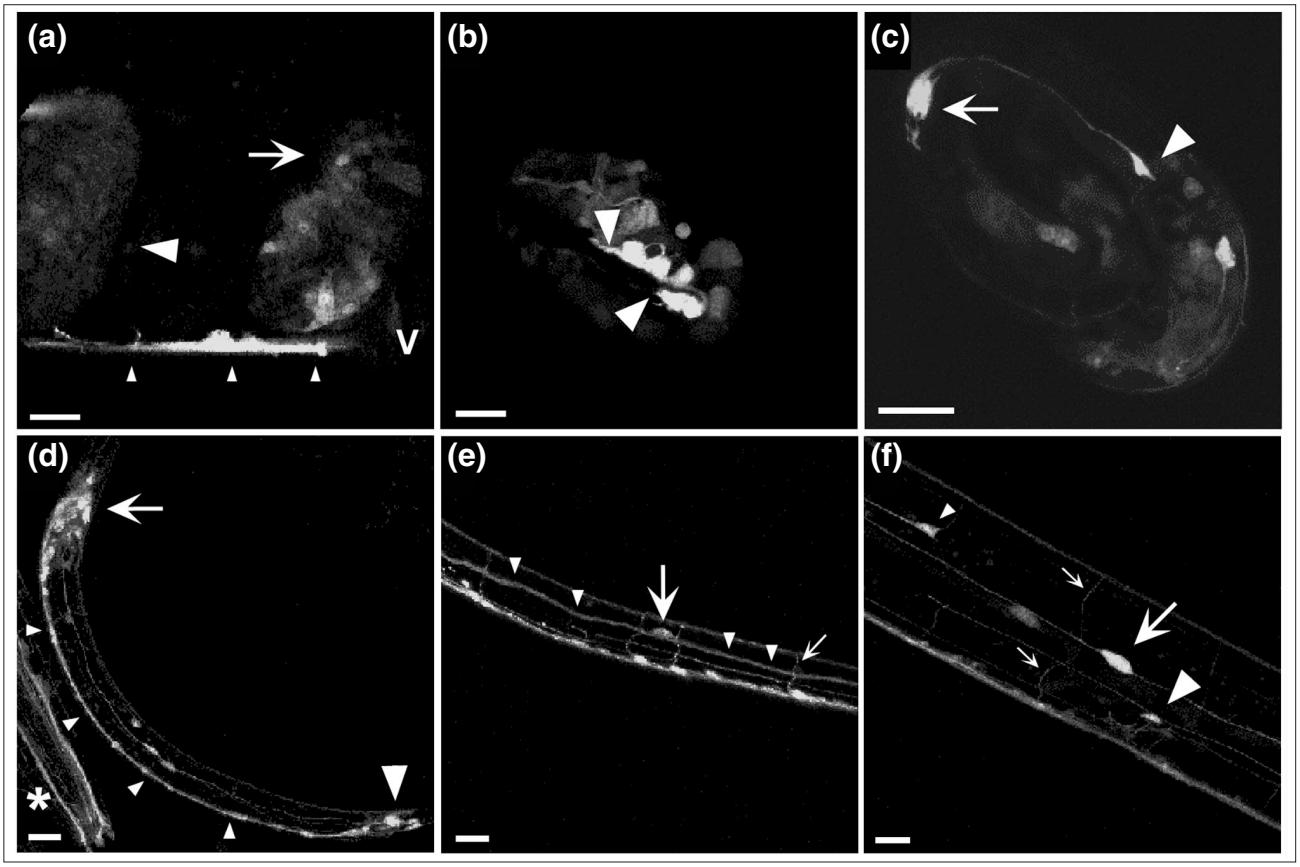

Figure 4
UNC-69::GFP is expressed in neurons. Confocal micrographs of mosaic animals expressing a rescuing carboxy-terminal UNC-69::GFP fusion. A 1 μm optical section is shown in **(a)**; all other panels are projections of optical series. (a) Late gastrula (large arrowhead) and early comma-stage embryo (arrow) with widespread expression of UNC-69::GFP. Embryos were still inside the mother. Small arrowheads indicate the maternal VNC; v indicates the maternal vulva. **(b)** A two-fold-stage embryo with strong UNC-69::GFP expression in VNC neurons (between arrowheads). **(c)** A three-fold embryo expressing UNC-69::GFP in a growth cone (arrowhead). The arrow indicates a neuronal cell body. **(d)** An L1-stage larva expressing UNC-69::GFP in neurons and axons in the head (arrow), VNC (small arrowheads) and tail (large arrowhead). The asterisk indicates reporter expression in labial sensory neuronal processes of an adjoining adult animal. **(e)** An L3 larva expressing UNC-69::GFP in the CAN neuron (large arrow), excretory canal (small arrowheads) and in commissural axons (e.g. small arrow). **(f)** An L4 larva expressing UNC-69::GFP in the CAN (large arrow), HSN (large arrowhead) and ALM (small arrowhead) neurons. Small arrows indicate commissures. All scale bars represent 10 μm. In all cases, anterior is to the left and dorsal is up.

UNC-69 is required for axonal outgrowth and guidance

The ventral coiler phenotype of *unc-69* mutants suggests a defect in nervous system development. Indeed, previous studies had reported axonal guidance defects of the D-type GABAergic motor neurons, mechanosensory neurons and the HSN neurons in *unc-69* mutants [23,24]. We confirmed these observations and extended them to other cell types (see Tables 1,2 and Figures 2, 5a-f). Incorrect targeting of the DD and VD motor axons is likely to contribute to the Unc phenotype of *unc-69* mutants. In addition to outgrowth and guidance defects, we also observed ectopic branching of the DD/VD neurons and mechanosensory neurons in *unc-69* mutants (Figure 5d,f). In a few cases the axons had unusual large swellings and occasionally meandered along the lateral body wall.

FMRF-amide (Phe-Met-Arg-Phe-NH_2) is a neuropeptide that serves as a neuromodulator, and is co-released together with other neurotransmitters. In examining other neuronal classes in *unc-69(e587)* mutants, we observed premature termination of axons of the FMRF-amide-positive neurons ALA, RID and AVKR, but not RMG (data not shown, and see Table 2). FMRF-amide-positive neurons are so-called neuropeptidergic neurons and could be sensory, motor or interneurons. We observed that 67% (20/30) of ALA axons

Table 2

Axon outgrowth and guidance defects of HSN, DD/VD, ALA and AVK neurons

Axon guidance phenotype	Defect in *unc-69(e587)* mutants (%)	*n*
HSN		
Ventral outgrowth	16	70
Midline crossover (HSNL)	38	40
Failure to reach nerve ring	99	59
DD/VD		
Dorsal outgrowth	33	45
ALA		
Premature termination	67	30
AVKR		
Premature termination or crossover	85	20

The morphology of HSN neurons was visualized using antibodies against serotonin; that of DD/VD neurons using antibodies against GABA; and that of ALA and AVKR neurons using antibodies against FMRF-amide. See Materials and methods for details. *n*, number of animals scored.

terminated prematurely, and ALA axons sometimes branched before termination. AVKR had frequent axonal outgrowth and guidance defects: 85% (17/20) of AVKR axons terminated prematurely or crossed from the left VNC (VNCL) to the right VNC (VNCR). Taken together, these observations support a role for *unc-69* in ventral and dorsal axonal guidance as well as in axonal elongation within the fascicles.

UNC-69 is required for fasciculation

As *unc-69* mutants have midline crossover defects (see Table 2), it is likely that axons running in the same fascicle lose cell-cell adhesion and fail to stay together. We constructed a series of electron micrograph (EM) cross-sections through the major nerve cords (DNC, VNCL and VNCR) that run antero-posteriorly in adult hermaphrodites. In wild-type animals, the composition of axons in any of these nerve cords is highly stereotyped, with four axons fasciculated to run in VNCL and the other ventral axons running within VNCR (Figure 5g) [25]. In *unc-69(e587)* and *unc-69(e602)* mutants, many fascicles split into two or more groups and in some cases defasciculated axons could be seen running alone along the hypodermal ridge. Moreover, some axons of both the DNC and VNCL appeared to be mislocalized and can be seen on the wrong side of the hypodermal ridge (Figure 5h and data not shown). Anti-tubulin and anti-GABA staining confirmed the observed fasciculation defects in *unc-69(e587)* mutants (data not shown).

UNC-69 acts cell autonomously to control neurite outgrowth

To determine whether *unc-69* expression is required in the growing neurites or in the surrounding tissues, we created *unc-69* transgenic lines expressing *unc-69(+)* specifically in the six touch neurons under the control of a *mec-7* promoter. We compared outgrowth and guidance defects of the ALM and AVM neurons in three such lines with those of *unc-69(lf)* mutants (see Table 1, Figure 2). In all three transgenic lines, the percentage of ALM neurites that failed to extend to full length or send a branch into the nerve ring

Figure 5 *(see figure on the next page)*
unc-69 is required for axonal outgrowth, guidance, branching and fasciculation in invertebrates and vertebrates. **(a,b)** Defect in the migration of the HSN neuron in *unc-69* mutant animals. In wild-type animals (a), the HSN axons (HSNL and HSNR) migrate ventrally until they reach the VNC, which they join and follow rostrally towards the head (arrow in (a)). In *unc-69* mutants (b), HSN axons occasionally fail to grow ventrally and instead project laterally along the body wall (arrow in (b)). Animals were stained with anti-serotonin antibodies to visualize the HSN neurons. Arrowheads indicate the vulva. Dotted lines mark the ventral margin of the body walls. **(c,d)** Commissures of D-type GABAergic neurons routinely reach the DNC in wild-type animals (c), but often fail in *unc-69(e587)* animals (d) and prematurely bifurcate (arrow). D-type GABAergic neurons were visualized with the *unc-47::gfp* transgene *oxIs12*. Asterisk in D marks a gap in the DNC. There are also often ectopic sprouts from the commissures (arrowheads in (d)) in *unc-69(e587)* mutants. **(e,f)** Images of the single ALM touch neuron in (e) wild-type and (f) *unc-69(e602)* animals. Many ectopic neurites branched out from the soma and the axonal shaft of the ALM neuron in *unc-69(e602)* mutant (arrowheads). **(g,h)** Tracings of representative electron micrographs of sections through the DNC and VNC. In the wild type (g), the position and content of the three major fascicles are highly stereotyped (black arrows). In *unc-69(e587)* mutants (h), defasciculated axons can often be found migrating separately along the body wall (open arrows). **(i,j)** Morphology of the bipolar AWC sensory neuron in (i) wild-type and (j) *unc-69(e587)* animals. Dendrites of AWC neurons in both animals reach the nose (arrows). Axonal shape is normal in wild-type worms (arrowhead in (i)), but abnormal in *unc-69(e587)* mutants, with ectopic bulges occasionally extending from the soma (arrowhead in (j)). **(k,l)** Expression pattern of *SCOCO* in stage 26 chick embryos. Sections were incubated with antisense (k) and sense (l) RNA probes for chick *SCOCO*. *SCOCO* was highly expressed in neural tissue and was most prominent in DRGs and in motoneurons of both the lateral motor column (LMC) and the medial motor column (MMC). Expression in the notochord (NC) and dermamyotome (DMT) was less pronounced. **(m,n)** *In ovo* RNAi of chick *SCOCO*. Embryos injected and electroporated with double-stranded RNA corresponding to (m) a *yfp*-containing plasmid or (n) chick *SCOCO* were immunostained with anti-neurofilament antibodies. In control embryos (m), the epaxial nerves extending dorsally toward their target, the epaxial muscle, were highly fasciculated. (n) RNAi of *SCOCO* led to defasciculation of epaxial nerve bundles and extensive branching between muscle segments (arrows). In all panels dorsal is up. Scale bars represent: (a-j) 10 μm, (k,l) 100 μm and (m,n) 500 μm.

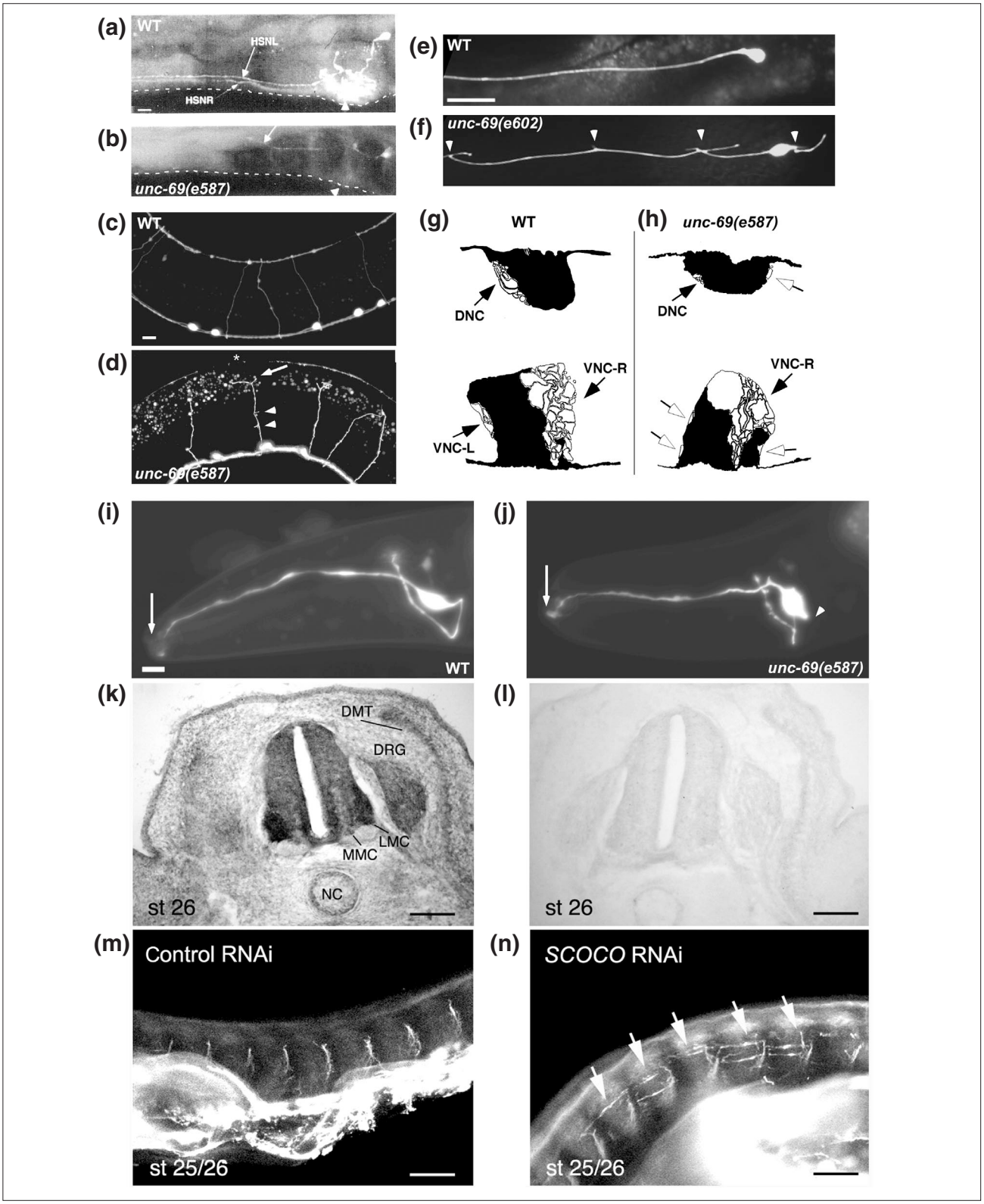

Figure 5 *(see legend on the previous page)*

dropped significantly. Similar observations were made for AVM outgrowth and branching. Note that none of the transgenic lines completely rescued the ALM outgrowth and branching defects. This could be due to loss or silencing of the transgene carried on the extrachromosomal array or could reflect a requirement for *unc-69* in other neuronal and/or non-neuronal cells. Nevertheless, we conclude that UNC-69 promotes outgrowth and guidance largely, if not completely, in a cell-autonomous manner.

UNC-69 is required for normal presynaptic organization

The *C. elegans* synaptobrevin/vesicle-associated membrane protein (VAMP) homolog SNB-1 is a vesicular soluble *N*-ethylmaleimide-sensitive factor attachment protein receptor (v-SNARE) on synaptic vesicles (SVs). Tagged SNB-1 can be used to follow SVs as they are transported to presynaptic regions [26]. We isolated an allele of *unc-69*, *ju69*, in a visual genetic screen for mislocalization of a SNB-1::GFP reporter in D-type GABAergic motor neurons. In wild-type worms, SNB-1::GFP expressed in the D neurons can be localized to discrete puncta along the VNC and DNC, at sites of neuromuscular junctions (Figure 6a,c). In *unc-69(ju69)* mutant nerve cords, SNB-1::GFP puncta were irregular in size and position, on average larger than in wild type, and often completely missing for extended stretches (Figure 6b,d,e). In addition, we occasionally observed puncta that abnormally diffused from the nerve cords into the commissures (Figure 6d). Despite the abnormal shape and distribution of presynaptic regions, the overall morphology of DD and VD neurons was grossly normal (Figure 6f-i) and only occasionally (<10%; n = 50) did one commissure fail to exit the VNC. We made similar observations in touch neurons using the P_{mec-4}*::gfp* transgene *zdIs5* (data not shown), a strain chosen for reconfirming findings made on D-type GABAergic motor neurons.

Much more dramatic SNB-1::GFP distribution defects were observed in the strong mutant *unc-69(e587)* (data not shown). Because of the extensive pathfinding defects observed in strong *unc-69* mutants, however, which might complicate interpretation of the SNB-1::GFP distribution defect, we restricted our subsequent analysis to the *unc-69(ju69)* background, in which axonal guidance is largely normal. Indeed, although *unc-69(ju69)* mutant worms are Unc, they move much better than strong *unc-69* mutants. Thus, the locomotion defect observed in *unc-69(ju69)* mutants is probably a consequence of a defect in transport or localization of axonal cargos rather than in axon guidance.

UNC-69 is not required for dendritic growth or for targeting proteins into dendrites

To determine whether the outgrowth defects we observed in *unc-69* mutants are specific to axons, we examined the morphology of the AWC class of sensory neurons using the *kyIs140* [P_{str-2}*::gfp*] transcriptional reporter, which is normally stochastically activated in either the right or left AWC neuron [27]. The bilaterally symmetric AWC neurons have a distinct bipolar structure, with a dendrite extending to the tip of the nose and an axon extending into the nerve ring (Figure 5i). In *unc-69(e587)* mutants, the axon of the AWC neuron often stopped prematurely (Figure 5j), and *str-2::gfp* expression was often silenced (see below). In contrast, the dendrite of the AWC neuron had no outgrowth defect, as 100% (136/136) of the AWC dendrites extended to their full length. In *unc-69(e587)* mutants, 73% (99/136) of AWC neurons had ectopic bulges or branches protruding from either the cell body or the axon (similar to what we observed in the mechanosensory neurons, Figure 5c). Ectopic branches only rarely extended from dendrites, however (data not shown). Dendritic morphology was also normal in the ASI neurons (visualized by the *str-3::gfp* transgene), the AWB, AWC, ASG, ASI, ASK, and ASJ neurons (visualized by the *tax-2Δ::gfp* transgene) [28,29], and the sensory neurons ASJ, ASH, ASI, ASK, ADL, and ADF (visualized by staining with the lipophilic dye DiI; data not shown). Finally, an odorant receptor was still properly localized to the cilia (see below). From these observations, we conclude that UNC-69 is probably not required for either cilia formation or dendritic elongation within the amphid sensilla, a sensory organ within the head of a worm.

In vesicle-trafficking mutants such as *unc-16 and unc-116*, markers for synaptic vesicles are also mis-sorted into dendrites [7]. We wondered whether *unc-69* mutants also show such a general sorting defect, or whether *unc-69* might be required more specifically for efficient trafficking within the axons. At the L1 larval stage, the thirteen VD neurons are not yet born, and the six DD neurons are the only D-type GABAergic motor neurons present in the VNC. At this stage, the DD neurons receive their synaptic inputs from the DNC and output onto the ventral body-wall muscles. In wild-type L1s, therefore, the SNB-1::GFP puncta can be seen only along the VNC. In *unc-69(ju69)* mutants, the synaptic GFP was not significantly mislocalized to the DNC (3.4%; n = 59; Figure 6k). In contrast, SNB-1::GFP puncta were frequently seen in the DNC in *unc-16(ju146)* mutant L1s (90.6%; n = 32; Figure 6k). We also made similar observations in worms carrying a *snb-1::gfp* transgene expressed in a pair of ASI sensory neurons, in which SNB-1::GFP was not significantly mislocalized to the ASI dendrites in *unc-69(ju69)* mutants (C-W.S., Y.J. and M.O.H., unpublished data).

We next asked whether UNC-69 has any role in transporting proteins within the dendrites. We used an *odr-10::gfp* transgene that is expressed in the AWB neurons to answer this question [30]. ODR-10 is an odorant receptor for diacetyl,

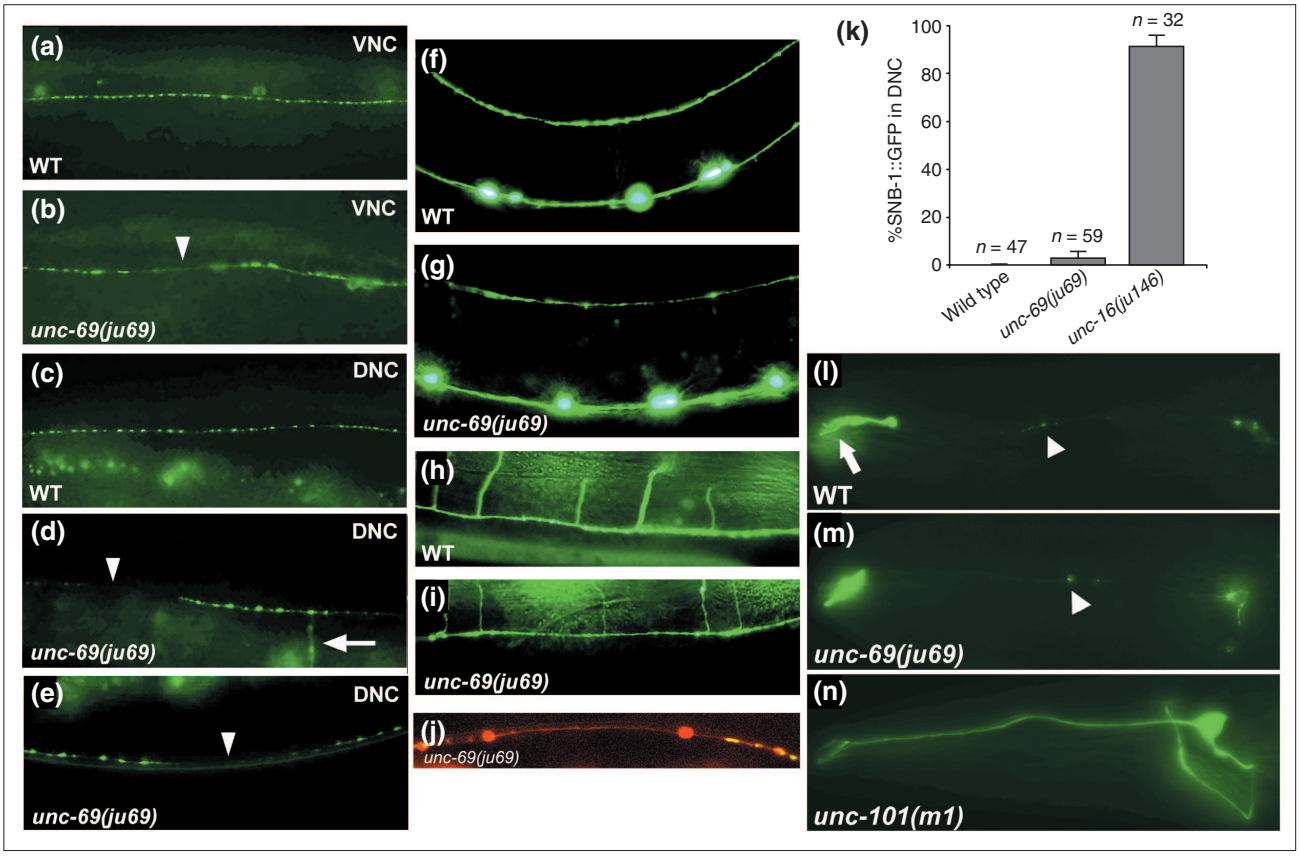

Figure 6

unc-69 affects axonal but not dendritic trafficking. **(a,c)** SNB-1::GFP is seen as evenly spaced puncta along the (a) VNC and (c) DNC in wild-type animals. **(b,d,e)** In *unc-69(ju69)* mutants, SNB-1::GFP puncta are on average bigger and often are absent from the VNC (arrowhead in (b)) and the DNC (arrowheads in (d,e)). In addition, SNB-1::GFP sometimes diffuses into the commissure (arrow in (d)). (a,b,e) Lateral views; (c,d) dorsal views of adult hermaphrodites. **(f-i)** As in wild-type animals (f,h), neuronal morphology is grossly normal in *unc-69(ju69)* mutants, and commissures still routinely reach the DNC (g,i). D-type GABAergic neuron morphology is visualized with the P_{unc-25}*::gfp* transgene *juIs76*. (f,g) Lateral views; (h,i) dorsal views. (j) Distribution of SNB-1::GFP puncta in a stretch of axon labeled with P_{unc-25}*::DsRed monomer* in the DNC in a *unc-69(ju69)* mutant hermaphrodite. SNB-1::GFP puncta are unevenly distributed, even though the DNC anatomy is grossly normal. **(k)** SNB-1::GFP is not significantly mislocalized into DD dendrites in *unc-69(ju69)* mutants. Animals carrying an *snb-1::gfp* transgene were scored at the L1 larval stage. Whereas 90% of *unc-16(ju146)* L1 larvae (n = 32) show dorsal GFP, 0% of wild-type L1s (n = 47) and 3% *unc-69(ju69)* L1s (n = 59) show dorsal GFP. Error bars represent the standard error of the mean. **(l-n)** The diacetyl odorant receptor ODR-10::GFP is targeted efficiently into AWB cilia both in (l) wild-type worms and (m) in *unc-69(ju69)* mutants. (n) In contrast, ODR-10::GFP becomes diffused in the dendritic targeting mutant *unc-101*. The arrow indicates the cilia; arrowheads indicate packets of ODR-10::GFP that shuttle in the dendrites. Anterior is to the left and dorsal is up.

and is actively transported in vesicles from the cell bodies to the cilia at the end of the dendrites, where the GFP fusion is deposited (Figure 6l). In dendritic targeting mutants, such as *unc-101* (which encodes the homolog of AP1 μ1 clathrin adaptor protein), ODR-10::GFP is not targeted to the AWB cilia [30] (Figure 6n); in contrast, in both *unc-69(ju69)* and *unc-69(e587)* mutants, ODR-10::GFP was still properly targeted (Figure 6m; data not shown). Taken together, our results suggest that dendritic development and transport of proteins into dendrites is not impaired in *unc-69* mutants. Thus, UNC-69 is possibly specifically required for axonal transport and outgrowth.

UNC-69 interacts physically with UNC-76

To identify potential UNC-69 interactors, we screened three *C. elegans* yeast two-hybrid libraries using full-length UNC-69 as bait. From these screens, we isolated at least 34 independent clones of UNC-76, a 385-amino-acid protein that was previously shown to be involved in axonal outgrowth and fasciculation in *C. elegans* [12-14]. The *Drosophila* homolog of UNC-76 was identified as a KHC-binding protein and shown to be a regulator of axonal transport [15]. A mammalian homolog of UNC-76, FEZ1, is a substrate for PKCχ [16]. Worm, fly and mammalian UNC-76 proteins are not only conserved in amino-acid sequence but

also have several conserved regions (Figure 7d) predicted to be capable of forming coiled-coil domains [14,15]. UNC-76 localizes to axons, and worms harboring mutations in *unc-76* have a severe Unc phenotype and coil ventrally, phenotypes very similar to those observed in *unc-69* mutants [14].

We used an *in vitro* glutathione *S*-transferase (GST) pull-down assay to verify the physical interaction between UNC-69 and UNC-76. As shown in Figure 7a, *in vitro* translated full-length UNC-76 (UNC-76FL) was pulled down efficiently by GST-UNC-69 but only minimally by GST-CBP, a eukaryotic transcription factor used as a negative control [31]. Conversely, *in vitro* translated adenoviral protein E1A efficiently bound to its cognate partner GST-CBP but not to GST-UNC-69. Therefore, the interaction between UNC-76 and UNC-69 is specific and most likely direct.

To narrow down the regions of interaction, we generated truncated proteins lacking various parts of UNC-76 (Figure 7b,d) and tested for their interaction with GST-UNC-69. We found that amino acids 281 to 299 of UNC-76 were necessary to interact with UNC-69 *in vitro*. Interestingly, this 19-amino-acid region overlaps with a region predicted to form a coiled-coil structure (amino acids 265-292; purple region

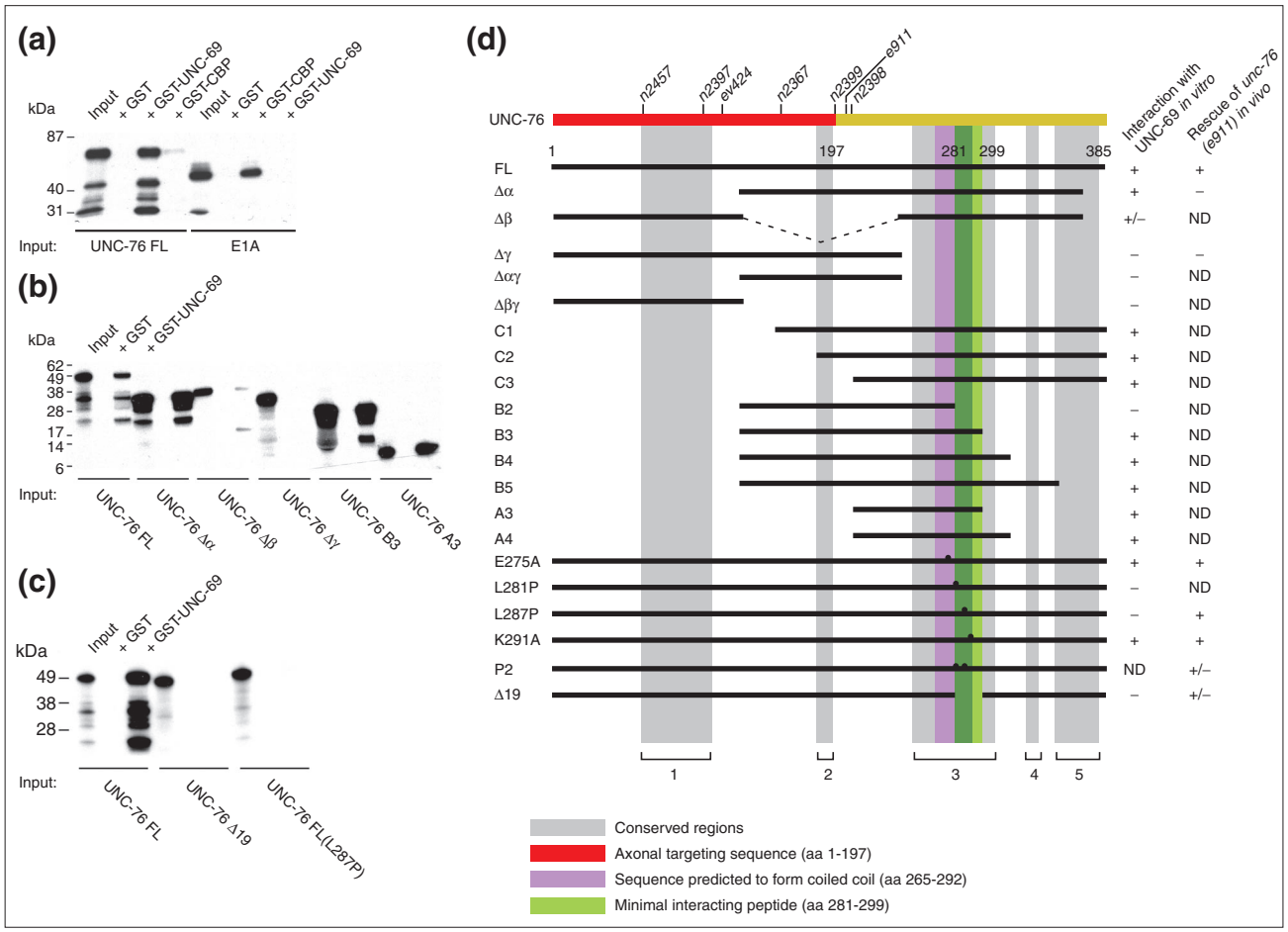

Figure 7
UNC-69 physically interacts with UNC-76, as shown by *in vitro* GST pull-down assays. (a) Full-length UNC-76 (UNC-76 FL) specifically binds to full-length GST-UNC-69 but not GST-CBP. The E1A-CBP interaction was used as a positive control. (b) Serial deletions of UNC-76: a portion of the carboxy-terminal region (deleted in UNC-76 Δγ but contained within UNC-76 B3 and A3) is necessary for interaction with GST-UNC-69. (c) Point mutation L287P or a small 19-amino-acid deletion (UNC-76 Δ19), which deletes amino acids 281-299, totally abolishes the ability of UNC-76 to bind GST-UNC-69. (d) Summary of the deletion analysis, as well as the results of rescuing experiments. Gray shading indicates conserved regions. Note that UNC-76 Δ19 not only loses its binding ability but also its rescuing activity for the *unc-76(e911)* mutants. The 19-amino-acid region (green) lies within a conserved region and overlaps with a region we predicted to form a coiled-coil domain (purple). A previously described axonal targeting sequence [14] is in red. The positions of different *unc-76* alleles are indicated.

in Figure 7d) and lies within a region conserved from worms to humans (gray-shaded region in Figure 7d).

UNC-76 may require interaction with UNC-69 to function *in vivo*

To corroborate the *in vitro* interactions with the *in vivo* function of UNC-76, we expressed truncated UNC-76 proteins tagged with yellow or cyan fluorescent protein (YFP or CFP) in *unc-76(e911)* mutant worms (Figure 7d) and assayed for rescue of the Unc phenotype. Both amino-terminally and carboxy-terminally tagged full-length UNC-76::YFP or CFP::UNC-76 fusion proteins were functional and rescued *unc-76(e911)* mutants (Figure 7d). The CFP::UNC-76 Δα fusion protein (which lacked the amino terminus of UNC-76) failed to rescue *unc-76(e911)* mutants, suggesting that the amino-terminal region of UNC-76 is required for its function *in vivo*. Bloom and Horvitz reported that amino acids 1-197 of UNC-76 are sufficient to direct proteins into the axons in *C. elegans* [14]. As the axonal targeting sequence of UNC-76 includes the region deleted in UNC-76 Δα, we speculated that CFP::UNC-76 Δα fusion proteins were not transported to axons. Indeed, the CFP signal was weak and seemed to congregate more around the soma (data not shown). In contrast, the CFP::UNC-76 Δγ fusion protein was both strongly expressed in soma and axons, but failed to rescue *unc-76(e911)* mutants, consistent with the hypothesis that binding to UNC-69 is critical for UNC-76 to function *in vivo*.

If coiled-coil structures are important for the UNC-76-UNC-69 interaction, any mutation that abolishes the coiled-coil structure would possibly also abolish physical interaction between the two proteins. To test this idea, we mutagenized four conserved residues in UNC-76: Glu275, Leu281, Leu287, and Lys291. Both UNC-76(E275A) and UNC-76(K291A) mutant proteins still bound UNC-69 *in vitro* (Figure 7d). Likewise, YFP fusions of these mutant proteins rescued *unc-76(e911)* mutants. In contrast, both UNC-76(L281P) and UNC-76(L287P) mutant proteins failed to bind UNC-69 *in vitro*. Surprisingly, UNC-76(L287P) was still able to rescue *unc-76(e911) in vivo* (Figure 7c,d; we did not test UNC-76(L281P) for rescue). These data suggest that a single -amino-acid substitution might not be potent enough to destroy the coiled-coil structure when UNC-76 protein is folded in its native state. Finally, we created a mutant protein carrying both L281P and L287P mutations (P2), as well as an internal deletion mutant, Δ19, which deletes amino acids 281-299 of UNC-76. Both P2 and Δ19 mutants largely failed to rescue *unc-76(e911) in vivo* (Figure 7d; occasionally, mutant hermaphrodites carrying the *unc-76 P2::yfp* or the *unc-76 Δ19::yfp* transgenes were slightly rescued as young adults). In summary, amino acids 281-299 of UNC-76 probably contain or overlap with an UNC-69-binding site, and UNC-76 may require interaction with UNC-69 to function *in vivo*.

UNC-69 and UNC-76 act in the same pathway to control axon extension

As both UNC-69 and UNC-76 are required for axon outgrowth and fasciculation, we asked whether they function in the same genetic pathway to regulate axon extension. We first tested whether overexpression of UNC-69 in *unc-76(lf)* mutants could bypass the *unc-76* mutant phenotype. We overexpressed a functional *unc-69::gfp* transgene as an extrachromosomal array in *unc-76(e911)* mutants but did not see any rescue in locomotion (three independent lines, data not shown). Likewise, overexpression of a functional *unc-76::yfp* transgene failed to rescue the locomotion defect of *unc-69(e587)* mutants (data not shown).

We also performed a double-mutant analysis to further address the question of whether *unc-69* and *unc-76* act in the same pathway. In *C. elegans*, expression of the odorant receptor gene *str-2* is randomly turned on in either the left or the right AWC sensory neuron (AWCL/R), but never in both [27]. In wild-type worms, this '1 AWC^{ON}' phenotype is determined by axonal contact and calcium signaling between AWCL and AWCR. In axonal guidance mutants such as *unc-76*, *sax-3* and *vab-3*, the two AWC axons often fail to meet, and $P_{str\text{-}2}$*::gfp* expression is consequently silenced in both AWCs, giving rise to a '2 AWC^{OFF}' phenotype [27]. We used this system to quantitatively score axon extension defects in the nerve ring in different *unc-69(lf)* and *unc-76(lf)* mutants as well as in *unc-69(lf); unc-76(lf)* double mutants.

In both strong loss-of-function mutants, *unc-69(e602)* and *unc-69(e587)*, 30-34% of animals showed a 2 AWC^{OFF} phenotype. In contrast, the hypomorphic allele *unc-69(ju69)* resulted in only 1% of mutant worms (n = 190) having $P_{str\text{-}2}$*::gfp* expression silenced in both AWCs (Table 3). This result was consistent with our previous observation that neuronal morphology is largely normal in *unc-69(ju69)* mutants. In agreement with previous studies [27], 47% of *unc-76(e911)* mutants (n = 101) had the 2 AWC^{OFF} phenotype; *e911* was the strongest allele among all the nine alleles that we tested. For the other *unc-76* alleles, the 2 AWC^{OFF} phenotype varied from 6% to 30%. Interestingly, the strength of the AWC expression defect (which is an indication of axon extension defects) showed an inverse colinear relationship with the position of each mutation in the open reading frame: the most 5′ mutation, *unc-76(n2457)*, showed the least defect in axon extension, whereas alleles located most carboxy-terminally showed greater defects than alleles located close to the amino terminus (Table 3). Interestingly, we did not observe enhancement of axon

Table 3

Quantitative analysis of axon extension defects in *unc-69(lf)*, *unc-76(lf)* and other mutants

Genotype	2 AWC^{OFF} (%)	1 AWC^{ON} (%)	2 AWC^{ON} (%)	*n*
Wild type	1	99	0	442
unc-69				
unc-69(ju69)	1	99	0	190
unc-69(e602)	34	66	0	119
unc-69(e587)	30	70	0	194
unc-76				
unc-76(rh116)	11	89	0	83
unc-76(n2457)	6	94	0	102
unc-76(n2397)	8	92	0	64
unc-76(ev424)	10	90	0	68
unc-76(n2367)	30	70	0	84
unc-76(n2399)	25	75	0	67
unc-76(e911)	47	53	0	101
unc-76(e911); lon-2(e678)	31	69	0	91
unc-76(n2398)	28	72	0	184
Double mutants				
unc-69(e602); unc-76(n2457)	35	65	0	106
unc-69(e602); unc-76(e911)	48	52	0	118
unc-69(e587); unc-76(n2457)	33	67	0	108
unc-69(e587); unc-76(e911)	31	69	0	143
Other axonal guidance mutants				
sax-3(ky123)	64	33	3	112
lon-2(e678) unc-6(n102)	38	62	0	65
vab-3(e648)	54	40	6	68
unc-33(e204)	7	73	20	135
unc-119(ed3)	12	48	39	99
Other double mutants				
unc-76(e911); sax-3(ky123)	95	5	0	22
unc-76(e911); lon-2(e678) unc-6(n102)	73	27	0	152
unc-76(e911); vab-3(e648)	63	27	10	62
unc-33(e204); unc-76(e911)	80	18	1	291
unc-119(ed3); unc-76(e911)	65	32	3	167

All animals scored had *kyIs140* ($P_{str\text{-}2}$::*gfp*) in the background, which turns on its expression in only one of the two AWC neurons (1 AWC^{ON}) in wild-type animals. In axon guidance mutants, $P_{str\text{-}2}$::*gfp* expression is silenced in both AWCs (2 AWC^{OFF}) owing to failure of axonal contact. All *unc-69* and *unc-76* alleles except *unc-76(rh116)* are arranged in order according to their physical position (5' to 3') in the open reading frame. *n*, number of animals scored.

extension defects in *unc-69; unc-76* double mutants: in all cases, the defect in the double mutant was no stronger than in the stronger of the single mutants (Table 3). In contrast, axon extension defects were greatly enhanced in *unc-76(e911); sax-3(ky123)*, *unc-76(e911); unc-6(n102)* and *unc-33(e204); unc-76(e911)*, and slightly enhanced in *unc-76(e911); vab-3(e648)* and *unc-119(ed3); unc-76(e911)* double mutants (Table 3). Because *unc-76* alleles failed to show any additivity with the candidate null alleles *unc-69(e587)* and *unc-69(e602)*, we conclude that UNC-69 and UNC-76 probably act in the same pathway to control axon extension, at least in the case of the AWC sensory neurons.

UNC-69 and UNC-76 regulate presynaptic organization cooperatively

We showed above that UNC-69 is required for localization of synaptic vesicles in axons. Does UNC-76 also have a role in this process, and if so, does UNC-76 control presynaptic organization together with UNC-69? Unfortunately, all existing *unc-76* alleles have severe axonal outgrowth defects, making interpretations of defect in synaptic vesicle localization difficult. To bypass this problem and to reveal possible genetic interactions between *unc-69* and *unc-76*, we looked at the localization of the synaptobrevin SNB-1::GFP puncta in *unc-69(lf)*/+; *unc-76(lf)*/+ double heterozygotes (Figure 8).

In wild-type adult hermaphrodites, SNB-1::GFP can be seen as evenly distributed puncta along the DNC [7] (Figure 8a,e). The distribution pattern of GFP puncta in DNC was not significantly different in *unc-69(e587)*/+ heterozygotes (Figure 8b) as compared with wild-type animals. However, in both *unc-69(e587)*/+; *unc-76(e911)*/+ and *unc-69(e587)*/+; *unc-76(n2457)*/+ double heterozygous hermaphrodites, SNB-1::GFP puncta were occasionally more diffused, larger, or completely absent within a stretch of DNC (Figure 8c,d,f); the absence of SNB-1::GFP puncta may be due to either transport or axon extension defects. In addition, *unc-69(e587)*/+; *unc-76(e911)*/+ and *unc-69(e587)*/+; *unc-76(n2457)*/+ double

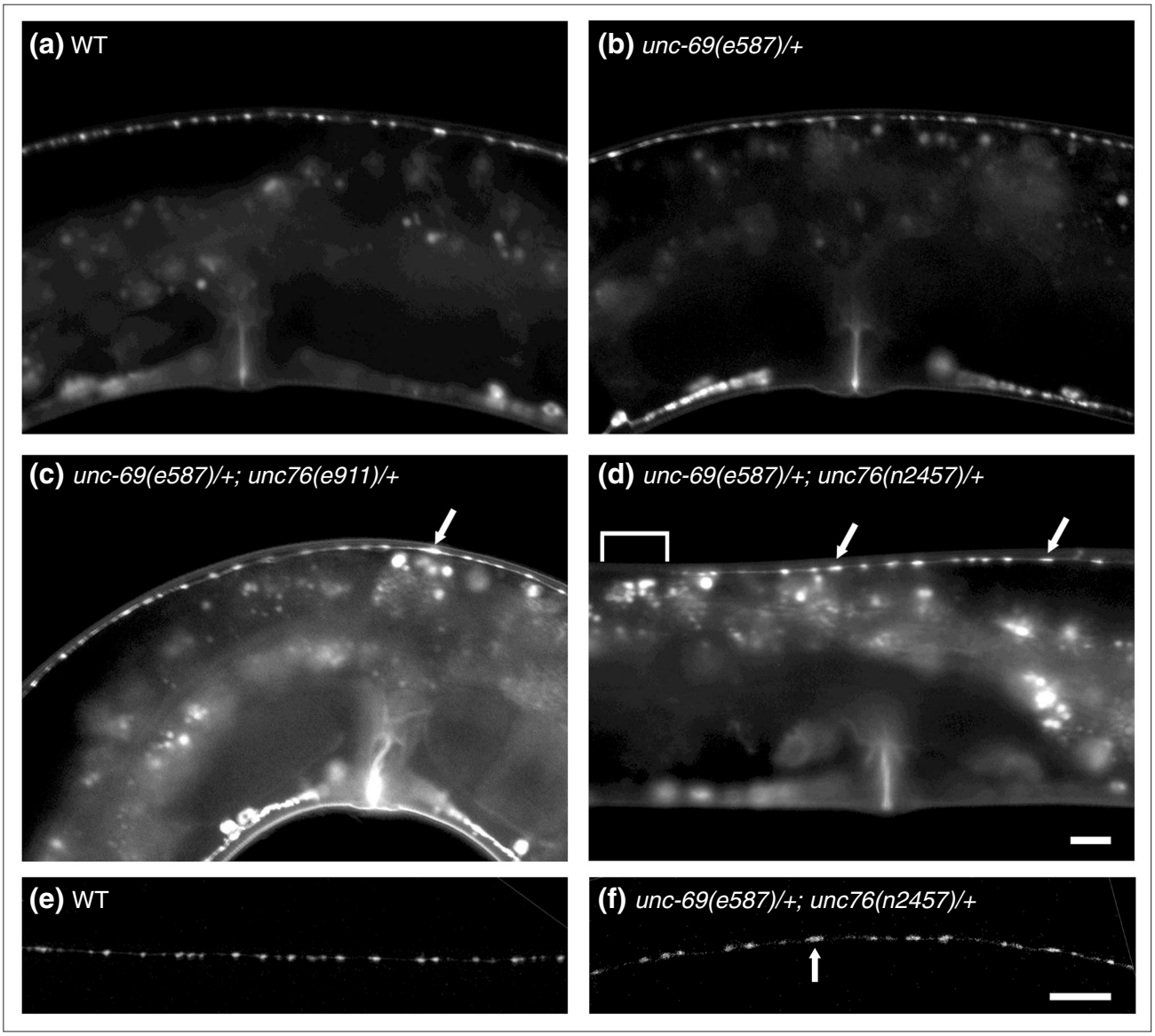

Figure 8
UNC-69 and UNC-76 cooperate to regulate the size and position of synaptic vesicles. (a-d) Lateral view of adult hermaphrodites 52-54 h after hatching, single section. (e,f) Lateral view of the DNC of adult hermaphrodites 52-54 h after hatching, flattened images of confocal z-stack. Anterior is to the left and dorsal is up. (a,e) SNB-1::GFP is evenly distributed along the DNC in wild-type animals. (b) Removing one copy of *unc-69* does not affect SNB-1::GFP distribution. (c,d,f) SNB-1::GFP becomes diffused and the puncta becomes larger (arrows) in *unc-69(e587)*/+; *unc-76(e911)*/+ and *(unc-69(e587)*/+; *unc-76(n2457)*/+ double heterozygotes. Occasionally, SNB-1::GFP is missing altogether from a stretch of the DNC (bracket in (d)). The genotypes are as follows: (a,e) *juIs1 [P_{unc-25}::snb-1::gfp]*, (b) *qC1/unc-69(e587); juIs1*, (c) *qC1/unc-69(e587); nT1[qIs51]/juIs1; nT1[qIs51]/unc-76(e911)*, (d,f) *qC1/unc-69(e587); nT1[qIs51]/juIs1; nT1[qIs51]/unc-76(n2457)*. Scale bars represent 10 μm.

heterozygotes occasionally had a slight Unc phenotype in locomotion, resembling weak synaptic transmission mutants. The weak locomotion defect could be a direct or indirect effect of the synaptic vesicle mislocalization defect.

In summary, the *unc-69*/+; *unc-76*/+ double heterozygotes show phenotypes that are similar, albeit significantly weaker, to those observed in *unc-69(ju69)* homozygotes. Haplo-insufficient genetic interactions of this type, commonly known as nonallelic (or unlinked) noncomplementation, are often observed with proteins that form heterodimers or function in a common protein complex (such as α- and β-tubulin; [32]). Several other explanations are also possible, however (discussed in [33]). Thus, our observations are compatible with, but do not definitively prove, the hypothesis that UNC-69 and UNC-76 act in a common pathway required for proper synaptic -vesicle localization.

UNC-69 and UNC-76 colocalize in punctate structures in axons and cell bodies

To determine the subcellular localization of UNC-69 and UNC-76, we coinjected P_{unc-69}*::cfp::unc-69* and P_{unc-76}*::unc-76::yfp* constructs at low concentration (5 ng/μl) into *unc-76(e911)* mutant hermaphrodites, and selected rescued transgenic animals for examination. At low concentration, both CFP::UNC-69 and UNC-76::YFP often appeared as puncta along the DNC, in CAN neurons, as well as in other neuronal processes that run along the subdorsal and subventral tracts (Figure 9a-f). Less frequently, these puncta could also be found in commissures that connect the DNC to the VNC. The punctate pattern of UNC-76 can also be observed when worms are stained with anti-UNC-76 antisera [14], consistent with this being the endogenous expression pattern of UNC-76. Both CFP::UNC-69 and UNC-76::YFP puncta were of variable size but were usually large and immobile, even in the commissures. Interestingly, CFP::UNC-69 and UNC-76::YFP proteins also colocalized in round, perinuclear dots in the soma (Figure 9j-l). These observations strengthen our belief that UNC-69 and UNC-76 coexist in a protein complex. The molecular nature of the observed UNC-69-UNC-76 puncta (multiprotein complexes or vesicles, perhaps) remains to be determined.

UNC-116/kinesin heavy chain is required for proper subcellular distribution of both UNC-69 and UNC-76

In *Drosophila*, Unc-76 associates and copurifies with KHC, which is the major component of the conventional kinesin motor Kinesin-1 required for axonal transport towards the plus ends of microtubules [15]. A similar biochemical interaction between UNC-76 and the *C. elegans* KHC ortholog UNC-116 [34] has not been reported so far. To determine whether the UNC-69-UNC-76 complex is transported to axons by UNC-116, or by another kinesin, the KIF1A homolog UNC-104 [35], we compared the subcellular localization of both CFP::UNC-69 and UNC-76::YFP in wild-type and in different kinesin mutant backgrounds.

In *unc-116(rh24)* mutants, UNC-76::YFP puncta were occasionally diffuse and sometimes failed to be accompanied by CFP::UNC-69 puncta in a stretch of axon (Figure 9g-i). In addition, both CFP::UNC-69 and UNC-76::YFP proteins

Figure 9 *(see figure on the following page)*
UNC-69 and UNC-76 colocalize as puncta in neuronal processes. (a-o) Functional P_{unc-69}*::cfp::unc-69* and P_{unc-76}*::unc-76::yfp* constructs were coinjected at 5 ng/μl each into *unc-76(e911)* mutants, and worms rescued for locomotion were selected. Note that the *unc-76(e911)* mutation was removed from the background in (g-o). (d-o) are deconvolved single-layer images. (a-c) Lateral view of an adult hermaphrodite from one line of transgenic animals with a wild-type phenotype. Both CFP::UNC-69 and UNC-76::YFP form discrete, large puncta in the DNC, as well as in the commissure (arrow). Vignette in (c) shows an enlarged image of colocalized puncta in the DNC from the rectangle. (d-f) Lateral view of an adult hermaphrodite from a second line of transgenic animals with a wild-type phenotype. Note that CFP::UNC-69 and UNC-76::YFP are both cytoplasmic and punctate, and the puncta are present in lateral and sublateral processes. (g-i) In *unc-116(rh24)* mutants, UNC-76::YFP puncta became diffuse in a stretch of axon in the VNC, and failed to colocalize with CFP::UNC-69 (arrows in (h,i)). (j-l) CFP::UNC-69 and UNC-76::YFP colocalize in perinuclear structures in the soma of a neuron in the tail ganglia. (m-o) In *unc-116(rh24)* mutants, both UNC-76::YFP and CFP::UNC-69 often appear as partially overlapping or non-overlapping aggregates in the soma of a preanal (i) and two tail ganglion neurons ((ii-iii)). (p-u) Expression pattern of (p-r) *opIs124* (P_{unc-69}*::unc-69::gfp*) and (s-u) *opIs130* (P_{unc-76}*::unc-76::yfp*). Both transgenes were integrated into the genome to ensure stable gene expression. All pictures show the CAN neuron soma (arrowhead) and its vicinity. (p,s) In wild-type worms, the CAN neuron extended its bipolar processes along the excretory canal, and the CAN neurites were filled with UNC-69::GFP and UNC-76::YFP. Note that puncta cannot be seen in these integrants owing to overexpression of the transgenes. (q) In *unc-104(e1265)* mutants, UNC-69::GFP accumulated near the CAN soma as well as in its neuronal processes (asterisks), giving it a notched appearance. (t) UNC-76::YFP localization appeared to be grossly normal in *unc-104(e1265)* mutants. (r,u) In *unc-116(rh24)* mutants, both UNC-69::GFP and UNC-76::YFP accumulated in CAN neurites (asterisk). UNC-69::GFP accumulation was prominent near the CAN soma and was accompanied by ectopic branches. In contrast, UNC-76::YFP aggregated and was evenly distributed along the CAN processes. The scale bar represents 20 μm. (v,w) The CAN neuron visualized by the integrated transgene *kyIs4* (P_{ceh-23}*::ceh-23::unc-76*$_{1-197}$*::gfp*). (v) In wild-type worms, GFP appeared as string of dots, reminiscent of endogenous UNC-76 expression pattern. (w) In *unc-116(rh24)* mutants, GFP dots became larger and more dispersed. (x,y) CAN neuron visualized by an extrachromosomal array *opEx901* (P_{unc-69}*::gfp*). Unlike the UNC-69::GFP fusion (r), GFP itself did not accumulate significantly around CAN soma in *unc-116(rh24)* mutants (y), although ectopic branches were frequently observed. (p-y) are confocal z-stack images. Anterior is to the left in (a-i) and (p-y); anterior is up and ventral is to the right in (j-o). All scale bars except in (p-u) represent 10 μm.

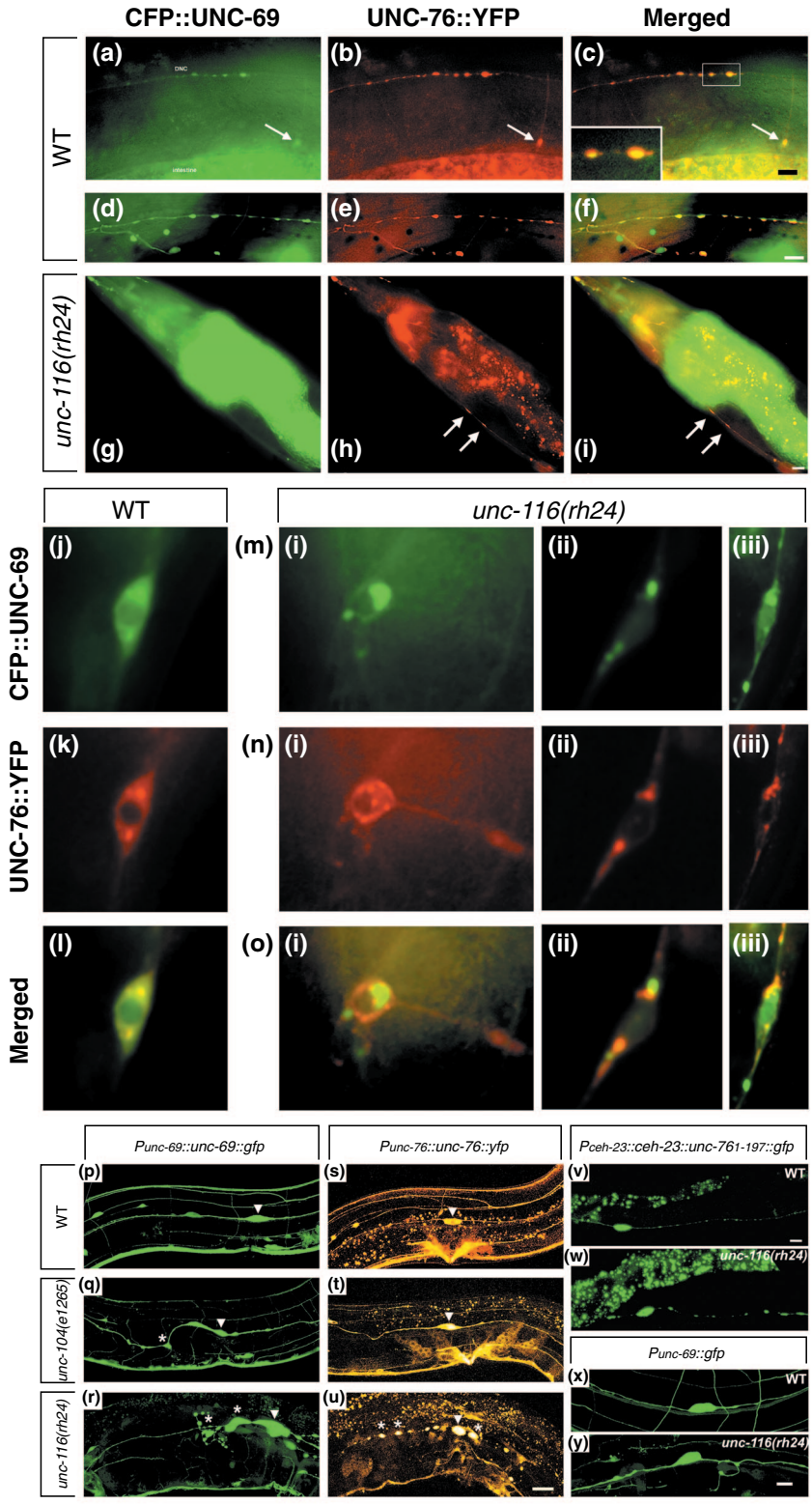

Figure 9 *(see legend on the previous page)*

often occupied distinct but partially overlapping perinuclear territories in the soma in *unc-116(rh24)* mutants (Figure 9m-o). Whereas perinuclear CFP::UNC-69 dots increased in size in *unc-116(rh24)* mutants, perinuclear UNC-76::YFP either split into several smaller dots (as in Figure 9n(i)) or formed irregular reticular structure (as in Figure 9n(iii)) in *unc-116(rh24)* mutants. The *unc-116(rh24)* mutants carry two missense mutations (I304M and E338K) at the end of the motor domain of KHC (amino acids 1-358) [34]. Thus, these mutations are likely to affect the processivity of KHC and cargo transport along the microtubules.

We also generated functional integrated UNC-69::GFP and UNC-76::YFP transgenes that were stably overexpressed in the nervous system and studied their subcellular localization in different kinesin mutant backgrounds. The CAN neurons are a pair of bilaterally symmetric neurons that send processes antero-posteriorly along the excretory canal (Figure 9p) [36]. In wild-type animals, UNC-69::GFP and UNC-76::YFP could be observed both in the CAN soma and throughout the processes (Figure 9p,s). In worms mutant for *unc-104(e1265)*, the *C. elegans KIF1A* homolog [35], subcellular distribution of UNC-69::GFP and UNC-76::YFP was not significantly altered (Figure 9q,t). In *unc-116(rh24)* mutants, overexpression pattern of UNC-69::GFP and UNC-76::YFP were both significantly different from wild-type animals. The CAN neuron accumulated UNC-69::GFP in the vicinity of its cell body, which was swollen and deformed. In addition, there were ectopic branches near the cell body, and UNC-69::GFP also accumulated in these processes (Figure 9r). Unlike UNC-69::GFP, UNC-76::YFP appeared as giant dots along the CAN processes in *unc-116(rh24)* mutant, as if UNC-76::YFP was removed from the cytoplasm and concentrated in certain subcellular compartments (Figure 9u). Moreover, a CEH-23::UNC-$76_{1\text{-}197}$::GFP fusion protein [37] also appeared as large aggregates along CAN processes in *unc-116(rh24)* mutants (Figure 9w).

In summary, our data show that the subcellular distribution of both UNC-69 and UNC-76 is altered in *unc-116(rh24)* mutants. It is striking that the nearly perfect co-localization of UNC-69 and UNC-76 is disrupted in *unc-116* mutants. We are still at a loss to explain the molecular basis of this unexpected finding. What is clear, however, is that axonal transport of UNC-69 and UNC-76 is still occurring in *unc-116(rh24)* mutants. Thus, other kinesin motors and/or additional factors probably contribute to transport of UNC-69 and UNC-76 along the axons.

UNC-69 does not interact with ARL-1, ARL-3, or ARFRP

UNC-69 homologs in *S. cerevisiae* and mammals have been reported to interact physically with members of the family of ARF-like small GTPases. To investigate whether a similar interaction occurs in *C. elegans*, we first used yeast two-hybrid assays to study protein-protein interactions between UNC-69 and three closely related but distinct ARF-like small GTPases, ARL-1 (F54C9.10), ARL-3 (F19H8.3), and ARFRP (Y54E10BR.2) [38]. Whereas UNC-69 readily interacted with the carboxyl terminus of UNC-76 (UNC-76γ), it did not interact with any of the three ARF-like proteins (Figure 10a). As human SCOCO was isolated as an effector for GTP-bound ARL-1 [20], we also tested the ability of UNC-69 to interact with GTPase-defective forms of ARL-1 and ARFRP. UNC-69 did not interact with either ARL-1(Q70L) or ARFRP(Q79L) (Figure 10a). Deletion of the amino-terminal myristoylation site [39] also had no effect: UNC-69 did not interact with the amino-terminal deletion ARL mutants, ARL-1Δ16 or ARL-3Δ17, with or without the GTPase-defective mutation (data not shown). In contrast, we readily detected the previously reported interaction between ARL-3 and UNC-119 [40], a homolog of human retinal gene 4 (HRG4) [41-43] (Figure 10b). Thus, the failure to detect any interaction between UNC-69 and the three ARF-like proteins might not have been due to inappropriate protein folding or subcellular compartmentalization in yeast.

UNC-69 and mannosidase II occupy partially overlapping subcellular regions

To address directly the question of whether UNC-69 is a Golgi-associating protein, we coexpressed CFP::UNC-69 and a YFP-tagged fragment of the *C. elegans* Golgi protein mannosidase II F58H1.1 (mansII::YFP) [44]. Unlike the colocalization pattern we observed previously for UNC-69 and UNC-76, UNC-69 and mansII only occasionally colocalized (Figure 11). Moreover, we clearly observed regions in which both UNC-69 and mansII occupied non-overlapping subcellular territories, even under overexpression conditions (arrows in Figure 11c,f,i). This mutual exclusion could not simply be explained by the squeezing out of UNC-69 from the mansII-containing territories as a result of spatial constraint, as UNC-69 and mansII territories did sometimes overlap (arrowheads in Figure 11c,i).

Taken together, our results suggest that any interaction between UNC-69 and Golgi is at best transient, and that the UNC-69 puncta probably represent a structure distinct from the Golgi.

UNC-69/SCOCO is required for axon pathfinding and fasciculation in chicken embryos

Although we failed to find any clear link between UNC-69 and Golgi-associated transport in *C. elegans*, two lines of evidence do suggest that the molecular function of UNC-69/SCOCO is conserved through evolution. First, the level

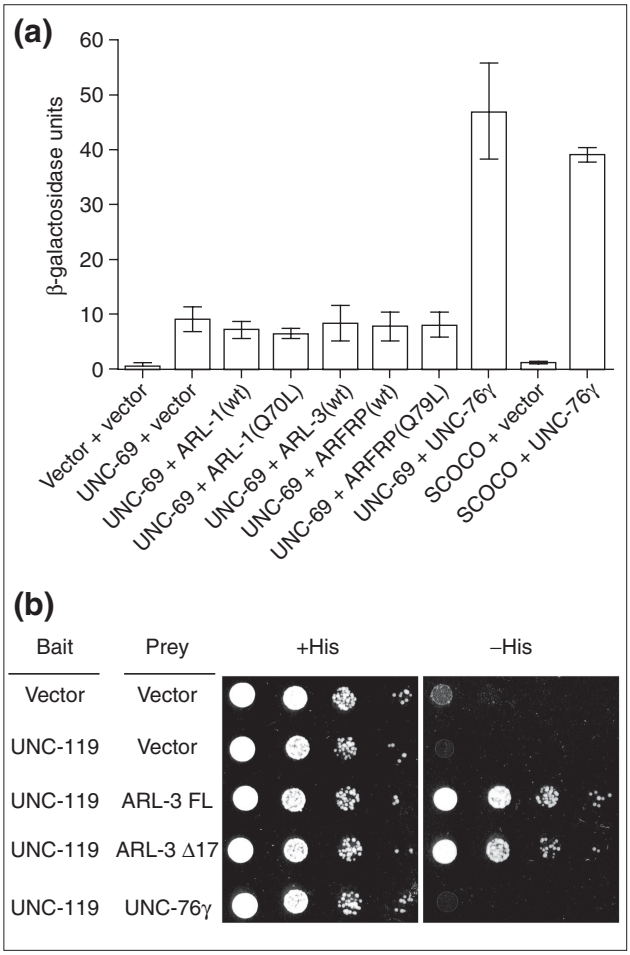

Figure 10
UNC-69 does not interact with ARL-1, ARL-3 or ARFRP. (c) Plasmids containing *LexA-unc-69* or *LexA-human SCOCO* were cotransformed into yeast cells with vector alone or vectors containing *GAD-unc-76γ*, *GAD-arl-1*, *GAD-arl-3*, *or GAD-arfrp*. Protein-protein interactions were measured as β-galactosidase activity by using ONPG liquid assays. UNC-69 did not interaction with any of the three ARL proteins. SCOCO did not interact with any of the three ARL proteins either (data not shown). (b) Auxotrophic growth assays for interactions between LexA-UNC-119 and GAD-ARL-3 or GAD-UNC-76γ. Cells (3×10^4) were plated onto +His or -His plates, and serial tenfold dilutions of cells were then subsequently plated. Cells were grown at 30°C for 48 h before images were taken. Note that the -His plate did not contain 3-amino triazol. The strength of interaction between UNC-119 and ARL-3Δ17 was only a fifth of that between UNC-119 and ARL-3 FL, as assayed by β-galactosidase activity (data not shown).

of conservation between family members is extremely high in all the metazoans analyzed (see Figure 3a). Second, overexpression of human SCOCO is sufficient to rescue the uncoordinated phenotype (and hence the axon guidance defects) of *unc-69* mutants, suggesting that human SCOCO can substitute for UNC-69 (see Figure 3c). There are, however, no reports so far on a possible role for UNC-69/SCOCO in vertebrate development. To address this issue, we studied the function of UNC-69/SCOCO in nervous system development of chicken embryos.

Expression of the chick homolog of *unc-69*/*SCOCO* was detected by *in situ* hybridization in the spinal cord of stage 22 embryos. Expression increased with time, peaking at around stage 26 (Figure 5k). In chicken embryos, SCOCO was expressed in motor neurons of both the lateral motor column (LMC) and the medial motor column (MMC). In addition to neural tissues, staining was also present in the dermamyotome (Figure 5k). Blocking the function of SCOCO with *in ovo* RNA interference (RNAi) [45] resulted in aberrant pathfinding of the epaxial nerve fibers (Figure 5n). The epaxial nerve is formed by axons of motoneurons of the MMC. These axons leave the spinal cord together with the neurons of the LMC to form the ventral root. Instead of growing into the developing limb, however, they leave the ventral root by a sharp dorsal turn. In control embryos, epaxial axons grew dorsally in a fasciculated manner and started branching only after reaching the territory of the prospective epaxial muscle (Figure 5m). In contrast, axons of epaxial motoneurons lacking UNC-69/SCOCO were strongly defasciculated and started to extend along the longitudinal axis of the embryo before reaching their dorsal destination (81% of *unc-69/SCOCO* RNAi treated embryos (n = 26) showed defects, versus 10% of control embryos (n = 20); Figure 5n and Additional data file 1). Because our *in ovo* RNAi approach selectively knocks down UNC-69/SCOCO expression in the spinal cord neurons, we conclude that the chick homolog of UNC-69/SCOCO is likely to function autonomously in epaxial nerve cells to control axon pathfinding, consistent with our observations in worms.

From the above analysis, we conclude that the function of UNC-69/SCOCO in axon guidance and nervous- system development is probably conserved through evolution. On the basis of its high degree of sequence conservation and its expression pattern, we predict that SCOCO is also required for nervous system development in mammals, including humans.

Discussion

UNC-69 is required for normal presynaptic organization and axonal outgrowth

In this work we show that mutations that affect the small 108-amino-acid protein UNC-69 abrogated a spectrum of processes, including synaptic-vesicle targeting, axonal outgrowth, pathfinding, and fasciculation. Although a weak reduction-of-function allele of *unc-69* results in a selective

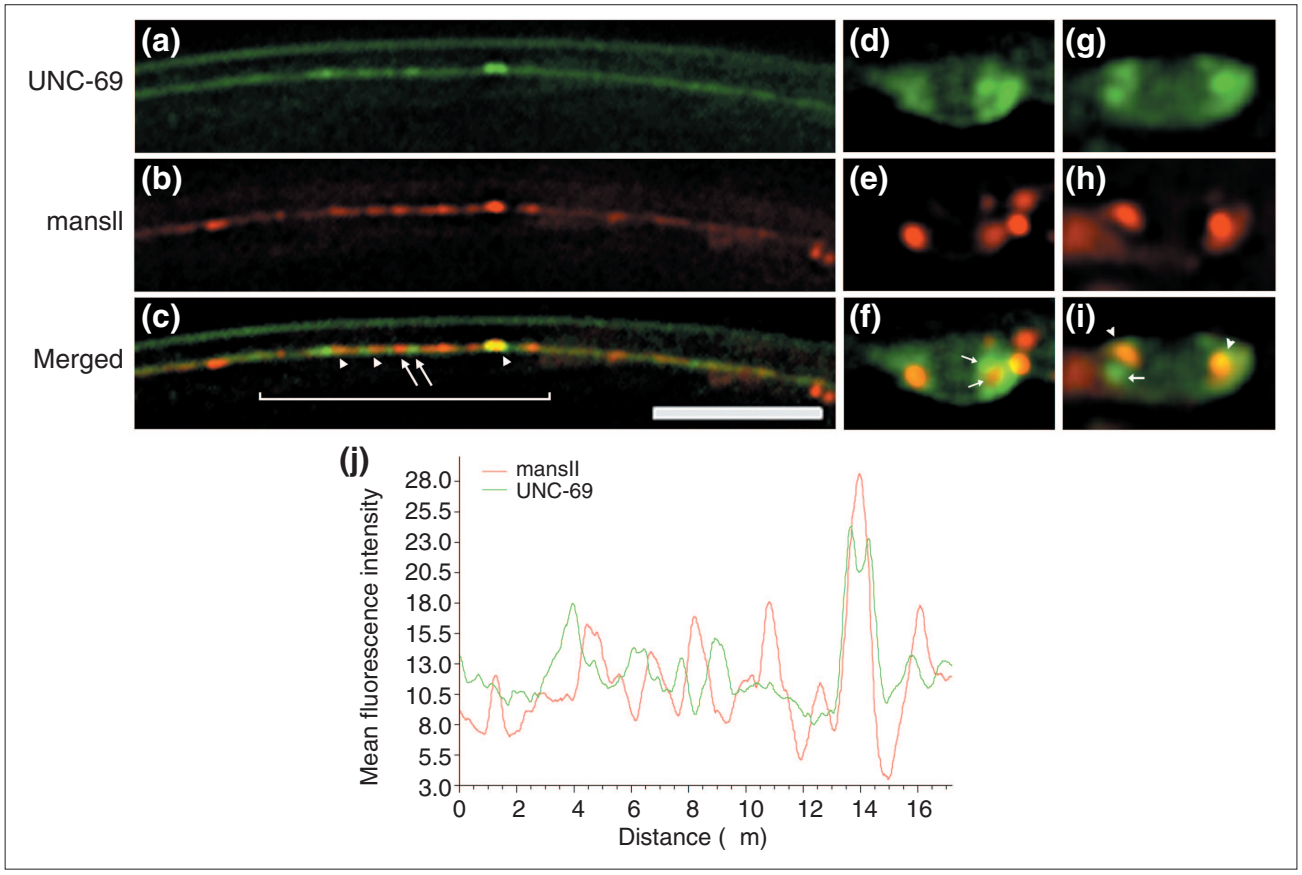

Figure 11
UNC-69 does not colocalize with the Golgi marker mansII. P_{unc-69}*::cfp::unc-69* and P_{unc-69}*::mansII::yfp* plasmids were coinjected at 5 ng/μl each into *unc-69(e587)* mutant hermaphrodites, and worms rescued for locomotion were selected for analysis. (a-c) Subcellular localization of CFP::UNC-69 and mansII::YFP in a stretch of axon in the DNC in an adult hermaphrodite animal. The scale bar represents 10 μm. (d-i) Subcellular localization of CFP::UNC-69 and mansII::YFP in the cell bodies of a tail neuron (d-f) and a neuron in the VNC (g-i) in adult hermaphrodite animals. UNC-69 and mansII usually occupied distinct subcellular regions (arrows in (c,f,i)); only occasionally did the expression patterns of the two proteins overlap (arrowheads in (c,i)). Anterior is to the left and dorsal is up in all pictures. All pictures are deconvolved single focal plane images. (j) Mean fluorescence intensity of CFP::UNC-69 and mansII::YFP along a 17 μm distance inside the bracketed region in (c).

defect in synaptic vesicle localization, strong *unc-69* mutants have extensive axonal outgrowth, fasciculation and guidance defects. Both of the strong *unc-69(lf)* alleles, *unc-69(e602)* and *unc-69(e587)*, truncate the coiled-coil domain of UNC-69. In contrast, the hypomorphic allele *unc-69(ju69)* results in a missense mutation of the start codon and presumably interferes with translation initiation. The lack of extensive axonal outgrowth defects in the *unc-69(ju69)* mutants suggests that UNC-69 protein translation might not be totally abolished and enough UNC-69 protein is still being produced to meet the requirement for growth-cone extension. In contrast, the process of proper localization of synaptic vesicles appears to be more sensitive to reduction in levels of UNC-69 protein. It is possible that *unc-69* mediates different cellular processes in parallel: axonal outgrowth, fasciculation and guidance on one hand, synaptic vesicle localization on the other.

UNC-69 is clearly different from most other molecules that have been implicated in axon outgrowth and guidance, which are either guidance cues, membrane receptors, or cell-adhesion proteins [46,47]. It is tempting to place UNC-69 downstream of these molecules, acting possibly as an integrator or transducer of extracellular guiding signals. Alternatively, and perhaps more likely, the axonal-outgrowth and fasciculation defects observed in strong *unc-69(lf)* mutants could be secondary to a more general transport defect, as loss of UNC-69 function might interfere not only with the transport of synaptic cargos but also with the transport of axonogenic vesicles to growth cones.

UNC-69 and UNC-76 interact *in vivo*

We identified UNC-76 as an UNC-69-interacting protein. UNC-76 is required for axonal outgrowth and fasciculation in worms and its homolog in *Drosophila* is an axonal transport protein [14,15]. We identified a 19-amino-acid segment (amino acids 281-299) in UNC-76 that is necessary for its interaction with UNC-69, and possibly for its *in vivo* function. Our genetic experiments suggest that both UNC-69 and UNC-76 act in the same pathway to regulate axon extension. In addition, we found that UNC-76 and UNC-69 cooperate to regulate the size and position of SNB-1::GFP puncta, a marker of presynaptic regions. Finally, we showed that UNC-69 and UNC-76 colocalize in neurons as puncta and that their normal subcellular distribution requires UNC-116/KHC. The physical interaction, subcellular colocalization, and similar mutant phenotypes all suggest that the UNC-69-UNC-76 protein complex acts as a functional unit that promotes transport of vesicles along axons.

A possible role for UNC-69 and UNC-76 in axonal transport?

Proper SNB-1::GFP localization in *C. elegans* requires many proteins, including UNC-116/KHC, KLC-2, UNC-14, UNC-51, as well as UNC-16, the worm homolog of *Drosophila* Sunday Driver, which serves as a scaffold protein receiving regulatory signals from the JNK pathway [7,9,48]. Both UNC-16 and UNC-14 are recruited to Kinesin-1 through their interaction with KLC-2 [9]. In UNC-116, KLC-2, UNC-14, and UNC-16 mutants, SNB-1::GFP is mislocalized from axons to dendrites. In contrast, SNB-1::GFP puncta were largely excluded from dendrites in *unc-69(ju69)* mutants, suggesting that UNC-69 is intrinsically different from these proteins. UNC-69 may function in a distinct step of axonal transport, and is possibly not involved in polarized sorting. Moreover, UNC-69 is unlikely to control general protein trafficking in neurons, as it was not required for dendritic transport of the transmembrane receptor ODR-10.

Kinesin-1 transports various cargos, including Golgi, endoplasmic reticulum, mitochondria and synaptic membrane proteins, but not synaptic vesicles, in the nervous system [34,49,50]. In contrast, UNC-104/KIF1A preferentially transports synaptic vesicle precursors [35,51]. Thus, the synaptic -vesicle marker mislocalization defects in various Kinesin-1 mutants [7,9,52,53] are probably secondary to a general defect of Kinesin-1-dependent cargo transport or other intracellular trafficking events within the axons. As subcellular localization of UNC-69 and UNC-76 is altered in the *unc-116(rh24)* mutants, but not in the *unc-104(e1268)* or *unc-104(rh43)* mutants (our unpublished observations), our data imply that UNC-69 and UNC-76 are possibly required for events other than transporting synaptic vesicles.

Indeed, the observation that *Drosophila* UNC-76 is a KHC-associating protein further suggests that the UNC-69-UNC-76 protein complex might constitute an alternative pathway for Kinesin-1-mediated transport. Association of the UNC-69-UNC-76 protein complex with the tail of KHC could either provide additional levels of regulation, or allow intracellular trafficking of a different repertoire of cargos. So far, however, we could not verify a direct physical interaction between *C. elegans* UNC-76 and the tail region (amino acids 696-815) of UNC-116 *in vitro* (C-W.S. and M.O.H., unpublished results). Further analysis will be required to definitively address this issue.

Implication of UNC-69 in mediating post-Golgi transport

UNC-69 is not predicted to have enzymatic activity and possibly functions only by interacting with other coiled-coil domain-containing proteins. The budding yeast and mammalian homologs of UNC-69, Slo1p and SCOCO, have been shown to interact, respectively, with Arl3p and ARL-1 - two related, Golgi-associated, GTP-binding ADP-ribosylation factor (ARF)-like proteins. Mammalian ARL-1 is involved in post-Golgi transport [20]. Yeast Arl3p could target Arl1p to the Golgi, where it then tethers vesicles derived from endosomes to the Golgi [21,54]. The fact that expression of human SCOCO rescues *unc-69* mutants suggests that a similar interaction occurs in *C. elegans*. We failed to detect any physical interaction between UNC-69 and either ARL-1 or ARFRP, however. Moreover, UNC-69 often appears to occupy subcellular regions distinct from those of the Golgi marker mansII. Thus, the exact step at which UNC-69 acts in vesicular transport (if at all) is still obscure.

Model for UNC-69-UNC-76 protein complex in vesicular trafficking

We propose that UNC-69 and UNC-76 participate in a protein complex that is localized to certain subcellular compartments in the cytoplasm to control vesicle transport between the Golgi and the plasma membrane. The whole UNC-69-UNC-76 protein complex might be recruited and targeted by Kinesin-1 to its final destination in axons. As multiple ectopic branches were consistently observed in both *unc*-69 and *unc-76* mutants, the UNC-69-UNC-76 protein complex might also help restrict membrane addition to growth cones during neuronal development, thereby preventing unwanted membrane extension elsewhere along the axons. Similar biochemical properties of the UNC-69-UNC-76 protein complex might be used to regulate synaptic vesicle clustering or maintenance in the presynaptic regions in the adult nervous system. UNC-69-UNC-76 puncta could reflect certain post-Golgi compartments that shuttle between their budding sites on the *trans*-Golgi and their docking sites near the plasma membrane. As such, an

UNC-69-UNC-76 protein complex might function at an intermediate step before vesicle maturation. Indeed, UNC-69-UNC-76 puncta were present along the commissures in addition to axons. As commissures do not form synapses [36], these puncta could define a sorting compartment from which functional vesicles are formed.

Functional conservation of UNC-69 and SCOCO through evolution

Several lines of evidence suggest that UNC-69/SCOCO has an evolutionarily conserved role in nervous -system development in different animal species. First, human SCOCO rescues the Unc defect of *C. elegans unc-69* mutants (see Figure 3c). Second, human SCOCO interacts with worm UNC-76γ in our yeast two-hybrid assays (Figure 10a), suggesting that the rescuing activity of human SCOCO is due at least in part to its ability to associate with UNC-76 in *C. elegans*. Third, human SCOCO and its chicken homolog are highly expressed in developing CNS neurons (see Figures 3b and 5k). Fourth, RNAi-mediated knockdown of chicken UNC-69/SCOCO results in guidance and fasciculation defects of the epaxial nerves (Figure 5m,n). It seems plausible from these observations that SCOCO also has an important role in promoting proper development (and possibly function) of the nervous system in mammals.

Conclusions

Our studies reveal an important role for the UNC-69-UNC-76 protein complex in axonal outgrowth, fasciculation and synapse formation. Our results suggest that UNC-69 and UNC-76 act as a functional unit to regulate one or multiple steps of vesicle dynamics in the *C. elegans* nervous system. On the basis of our transgenic rescue and RNAi experiments, we suggest that vertebrates also use the UNC-69-UNC-76 complex in a similar fashion to control synapse formation and axonal outgrowth. We expect further studies to shed light on this hitherto less noticed branch of axonal guidance.

Materials and methods

C. elegans strains and genetics

C. elegans strains were maintained as described [18]. All strains were grown at 20°C, except *dpy-20(e1282ts)* and *lin-15(n765ts)* mutants, which were grown at 15°C before injection to improve viability and at 25°C following injection to enhance selection of transgenic F1 animals. Wild-type worms were of the Bristol N2 strain.

Cloning of *unc-69*

All genetic mapping data were deposited into WormBase [55].The *unc-69* gene is tightly linked to RFLP *nP55*, which is recognized by cosmid C15B3. The three overlapping cosmids C15B3, C41B4 and F11D2, but not the flanking cosmids C30B11 and F46H1, rescued the Unc phenotype of *unc-69(e587)* mutant. Subsequent subclonings identified a 1.2-kb *Eco*RI-*Sac*I rescuing genomic fragment, which contained a single gene composed of three exons. A frameshift mutation was introduced into the *unc-69* open reading frame of the rescuing *Eco*RI-*Sac*I fragment by cutting and filling the unique *Mlu*I restriction site, followed by religation of the blunt ends. The frameshifted construct failed to rescue *unc-69* mutant worms. To identify the molecular lesion(s) present in *unc-69* mutants, the *unc-69* locus from wild-type and *unc-69* mutants was amplified using primers flanking the gene (5′-GCTCCGCAGTACGTCTTCTAAGCCC-3′ and 5′-GCGAGAATGGAACAATCAATGG-ACG-3′) and sequenced. In addition to the stop codon, *e602* also contains a silent (third base) G-to-A transition in Lys107.

Egg-laying assay

Assays of egg-laying behavior were performed either in M9 buffer [56] or on plates. For M9 assays, gravid hermaphrodites were individually transferred to microtiter wells containing either M9 or a 5 mg/ml solution of serotonin (5-HT, Sigma, St. Louis, USA) in M9 and the number of eggs laid after 60 min was determined. For plate assays, five gravid hermaphrodites were transferred onto fresh plates with or without food, and the total number of eggs laid after 90 min was determined.

Immunocytochemistry and fluorescence microscopy

Indirect immunofluorescence staining for serotonin and GABA were performed as previously described [57-59]. Anti-serotonin and anti-GABA antisera were generously provided by H. Steinbusch (Free University, Amsterdam, The Netherlands) and used at 1%. Neuronal morphology was observed on a Zeiss Axioplan microscope equipped for epifluorescence, using the Zeiss filter set 488005 (excitation: 395-440 nm band-pass filter; emission: 470 nm long-pass filter). For colocalization studies, animals were anesthetized with 10 mM levamisole and mounted on 4% agarose pads in M9. A Leica DMRA2 microscope equipped with a Hamamatsu ORCA-ER CCD camera, a Leica Fluotar 40X oil objective, and appropriate filter sets was used to visualize YFP and CFP. Images were taken and deconvoluted using the Openlab software (Improvision, Coventry, UK), and analyzed using ImageJ. For confocal microscopy, a Zeiss 510 or a Leica DMRE confocal laser-scanning microscope equipped with TCS SP2 AOBS and PL APO objectives was used.

Electron microscopy

Adult hermaphrodites were fixed in 0.8% glutaraldehyde, 0.7% OsO_4 and 0.1 M cacodylate buffer for 1 h on ice. Subsequently, samples were cut and postfixed in 2% OsO_4 and

0.1 M cacodylate buffer, mounted into an agar block, dehydrated in series of alcohols, and embedded in a mixture of epon-araldite. Thin sections (50 nm) were cut on an Ultracut E and pictures were taken with a JEOL 1200X at 80 kV.

Dye filling

Adult worms were soaked in 10 μg/ml DiI (Molecular Probes, Eugene, USA) in M9, and incubated in the dark for 2 h at 20°C, followed by several washes in M9 buffer. Staining was analyzed using appropriate filters.

cDNA screening and northern blot

A rescuing 2.8 kb *Eco*RI genomic fragment was used to probe a *C. elegans* lambdaZAP cDNA library (gift of R. Barstead). From approximately 300,000 plaques we isolated four cDNAs. The sequences present at the ends of the inserts were determined for all four clones, and the DNA sequence of the longest intact clone was determined (one strand only). A random-primed, ^{32}P-labeled *unc-69* cDNA was used to probe a northern blot of wild-type poly(A)$^+$ RNA. The blot was visualized and band intensities quantified using a Fuji Film phosphor imager. Poly(A)$^+$ RNA was isolated from purified embryos or mixed stages of wild-type strain N2 as described by Sambrook *et al.* [60], except that FastTrack columns (Invitrogen, San Diego, USA) were used (according to the manufacturer's protocols) instead of standard oligo(dT) columns. Likewise, a human fetal multiple tissue northern blot was probed with a portion of the *SCOCO* cDNA.

Molecular biology

All manipulations were done following standard protocols [60]. A 1.5 kb *unc-69* genomic fragment containing 700 bp upstream and 300 bp downstream of the coding region was engineered through site-directed mutagenesis to construct various amino- and carboxy-terminal CFP or GFP fusions (pgfpu69, pu69gfp and pSU083). The rescuing ability of the constructs was tested for both amino- and carboxy-terminal GFP fusions. A full-length *unc-69* cDNA was cloned into pGEX-4T1 to generate a prokaryotic expression *unc-69-gst* construct. To generate a full-length *unc-76* major splicing form cDNA (pSU001), the *Eco*RI-*Xba*I fragment of p76-c4 [14] was replaced by the *Eco*RI-*Bam*HI fragment of *yk784h09* and the *Xba*I-*Bam*HI fragment of p76-c7, using three-way ligation. Progressive *unc-76* deletions were made either by a PCR-based method, or using ExoIII and S1 nucleases following Erase-a-Base (Promega, Madison, USA) and ExoIII/S1 Deletion Kit (Fermentas, Hanover, USA) protocols. To generate genomic *unc-76* constructs, an *Asc*I site was engineered 5′ to the start ATG and was used to insert a 1 kb *Kpn*I-*Asc*I *unc-76* promoter region up to the start codon. Subsequently a *Bgl*II-*Sph*I genomic fragment encompassing exons 1 to 3 was used to replace the corresponding region of the cDNA. An *Asc*I CFP cassette was inserted in-frame to create the amino-terminal CFP fusion plasmid (pSU065). Likewise, a *Not*I site was engineered immediately 5′ to the stop codon to allow creation of the carboxy-terminal YFP fusion plasmid (pSU026). A genomic fragment containing the first 82 amino acids of mannosidase II was placed 3′ to the *unc-69* promoter and was carboxy-terminally fused with YFP to create pSU137. Full-length and truncated cDNAs of *unc-69*, *scoco*, *unc-76*, *arl-1*, *arl-3*, *arfrp*, and *unc-119* were amplified from mixed-stage N2 mRNA pool or existing cDNA clones and subsequently subcloned into pRE192 and pRH143 to create LexA-bait and GAD-prey plasmids. pRE192 and pRH143 are derivatives of pBTM116 and pGAD424, respectively, and are gifts of K. Basler (University of Zurich).

Single- amino-acid changes were made following QuikChange Site-Directed Mutagenesis Kit protocols (Stratagene, La Jolla, USA). Sequences for each of the mutations are as follows: UNC-76(E275A): GAG→GCG; UNC-76(L281P): CTG→CCA; UNC-76(L287P): CTG→CCG; UNC-76(K291A): AAA→GCC; ARL-1(Q70L): CAA→CTA; ARFRP(Q79L): CAG→CTG. Mutations were confirmed by sequencing and swapped back into the original plasmids before further subcloning. All plasmids and construct sequences are available upon request.

Protein sequence analysis

Prediction of coiled-coil structures was carried out using the COILS version 2.1 program [61]. The coiled-coil regions of UNC-69, UNC-76 and their homologs were assigned on the basis of a greater than 80% probability of forming coiled coils according to this program. We used ClustalW or T-Coffee for multiple sequence alignment and shaded the ClustalW alignment using BOXSHADE.

Yeast two-hybrid

Random- and dT-primed yeast two-hybrid phage libraries were generous gifts from R. Barstead (Oklahoma Medical Research Foundation, Oklahoma City, USA). A further random-primed library was provided by M. Vidal (Harvard Medical School, Boston, USA). The *unc-69* cDNA was subcloned into pDBTrp and pDBLeu vectors (PROQUEST Two-Hybrid System, GibcoBRL, Carlsbad, USA) and cotransformed with the AD plasmids. Transformed yeast reporter strain Mav203 (GibcoBRL) was patched onto plates lacking Leu and Trp (LW plates), and then replica plated onto plates lacking Leu, Trp and His with 75 mM 3-amino triazol (LWH/3AT plates), onto plates lacking uracil (URA plates) and onto filters for β-galactosidase assays. Only clones that activated all three (His, Ura, LacZ) reporter genes were kept for further analysis. Plasmid DNAs were purified from positive clones and retested for interaction with the bait plasmid.

To study the interactions between UNC-69 and various ARL proteins, we used the yeast reporter strain L40, and followed Clontech's Yeast Protocols Handbook for *o*-nitrophenyl β-D-galactopyranoside (ONPG) and auxotrophic assays.

In vitro translation and GST pull-down assay

In vitro transcription and translation of *unc-76* was performed following protocols of the TNT-coupled reticulocyte lysate system (Promega) in the presence of ^{35}S-labeled methionine (Amersham, Little Chalfont, UK). For pull-down experiments, purified recombinant GST and UNC-69-GST proteins were first immobilized on glutathione beads (Amersham). Immobilized proteins (2-10 μg) were incubated with 1-20 μl *in vitro* translated UNC-76 (depending on binding efficiency) in 1x interaction buffer (20 mM HEPES pH 7.9, 5 mM $MgCl_2$, 0.2% NP40, 0.2% BSA, 7.5% glycerol and protease inhibitor cocktail (Complete Mini, Roche, Indianapolis, USA)) at 4°C for 1.5-2 h. The beads were washed three times in washing buffer (100 mM KCl, 20 mM HEPES pH 7.9, 5 mM $MgCl_2$, 0.2% NP40 and protease inhibitor cocktail (Roche)), resuspended in 20 μl 2x SDS sample buffer, boiled and analyzed by SDS-PAGE and autoradiography.

Germline transformations and array integration

For high-copy overexpression, plasmids were injected into the germline of adult hermaphrodites [62] at 50 ng/μl together with 150 ng/μl rescuing *dpy-20(+)* or pL15-EK *lin-15(+)* genomic fragments. To generate low-copy extrachromosomal arrays, plasmids were individually or co-injected each at 5 ng/μl together with 195 ng/μl pL15-EK. Transgenic progeny of injected animals were selected as non-Dpy or non-Muv animals at 25°C. Stably transmitting extrachromosomal arrays were integrated by γ-irradiation at 120 kV for 4.2 min.

In ovo RNAi in chicken embryos

We obtained a cDNA clone of chick *SCOCO*, ChEST376p13, from the HGMP Research Center [63]. Double-stranded RNA for *in ovo* RNAi was transcribed *in vitro* as described [45]. Embryos were injected at stage 17-18 with 0.1 μl dsRNA (500 ng/μl) or a plasmid encoding YFP in PBS followed by electroporation. Stage 25-26 embryos [64] were stained and examined under a dissecting microscope with epifluorescence. With the site of injection chosen, we knocked down SCOCO only in MMC/LMC motor neurons, not in cells of the dermamyotome and/or the epaxial mesenchyme.

Immunostaining of chicken embryos

For whole-mount immunostaining, staged embryos were dissected and fixed as described [45]. Embryos were permeabilized with 1% Triton X-100 in PBS, incubated in 20 mM lysine and 0.1 M sodium phosphate (pH 7.4), and in blocking solution (10% FCS in -PBS) to reduce nonspecific staining. Mouse anti-neurofilament antibodies (RM0270, Zymed, San Francisco, USA) were used at 1:1,500 and applied for 48 h at 4°C. Embryos were washed in PBS at 4°C, and incubated in blocking solution before addition of secondary antibody (goat anti-mouse Cy3, 1:250; Jackson Laboratories, West Grove, USA). Embryos were dehydrated by sequential incubation in 25%, 50%, 75%, and 100% methanol. The tissue was cleared by transferring the embryos to BBBA (benzyl-benzoate:benzyl-alcohol = 2:1). The embryos were gently agitated until translucent, and were analyzed by fluorescent microscopy.

In situ hybridization of chicken embryos

Embryos were sacrificed at different developmental stages (from stage 17 to 33) and fixed in 4% paraformaldehyde. The tissue was cryoprotected in 25% sucrose, and 20-μm - thick transverse sections of the lumbosacral spinal cord were used for the analysis of *SCOCO* expression as described previously [65].

Additional data files

The following files are available: Supplementary results and tables (Additional data file 1); a figure showing that the overexpression of a full-length UNC-69(M1I)::GFP protein rescues locomotion defects of the *unc-69(e587)* mutants (Additional data file 2); a figure showing the extent of the *ok339* deletion (Additional data file 3); and a figure showing that RNAi knockdown of chicken UNC-69/SCOCO results in epaxial nerve pathfinding defects (Additional data file 4).

Acknowledgements

We thank A. Hajnal and J. M. Kinchen for critical reading of the manuscript, B. Dickson for thoughtful comments, and W-C. Chou, R. Staedeli, H-H. Chen, L. Martin, P. Gisler, E. Horvath and G. Stergiou for other help. We thank E. Hartwieg for assistance with the EM sections; D. Baillie for the *C. briggsae* genomic library; S. Clark for the *mec-4::gfp* plasmid; R. Barstead, M. Vidal and K. Basler for Y2H libraries and plasmids; H. Steinbusch for antisera; R. Eckner for the E1A and CBP plasmids; Y. Kohara for cDNAs; and C. Bargmann for the *kyIs4* strain. Some strains were contributed by the *Caenorhabditis* Genetics Center (CGC), which is funded by the National Institutes of Health (NIH) Center for Research Resources. We would also like to thank G. Moulder at the *C. elegans* Gene Knockout Consortium for providing us with the *unc-69(ok339)* deletion strain. This work was funded by grants from the Rita Allen Foundation, March of Dimes, Ernst Hadorn Foundation, and Swiss National Science Foundation to M.O.H. The work at MIT was supported by NIH Grant GM24663 to H.R.H. H.R.H. and Y.J. are investigators of the Howard Hughes Medical Institute. C.R. is supported by the research fund of the University of Zurich. C-W.S. is supported by the Ernst Hadorn Foundation and a Zentrum für Neurowissenschaften Zürich (ZNZ) Ph.D. fellowship.

References

1. Martinez-Arca S, Coco S, Mainguy G, Schenk U, Alberts P, Bouille P, Mezzina M, Prochiantz A, Matteoli M, Louvard D, *et al.*: **A common exocytotic mechanism mediates axonal and dendritic outgrowth.** *J Neurosci* 2001, **21:**3830-3838.

2. Washbourne P, Bennett JE, McAllister AK: **Rapid recruitment of NMDA receptor transport packets to nascent synapses.** *Nat Neurosci* 2002, **5:**751-759.
3. Ahmari SE, Buchanan J, Smith SJ: **Assembly of presynaptic active zones from cytoplasmic transport packets.** *Nat Neurosci* 2000, **3:**445-451.
4. Burack MA, Silverman MA, Banker G: **The role of selective transport in neuronal protein sorting.** *Neuron* 2000, **26:**465-472.
5. Horton AC, Ehlers MD: **Neuronal polarity and trafficking.** *Neuron* 2003, **40:**277-295.
6. Vale RD: **The molecular motor toolbox for intracellular transport.** *Cell* 2003, **112:**467-480.
7. Byrd DT, Kawasaki M, Walcoff M, Hisamoto N, Matsumoto K, Jin Y: **UNC-16, a JNK-signaling scaffold protein, regulates vesicle transport in *C. elegans.*** *Neuron* 2001, **32:**787-800.
8. Koushika SP, Schaefer AM, Vincent R, Willis JH, Bowerman B, Nonet ML: **Mutations in *Caenorhabditis elegans* cytoplasmic dynein components reveal specificity of neuronal retrograde cargo.** *J Neurosci* 2004, **24:**3907-3916.
9. Sakamoto R, Byrd DT, Brown HM, Hisamoto N, Matsumoto K, Jin Y: **The *C. elegans* UNC-14 RUN domain protein binds to the Kinesin-1/UNC-16 complex and regulates synaptic vesicle localization.** *Mol Biol Cell* 2005, **16:**483-496.
10. Lai T, Garriga G: **The conserved kinase UNC-51 acts with VAB-8 and UNC-14 to regulate axon outgrowth in *C. elegans.*** *Development* 2004, **131:**5991-6000.
11. Ogura K, Shirakawa M, Barnes TM, Hekimi S, Ohshima Y: **The UNC-14 protein required for axonal elongation and guidance in *Caenorhabditis elegans* interacts with the serine/threonine kinase UNC- 51.** *Genes Dev* 1997, **11:**1801-1811.
12. Hedgecock EM, Culotti JG, Thomson JN, Perkins LA: **Axonal guidance mutants of *Caenorhabditis elegans* identified by filling sensory neurons with fluorescein dyes.** *Dev Biol* 1985, **111:**158-170.
13. McIntire SL, Garriga G, White J, Jacobson D, Horvitz HR: **Genes necessary for directed axonal elongation or fasciculation in *C. elegans.*** *Neuron* 1992, **8:**307-322.
14. Bloom L, Horvitz HR: **The *Caenorhabditis elegans* gene *unc-76* and its human homologs define a new gene family involved in axonal outgrowth and fasciculation.** *Proc Natl Acad Sci USA* 1997, **94:**3414-3419.
15. Gindhart JG, Chen J, Faulkner M, Gandhi R, Doerner K, Wisniewski T, Nandlestadt A: **The Kinesin-associated protein UNC-76 is required for axonal transport in the *Drosophila* nervous system.** *Mol Biol Cell* 2003, **14:**3356-3365.
16. Kuroda S, Nakagawa N, Tokunaga C, Tatematsu K, Tanizawa K: **Mammalian homologue of the *Caenorhabditis elegans* UNC-76 protein involved in axonal outgrowth is a protein kinase C zeta-interacting protein.** *J Cell Biol* 1999, **144:**403-411.
17. Okumura F, Hatakeyama S, Matsumoto M, Kamura T, Nakayama KI: **Functional regulation of FEZ1 by the U-box-type ubiquitin ligase E4B contributes to neuritogenesis.** *J Biol Chem* 2004, **279:**53533-53543.
18. Brenner S: **The genetics of *Caenorhabditis elegans.*** *Genetics* 1974, **77:**71-94.
19. Hengartner MO, Horvitz HR: ***C. elegans* cell survival gene *ced-9* encodes a functional homolog of the mammalian proto-oncogene *bcl-2*.** *Cell* 1994, **76:**665-676.
20. Van Valkenburgh H, Shern JF, Sharer JD, Zhu X, Kahn RA: **ADP-ribosylation factors (ARFs) and ARF-like 1 (ARL1) have both specific and shared effectors: characterizing ARL1-binding proteins.** *J Biol Chem* 2001, **276:**22826-22837.
21. Panic B, Whyte JR, Munro S: **The ARF-like GTPases Arl1p and Arl3p act in a pathway that interacts with vesicle-tethering factors at the Golgi apparatus.** *Curr Biol* 2003, **13:**405-410.
22. Huang CF, Buu LM, Yu WL, Lee FJ: **Characterization of a novel ADP-ribosylation factor-like protein (yARL3) in *Saccharomyces cerevisiae.*** *J Biol Chem* 1999, **274:**3819-3827.
23. Siddiqui SS: **Mutations affecting axonal growth and guidance of motor neurons and mechanosensory neurons in the nematode *Caenorhabditis elegans.*** *Neurosci Res Suppl* 1990, **13:**S171-S190.
24. Wightman B, Baran R, Garriga G: **Genes that guide growth cones along the *C. elegans* ventral nerve cord.** *Development* 1997, **124:**2571-2580.
25. White JG, Southgate E, Thomson JN, Brenner S: **The structure of the ventral nerve cord of *Caenorhabditis elegans.*** *Philos Trans R Soc Lond B Biol Sci* 1976, **275:**327-348.
26. Nonet ML: **Visualization of synaptic specializations in live *C. elegans* with synaptic vesicle protein-GFP fusions.** *J Neurosci Methods* 1999, **89:**33-40.
27. Troemel ER, Sagasti A, Bargmann CI: **Lateral signaling mediated by axon contact and calcium entry regulates asymmetric odorant receptor expression in *C. elegans.*** *Cell* 1999, **99:**387-398.
28. Peckol EL, Zallen JA, Yarrow JC, Bargmann CI: **Sensory activity affects sensory axon development in *C. elegans.*** *Development* 1999, **126:**1891-1902.
29. Coburn CM, Bargmann CI: **A putative cyclic nucleotide-gated channel is required for sensory development and function in *C. elegans.*** *Neuron* 1996, **17:**695-706.
30. Dwyer ND, Adler CE, Crump JG, L'Etoile ND, Bargmann CI: **Polarized dendritic transport and the AP-1 mu1 clathrin adaptor UNC-101 localize odorant receptors to olfactory cilia.** *Neuron* 2001, **31:**277-287.
31. Eckner R, Yao TP, Oldread E, Livingston DM: **Interaction and functional collaboration of p300/CBP and bHLH proteins in muscle and B-cell differentiation.** *Genes Dev* 1996, **10:**:2478-2490.
32. Stearns T, Botstein D: **Unlinked noncomplementation: isolation of new conditional-lethal mutations in each of the tubulin genes of *Saccharomyces cerevisiae.*** *Genetics* 1988, **119:**249-260.
33. Belanger KD, Kenna MA, Wei S, Davis LI: **Genetic and physical interactions between Srp1p and nuclear pore complex proteins Nup1p and Nup2p.** *J Cell Biol* 1994, **126:**619-630.
34. Patel N, Thierry-Mieg D, Mancillas JR: **Cloning by insertional mutagenesis of a cDNA encoding *Caenorhabditis elegans* kinesin heavy chain.** *Proc Natl Acad Sci USA* 1993, **90:**9181-9185.
35. Hall DH, Hedgecock EM: **Kinesin-related gene *unc-104* is required for axonal transport of synaptic vesicles in *C. elegans.*** *Cell* 1991, **65:**837-847.
36. White JG, Southgate E, Thomson JN, Brenner S: **The structure of the nervous system of the nematode *Caenorhabditis elegans.*** *Philos Trans R Soc Lond B Biol Sci* 1986, **314:**1-340.
37. Zallen JA, Kirch SA, Bargmann CI: **Genes required for axon pathfinding and extension in the *C. elegans* nerve ring.** *Development* 1999, **126:**3679-3692.
38. Li Y, Kelly WG, Logsdon JM, J**r.**, Schurko AM, Harfe BD, Hill-Harfe KL, Kahn RA: **Functional genomic analysis of the ADP-ribosylation factor family of GTPases: phylogeny among diverse eukaryotes and function in *C. elegans.*** *FASEB J* 2004, **18:**1834-1850.
39. Pasqualato S, Renault L, Cherfils J: **Arf, Arl, Arp and Sar proteins: a family of GTP-binding proteins with a structural device for 'front-back' communication.** *EMBO Rep* 2002, **3:**1035-1041.
40. Li S, Armstrong CM, Bertin N, Ge H, Milstein S, Boxem M, Vidalain PO, Han JD, Chesneau A, Hao T, *et al.*: **A map of the interactome network of the metazoan *C. elegans.*** *Science* 2004, **303:**540-543.
41. Maduro M, Pilgrim D: **Identification and cloning of *unc-119*, a gene expressed in the *Caenorhabditis elegans* nervous system.** *Genetics* 1995, **141:**977-988.
42. Higashide T, Inana G: **Characterization of the gene for HRG4 (UNC119), a novel photoreceptor synaptic protein homologous to Unc-119**. *Genomics* 1999, **57:**446-450.
43. Swanson DA, Chang JT, Campochiaro PA, Zack DJ, Valle D: **Mammalian orthologs of *C. elegans unc-119* highly expressed in photoreceptors.** *Invest Ophthalmol Vis Sci* 1998, **39:**2085-2094.
44. Rolls MM, Hall DH, Victor M, Stelzer EH, Rapoport TA: **Targeting of rough endoplasmic reticulum membrane proteins**

and ribosomes in invertebrate neurons. *Mol Biol Cell* 2002, **13:**1778-1791.
45. Pekarik V, Bourikas D, Miglino N, Joset P, Preiswerk S, Stoeckli ET: **Screening for gene function in chicken embryo using RNAi and electroporation.** *Nat Biotechnol* 2003, **21:**93-96.
46. Yu TW, Bargmann CI: **Dynamic regulation of axon guidance.** *Nat Neurosci* 2001, **4 Suppl:**1169-1176.
47. Kiryushko D, Berezin V, Bock E: **Regulators of neurite outgrowth: role of cell adhesion molecules.** *Ann NY Acad Sci* 2004, **1014:**140-154.
48. Crump JG, Zhen M, Jin Y, Bargmann CI: **The SAD-1 kinase regulates presynaptic vesicle clustering and axon termination.** *Neuron* 2001, **29:**115-129.
49. Hirokawa N: **Kinesin and dynein superfamily proteins and the mechanism of organelle transport.** *Science* 1998, **279:**519-526.
50. Gho M, McDonald K, Ganetzky B, Saxton WM: **Effects of kinesin mutations on neuronal functions.** *Science* 1992, **258:**313-316.
51. Okada Y, Yamazaki H, Sekine-Aizawa Y, Hirokawa N: **The neuron-specific kinesin superfamily protein KIF1A is a unique monomeric motor for anterograde axonal transport of synaptic vesicle precursors.** *Cell* 1995, **81:**769-780.
52. Hurd DD, Saxton WM: **Kinesin mutations cause motor neuron disease phenotypes by disrupting fast axonal transport in *Drosophila*.** *Genetics* 1996, **144:**1075-1085.
53. Gindhart JG, Jr., Desai CJ, Beushausen S, Zinn K, Goldstein LS: **Kinesin light chains are essential for axonal transport in *Drosophila*.** *J Cell Biol* 1998, **141:**443-454.
54. Munro S: **The Arf-like GTPase Arl1 and its role in membrane traffic.** *Biochem Soc Trans* 2005, **33:**601-605.
55. **Wormbase** [http://www.wormbase.org]
56. Sulston J, Hodgkin J: **Methods.** In: *The Nematode* Caenorhabditis elegans. Edited by Wood WB. Cold Spring Harbor, New York: Cold Spring Harbor Laboratory Press; 1988: 587-606.
57. Desai C, Garriga G, McIntire SL, Horvitz HR: **A genetic pathway for the development of the *Caenorhabditis elegans* HSN motor neurons.** *Nature* 1988, **336:**638-646.
58. McIntire SL, Jorgensen E, Horvitz HR: **Genes required for GABA function in *Caenorhabditis elegans*.** *Nature* 1993, **364:**334-337.
59. McIntire SL, Jorgensen E, Kaplan J, Horvitz HR: **The GABAergic nervous system of *Caenorhabditis elegans*.** *Nature* 1993, **364:**337-341.
60. Sambrook J, Fritsch EF, Maniatis T: *Molecular Cloning: A Laboratory Manual.* Cold Spring Harbor, New York: Cold Spring Harbor Laboratory Press; 1989.
61. Lupas A, Van Dyke M, Stock J: **Predicting coiled coils from protein sequences.** *Science* 1991, **252:**1162-1164.
62. Mello CC, Kramer JM, Stinchcomb D, Ambros V: **Efficient gene transfer in *C. elegans*: extrachromosomal maintenance and integration of transforming sequences.** *EMBO J* 1991, **10:**3959-3970.
63. **BBSRC ChickEST Database** [http://www.chick.umist.ac.uk]
64. Hamburger V, Hamilton HL: **A series of normal stages in the development of the chick embryo.** *J Morphol* 1951, **88:**49-92.
65. Schaeren-Wiemers N, Gerfin-Moser A: **A single protocol to detect transcripts of various types and expression levels in neural tissue and cultured cells: *in situ* hybridization using digoxigenin-labelled cRNA probes.** *Histochemistry* 1993, **100:**431-440.

SUPPLEMENTARY RESULTS

SCOCO and FEZ1 are cytoplasmic proteins

In order to determine the subcellular localization of SCOCO and FEZ1, I expressed $(Myc)_2$-tagged SCOCO (Myc-SCOCO) and V5-$(His)_6$-tagged FEZ1 (V5-FEZ1) in different cell lines. First, V5-FEZ1 and Myc-SCOCO expression was analyzed in COS-7 and 293T cells. V5-FEZ1 was observed in a punctuate pattern in the cytoplasm and seemed to be enriched in the perinuclear region indicating Golgi-localization (Figure 1A, 1B). Myc-SCOCO staining was present throughout the cytoplasm in small dots, although the signal was less strong compared to V5-FEZ1, probably due to the polyclonal anti-myc antibody (data not shown). Unpermeabilized cells did not stain. Next, I tested a neuronal cell line since FEZ1 and SCOCO are known to be expressed in the brain. NG108 cells are hybrids derived of mouse neuroblastoma and rat glioma cells and were shown to display a broad spectrum of neuronal properties (Hamprecht et al., 1985). In NG108 cells, V5-FEZ1 prominently localized to axon-like projections, in addition to the overall cytoplasmic staining (Figure 1C). Likewise, Myc-SCOCO was present in the cytoplasm and cellular projections (Figure 1D, 1E). In order to visualize the Golgi/Endosomal compartment, the cells were incubated with fluorochrome-coupled wheat germ agglutinin. FEZ1 showed overlapping localization with the Golgi-compartment, which was not the case for Myc-SCOCO suggesting that the two proteins might mainly interact in the cytoplasm (data not shown). However, in a previous study, SCOCO has been found to localize to Golgi-membranes using polyclonal rabbit antibodies raised against recombinant human $(His)_6$-SCOCO (Van Valkenburgh et al., 2001). These findings indicate that SCOCO and FEZ1 might also interact at the interface of Golgi and cytoplasm.

To verify the correct expression of Myc-SCOCO and V5-FEZ1, transfected COS-7 cells were lysed for western blot analysis. The blots were probed with rabbit polyclonal anti-Myc or mouse monoclonal anti-V5 antibodies. V5-$(His)_6$-FEZ1 was detected as a 57kDa band that was absent in the control lanes containing lysates from untransfected or mock transfected cells (empty vector) (Figure 1F). It has been previously reported that the molecular weight of FEZ1, when expressed in COS-7 cells, is 10kD larger than *in vitro* translated FEZ1 (45kDa), probably due to posttranslational modifications. FEZ1 contains four N-glycosylation and various phosphorylation sites (Kuroda et al., 1999).

A band at 15kDa appeared to be specific for MYC-SCOCO. The molecular weight also ranged above the expected 12kDa deduced form the amino acid sequence indicating

posttranslational modification steps (Figure 1F). A SCOCO-specific band present at 30kDa is likely to correspond to a SCOCO-dimer form.

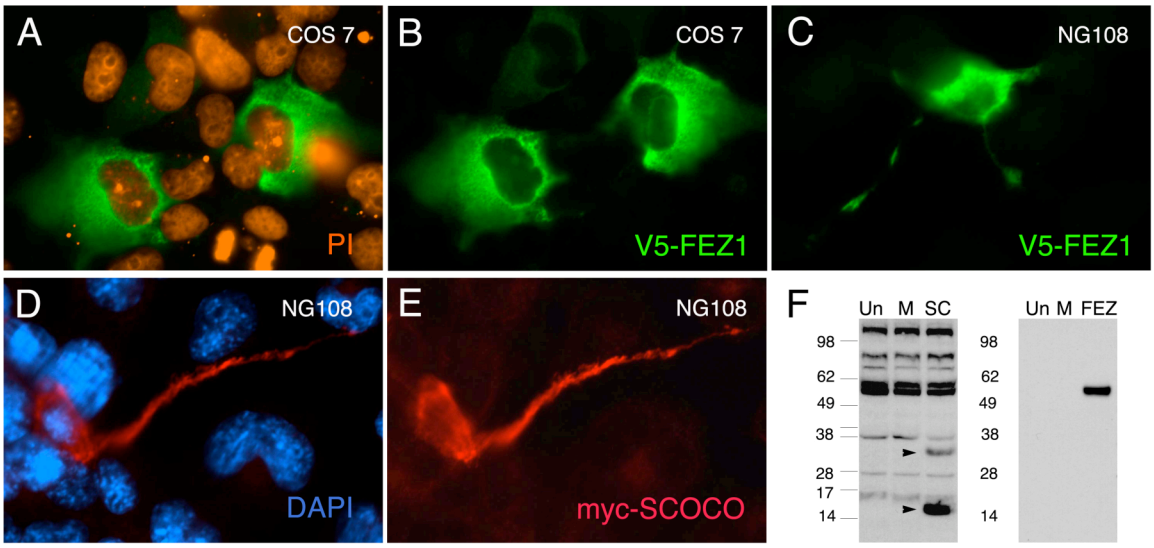

Figure 1. Subcellular localization of FEZ1 and SCOCO

Immunostaining for V5-FEZ1 (green) in COS-7 and NG108 cells **(A, B, C)** and for Myc-SCOCO (red) in NG108 cells **(D, E)**. Cell nuclei are visualized in orange with propidium iodine (PI) **(A)** and in blue with DAPI **(D)**. **(F)** Lysates from untransfected (Un), mock transfected (M) (empty vector) and *$(myc)_2$–scoco* (SC) or *V5-$(His)_6$-fez1* (FEZ) transfected cells were analyzed by western blotting. Specific bands for Myc-SCOCO are detected at 15 kDa and 30 kDa (dimer) (arrowheads). V5-FEZ1 corresponds to a band at around 57 kDa.

Potential interaction between SCOCO and FEZ1

The worm homologs UNC-69 and UNC-76 have been shown to directly interact with each other in yeast-two-hybrid and GST pull-down experiments (Su et al., 2006). In order to test if this interaction is conserved in mammals, I performed immunoprecipitation assays with Myc-SCOCO and V5-FEZ1. NG108 cells were transfected with the constructs for *$(myc)_2$–scoco* and *V5- $(His)_6$-fez1*. Then, V5-FEZ1 was immunoprecipitated from cell lysates with monoclonal mouse anti-V5 antibodies and the blot was probed with rabbit polyclonal anti-myc antibodies and vice versa. In preliminary experiments, the two proteins could not be precipitated together. This could mean that they do not directly bind to each other or that they interact only very transiently.

Generation of monoclonal anti-human SCOCO antibodies

Several lines of evidence point to a conserved role of UNC-69/SCOCO in nervous system development. Human SCOCO was found to be enriched in fetal brain and chicken SCOCO turned out to be highly expressed in the central nervous system of developing chicken embryos (Su et al., 2006). The coiled-coil domains of UNC-69/SCOCO from C. *elegans, Drosophila,* mouse and humans show 74% sequence identity. Based on this high identity in the protein sequence, we decided to generate antibodies against the human SCOCO form, which essentially consist of the coiled-coil domain of UNC-69. To this end, I expressed and purified human SCOCO-GST from bacteria (Figure 2A). We expected that some antibodies that recognize human SCOCO, might also cross-react with mouse and chicken SCOCO. Monoclonal antibodies were selected based on a phage display technology offered by the company MorphoSys/AntibodiesbyDesign. The screening procedure of Morphosys excludes antibodies that react with the GST-tag alone.

From several selection rounds, we have obtained ten myc-tagged bivalent mini-antibodies ($F(ab')_2$ format), which were selected as the ten best binders in an ELISA assay. Except for one antibody, Ab438, all tested antibodies recognized the purified human SCOCO protein and reacted only weakly with GST (Figure 2B). Ab435 showed strong binding to human SCOCO and very low background interaction with GST. None of the six antibodies analyzed so far, cross-reacted with GST-UNC-69. Next, it will be necessary to determine if the antibodies also show a high specificity for SCOCO in total cell lysates. Furthermore, it will be interesting to see if some of the antibodies cross-react with chicken and mouse SCOCO.

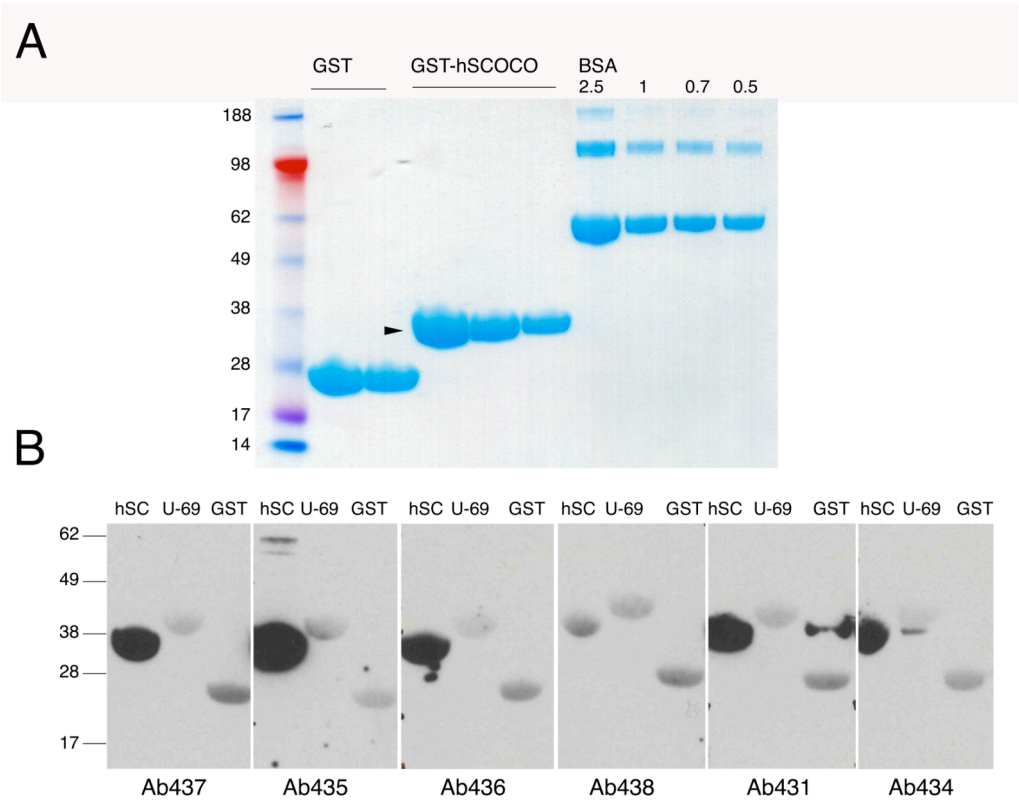

Figure 2. Generation of monoclonal anti-SCOCO antibodies

(A) Eluted GST and GST-humanSCOCO fractions (arrowhead). BSA standards (mg/ml) are shown to estimate protein concentration. **(B)** Western blots for six of the generated anti-SCOCO antibodies. The Antibodies were assayed for their binding specificity to human SCOCO (hSC) versus GST and for potential cross-reactivity with *C. elegans* GST-UNC-69 (U-69).

Mapping of *unc-69* suppressors

From a screen for suppression of the locomotion defects of *unc-69* worms, performed by Cheng-Wen Su, seven strong *unc-69* suppressors were selected for further investigation. I backcrossed the suppressors *op345*, *op350* and *op377* three times to the *unc-69(ju69)* background to remove unlinked mutations. The three suppressors were all dominant suppressors because wild-type hermaphrodites were observed in the F1 generation when suppressed males were mated with *unc-69 (ju69)* hermaphrodites. *op345* and *op350* could not be homozygoused suggesting that they are homozygous lethal. In contrast, *op377* was homozygous viable and could be assigned to a chromosome by classical genetic mapping with visible markers. *op377; unc-69 (ju69)* males were crossed to *dpy-5 (e61)* I; *rol-6 (e187)* II; *unc-69 (ju69)* III hermaphrodites. In the F2, 48 *Unc* (non-suppressed) animals were singled out and the progeny was analyzed for the distribution of *Dpy* and *Rol* phenotypes: 31 of 48

plates contained *Rol* animals, 29 out of 48 contained *Dpy* worms. In a second cross *op377; unc-69 (ju69)* males were crossed to *unc-69 (ju69)* III; *bli-6 (sc16)* IV; *dpy-11 (e224)* V; *lon-2 (e678)* X hermaphrodites. 13 out of 23 *Unc* F2 worms segregated *Bli*, 13 segregated *Dpy* and 20 *Lon*. This mapping data suggests that *op377* is located on chromosome X.

MATERIAL AND METHODS

Immunocytochemistry

COS-7, 293T cells or NG108 cells were transfected with pUB6 containing the FEZ1 cDNA or pcDNA3 containing the SCOCO cDNA using the Fugene kit (Roche). SCOCO and FEZ-1 were expressed as myc_2-tagged (pcDNA3) and V5-$(His)_6$-tagged (pUB6) proteins, respectively. Cells were fixed in 4% paraformaldehyde for 25 min (permeabilized cells) or 15 minutes in 2% paraformaldehyde (unpermeabilized cells). Unpermeabilized cells were shown to be intact by addition of Trypan Blue. To permeabilize, cells were incubated in 0.1% TritonX, 1%BSA in PBS, followed by blocking with 10% FCS, 0.05% NaN_3 in PBS. Then, cells were washed with 0.05% Tween in PBS and subsequently incubated with either rabbit polyclonal antibody against human c-myc (Covance) (1:400 immuno; 1:1000 WB) or mouse monoclonal antibody against the V5-tag (Invitrogen) (1:400 immuno; 1:5000 WB). Secondary antibodies coupled to Alexa-488 and Alexa-596 were applied 1:1000 after washing steps. Cells were mounted for microscopy with SlowFade antifade kit (Molecular Probes). For western blotting, secondary HRP-coupled antibodies were used. For all experiments, NG108 cells were kept in an undifferentiated state by incubation in DMEM/10%FCS.

Immunoprecipitation

NG108 cells were transfected with *$(myc)_2$–scoco* and *V5-$(His)_6$-fez1* to perform immunoprecipitation experiments. SCOCO was immunoprecipitated from lysates with rabbit polyclonal anti-myc antibodies (Covance) overnight at 4° C, on a rotating wheel. Thereafter, the antibodies were bound to protein A-coupled sepharose beads, followed by three washing steps with lysis buffer and protease inhibitors (50mM Tris, pH 7.8, 150mM NaCl, 1% NP-40). Bound proteins were eluted from the beads by boiling and separated by SDS-PAGE for western blotting. Blots were probed with mouse monoclonal specific for V5-FEZ1 (Invitrogen). The same experiment was conducted by immunoprecipitating FEZ1 first, with subsequent western blotting for SCOCO.

Protein purification

The human cDNA of SCOCO was cloned into the BamH1 site of the pGEX4T-2 vector (pGEX-SCOCO) and the plasmid was transfected into Bcl-21 bacteria. Bacteria containing pGEX-SCOCO and pGEX4T-2 were grown to an OD of 0.7 in 200ml LB/ampicillin. Protein expression was induced with 0.5 mM IPTG for 3h at 37°C. Afterwards, the bacteria were centrifuged for 10 min at 5000 rpm and the pellets were frozen at –80°C. Later, the frozen pellets were resuspended in 20 ml lysis buffer (10mM Tris-HCl, 1mM EDTA, 150 mM NaCl, 1.5% sarcosyl) with protease inhibitors (CompleteMini) (Roche). The suspension was incubated on ice for 10 min before addition of 100 µl 1M DTT. Then, the bacteria were lysed on ice by sonication for three times 20 s. After addition of 2 ml of 20% Triton-X, the lysates were centrifuged for 15 min at 7000 and the supernatant was mixed with 1ml glutathione beads. Beads and lysates were incubated for 2 h at 4° C on a rotating wheel and subsequently washed four times with washing buffer (20mM Tris, pH 8, 200mM NaCl, 1mM EDTA, 1mM $MgCl_2$, 0.5% NP-40, 1mM DTT) and two times with 20mM Tris, pH8, 120 mM NaCl. GST and GST-SCOCO were eluted with elution buffer (100mM Tris HCl, pH8, 120 mM NaCl, 20mM reduced glutathione) in several 1ml fractions. Purified protein fractions were dialyzed against PBS, pH 7.2, before sending them to MorphoSys to generate monoclonal antibodies. The ten best binders (myc-tagged bivalent mini-antibodies, $(F(ab')_2)$ in an ELISA were tested on western blots. Mini-antibodies were applied 1:2000, followed by mouse α-myc (E910) ascites 1:3000 and goat α-mouse-HRP 1:25 000.

REFERENCES

Hamprecht B, Glaser T, Reiser G, Bayer E, Propst F (1985). Culture and characteristics of hormone-responsive neuroblastoma X glioma hybrid cells. Methods Enzymol. 109: 316-341.

Kuroda S, Nakagawa N, Tokunaga C, Tatematsu K, Tanizawa K (1999). Mammalian homologue of the *Caenorhabditis elegans* UNC-76 protein involved in axonal outgrowth is a protein kinase C zeta-interacting protein. J Cell Biol. 144: 403-411.

Van Valkenburgh H, Shern JF, Sharer JD, Zhu X, Kahn RA (2001). ADP-ribosylation factors (ARFs) and ARF-like 1 (ARL1) have both specific and shared effectors: characterizing ARL1-binding proteins. J Biol Chem. 276: 22826-22837.

Su CW, Tharin S, Jin Y, Wightman B, Spector M, Meili D, Tsung N, Rhiner C, Bourikas D, Stoeckli E, Garriga G, Horvitz HR, Hengartner MO (2006). The short coiled-coil domain-containing protein UNC-69 cooperates with UNC-76 to regulate axonal outgrowth and normal presynaptic organization in *Caenorhabditis elegans*. J Biol. 5:9 [Epub ahead of print].

CHAPTER 6

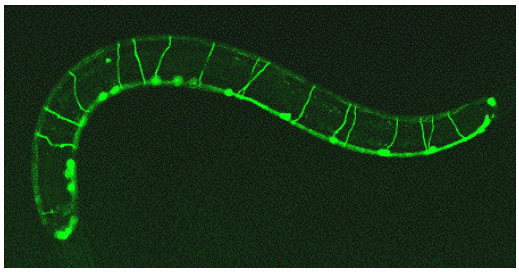

Perspectives

AXON GUIDANCE: PAST AND PRESENT RESEARCH

Fifteen years ago, only very few molecules were known that guide axons in vivo. In 1990, Hedgecock, Culotti and Hall presented three *C. elegans* mutants, which showed specific defects in cell migration and axon guidance along the ventral-dorsal axis. The affected genes were *unc-6*, *unc-5* and *unc-40* and identified at once the evolutionary conserved guidance cue netrin and its cognate receptors UNC-5 and DCC (Hedgecock et al., 1990). This impressively demonstrated, that the essential axon guidance molecules required for the correct wiring of a complex nervous system can be elucidated by screening for axon guidance mutants in the nematode *C. elegans*. In the following ten years, genetic, biochemical and molecular approaches led to the identification of four conserved families of guidance cues, which direct axons to their target area: netrins, Slits, semaphorins and ephrins (Dickson, 2002, Chilton, 2006).

More recent efforts have concentrated to understand how axon guidance signaling downstream of the identified cell surface receptors causes growth cone turning and correct navigation. Rho GTPases and their effectors such as Pak and Rho kinases turned out to be important downstream components that relay axon guidance signals to the actin cytoskeleton. Several axon guidance receptors were shown to directly bind to GTPases, regulatory GTPase activating proteins or guanine nucleotide exchange factors (Dickson, 2002). Ena/VASP proteins, which antagonize actin-capping proteins, are also required for the transduction of guidance signals to actin filaments (Dickson, 2002). Another branch of research has provided considerable evidence for an important role of calcium signaling in promoting growth cone turning (Wen and Zheng, 2006).

In addition to studying signal transduction, researchers in the axon guidance field have explored two other main roads in the past five years. First, the search for new guidance molecules, which escaped detection in the previous screens and second, the study of regulatory mechanisms in axon guidance that allow highly differentiated responses for navigating axons. A surprising finding concerning the first aspect was the discovery of morphogens as axon guidance molecules: Several recent studies could show that members of the three classical morphogen families, Hedgehog, Wnt and BMP, function as guidance cues during later developmental stages (Schnorrer and Dickson, 2004; Stoeckli, 2006). The second focus of axon guidance research provided insight into several mechanisms that enable modulation of axon guidance signaling. These include crosstalk between different receptors

(Hong et al., 1999; Stein et al., 2001; Sabatier et al., 2004; Chang et al., 2004), post-translational control of receptor exposure (Keleman et al., 2002), regulation of the distribution of extracellular signals (Hiramoto et al., 2000) and local control of protein synthesis (Brittis et al., 2002). In very recent genetic experiments, heparan sulfate proteoglycans (HSPGs) were identified as critical regulators of axon guidance signaling (Lee and Chien, 2004). The mechanism, by which HSPGs control neuronal migration and axon guidance is not clear yet and will remain an important question to be addressed in the future.

HSPGs IN *C. ELEGANS* NERVOUS SYSTEM DEVELOPMENT: AN OUTLOOK

1. Syndecan function in neuronal migration and axon guidance.

The main objective of my thesis project was to study the role of HSPGs in nervous system development of *C. elegans*. To this end, I characterized in detail the function of the cell surface HSPG syndecan SDN-1, which I found to play a crucial role in neuronal migration and axon guidance (Chapter 2) and analyzed other available HSPG mutants for neural defects (Chapter 3). In order to uncover additional components of HS-dependent axon guidance signaling pathways, I designed several modifier screens and characterized seven *hse-5* enhancer mutations (Chapter 4) that are likely to identify new genes in the axon guidance pathway regulated by SDN-1.

In my view, the functional rescue assays in *sdn-1* mutants provide a powerful tool to further elucidate the molecular mechanism through which SDN-1 controls axon guidance signaling. Evaluating the rescue activity of a construct encoding for a verified HS-less SDN-1 (by mutating HS attachment sites) or for a transmembrane SDN-1 lacking the cytoplasmic domain would lead to a more complete data set to make strong claims about a purely "sugar-based" function of SDN-1 in neuronal processes. As a side aspect of this project, we have started a collaboration with Fred Hagen where we aim to map all the potential HS and mucin glycosylation sites on SDN-1.

The second type of experiments, I envisage to provide mechanistic clues about SDN-1 function, are ectopic expression studies. If SDN-1 affects indeed the extracellular distribution of Slit SLT-1, as it has been deduced from an experiment in *Drosophila* (Johnson et al., 2004), ectopic expression of SDN-1 in dorsal body wall muscles would be expected to perturb ventral axon guidance. In *C. elegans* larvae, SLT-1 is expressed by dorsal muscles and repels axons (for example from AVM) to the ventral side, in parallel to attraction by UNC-6/netrin

(Hao et al., 2001). Of course, the comparison of SLT-1 gradients in *sdn-1* null mutants and wild-type worms could provide the same answer in a more direct way. However, this experiment is technically extremely difficult in *C. elegans*, compared to the situation in *Drosophila*, although not impossible as demonstrated by the recent visualization of a Wnt gradient in *C. elegans* (Coudreuse et al., 2006). Except for the structure/function experiments, the above experiments are not new approaches, but would rather reconfirm or reevaluate previous observations in *C. elegans.*

This project was started two and a half years ago from scratch, without previous knowledge of axon guidance signaling genetics and only very little expertise in neurobiology. In order to remain competitive in this field, I believe that future efforts have to concentrate on the identification of the enhancers identified in the screens, which represent a novel approach. Experiments attempting to verify the existence of the proposed HS sugar code by ectopic expression of HS-modifying enzymes are of course perfectly obvious as well, but are already intensively pursued by the group of Prof. Oliver Hobert at Columbia University.

2. Identification of new components in HS-dependent axon guidance signaling

To analyze available HSPG mutants for neural phenotypes (Chapter 3) did not help me to pinpoint an additional HSPG that could possibly act in parallel of SDN-1, as proposed in Chapter 2. To select *C. elegans* genes predicted to encode HSPGs based on homology with other species is a valid strategy, as shown for CLE-1, but bears the disadvantage to be biased towards known HSPGs. Therefore, I have initiated a biochemical approach to specifically purify HSPGs from *C. elegans* to determine their identities (in collaboration with Enrique Brandan). Once the isolation of HSPGs is optimized to a degree that single bands are obtained in the gel, they can be analyzed by mass spectrometry. Comparison of the peptides against the *C. elegans* proteome database, created by the Hengartner proteome group, is likely to unambigously identify the purified HSPGs. The lab of Enrique Brandan has already achieved to isolate clean HSPG bands corresponding to 30 and 80kDa. It will be highly interesting to determine their molecular identity. In the mean time, analysis of newly generated HSPG mutants, such as a deletion in the *C. elegans* testican gene, should be continued.

But as already stated, the main emphasis of future research on neural functions of HSPGs should lie on the mapping of the enhancer mutations obtained in the *hse-5* background, in parallel to additional screening for enhancers in the *sdn-1* null background. A safe approach

might be to concentrate on the mapping of *op459* on chromosome II, which is likely to identify a new gene required for commissural guidance based on extensive literature review. However, if complementation tests demonstrate that the enhancers on chromosome IV are neither hypomorphic alleles of *unc-5*, *ced-10*, *unc-44* nor alleles of *zag-1*, I propose to map the strongest enhancer *op468*. Having mentioned a safe approach, one has to recognize that a hunt for a mutant in a forward genetic screen is always a random process and that the preconceived ideas about what genes will be identified might be wrong, especially when the screening design is used for the first time. But since only further analysis of the genes will tell us the truth in the end, I believe that the development of an effective RNAi strategy will be decisive to speed up the time-consuming mapping of enhancers. I would cross *eri-1(mg366)*, *lin-15(n744)* or *lin-35(n745)* into *hse-5(tm472); oxIs12* worms and test the suitability of these strains to map enhancers of *hse-5* by performing RNAi against *sdn-1*. All three mutations can sensitize worms to the effect of RNAi in neurons (Wang et al., 2005). These newly discovered genetic backgrounds offer now the possibility to do reverse genetic screens for neural processes, but it will be important to select strains that do not interfere with neural development, which could confound RNAi results.

From *C. elegans* proteins to mammalian homologs

In my second project, I have established new approaches for our lab that enable to test the functional conservation of identified *C. elegans* axon guidance genes in higher vertebrates (Chapter 5). In collaboration with the group of Prof. Esther Stoeckli, we could show that the chicken homolog of UNC-69 is highly expressed in the developing chicken nervous system and that interference with its function by in-ovo RNAi perturbs an axonal guidance process. This approach is especially powerful if there are no other redundant gene family members, which could compensate for the knock-down of the targeted gene.

In my opinion, also experiments in neural cell lines can provide valuable information that can complement the genetic studies performed in our lab. The cell culture offers increased resolution to determine the subcellular localization of proteins, compared to the small cells of the worm. This could be especially important for experiments that attempt to show colocalization of two proteins or the distribution of receptors at the cell membrane.

CONCLUDING REMARKS

When Sidney Brenner introduced *C. elegans* as a new model organism in the 1970s, he foresaw that the worm would become a powerful system to study nervous system development and behavior. This prediction turned out to be entirely true. In addition to developmental questions, neurobiological research in *C. elegans* has now moved on to uncover the genetic basis of behavior and even learning. Nevertheless, many aspects of nervous system development are not understood yet. I envision that the following processes in axon guidance will become the center of intense investigation in the future: First, the question of how axon guidance signals are integrated and segregated within the axonal growth cone. Second, the elucidation of the molecular signals that mediate the ultimate fine mapping of axons to the correct neuron, once they have reached the target area. And third, there is still little knowledge about factors that mediate interactions among axons or conversely, signals that trigger defasciculation of an axon from a common nerve track. However, by asking all these questions, it should not be forgotten that the process of axon guidance, which is crucial for the initial wiring of the neural connections, is also implicated in the rewiring of regenerating axons after nerve injury. Therefore, I believe that we have to undertake major efforts to study not only the developmental aspects of the nervous system, but also the pathological conditions.

REFERENCES

Brittis PA, Lu Q, Flanagan JG (2002). Axonal protein synthesis provides a mechanism for localized regulation at an intermediate target. Cell. 110: 223-235.

Chang C, Yu TW, Bargmann CI, Tessier-Lavigne M (2004). Inhibition of netrin-mediated axon attraction by a receptor protein tyrosine phosphatase. Science. 305: 103-106.

Chilton JK (2006). Molecular mechanisms of axon guidance. Dev Biol. 292: 13-24.

Coudreuse DY, Roel G, Betist MC, Destree O, Korswagen HC (2006). Wnt gradient formation requires retromer function in Wnt-producing cells. Science. 312: 921-4.

Dickson BJ (2002). Molecular mechanisms of axon guidance. Science. 298:1959-1964.

Hedgecock EM, Culotti JG, Hall DH (1990). The *unc-5*, *unc-6*, and *unc-40* genes guide circumferential migrations of pioneer axons and mesodermal cells on the epidermis in *C. elegans*. Neuron. 4: 61-85.

Hiramoto M, Hiromi Y, Giniger E, Hotta Y (2000). The *Drosophila* Netrin receptor Frazzled guides axons by controlling Netrin distribution. Nature. 406: 886-889.

Hong K, Hinck L, Nishiyama M, Poo MM, Tessier-Lavigne M, Stein E (1999). A ligand-gated association between cytoplasmic domains of UNC5 and DCC family receptors converts netrin-induced growth cone attraction to repulsion. Cell. 97:927-941.

Johnson KG, Ghose A, Epstein E, Lincecum J, O'Connor MB, Van Vactor D (2004). Axonal heparan sulfate proteoglycans regulate the distribution and efficiency of the repellent slit during midline axon guidance. Curr Biol. 14: 499-504.

Keleman K, Rajagopalan S, Cleppien D, Teis D, Paiha K, Huber LA, Technau GM, Dickson BJ (2002). Comm sorts robo to control axon guidance at the *Drosophila* midline. Cell. 110: 415-427.

Lee JS, Chien CB (2004). When sugars guide axons: insights from heparan sulphate proteoglycan mutants. Nat Rev Genet. 5: 923-935.

Sabatier C, Plump AS, Le Ma, Brose K, Tamada A, Murakami F, Lee EY, Tessier-Lavigne M (2004). The divergent Robo family protein rig-1/Robo3 is a negative regulator of slit responsiveness required for midline crossing by commissural axons. Cell. 117: 157-169.

Schnorrer F, Dickson BJ (2004). Axon guidance: morphogens show the way. Curr Biol. 14: R19-21.

Stein E, Tessier-Lavigne M (2001). Hierarchical organization of guidance receptors: silencing of netrin attraction by slit through a Robo/DCC receptor complex. Science. 291: 1928-1938.

Stoeckli ET (2006). Longitudinal axon guidance. Curr Opin Neurobiol. 16: 35-39.

Wen Z, Zheng JQ (2006). Directional guidance of nerve growth cones. Curr Opin Neurobiol. 16: 52-58.